TU
TECHNISCHE UNIVERSITÄT WIEN

Dissertation

CO Oxidation and Preferential CO Oxidation on Cobalt Oxide Catalysts

ausgeführt zum Zwecke der Erlangung des akademischen Grades eines Doktors der technischen Wissenschaften unter der Leitung von

Univ.Prof. Mag.rer.nat. Dr.rer.nat. Günther Rupprechter

und

Assistant Prof. Dip-Ing. Dr.techn. Karin Föttinger

Institut für Materialchemie E165

eingereicht an der Technischen Universität Wien Fakultät für Technische Chemie

von

MSc. Liliana Lukashuk

Matrikelnummer: 1228509

21 Summerhouse Square, TS20 1BH, Stockton-on-Tees, United Kingdom

Stockton-on-Tees, am 06/11/2016

Two roads diverged in a wood, and I—
I took the one less travelled by,
And that has made all the difference.

Robert Frost

STATEMENT OF AUTHORSHIP

I hereby declare that this PhD thesis is the result of my own scientific research work conducted during the course of my PhD study at the Institute of Materials Chemistry, Technische Universität Wien from October 2012 to November 2015, unless otherwise acknowledged in the text. The chapters represent papers that were published or are being prepared for submission to international journals. All references and verbatim extracts have been quoted, and all sources of information have been specifically acknowledged. This thesis has not been submitted for any other degree.

Stockton-on-Tees, 06/11/2016

_____ Liliana Lukashuk

ZUSAMMENFASSUNG

Die katalytische CO Oxidation ist eine der am häufigsten untersuchten Reaktionen. Das große Interesse an dieser Reaktion kann durch zwei Gegebenheiten erklärt werden: a) Die katalytische CO Oxidation ist von großer praktischer Relevanz in der Fahrzeug-Abgaskontrolle, der Luftreinigung und der H_2 Aufreinigung für Polymerelektrolytbrennstoffzellen (i.e. präferenzielle CO Oxidation (PROX)); b) die CO Oxidation wird oft als Modellreaktion verwendet, die dazu dienen kann, die Natur von aktiven Zentren und von Reaktionsmechanismen aufzuklären. Vielversprechende Katalysatoren für sowohl die CO Oxidation als auch PROX sind Materialien aus Kobaltoxid. Trotz zahlreicher Untersuchungen dieser Katalysatoren in der CO Oxidation blieb die Natur der aktiven Zentren und der Reaktionsmechanismus ungeklärt. Es bestehen immer noch offene Fragen und Unstimmigkeiten bezüglich z.B. der Rolle von Co^{2+}/Co^{3+} Spezies und von Promotoren, verschiedenster Sauerstoffspezies, Sauerstofffehlstellen, der Bildung von Karbonaten, des Einflusses der Vorbehandlung und der Deaktivierung des Katalysators.

Basierend auf den ungeklärten Fragen besteht das Ziel dieser Arbeit darin, einen Einblick in mechanistische Vorgänge der (präferenziellen) CO Oxidation in Gegenwart von Co_3O_4 bzw. CeO_2-Co_3O_4 zu erhalten. Um dieses Ziel zu erreichen wurden verschiedenste operando Methoden eingesetzt: Fourier Transformations-IR-Spektroskopie (FTIR), Synchrotron-Röntgenphotoelektronenspektroskopie nahe dem Umgebungsdruck (Near Atmospheric Pressure, NAP-XPS), Röntgendiffraktion (XRD) und Röntgenabsorptionsspektrokopie (XAS). Sie dienten im Speziellen dazu, Änderungen der Oberfläche und des Volumens des Katalysators unter Reaktionsbedingungen (CO und O_2; CO, O_2 und H_2), in CO Atmosphäre und während eines Wechsels von CO auf O_2 zu verfolgen.

Im ersten Teil der Arbeit wird auf die oberflächennahe Zusammensetzung von Kobaltoxid unter reduzierender (CO) und oxidierender (O_2) Atmosphäre eingegangen. Die Anwendung von Synchrotron-basiertem in situ **NAP-XPS** (inklusive Tiefenprofilmessungen mittels Variation der Photonenenergie) und Röntgen-Nahkanten-Absorptions-Spektroskopie (NEXAFS) an der Co $L_{3,2}$ Kante (im Modus „Total Electron Yield Detection") ermöglichte es, elektronische und strukturelle oberflächennahe Änderungen von Co_3O_4 zu detektieren. Des Weiteren konnte hiermit die Entstehung und das Verschwinden von Adsorbaten und Sauerstofffehlstellen während der CO Reduktion und anschließender O_2 Reoxidation beobachtet werden. Die zu unterschiedlichen Probentiefen zugehörigen Ergebnisse ermöglichten es, die Bildung von Sauerstofffehlstellen an der Oberfläche (RT-150 °C; durch Oberflächenreduktion mit CO) von Fehlstellen im Volumen (200-250 °C; durch die Mobilität von Gittersauerstoff) zu unterscheiden. Außerdem wurde während der Reduktion von Co_3O_4 in CO bei 250 °C die Entstehung eines Mischoxids aus kubischem CoO (Steinsalzstruktur) und metastabilem hexagonalem CoO (Wurtzitstruktur) im oberflächennahen Bereich (3-5 nm) verzeichnet. Die Messungen zeigten, dass die Temperaturen der Reduktion von Co_3O_4 und der Reoxidation von metallischem Co deutlich unterschiedlich sind. All diese Beobachtungen liefern neue Einblicke in die Oberflächenchemie

von Co_3O_4 und den Mechanismus der CO Oxidation auf Co_3O_4. Nicht zuletzt geben sie auch Aufschluss über die Deaktivierung und die Regenerierung von aus metallischem Kobalt bestehenden Fischer-Tropsch-Katalysatoren unter oxidierenden Bedingungen.

Als nächstes wurde die CO Oxidation über Kobaltoxid Katalysatoren mit operando-Techniken untersucht. Operando FTIR, NAP-XPS, XRD und XAS wurden angewandt, um Oberflächen- und Volumenänderungen unter stationären Reaktionsbedingungen (CO und O_2), in CO Atmosphäre und während dem Wechsel von CO auf O_2 aufzuzeichnen. Operando NAP-XPS hat gezeigt, dass unter Reaktionsbedingungen bis zu 200 °C ein vollständig oxidiertes Co_3O_4 vorliegt, während in reinem CO eine Reduktion der Co_3O_4 Oberfläche bereits bei 100 °C von statten ging. In den „switching" Experimenten von CO auf O_2 wurden deutliche Änderungen des Co^{3+}/Co^{2+} Verhältnis beobachtet: 25% Co^{3+} in CO vs. 28% Co^{3+} in O_2 bei 150 °C, und 24% Co^{3+} in CO vs 28% Co^{3+} in O_2 bei 200 °C. In der C 1s Region der XPS Spektren wurden Karbonate, molekular absorbiertes CO an Co Kationen und elementarer Kohlenstoff detektiert. Elementarer Kohlenstoff deutet auf eine CO Dissoziation während der CO Oxidation hin.

Die Ergebnisse der FTIR Spektroskopie haben deutlich gezeigt, dass CO unterschiedlich koordinierte Karbonate auf der Co_3O_4 Oberfläche bildete, wobei diese in Gegenwart des Reaktionsgemisches mit der Zeit abnahmen. Basierend auf der Kombination von operando NAP-XPS und operando FTIR Spektroskopie (inklusive stationärer und dynamischer „switching" Experimente) gibt es eindeutige Indizien, dass die Reaktion auf Co_3O_4 bei hohen Temperaturen über einen Redox Mars-van-Krevelen Mechanismus abläuft, bei dem der Redoxzyklus zwischen Co^{3+} und Co^{2+} ein wichtiger Teilschritt ist. Im Gegensatz dazu verläuft die CO Oxidation bei niedrigen Temperaturen wahrscheinlich über einen Langmuir-Hinshelwood Mechanismus ab. Des Weiteren geben die Resultate Aufschluss über weitere Reaktionswege, welche zur Gesamtreaktion beitragen können, wie a) die Bildung von Karbonaten gefolgt von ihrer Zersetzung und b) die CO Dissoziation mit anschließender Reoxidation von elementarem Kohlenstoff.

Zusätzlich wurde ein Vergleich zu CoO Materialien mit unterschiedlicher Partikelgröße durchgeführt. Für CoO Partikelgrößen im Bereich 20-50 nm wurde während der CO Oxidation eine Reoxidation von CoO zu Co_3O_4 (an der Oberfläche und im oberflächennahen Bereich) bei 200 °C aufgezeichnet. Im Gegensatz dazu wurde für makroskopisches CoO (1 μm) keine Volumenoxidation zu Co_3O_4 unter Reaktionsbedingungen bis zu Temperaturen von 360 °C beobachtet.

Der dritte Teil der Arbeit fokussiert sich auf die präferenzielle CO Oxidation in Gegenwart von Co_3O_4 und CeO_2-Co_3O_4 Katalysatoren. Hierbei wurden zugleich der Oxidationszustand und die katalytische Aktivität des Co_3O_4 Katalysators während der PROX Reaktion aufgezeichnet. Die Co_3O_4 Reduktion wurde in der Reaktionsmischung (CO, O_2 und H_2) sowohl als auch in reinem CO und H_2 untersucht. Während der PROX Reaktion über Co_3O_4 erschien der Katalysator zur Gänze im oxidierten

Zustand (sowohl im Volumen als auch auf der Oberfläche bei Temperaturen bis zu 250 °C). Referenzmessungen in reiner CO Atmosphäre zeigten allerdings, dass CO die Katalysatoroberfläche bei 100 °C zu reduzieren beginnt, in dem es mit Gittersauerstoff aus der Oberfläche reagiert. Jedoch verläuft die Reoxidation mit O_2 während der PROX Reaktion so rasch, dass es hierbei nicht zu einer merklichen Reduktion des Katalysators kommt (ähnlich wie im Falle der CO Oxidation). Abgesehen von der niedrigen Konzentration von Sauerstofffehlstellen unter stationären PROX Bedingungen wird vermutet, dass die selektive CO Oxidation in Gegenwart von H_2 vorwiegend über den Mars-van-Krevelen Mechanismus verläuft, was aus den CO-O_2 „switching" Experimenten hervorgeht. In reiner H_2 Atmosphäre wird eine Reduktion des Co_3O_4 Volumens und seiner Oberfläche erst bei Temperaturen von über 250 °C initiiert. Während sich die Änderung der Selektivität für die Methanisierung bei ungefähr 250 °C durch die Reduktion von Co_3O_4 zu CoO erklären lässt, kann die Änderung der Selektivität von der CO Oxidation zur Oxidation von CO und H_2 bei 170 °C nicht durch eine Änderung des Oxidationszustandes der Oberfläche erklärt werden. Stattdessen sind für die Erniedrigung der Selektivität für die CO Oxidation bei Erhöhung der Temperatur zwei andere wesentliche Faktoren verantwortlich: a) Der stärkere Anstieg der Reaktionsgeschwindigkeit der H_2 Oxidation gegenüber der CO Oxidation und b) die Konkurrenz um die limitierende Menge an O_2 für die Oxidation. Zuletzt wurde der Effekt der Zugabe von CeO_2 (ein weniger aktives Material) zu Co_3O_4 untersucht. Durch den Zusatz von 10 wt% CeO_2 wurde die Reduktionstemperatur des Katalysators in CO und H_2 erhöht und zudem eine Erhöhung der Aktivität in der PROX Reaktion festgestellt. Da CeO_2 eine geringere Aktivität als Co_3O_4 hat, kann die erhöhte Aktivität nur auf bestehende Co-O-Ce Ensembles zurückgeführt werden.

ABSTRACT

Catalytic CO oxidation is one of the most extensively studied reactions. The interest in this reaction can be explained by two main reasons: a) catalytic CO oxidation is of great practical importance in automotive exhaust gas control, air purification, and H_2 purification for proton exchange membrane fuel cells (i.e., preferential CO oxidation (PROX)); b) CO oxidation is a simple model reaction that can provide insights into the nature of active sites of catalysts and mechanisms of catalytic processes. Cobalt oxide materials are promising catalysts for CO oxidation and PROX. Although many efforts have been made to explore the potential of cobalt oxide catalysts for the CO oxidation reaction, the nature of the active sites and the reaction mechanism are still not well understood. Open questions and contradicting results concern, for instance, the role of Co^{2+}/Co^{3+}, different oxygen species, oxygen vacancies, the role of promoters, formation of carbonates, influence of pretreatment, and catalyst deactivation. Therefore, the goal of this thesis was to gain mechanistic understanding of cobalt oxide and promoted cobalt oxide catalysts for CO oxidation and preferential CO oxidation reactions. For this purpose, a combined operando approach was employed: Fourier transform infrared spectroscopy (FTIR), near atmospheric pressure X-ray photoelectron spectroscopy (NAP-XPS), X-ray diffraction (XRD), and X-ray absorption spectroscopy (XAS) were used to monitor surface and bulk changes of catalysts under reaction conditions (CO and O_2: CO, O_2 and H_2), in CO atmosphere and upon switching from CO to O_2.

The (near)surface composition of cobalt oxide under reducing (CO) and oxidizing (O_2) atmospheres was studied first. Using synchrotron-based in situ NAP-XPS, including depth profiling by photon energy variation, and near-edge X-ray absorption fine structure (NEXAFS) at the Co $L_{3,2}$ edge (total electron yield detection), the (near)surface electronic and structural changes of Co_3O_4, adsorbates and oxygen vacancies evolution during CO reduction and subsequent O_2 reoxidation were monitored. The results obtained by combining information from different information depths allowed to distinguish surface vacancy formation during reduction of Co_3O_4 in CO atmosphere (RT-150 ºC) from the oxygen vacancies created by mobility of bulk lattice oxygen (200-250 ºC). Additionally, formation of a mixed phase of rocksalt-type CoO and metastable wurtzite-type CoO in the near-surface (~ 3-5 nm) during reduction of Co_3O_4 in CO atmosphere at 250 ºC were identified. Moreover, the obtained data revealed that the temperatures for reduction of cobalt oxide and the reoxidation of metallic cobalt did not coincide. This provides new insights into the surface chemistry of Co_3O_4 and shed light on the CO oxidation mechanism on cobalt oxide, as well as the deactivation and regeneration of metallic cobalt Fischer-Tropsch catalysts under oxidizing conditions.

CO oxidation over cobalt oxide catalysts by means of operando techniques was studied next. Operando FTIR, NAP-XPS, XRD, and XAS were employed to monitor surface and bulk changes in the catalyst under static reaction conditions (CO and O_2), in CO atmosphere and upon switching from CO to O_2. Operando NAP-XPS revealed fully oxidized Co_3O_4 during CO oxidation up to 200 ºC, whereas in

(pure) CO the surface reduction of Co_3O_4 started around 100 ^{o}C. Significant changes in the Co^{3+}/Co^{2+} ratio were observed upon switching from CO to O_2: 25% Co^{3+} in CO vs 28% Co^{3+} in O_2 at 150 ^{o}C; and 24% Co^{3+} in CO vs 28% Co^{3+} in O_2 atmosphere at 200 ^{o}C. In the C 1s region, carbonates, molecular CO adsorbed on cobalt cations, and elementary carbon were observed, the latter indicating CO dissociation during CO oxidation. FTIR spectroscopy clearly showed that CO formed surface carbonate species with Co_3O_4 (i.e., monodentate and at higher temperatures bidentate), while during the reaction the amount of carbonates decreased. The combined results of operando NAP-XPS and operando FTIR spectroscopy (i.e., static steady-state and dynamic switching experiments) indicate a redox Mars-van-Krevelen mechanism of CO oxidation on Co_3O_4, involving the Co^{3+}/Co^{2+} cycle and oxygen vacancy formation at higher temperatures and likely the Langmuir–Hinshelwood mechanism at lower temperature. Moreover, the results point to additional reaction pathways such as: 1) carbonate formation followed by decomposition; 2) CO dissociation followed by elementary carbon reoxidation in the overall CO oxidation reaction mechanism on Co_3O_4. An effect of the particle size of CoO materials on the catalytic activity was revealed. For CoO with particles of 20-50 nm, reoxidation of CoO to Co_3O_4 during CO oxidation (surface and near-surface) at 200 ^{o}C was monitored. In contrast, for macroscopic CoO (1 μm) no bulk oxidation of CoO to Co_3O_4 was observed during CO oxidation at temperatures as high as 360 ^{o}C.

Preferential CO oxidation on Co_3O_4 and CeO_2-Co_3O_4 catalysts was studied third. The Co_3O_4 catalyst oxidation state during the PROX reaction was examined while simultaneously monitoring catalytic activity. Apart from the reaction mixture (CO, O_2, H_2), Co_3O_4 reduction in pure CO or H_2 atmospheres were additionally examined. During PROX on Co_3O_4 the catalyst appears fully oxidized (i.e., both the surface and bulk oxidation state do not change up to 250 °C). However, as revealed by reference measurements in (pure) CO, CO reduces the catalyst (surface) starting around 100 °C via reaction with lattice oxygen. However, the reoxidation by O_2 during PROX is fast enough to prevent overall reduction. Despite a very low concentration of oxygen vacancies under steady state PROX conditions, it is suggested that selective oxidation of CO to CO_2 in an excess of H_2 follows predominantly the Mars-van-Krevelen mechanism, referring to the information obtained from CO-O_2 switching experiments. In (pure) H_2, surface and bulk reduction both start above 250 °C. Whilst the Co_3O_4 reduction to CoO and Co around 250 °C explains the selectivity change to methanation, the change in selectivity around 170 °C from PROX (with predominantly CO oxidation) to both CO and H_2 oxidation cannot be explained by a change in (surface) oxidation state. Upon increasing the temperature the difference in the increase of H_2 oxidation rate vs CO oxidation rate (higher apparent activation energy for H_2 oxidation), as well as the competition for the limited amount of O_2, are responsible for the decreasing CO oxidation selectivity. Furthermore, the effect of adding CeO_2 (a less active material) to Co_3O_4 was studied. Promotion of Co_3O_4 with 10 wt% CeO_2 increased the reduction temperatures in CO and H_2 and enhanced the PROX activity. Since CeO_2 is a less active material, this can only be explained by a higher activity of Co-O-Ce ensembles.

ACKNOWLEDGMENT

SYMBOLS

Symbol	Unit	Meaning
2θ	°	diffraction angle
A_{BET}	$m^2\,g^{-1}$	specific BET-surface area
D_p	nm	pore diameter
c	$mol\,L^{-1}$	concentration
V_{spec}	$cm^3\,g^{-1}$	specific pore volume
λ	nm	wavelength

ABREVIATIONS

BE	Binding Energy
DOS	Density of States
EELS	Electron Energy Loss Spectroscopy
EXAFS	Extended X-ray Absorption Fine Structure
FID	Flame Ionization Detector
FTIR	Fourier Transformed Infrared
FWHM	Full Width at Half Maximum
KE	Kinetic Energy
MCT	Mercury Cadmium Telluride
MFC	Mass Flow Controller
MS	Mass Spectrometry
NAP-XPS	Near Atmospheric Pressure X-Ray Photoelectron Spectroscopy
NEXAFS	Near Edge X-Ray Absorption Fluorescence Spectroscopy
NIST	National Institute of Standards and Technology
OSC	Oxygen Storage Capacity
PEMFC	Proton Exchange Membrane Fuel Cell
PROX	Preferential Oxidation
RT	Room Temperature
SEM	Secondary Electron Multiplier
SSA	Specific Surface Area
TCD	Thermal Conductivity Detector
TEM	Transmission Electron Microscopy
TOF	Turn Over Frequency
TPD	Temperature Programmed Desorption

TPO	Temperature Programmed Oxidation
TPR	Temperature Programmed Reaction
TWC	Three Way Catalyst
UPS	Ultraviolet Photoelectron Spectroscopy
VB	Valence Band
XANES	X-Ray Near Edge Structure
XPS	X-Ray Photoelectron Spectroscopy
XRD	X-Ray Diffraction

TABLE OF CONTENTS

CHAPTER 1

INTRODUCTION AND STATE OF THE ART

1.1 GENERAL

In today's world it is difficult to imagine everyday life without the contribution of catalysis. 85% of all chemical production processes of industrial chemicals and derivatives use catalysts.[1] Moreover, about 80% of these catalytic processes are heterogeneously catalyzed, which means that the catalyst is in a different phase than the educts and products. In the majority of the cases the catalyst is a solid. This is simply explained by the fact that for large-scale industrial production the separation of the products and educts from the catalyst is a crucial step that is often followed by recycling and regeneration of spent catalysts.[1] Generally, catalyst separation is more easily achieved for solid catalysts. Homogeneous catalysis is mainly associated with those reactions, where solid catalysts are still not applicable. However, many research efforts are currently directed toward the immobilization of molecular catalysts on solid supports and replacement of homogeneous processes to heterogeneous ones.

Economic issues and environmental regulations that have changed and become more restrictive over time increase the need for the improvement of catalytic processes. The improvement of catalytic processes is strongly related to the better performance of catalysts (i.e., higher conversion, selectivity, yield, and stability). Furthermore, the desired catalysts additionally have to meet the requirements of being "low cost" as well as "environmentally and user-friendly". All these requirements can be met only by catalyst development and optimization following new approaches in the design and synthesis.

Research and development of more efficient and sustainable catalysts that either refers to the development of completely new catalysts or optimization of existing ones, is a vital part of industrial and academic research. It encompasses different approaches for reaching the aimed results. One strategy is based on the synthesis of a series of catalysts, followed by the screening of the catalytic activity (i.e., "high-throughput synthesis and screening"). However, using such an approach alone without understanding activity-controlling factors often does not lead to a gain in knowledge and a deeper understanding of factors driving the activity and selectivity of catalysts (i.e., the nature of active sites and reaction mechanisms). One out of a hundred synthesized catalysts using "high-throughput synthesis" might be very active for a particular reaction (i.e., a "lucky catalyst"). However, without a deeper understanding of how the electronic and geometric properties of this particular catalyst correlate with its catalytic performance, it is not possible to transfer knowledge to similar processes or even further improve and optimize the current catalyst. Thus, the development of a new better catalyst starts again from scratch and involves high costs as well as time for finding the next "lucky catalyst".

Therefore, the *"understanding of structure-performance relationships of catalysts"* is a crucial step for the successful development of the next generation of more efficient catalysts and covers different aspects. Some research lines focus on the preparation of catalysts varying certain parameters (e.g., preparation methods, elemental

composition, loading etc.), and then they correlate catalytic properties of the synthesized materials with their electronic and geometric structure, reducibility, tendency to adsorption/desorption of the educts and products for a particular reaction. This gives rather a macroscopic picture on the *"understanding of structure-performance relationships of catalysts"* omitting the detailed microscopic insights into the activity-controlling factors driving a particular reaction.

Another line of research dealing with the *"understanding of structure-performance relationships of catalysts"* focuses on microscopic insights and explores the nature of the reaction sites of catalysts and mechanisms of reactions. For studying the nature of active sites and reaction mechanisms, two methodologies are commonly used nowadays. The first one is based on the detailed study of reaction kinetics (i.e., reaction rates, determining the orders of reactions and the rate law). It takes its roots back to 1921, when the mechanism of the catalytic action of platinum in the reactions of CO oxidation and hydrogen oxidation was described with the help of kinetics by Irving Langmuir, and presented at a Discussion of the Faraday Society held in September 1921 at the Institution of Electrical Engineers in London.[2] Further, his work was elaborated by Cyril Hinshelwood.[3] The joined work of Irving Langmuir and Cyril Hinshelwood is known today as the Langmuir-Hinshelwood mechanism and is one of the most common reaction mechanisms describing numerous catalytic reactions. According to the Langmuir-Hinshelwood mechanism, a catalytic act is a reaction between two molecules, adsorbed on neighboring sites. Some years later, in 1938, Dan Eley and proposed the Eley-Rideal mechanism, in which a catalytic act is a reaction between an adsorbed molecule and a molecule from the gas phase.[3] Later works of Mars and Van Krevelen on reducible oxides (1954) suggested another mechanism that today is called the Mars -Van Krevelen-type mechanism. According to this mechanism, one reactant forms a chemical bond with the catalytic surface; the other reactant reacts directly from the gas phase. A vacancy/surface defect that is formed, when the reaction product desorbs, is filled with an atom from the bulk.[3] However, nowadays it is generally accepted that the vacancy created by the reaction is filled with the first reactant again.[4]

Although studying the kinetics of reactions is a powerful tool for identifying some steps of the reaction cycle and for obtaining hints about active sites, it does not allow for the complete picture of the reaction mechanism to be obtained. Often several reaction mechanisms can run in parallel; therefore, an exact identification of the reaction mechanism is not feasible. Moreover, for heterogeneous catalytic reactions, the identification of active sites is rather vague especially for solid catalysts because of their complexity. Often solid catalysts are multicomponent and multielement materials. Furthermore, the structures of solid catalysts are usually not well defined, and, thus, several sites might serve as active sites, and, as a result, different reaction pathways might simultaneously run on different reaction sites, or different reaction pathways might occur in different temperature regimes. The complementary methodology that is based on the use of in situ/operando techniques for studying the catalyst under reaction conditions can overcome some of the limitations of the traditional kinetic methodology and provide a broader insight on the

complex network of reaction pathways. Using in situ/operando techniques allows monitoring the reaction sites of catalysts on a rather local level and can strongly contribute to the *"understanding of the structure-performance relationships of catalysts"*, the nature of active sites, and reaction mechanisms.

For the successful development of the next generation of more efficient catalysts, a combination of all the approaches mentioned above is required: 1) preparation of a set of catalysts by varying certain parameters (e.g., preparation methods, elemental composition, loading etc.) and correlating their catalytic performance with the electronic and geometric structure; 2) studying the kinetics of reactions; 3) in situ/operando investigation of catalysts under reaction conditions. Using such a combined approach and interconnecting the obtained information is a powerful research tool that can boost the research and development of more efficient catalysts with the desired catalytic properties.

1.2 IN SITU/OPERANDO APPROACH FOR A BETTER UNDERSTANDING OF CATALYSIS

Solid catalysts are very dynamic under working conditions when high temperatures and pressures are applied. Freshly prepared catalysts often undergo structural changes under activation/pretreatment conditions and further under reaction conditions. Thus, simply speaking, catalysts "adjust" to the reaction environment.[5] Monitoring such environment-induced changes of catalysts and understanding why it happens should be taken into account during the design of catalysts. The "old-fashioned" approach to gain insights into the environment-induced changes was and still is in many cases to study catalysts ex situ (i.e., outside, off site, out of place, away from the catalytic reactor and at ambient conditions).[6 7 8] However, it does not allow a clear picture of working catalysts to be obtained. The famous saying of Gabor Somorjai highlights this: "Knowing the 'before-reaction part' or 'after-reaction part' is like studying a life with access only to the prenatal and postmortem states".[9] Moreover, exposing the catalyst to ambient conditions after a catalytic reaction might again change the catalyst structural and electronic properties and lead to data misinterpretation.

A more informative way is to monitor the catalyst directly under reaction conditions, in situ (i.e., on site or in position, undisturbed).[9] Combining "watching catalysis under reaction conditions" by physical-chemical methods with simultaneously recording catalytic data using a mass spectrometer or a gas chromatograph is an even more sophisticated way that allows correlating the catalytic properties **directly** with the electronic and structural changes of the catalyst. This approach is called "operando".[10] Such an operando approach is not only applied for studying catalysts under working condition, but is also applied in the preparation stage of catalysts. For instance, application of tomographic energy dispersive diffraction imaging during the calcination of $[Ni(en)(H_2O)_4]Cl_2/\gamma-Al_2O_3$ and $[Ni(en)_3](NO_3)_2/\gamma-Al_2O_3$ hydrogenation catalyst bodies

was used to study the changes in the structural composition of catalysts at the macroscopic level.[11] Generally, an operando/in situ approach allows one to study "*birth*, *life,* and *death* of catalysts", a concept that was recently introduced by Bert Weckhuysen.[5] According to his concept, "birth" is referred to the stage when a catalyst is prepared, as it is essential to understand how catalytic solids are formed; "life" describes how a catalyst functions and performs in a catalytic reaction; "death" explains how a catalyst undergoes deactivation.

Generally, operando investigation of catalysts includes spectroscopic techniques (e.g., Raman spectroscopy, infrared spectroscopy (IR), X-ray photoelectron spectroscopy (XPS), X-ray absorption spectroscopy (XAS), ultraviolet-visible spectroscopy (UV-Vis), electron paramagnetic resonance spectroscopy (EPR) etc.), but also microscopy (e.g., environmental transmission electron microscopy and environmental scanning electron microscopy), X-ray diffraction (XRD), and X-ray total scattering. The challenge that the operando/in situ approach currently faces is the time scale (i.e., the time resolution at which reaction events on catalysts might be followed). Often under catalytic conditions the structure of catalysts might be very dynamic adjusting to the reaction environment quickly particularly for noble metal catalysts. For instance, a fast response of Pd and Pt to the reaction environment (CO/NO and CO/O_2) has been observed for Pt and Pd supported on inert Al_2O_3 and for Pd supported on ceria-zirconia, where dynamic electronic changes were detected for Pd as well as for ceria.[12] [13] [14] [15] [16] In a study of our research group on methanol steam reforming over Pd supported on reducible Ga_2O_3 and ZnO, highly dynamic behavior for Pd and for ZnO/Ga_2O_3 was observed.[17] [18] Therefore, many efforts nowadays are directed toward the development of fast time-resolved in situ/operando techniques for studying the dynamic changes of catalysts under working conditions. The main current challenge for improving time resolution is the development of detectors for the fast data/signal read out.

Another line of current operando/in situ research interest is using an integrated approach, applying simultaneously several techniques (e.g., IR, Raman, XRD, and XAS), for studying catalysts under reaction conditions. Such an approach is successfully employed in the BM01B beamlines at the European Synchrotron Research Facility (ESRF), where in situ XRD and XAS are combined.[19] Other synchrotron facilities also currently follow this direction. For instance, a new BALDER XAS beamline which will be operated in the MAX-lab IV will combine XAS with Diffuse Reflectance Infrared Fourier Transform Spectroscopy (DRIFTS) and Attenuated Total Reflection Infrared Spectroscopy (ATR-IR).[20] Using such an integrated approach requires special reaction cells that allow carrying out in situ experiments either simultaneously or one after another in the same cell. Therefore, many efforts are directed toward the development of cells that can be used for combined measurements. For instance, Davide Ferri and his group have developed a new IR/XRD/XAS in situ cell that enables using the same cell for IR, XRD, and XAS.[21] We have recently also developed and constructed a new combined XAS/XRD cell that allows

performing fast time-resolved measurements in the same cell. More details about this cell will be presented in the experimental part of this thesis.

The increased interest in the situ/operando approach for studying catalysis is demonstrated by the increased number of research papers where in situ/operando techniques are employed. A lot of money is currently invested into the building and improvement of synchrotron facilities as well as dedicated beamlines for in situ/operando studies. In situ/operando is one of the topics in most catalysis conferences. Moreover, a dedicated conference on operando spectroscopy was launched in 2003 in Lunteren (the Netherlands) and has been held every 3 years since.

1.3 SYSTEM OF INTEREST FOR THIS WORK: PROMOTED AND UNPROMOTED COBALT OXIDE FOR OXIDATION REACTIONS

Catalytic CO oxidation ($CO+0.5O_2{\rightarrow}CO_2$) is one of the most extensively studied reactions. The interest in this reaction can be explained by two main reasons: a) catalytic CO oxidation is of great practical importance in automotive exhaust gas control, air purification, and H_2 purification for proton exchange membrane fuel cells (i.e., preferential CO oxidation (PROX)); b) CO oxidation is a simple model reaction that can provide insights into the nature of active sites of catalysts and mechanisms of catalytic processes. Regarding the automotive exhaust gas control, the problem that arises is controlling automotive emissions during the cold start of a car (i.e., "cold-start extra emissions" - the additional emissions during the warm-up phase). To meet the upcoming "Euro" and "Tier" emission standards that become stricter with time, three-way-catalyst (TWC) technology requires continuous development and innovation to lower the concentration of CO emission at low temperatures. However, controlling automotive emissions during the cold start of a car is still a challenge. In fact, 80% of the emissions result from the cold-start period. Conventional TWCs, composed of a ceramic ("honeycomb") substrate coated with alumina, ceria, and dispersed noble metal nanoparticles (Pt, Pd, and Rh), are inactive at ambient temperatures, because the noble metals are poisoned by strongly adsorbed CO. Thus, elevated temperatures (higher than 200 ^{o}C) are required to desorb CO, adsorb and dissociate oxygen, and to initiate CO oxidation.[22] To reduce cold-start CO emissions, several approaches have been developed, for example pre-heating the TWC converter, which obviously requires external energy. A better approach is to utilize catalysts that are less prone to CO adsorption at low temperatures (<200 °C). Therefore, many efforts are directed toward the design and development of catalysts with lower CO oxidation light-off temperatures (i.e., the temperature at which catalytic reactions are initiated).

Another line of research, that has a strong connection to CO oxidation, is H_2 purification for obtaining CO-free H_2 for hydrogen-fueled proton exchange membrane fuel cells (PEMFC). A PEMFC is an attractive pollution-free and energy-saving power source for portable and stationary applications, but an efficient operation of PEMFC strongly depends on the availability of high-purity H_2. Even ppm concentrations of CO severely poison the Pt anode catalyst, therefore, very deep H_2 purification for obtaining CO-free H_2 is crucial.[23] In this regard, catalytic preferential CO oxidation (PROX) (i.e., $CO+H_2+0.5O_2 \rightarrow CO_2+H_2$) is a key reaction for removing traces of CO from the H_2-rich stream and requires efficient and selective catalysts.[24][25] These catalysts should be able to operate at 80 °C to be coupled with PEMFC.

The search for efficient catalysts with lower CO oxidation light-off temperatures is still ongoing. For example, nanoparticles of Au (2-4 nm size) supported on reducible oxides (e.g., TiO_2, CeO_2) have been found to be very active for low temperature CO oxidation.[26][27] Nevertheless, the commercialization is hindered by catalyst deactivation under working conditions due to the sintering of Au particles and the accumulation of inactive surface carbonate species on the catalyst surface.[28][29][30] Moreover, the price and the limited availability of gold motivate researchers to find other catalysts. As a result, in recent years much attention has been paid to the design and development of noble metal-free catalysts. An alternative to noble metal catalysts are transition metal oxides and mixed oxides. Therefore, in the last decades the research focus has moved to efficient and low-cost noble metal-free transition metal oxide catalysts.[31] Among these oxides especially cobalt oxides have turned out to be promising for low temperature CO oxidation.[32][33][34][35] The high activity of cobalt-based catalysts for CO oxidation was related to the redox properties of cobalt oxides (i.e., the ease of lattice oxygen release and formation of oxygen vacancies that might further serve as active sites).[32][33] Therefore, the reaction mechanism suggested for CO oxidation on cobalt oxides is often related to the Mars-Van Krevelen-type mechanism, which is also supported by theoretical studies.[36][37][38] Generally, it is assumed that Co^{3+} is the active site and supplies oxygen to CO forming Co^{2+}, consequently causing gradual catalyst deactivation. The active Co^{3+} sites were shown to be recovered only by high temperature treatments in oxygen atmosphere (>250 °C).[32] Moreover, cobalt oxide catalysts are very sensitive to water, which is another source of catalyst deactivation, in particular at low reaction temperatures. Overcoming these instability issues and further improving the "low cost" CO oxidation cobalt oxide catalysts that are able to operate at ambient conditions requires the tuning of the electronic structure of cobalt oxides and modification of the cobalt oxide redox properties (i.e., enhancing the oxygen mobility and making more oxygen available for the oxidation process).

One effective approach for the development of efficient cobalt-based CO oxidation catalysts is modification of the cobalt oxide redox properties by doping with ceria.[39][40][41] Moreover, when "mixed" Co_3O_4-CeO_2 catalysts are used, the favorable activity of cobalt oxide can be combined with the high oxygen storage capacity (OSC) and unique redox properties of ceria that is important for the operation of

automotive exhaust TWCs. Also, such catalysts have recently been found to be active for preferential CO oxidation, hydrocarbon, and diesel soot oxidation.[39] [40] [42] [43] [44]

The role of the ceria addition to Co_3O_4 has been recently extensively investigated, and it was found that addition of ceria to Co_3O_4 modifies structural as well as redox properties of Co_3O_4. [43] [44] With respect to the structural properties, several studies show that Co_3O_4 modified with CeO_2 has a higher specific surface area (SSA) because of the mesoporosity induced by CeO_2 (cobalt oxide materials are often macroporous). Mesoporosity and the resulting higher SSA lead to a higher Co_3O_4 dispersion compared to pure Co_3O_4. This, as a result, leads to the higher oxidation activity of Co_3O_4-CeO_2 in comparison with Co_3O_4 due to more exposed active sites.[43] In addition to the modification of the structural properties, the addition of CeO_2 to cobalt oxides modifies the redox properties through formation of oxygen vacancies that enhance the oxygen mobility, making more oxygen available for the oxidation process and improving the activity and stability of cobalt oxide catalysts.[41]

Despite intensive studies of cobalt-based catalysts and their potential commercialization as catalysts for TWC and PROX, the nature of the active sites as well as the reaction and deactivation mechanisms are still under debate. Open questions and contradicting results concern, for instance, the role of Co^{2+}/Co^{3+}, different oxygen species, oxygen vacancies, formation of carbonates, the influence of pretreatment, and the cause of catalyst deactivation. This is due to the fact that the current understanding of CO oxidation and PROX is mostly based only on ex situ analysis of the catalysts and on kinetic experiments.[35] [42] [45] Very little is known about the structure and surface chemistry of these catalysts under reaction conditions. Moreover, the origin of the enhanced catalytic activity when CeO_2 is added to Co_3O_4 as well as the nature of the active sites and reaction mechanisms is not fully understood. Therefore, an in-depth and comprehensive in situ/operando investigations of the structural and electronic changes of cobalt oxide and promoted cobalt oxide catalysts, occurring under catalytic working conditions, are needed.

1.4 OBJECTIVES AND THE CONTEXT OF THE THESIS

The ultimate goal of the research described in this doctoral thesis was to improve the fundamental understanding of CO oxidation and PROX on cobalt-oxide catalysts and to reveal the role of CeO_2 for enhancing the catalytic activity of cobalt oxide catalysts. The following scientific questions were addressed:

1) What is the nature of active sites, reaction and deactivation mechanism of cobalt oxide catalysts in CO oxidation and PROX?

2) Co_3O_4 vs CoO: what is the active phase of the catalyst under CO oxidation reaction conditions? Is CoO oxidized to Co_3O_4?

3)   What is the effect of CeO_2 on the activity of Co_3O_4 in the preferential oxidation of CO?

Answering all these research questions is the objective of this doctoral thesis.

To reach the objectives of the thesis, an integrated approach was applied, based on the combination of: 1) preparation and characterization of catalysts and correlating structural and reduction properties of catalysts with their catalytic performance; 2) kinetic studies; 3) application of in situ/operando techniques for studying catalysts under working conditions: Infrared spectroscopy (IR) and near atmospheric pressure X-ray photoelectron spectroscopy (NAP-XPS) for detecting the surface changes and surface species; X-ray absorption spectroscopy (XAS) and X-ray diffraction (XRD) for revealing bulk electronic and structural changes. The results of this thesis are aimed to make a strong contribution to fundamental and applied research in catalytic CO oxidation and advance the future development of novel catalysts for oxidation reactions.

In **Chapter 2**, the preparation of catalysts and the details of the catalyst characterization will be described. Further, background information on XPS, IR, and XAS, which were used for studying the catalysts in situ/operando, will be summarized. This will help the reader to better understand the results and discussion part of the thesis. In addition, the details of the in situ techniques, experimental setups and the reaction cells that were used in this work will be described. At the end of **Chapter 2** the current state of the art for the development of in situ XAS and XRD cells will be discussed briefly, and the combined XAS/XRD in situ reaction cell that was constructed within this doctoral project will be presented and discussed in terms of its application for in situ XAS and XRD experiments.

Chapter 3 is dedicated to the investigation of the oxidation states and geometric structure of cobalt in Co_3O_4, and the surface composition under reducing (CO) and oxidizing (O_2) atmospheres in a wide temperature range using synchrotron-based NAP-XPS, including depth profiling, Near-edge X-ray absorption fine structure spectroscopy (NEXAFS) at the Co $L_{3,2}$ edge in the total electron yield mode (TEY), and valance band spectra. The results obtained for different information depths during CO-TPR and O_2-TPO are discussed together with the implication on mechanistic aspects of CO oxidation.

Chapter 4 explains in more detail the reaction mechanism of CO oxidation on Co_3O_4 based on operando FTIR and NAP-XPS results, including dynamic experiments with changing reaction atmospheres (i.e., CO vs O_2). Moreover, the phase dependence of CO oxidation (CoO vs Co_3O_4) is explained with the help of kinetic measurements, NAP-XPS and XAS.

The main focus of **Chapter 5** is to improve the understanding of PROX over Co_3O_4 and to reveal the effect of CeO_2 on the activity of Co_3O_4 in PROX. To boost the understanding of PROX on Co_3O_4, cobalt oxide reduction in pure CO and H_2 atmospheres was studied and compared with PROX conditions. Operando XAS at the Co K edge was applied to reveal bulk structure changes, whereas operando NAP-XPS was used to monitor surface composition changes. This chapter is based on the publication: "Operando XAS and NAP-XPS studies of preferential CO oxidation on Co_3O_4 and CeO_2-Co_3O_4 catalysts", Liliana Lukashuk *et al.*, published in Journal of Catalysis 344, 2016, pp.1-15. The results presented in this paper are the result of my own scientific research work and I wrote the manuscript for this paper.

Chapter 6 summarizes the main findings and conclusions of this thesis.

1.5 REFERENCES

1.   Hagen, J., In *Industrial Catalysis: A Practical Approach*, Wiley-VCH Verlag GmbH & Co. KGaA: Weinheim, Germany, 2006.

2.   Langmuir, I., The mechanism of the catalytic action of platinum in the reactions $2CO + O_2 = 2CO_2$ and $2H_2 + O_2 = 2H_2O$. *Transactions of the Faraday Society* **1922,** *17* (0), 621-654.

3.   Masel, R. I., *Principles of Adsorption and Reaction on Solid Surfaces*. John Wiley & Sons, Inc: Hoboken, NJ, 1996.

4.   Duprez, D., Study of surface reaction mechanisms by $^{16}O/^{18}O$ and H/D isotopic exchange. *Catalysis Today* **2006,** *112* (1–4), 17-22.

5.   Weckhuysen, B. M., Studying birth, life and death of catalytic solids with operando spectroscopy. *National Science Review* **2015,** *2* (2), 147-149.

6.   Schimanke, G.; Martin, M.; Kunert, J.; Vogel, H., Characterization of Mo-V-W Mixed Oxide Catalysts by ex situ and in situ X-Ray Absorption Spectroscopy. *Zeitschrift für anorganische und allgemeine Chemie* **2005,** *631* (6-7), 1289-1296.

7.   Wu, J.; Shan, S.; Petkov, V.; Prasai, B.; Cronk, H.; Joseph, P.; Luo, J.; Zhong, C.-J., Composition–Structure–Activity Relationships for Palladium-Alloyed Nanocatalysts in Oxygen Reduction Reaction: An Ex-Situ/In-Situ High Energy X-ray Diffraction Study. *ACS Catalysis* **2015,** *5* (9), 5317-5327.

8.   Kuznetsov, V. L.; Krasnikov, D. V.; Schmakov, A. N.; Elumeeva, K. V., In situ and ex situ time resolved study of multi-component Fe☐Co oxide catalyst activation during MWNT synthesis. *physica status solidi (b)* **2012,** *249* (12), 2390-2394.

9.   Weckhuysen, B. M., Snapshots of a working catalyst: possibilities and limitations of in situ spectroscopy in the field of heterogeneous catalysis. *Chemical Communications* **2002,** (2), 97-110.

10.   Bañares, M. A., Operando methodology: combination of in situ spectroscopy and simultaneous activity measurements under catalytic reaction conditions. *Catalysis Today* **2005,** *100* (1–2), 71-77.

11.   Espinosa-Alonso, L.; O'Brien, M. G.; Jacques, S. D. M.; Beale, A. M.; Jong, K. P. d.; Barnes, P.; Weckhuysen, B. M., Tomographic Energy Dispersive Diffraction Imaging To Study the Genesis of Ni Nanoparticles in 3D within γ-Al₂O₃ Catalyst Bodies. *Journal of the American Chemical Society* **2009,** *131* (46), 16932-16938.

12.   Ferri, D.; Kumar, M. S.; Wirz, R.; Eyssler, A.; Korsak, O.; Hug, P.; Weidenkaff, A.; Newton, M. A., First steps in combining modulation excitation spectroscopy with synchronous dispersive EXAFS/DRIFTS/mass spectrometry for in situ time resolved study of heterogeneous catalysts. *Physical Chemistry Chemical Physics* **2010,** *12* (21), 5634-5646.

13.   Newton, M. A.; Chapman, K. W.; Thompsett, D.; Chupas, P. J., Chasing Changing Nanoparticles with Time-Resolved Pair Distribution Function Methods. *Journal of the American Chemical Society* **2012,** *134* (11), 5036-5039.

14.   Newton, M. A.; Michiel, M. D.; Kubacka, A.; Fernández-García, M., Combining Time-Resolved Hard X-ray Diffraction and Diffuse Reflectance Infrared Spectroscopy To Illuminate CO Dissociation and Transient Carbon Storage by Supported Pd Nanoparticles during CO/NO Cycling. *Journal of the American Chemical Society* **2010,** *132* (13), 4540-4541.

15.   Szlachetko, J.; Ferri, D.; Marchionni, V.; Kambolis, A.; Safonova, O. V.; Milne, C. J.; Kröcher, O.; Nachtegaal, M.; Sá, J., Subsecond and in Situ Chemical Speciation of Pt/Al₂O₃ during Oxidation–Reduction Cycles Monitored by High-Energy Resolution Off-Resonant X-ray Spectroscopy. *Journal of the American Chemical Society* **2013,** *135* (51), 19071-19074.

16.   Ferri, D.; Newton, M. A.; Di Michel, M.; Chiarello, G. L.; Yoon, S.; Lu, Y.; Andrieux, J., Revealing the Dynamic Structure of Complex Solid Catalysts Using Modulated Excitation X-ray Diffraction. *Angewandte Chemie International Edition* **2014,** *53* (34), 8890-8894.

17.   Föttinger, K.; van Bokhoven, J. A.; Nachtegaal, M.; Rupprechter, G., Dynamic Structure of a Working Methanol Steam Reforming Catalyst: In Situ Quick-EXAFS on Pd/ZnO Nanoparticles. *The Journal of Physical Chemistry Letters* **2011,** *2* (5), 428-433.

18.   Föttinger, K.; Rupprechter, G., In Situ Spectroscopy of Complex Surface Reactions on Supported Pd–Zn, Pd–Ga, and Pd(Pt)–Cu Nanoparticles. *Accounts of Chemical Research* **2014,** *47* (10), 3071-3079.

19.   http://www.esrf.eu/UsersAndScience/Experiments/CRG/BM01/bm01b.

20.   https://www.maxlab.lu.se/balder.

21.   Chiarello, G. L.; Nachtegaal, M.; Marchionni, V.; Quaroni, L.; Ferri, D., Adding diffuse reflectance infrared Fourier transform spectroscopy capability to extended x-ray-absorption fine structure in a new cell to study solid catalysts in combination with a modulation approach. *Review of Scientific Instruments* **2014,** *85* (7), 074102.

22.   Ertl, G., Reactions at Surfaces: From Atoms to Complexity (Nobel Lecture). *Angewandte Chemie International Edition* **2008,** *47* (19), 3524-3535.

23.   Jiménez, S.; Soler, J.; Valenzuela, R. X.; Daza, L., Assessment of the performance of a PEMFC in the presence of CO. *Journal of Power Sources* **2005,** *151*, 69-73.

24.   Park, E. D.; Lee, D.; Lee, H. C., Recent progress in selective CO removal in a H_2-rich stream. *Catalysis Today* **2009,** *139* (4), 280-290.
25.   Liu, K.; Wang, A.; Zhang, T., Recent Advances in Preferential Oxidation of CO Reaction over Platinum Group Metal Catalysts. *ACS Catalysis* **2012,** *2* (6), 1165-1178.
26.   Haruta, M.; Daté, M., Advances in the catalysis of Au nanoparticles. *Applied Catalysis A: General* **2001,** *222* (1–2), 427-437.
27.   Acosta, B.; Smolentseva, E.; Beloshapkin, S.; Rangel, R.; Estrada, M.; Fuentes, S.; Simakov, A., Gold supported on ceria nanoparticles and nanotubes. *Applied Catalysis A: General* **2012,** *449*, 96-104.
28.   Fan, H.-Y.; Shi, C.; Li, X.-S.; Zhang, S.; Liu, J.-L.; Zhu, A.-M., In-situ plasma regeneration of deactivated Au/TiO_2 nanocatalysts during CO oxidation and effect of N_2 content. *Applied Catalysis B: Environmental* **2012,** *119–120*, 49-55.
29.   Denkwitz, Y.; Zhao, Z.; Hörmann, U.; Kaiser, U.; Plzak, V.; Behm, R. J., Stability and deactivation of unconditioned Au/TiO_2 catalysts during CO oxidation in a near-stoichiometric and O_2-rich reaction atmosphere. *Journal of Catalysis* **2007,** *251* (2), 363-373.
30.   Yang, F.; Chen, M. S.; Goodman, D. W., Sintering of Au Particles Supported on TiO_2(110) during CO Oxidation. *The Journal of Physical Chemistry C* **2009,** *113* (1), 254-260.
31.   Royer, S.; Duprez, D., Catalytic Oxidation of Carbon Monoxide over Transition Metal Oxides. *ChemCatChem* **2011,** *3* (1), 24-65.
32.   Jansson, J., Low-Temperature CO Oxidation over Co_3O_4/Al_2O_3. *Journal of Catalysis* **2000,** *194* (1), 55-60.
33.   Jansson, J.; Skoglundh, M.; Fridell, E.; Thormählen, P., A Mechanistic Study of Low Temperature CO Oxidation over Cobalt Oxide. *Topics in Catalysis* **2001,** *16-17* (1-4), 385-389.
34.   Jia, C.-J.; Schwickardi, M.; Weidenthaler, C.; Schmidt, W.; Korhonen, S.; Weckhuysen, B. M.; Schüth, F., Co_3O_4–SiO_2 Nanocomposite: A Very Active Catalyst for CO Oxidation with Unusual Catalytic Behavior. *Journal of the American Chemical Society* **2011,** *133* (29), 11279-11288.
35.   Xie, X.; Li, Y.; Liu, Z.-Q.; Haruta, M.; Shen, W., Low-temperature oxidation of CO catalysed by Co_3O_4 nanorods. *Nature* **2009,** *458* (7239), 746-749.
36.   Wang, H.-F.; Kavanagh, R.; Guo, Y.-L.; Guo, Y.; Lu, G.; Hu, P., Origin of extraordinarily high catalytic activity of Co_3O_4 and its morphological chemistry for CO oxidation at low temperature. *Journal of Catalysis* **2012,** *296*, 110-119.
37.   Pang, X.-Y.; Liu, C.; Li, D.-C.; Lv, C.-Q.; Wang , G.-C., Structure Sensitivity of CO Oxidation on Co_3O_4: A DFT Study. *ChemPhysChem* **2013,** *14* (1), 204-212.
38.   Broqvist, P.; Panas, I.; Persson, H., A DFT Study on CO Oxidation over Co_3O_4. *Journal of Catalysis* **2002,** *210* (1), 198-206.
39.   Yang, J.; Lukashuk, L.; Akbarzadeh, J.; Stöger-Pollach, M.; Peterlik, H.; Föttinger, K.; Rupprechter, G.; Schubert, U., Different Synthesis Protocols for Co_3O_4–CeO_2 Catalysts—Part 1: Influence on the Morphology on the Nanoscale. *Chemistry – A European Journal* **2015,** *21* (2), 885-892.
40.   Tang, C.-W.; Wang, C.-B.; Chien, S.-H., Abatement of Carbon Monoxide over CeO_2–CoO_x Catalysts: Effect of Preparation Method. *Catalysis Letters* **2009,** *131* (1-2), 76-83.
41.   Li, J.; Lu, G.; Wu, G.; Mao, D.; Wang, Y.; Guo, Y., Promotional role of ceria on cobalt oxide catalyst for low-temperature CO oxidation. *Catalysis Science & Technology* **2012,** *2* (9), 1865-1871.
42.   Woods, M. P.; Gawade, P.; Tan, B.; Ozkan, U. S., Preferential oxidation of carbon monoxide on Co/CeO_2 nanoparticles. *Applied Catalysis B: Environmental* **2010,** *97* (1–2), 28-35.
43.   Liotta, L. F.; Di Carlo, G.; Pantaleo, G.; Deganello, G., Catalytic performance of Co_3O_4/CeO_2 and Co_3O_4/CeO_2–ZrO_2 composite oxides for methane combustion: Influence of catalyst pretreatment temperature and oxygen concentration in the reaction mixture. *Applied Catalysis B: Environmental* **2007,** *70* (1–4), 314-322.
44.   Dhakad, M.; Mitshuhashi, T.; Rayalu, S.; Doggali, P.; Bakardjiva, S.; Subrt, J.; Fino, D.; Haneda, H.; Labhsetwar, N., Co_3O_4–CeO_2 mixed oxide-based catalytic materials for diesel soot oxidation. *Catalysis Today* **2008,** *132* (1–4), 188-193.
45.   Yung, M. M.; Zhao, Z.; Woods, M. P.; Ozkan, U. S., Preferential oxidation of carbon monoxide on CoO_x/ZrO_2. *Journal of Molecular Catalysis A: Chemical* **2008,** *279* (1), 1-9.

CHAPTER 2

EXPERIMENTAL

2.1 MATERIALS AND METHODS

2.1.1 PREPARATION OF CATALYSTS

Co_3O_4: Co_3O_4 was used as received from Fluka, purity 99.5%.

CoO: CoO was used as received from VWR, purity 99.5%.

CeO_2-Co_3O_4: CeO_2-Co_3O_4 with 10 wt% CeO_2 loading was prepared via wet impregnation of Co_3O_4. In a typical synthesis, 0.504 g of $Ce(NO_3)_3 \cdot 6H_2O$ was dissolved in 7 mL of distilled water, added to 1.8 g of Co_3O_4 and stirred overnight. After that, the catalyst was dried at 110 ^{o}C for 3 h, and subsequently calcined at 400 ^{o}C for 2 h.

2.1.2 CHARACTERIZATION OF CATALYSTS

N_2 adsorption-desorption

N_2 adsorption-desorption isotherms were recorded at -196 ^{o}C using an ASAP 2020 instrument from Micromeritics. Before each run, a known mass of sample (ca. 0.12 g) was heated to 80 ^{o}C under vacuum for 3 h. Specific surface areas (SSAs) were calculated from the linear part of the Brunauer-Emmett-Teller line. Pore-size distributions were obtained applying the Barrett-Joyner-Halenda (BJH) equation to the desorption branch of the isotherm. The total pore volume was estimated from the N_2 uptake at a P/P_0 value of 0.99.

X-ray powder diffraction

X-ray powder diffraction (XRD) measurements were performed on a Philips X'Pert diffractometer using Cu-Kα radiation (0.154 nm) (X-ray tube was operated at 40 kV and 40 mA) operating in Bragg-Brentano reflection geometry. The scanning range was 5-120° (2θ) in step scan mode of 0.05° (2θ), with 4.5 s per step.

High-resolution transmission electron microscopy

High-resolution transmission electron microscopy (HRTEM) was performed on a TECNAI F20 microscope operated at 200 kV for CoO, Co_3O_4 and CeO_2-Co_3O_4 samples in the USTEM Center, Technische Universität Wien. High-angle annular dark-field scanning TEM (HAADF-STEM) and electron energy loss spectroscopy (EELS) were employed to determine the elemental distribution in CeO_2-Co_3O_4 and the particle size of CeO_2.

Temperature programmed reduction (CO-TPR, H$_2$-TPR) and temperature programmed desorption (CO-TPD, O$_2$-TPD)

CO temperature programmed reduction (CO-TPR), H$_2$ temperature programmed reduction (H$_2$-TPR), CO temperature programmed desorption (CO-TPD), and O$_2$ temperature programmed desorption (O$_2$-TPD) on catalysts (ca. 20 mg) were performed in a continuous-flow fixed-bed quartz reactor under atmospheric pressure. Before each experiment, the catalysts were pretreated with synthetic air (50 mL min^{-1}) at 400 ^{o}C for 30 min (heating rate of 10 ^{o}C min^{-1}).

CO-TPR, H$_2$-TPR: For the CO-TPR, the pretreated sample was exposed to 5 vol.% CO and 95 vol.% He mixture (total flow 50 mL min^{-1}) at RT. For the H$_2$-TPR, either 5 vol.% H$_2$ and 95 vol.% He mixture (total flow 50 mL min^{-1}) or 50 vol.% H$_2$ and 50 vol.% He mixture (total flow 50 mL min^{-1}) were used. Then the system was heated up to 700 ^{o}C with a heating rate of 10 ^{o}C min^{-1}.

CO-TPD, O$_2$-TPD: The pretreated sample was exposed either to 5 vol.% CO and 95 vol.% He mixture (total flow 50 mL min^{-1}) at RT or to 5 vol.% O$_2$ and 95 vol.% He mixture (total flow 50 mL min^{-1}) at 500 ^{o}C for 30 min and cooled down to RT in O$_2$. At RT pure He (total flow 50 mL min^{-1}) was purged through the catalyst for 30 min. Then the system was heated in He (total flow 50 mL min^{-1}) to 700 ^{o}C with a heating rate of 10 ^{o}C min^{-1}.

For all experiments the gas stream was analyzed by an online quadrupole mass spectrometer (QMS) (Prisma Plus QMG 220, Pfeiffer Vacuum) equipped with a Faraday detector. No cooling traps and cartridges were used for TPR and TPD experiments.

2.1.3 CATALYTIC CO OXIDATION AND PREFERENTIAL CO OXIDATION

CO oxidation and preferential CO oxidation reactions on the catalysts were performed in a continuous-flow fixed-bed quartz reactor under atmospheric pressure. The sample (ca. 20 mg), mixed with quartz powder (1 :10) to avoid mass- and heat-transfer limitations, was loaded into the reactor and pretreated with synthetic air (50 mL min^{-1}) at 400 ^{o}C for 30 min (heating rate of 10 ^{o}C min^{-1}). The sample was then cooled to 30 ^{o}C under a flow of synthetic air. The concentrations of CO and CO$_2$ in the outlet stream were monitored by gas chromatography using a HP-PLOT Q column and a flame-ionization detector with a methanizer.

Temperature dependent CO oxidation experiments: temperature dependent CO oxidation experiments with 5 vol.% CO, 10 vol.% O$_2$ in He mixture (total flow 50 mL min^{-1}) were performed by heating the catalyst from RT to 200 ^{o}C with a heating rate of 2 ^{o}C min^{-1}.

Temperature dependent preferential CO oxidation (PROX) experiments: the pretreated sample was exposed to a 1 vol.% CO, 1 vol.% O_2, 50 vol.% H_2 and 48 vol.% He mixture (total flow 50 mL min^{-1}). The system was heated to 200 ^oC with a heating rate of 2 ^oC min^{-1}.

Temperature programmed reaction experiments: temperature programmed CO methanation (1 vol.% CO, 50 vol.% H_2 in He), reverse water gas shift (1 vol.% CO_2, 50 vol.% H_2 in He), hydrogen oxidation (1 vol.% O_2, 50 vol.% H_2 in He), water gas shift (1 vol.% CO, 3 vol.% H_2O in He), PROX (1 vol.% CO, 1 vol.% O_2, 50 vol.% H_2 in He), CO oxidation (1 vol.% CO, 1 vol.% O_2 in He) reactions (total flow 50 mL min^{-1}) were carried out similarly to the temperature dependent CO oxidation and PROX experiments described above. The gas stream was analyzed by an online quadrupole mass spectrometer (PrismaPlus QMG 220, Pfeiffer Vacuum) equipped with a Faraday detector during heating the catalyst in the reaction mixtures from RT to 350 ^oC with a heating rate of 2 ^oC min^{-1}.
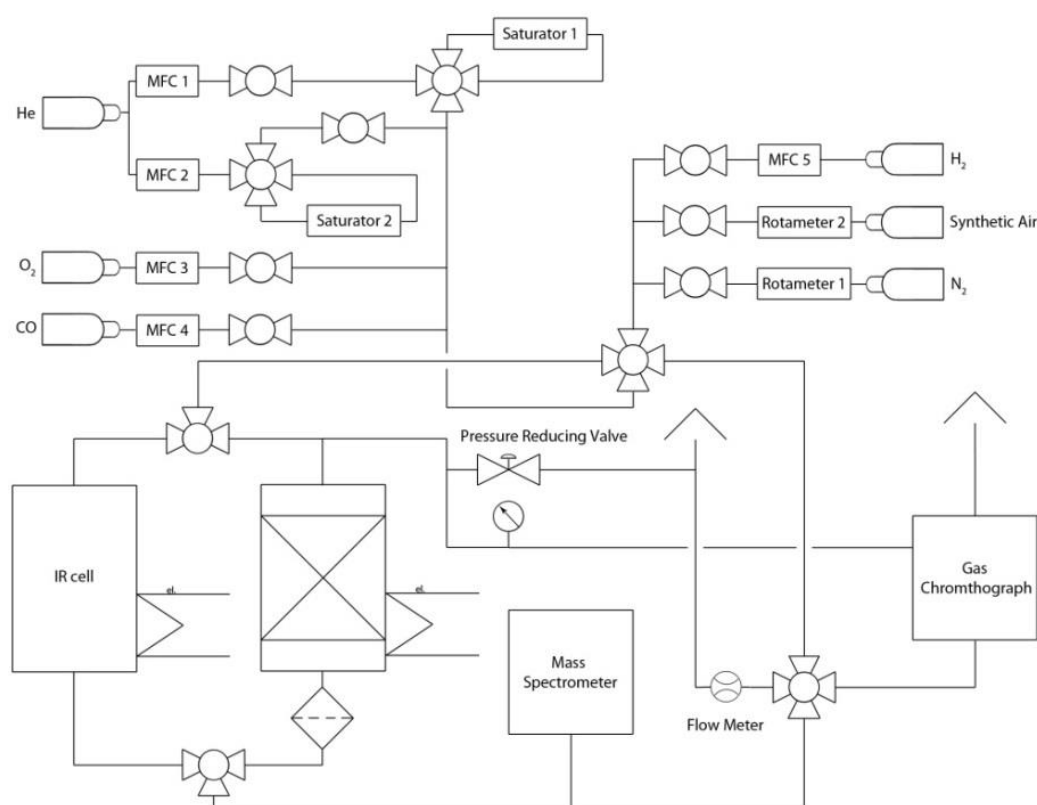
Figure 1. Schematic representation of the experimental setup for the kinetic, TPR, TPD, and operando infrared spectroscopy measurements.[1]

2.2 IN SITU/OPERANDO STUDIES OF CATALYSTS

2.2.1 X-RAY PHOTOELECTRON SPECTROSCOPY

2.2.1.1 FUNDAMENTALS OF X-RAY PHOTOELECTRON SPECTROSCOPY

X-ray photoelectron spectroscopy (XPS) is one of the most powerful spectroscopic tools that allows obtaining chemical information about surfaces of solid materials. It is based on the photoelectric effect theory (i.e., ejection of electrons from the surface in response to incident light/photons) (**Figure 2**).
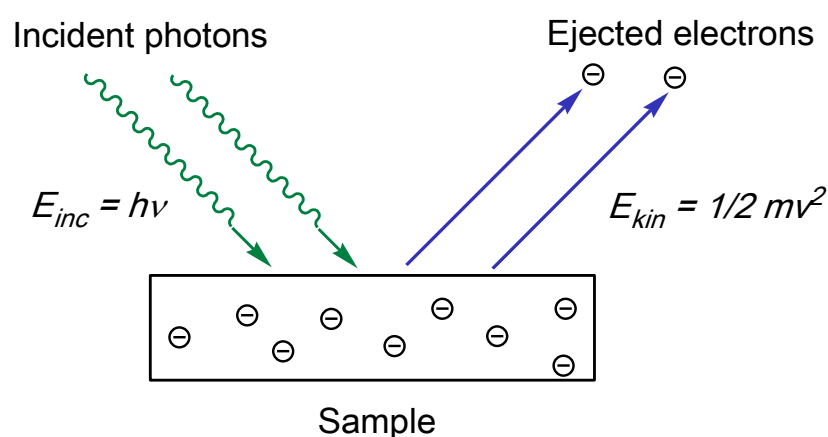
Figure 2. Schematic representation of the photoelectric effect.

In X-ray photoelectron spectroscopy the number of ejected electrons created by photons due to the photoelectric effect is measured as a function of their kinetic energy. Upon electron ejection by incident photons, an outer electron fills a core hole. The energy of this transition is then balanced by the emission either of an Auger electron or a characteristic X-ray. The ejection of electrons might occur either from the inner core-orbitals or from the outer valence shells depending on the photon source. Typically, if X-ray radiation is used, the ejected electron comes from the inner core-orbitals. In the case of ultraviolet radiation the ejection of electrons occurs from the outer valence shells.

According to Einstein's law of the photoelectric effect, the kinetic energy (E_{kin}) of ejected electrons is equal to the difference between the energy of the incoming radiation ($h\nu$) and the binding energy (E_{bin}) of a certain orbital shell (equation (1)):

$$E_{kin} = h\nu - E_{bin} \tag{1}$$

where h is the Planck constant and ν is the frequency of the incident photons. Usually the bond energy is defined as the difference of energies between the states with N-1 electrons and the state with N electrons. Therefore, the kinetic energy is expressed by the following equation:

$$E_{kin} = h\nu - E_{bin} = h\nu - [E^{N-1} - E^N] \tag{2}$$

In this equation, the binding energy is calculated with a reference to the vacuum level. However, this assumption is only valid for a free atom or a molecule. For solid materials the bond energy is calculated from the Fermi level as a reference (**Figure 3**). Therefore, the term related to the work function of an analyzer/spectrometer (i.e., φ_a) should be subtracted from equation **(2)**. Thus, the equation that describes the photoelectric effect for solid samples is presented by equation **(3)**:

$$E_{kin} = h\nu - E_{bin} = h\nu - [E^{N-1} - E^N] - \varphi_a \tag{3}$$

From equation (3) it follows that the detected energy of a photoemitted electron is a function of the binding energy. This binding energy is characteristic of an element that is present in the sample and corresponds to a peak in the XPS spectrum. The area under a peak in a spectrum represents the relative amount of the element, whereas the peak shape and its position indicate the chemical state (e.g., oxidation state) of an element.
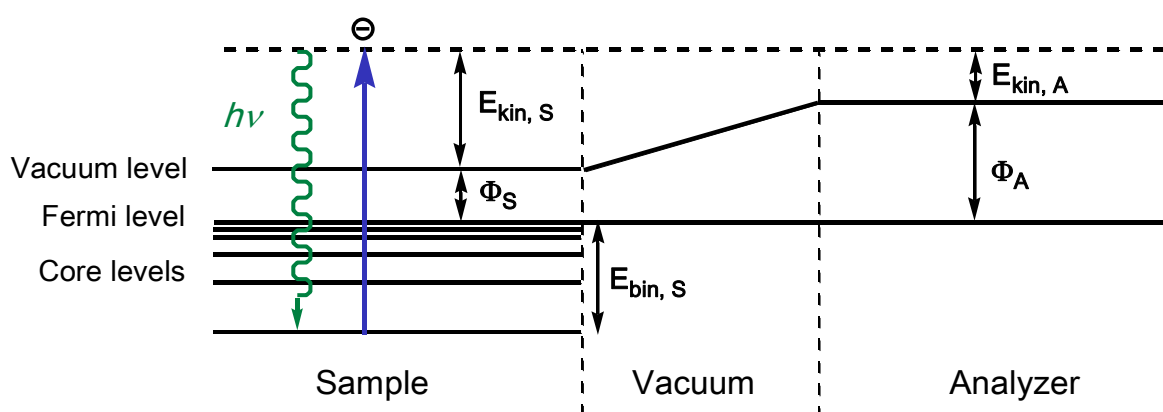
Figure 3. Schematic representation of the physical principles of X-ray photoelectron spectroscopy.

2.2.1.2 NEAR ATMOSPHERIC PRESSURE X-RAY PHOTOELECTRON SPECTROSCOPY. THE ISISS BEAMLINE, BESSY II EXPERIMENTAL SETUP

Traditionally, XPS is known to be an UHV technique that can only operate at pressures below 10^{-9} mbar because of the strong scattering of photoelectrons by gas molecules. For a long time this did not allow using this technique for investigation of catalyst surfaces under reaction conditions and studying catalysts in situ/operando. To overcome this limitation and to enable investigation of catalysts with in situ XPS, a new type of photoemission spectrometer, based on several differential pumping stages with electrostatic lenses between the sample surface and the photoelectron detection, was developed. A schematic representation of the differential pumping system of the near atmospheric pressure XPS (NAP-XPS) setup from the ISISS beamline (Innovation Station for In Situ Spectroscopy), BESSY II is given in **Figure 4**. This setup enables operation at pressures close to ambient (e.g., up to 20 mbar). Although these pressures are still far away from pressures used in fixed-bed flow reactors, NAP-XPS experiments can model the reaction environment and allows studying the dynamic variations between the surface of a catalyst and its catalytic properties.
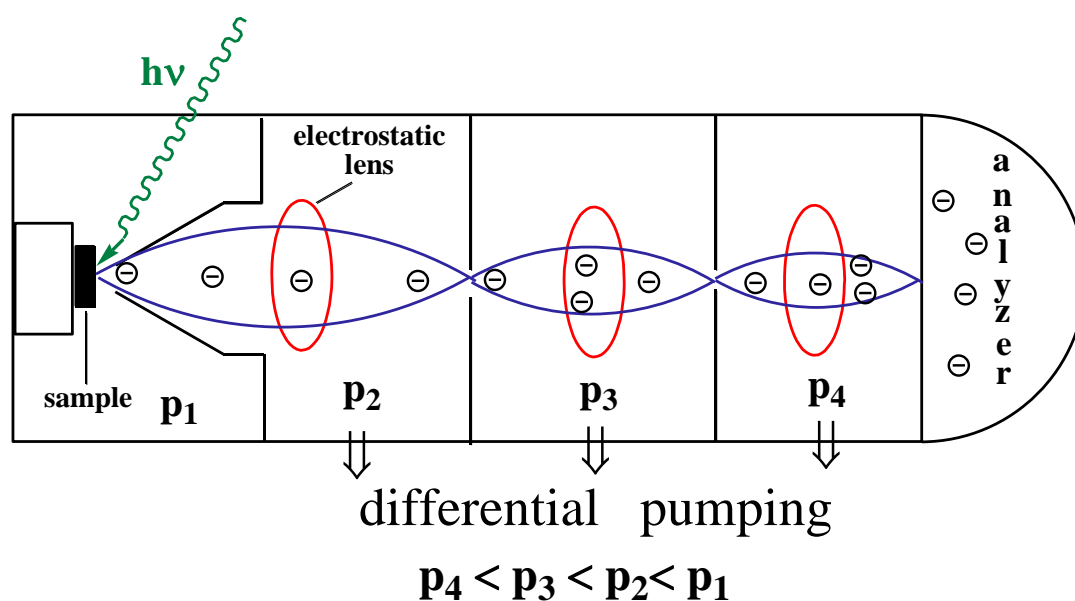
Figure 4. Schematic representation of the differential pumping from the ISISS beamline, BESSY.

To understand the dynamic surface variation of cobalt oxide catalysts and to reach a pressure of several mbar, operando near atmospheric pressure X-ray photoelectron spectroscopy experiments on cobalt oxide system were performed at the ISISS beamline, BESSY II in Berlin, Germany.[2] This NAP-XPS setup is designed to operate using high brilliance synchrotron radiation (i.e., the photon flux is 6*1e10 photons/s/0.1A). This provides an opportunity to vary the kinetic energy for the same photoelectron spectrum and, as a result, to perform depth-profiling measurements in order to distinguish surface species from subsurface species. In addition, the usage of high brilliance synchrotron radiation for XPS analysis,

instead of non-monochromatic radiation, automatically provides a better resolution in an XPS spectrum and increases the signal-to-noise ratio. This is essential for in situ/operando XPS experiments because of the attenuation of the signal due to the strong scattering of photoelectrons by gas molecules. The NAP-XPS setup at BESSY II that is presented in **Figure 5** consists of a reaction cell attached to a set of differentially pumped electrostatic lenses and a separately pumped analyzer (Phoibos 150 Plus, SPECS GmbH).[3] These electrostatic lenses or "transfer part" is the "heart" of the NAP-XPS setup. The first aperture is a conically shaped nozzle, as shown in **Figure 6a**. The function of this aperture is to bring the pressure down to the 10^{-3} mbar range. Behind the nozzle, a deceleration lens creates images of the beam that is analyzed at the entrance aperture of the second lens stage. Further, a quadrupole lens guides the beam to the entrance of the hemispherical analyzer.[4] All four pressure stages are separated by apertures, as shown in **Figure 4**.

The high pressure XPS cell is connected to a gas manifold system with calibrated mass flow controllers that allow the gases to be mixed in a controlled way at variable feed gas compositions. An electron impact Quadrupole mass spectrometer and a multichannel gas chromatograph can be connected to the XPS cell via a gas dosing valve for on-line analysis of the gas phase composition which gives excellent possibilities to correlate the XPS spectra with the reactivity of a catalyst.
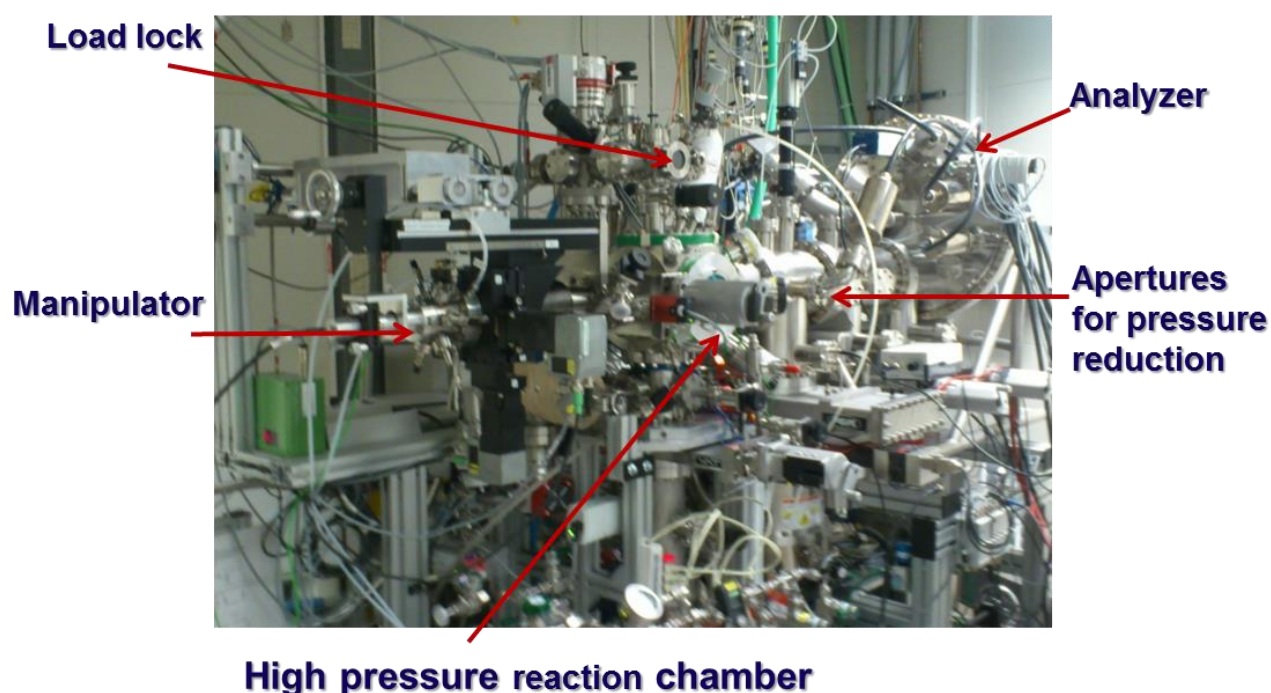
Figure 5. Picture of the NAX-XPS setup from ISISS beamline, BESSY II.

For our experiments, the powder sample (ca. 30 mg) was pressed into a Tantalum grid of 99.85% purity (0.08 mm wire diameter), supplied by GLC Alloys, in order to minimize charging effects together with a K-type thermocouple, fixed to a sapphire sample holder (**Figure 6a**), and mounted inside the NAP-XPS reaction cell in front of the first aperture of the differentially pumped electrostatic lens system (**Figure 6b**). The heating of the sample was done from the back using an infrared laser.
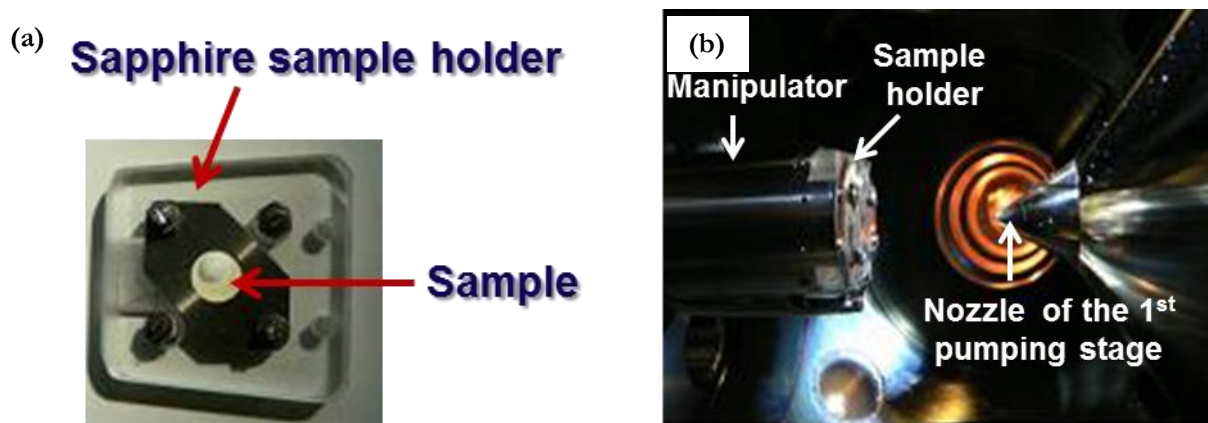
Figure 6. Picture of the sapphire sample holder together with a sample for NAP-XPS (a); the sample holder inserted into the NAP-XPS chamber in close proximity to the nozzle from the first pumping stage (b) (ISISS beamline, BESSY II).

2.2.1.3   E X P E R I M E N T A L   C O N D I T I O N S   O F   O P E R A N D O   N A P - X P S   M E A S U R E M E N T S   A N D   D A T A   A N A L Y S I S

Before each experiment, the sample (as samples Co_3O_4, CeO_2-Co_3O_4 were used) was pretreated in the XPS reaction cell by oxidation (0.5 mbar O_2 at 400 ^oC) until all residual surface carbon and carbonates disappeared. After cooling the sample to RT, either CO (0.15 mbar), O_2 (0.15 mbar), H_2 (0.4 mbar), $CO+O_2$ (1/2 ratio at 0.5 mbar), or the $CO+O_2+H_2$ PROX mixture (1/1/12 ratio at 0.5 mbar) were introduced with the partial pressure of the gases controlled by calibrated mass flow controllers, and photoemission spectra were recorded. During cycling experiments CO (0.15 mbar) was followed by O_2 (0.15 mbar). Then the sample was heated to 100, 150, 200, 250 and 300 ^oC with a heating rate of 5 ^oC min^{-1}, and photoemission spectra were acquired at these temperatures. To ensure surface specificity, the Co 2p, Ce 3d, and C 1s core-level regions and the valence band were recorded using selected photon energies that resulted in photoelectrons with 200 eV kinetic energy and ~0.6 nm inelastic-mean-free path for Co. To obtain depth-resolved information, the photoelectron spectra were taken also at higher kinetic energies: 400 eV and 600 eV that results in ~0.8 nm and ~1.1 nm inelastic-mean-free path for Co,

respectively, calculated from the NIST (National Institute of Standards and Technology) electron-inelastic-mean-free-path database. In addition, in situ NEXAFS measurements were performed on Co_3O_4 in the same setup for CO-TPR and O_2-TPO experiments. NEXAFS Co $L_{3,2}$ edge spectra were obtained in the total electron yield mode (TEY) using the electron spectrometer as a detector. The CoO sample was obtained by heating Co_3O_4 in the NAP-XPS chamber under vacuum to 615 ^oC. The gas phase composition was monitored on-line by an electron impact Quadrupole mass spectrometer and multichannel gas chromatograph which were connected to the XPS cell via a leak valve.

All XPS spectra were analyzed using the CasaXPS software package. The binding energies (BE) were calibrated using the O 1s second-order peak. The accuracy of the BE calibration was estimated to be around 0.05 eV. To fit the high-resolution spectra, a Shirley-type function was first used to remove the background arising from energy loss for the Co 2p, a linear function was used in the case of the Ce 3d, because the Ce 3d sits on the slope of the O_{KLL} Auger peak and the Co 2p core level peak. Either a Shirley-type function or a linear function was used in the case of the C 1s. The extracted spectra were then fitted with a combined Gaussian and Lorentzian line profile that takes into account the spectrometer and lifetime broadening.

2.2.2 INFRARED SPECTROSCOPY

2.2.2.1 FUNDAMENTALS OF INFRARED SPECTROSCOPY

In a first approximation vibrations of diatomic molecules can be considered as oscillations of a simple harmonic oscillator. The potential energy of this oscillator is described by equation (4):

$$U = 1/2 \, kq^2 \tag{4}$$

where k is the force constant, q is a vibration coordinate (i.e., $q = r - r_e$, where r_e is an equilibrium distance between the atoms). A vibration coordinate is a value that characterizes the deviation of atoms from the equilibrium state (i.e., the change in the bond length). Therefore, the dependence of vibrations for a diatomic molecule from q has the form of a parabola in the harmonic oscillator approximation, as presented in **Figure 7**.

According to the classical theory, the molecule can be in any part of the potential curve; therefore, the vibration energy of the molecule can have different values. But quantum theory restricts this. According to

quantum theory, the vibrational energy of the molecule is quantized, thus, the molecule can only be in certain discrete energy states. The energy is given by the following equation:

$$E = (\upsilon + 1/2)h\nu \qquad \textbf{(5)}$$

where υ is a vibrational quantum number that can only have integer values, $\upsilon = 0, 1, 2$, etc; while ν is the frequency of vibrations. From equation **(5)** it follows that the energy levels of diatomic molecules correspond to different quantum numbers υ. The vibration frequency of diatomic molecules in the harmonic oscillator approximation is given by:

$$\nu = \frac{1}{2\pi} \sqrt{\frac{k}{\mu}}, \quad \text{where} \qquad \textbf{(6)}$$

$$\mu = \frac{1}{m_1} + \frac{1}{m_2} = \frac{m_1 + m_2}{m_1 m_2} \qquad \textbf{(7)}$$

μ is the reduced mass, m_1 and m_2 are the masses of atoms, and k is the force constant. For a harmonic oscillator, the only transition with $\Delta\upsilon = \pm1$ are allowed. All others transitions are forbidden.
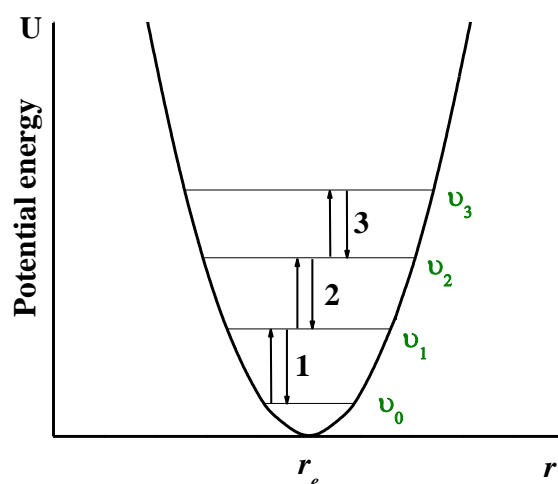
Figure 7. Potential energy curve of a harmonic oscillator.

However, at the lowest vibration levels υ_0 a molecule is not "frozen", and even at absolute zero temperature varies with some frequency around the equilibrium position. This is a consequence of the Heisenberg uncertainty principle, according to which it is impossible to determine the coordinates of

23

atoms, and, thus, an exact distance between atoms. Therefore, the vibrations in real molecules are inharmonic, and the potential energy of a molecule is described with the Morse function/potential shown in **Figure 8**. The vibration energy levels are not equidistant, and with an increase of υ, the energy levels gradually converge and merge when the energy approaches the dissociation energy. The vibrational energy values in the inharmonic oscillator approximation are described with a more complex expression than for the harmonic oscillator. For inharmonic vibrations selection rules might be omitted. As a result, some of the forbidden transitions become possible: (a) (i.e., $\upsilon_o, \rightarrow \upsilon_2$, $\Delta\upsilon = +2$) and (b) (i.e., $\upsilon_o, \rightarrow \upsilon_3$, $\Delta\upsilon = +3$) (**Figure 8**). Transitions (a) and (b) are called the first and the second overtones. For IR spectroscopy, since the vibration is excited by electromagnetic radiation, the dipole moment of the molecule must change. Importantly, the intensity of the vibration mode depends on the change in the dipole moment as well as the concentration of the species.
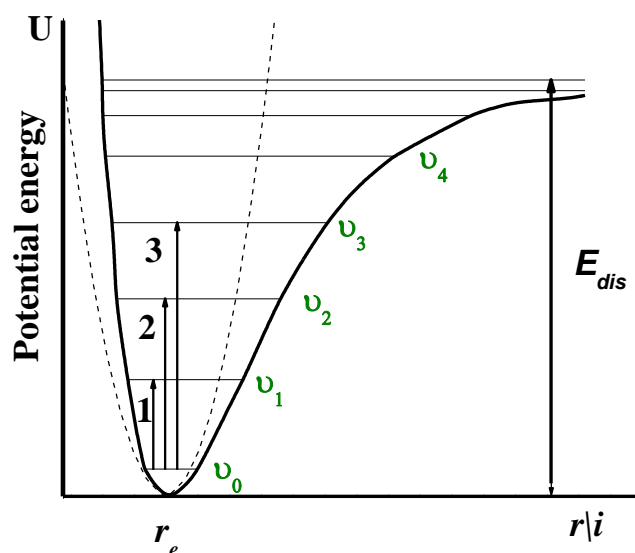
Figure 8. Potential energy curve of a two-atom molecule in the inharmonic oscillator approximation.

2.2.2.2 VIENNA FTIR EXPERIMENTAL SETUP FOR OPERANDO STUDIES

Operando FTIR studies of the cobalt oxide catalysts were carried out in transmission mode using a Bruker Vertex 70 spectrometer (liquid N_2-cooled MCT detector, resolution of 4 cm^{-1}) with a stainless steel transmission flow cell equipped with CaF_2 windows. The inlet of the cell is connected to a gas manifold system with calibrated mass flow controllers, as pictured in **Figure 9**; the outlet of the cell is connected to a mass spectrometer and a gas chromatograph. The sample (ca. 4-5 mg) was pressed into a pellet, which consisted of a thin catalyst layer supported on a KBr pellet and placed in a small, cylindrical stainless steel sample holder equipped with a ring-shaped furnace and a type-K thermocouple mounted to the sample holder.
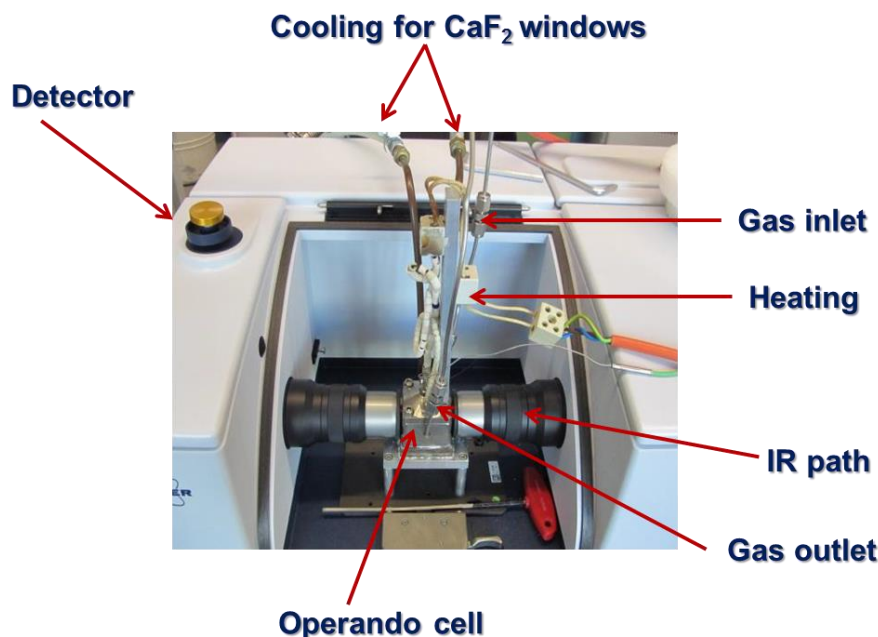
Figure 9. Picture of the operando FTIR setup at IMC, Vienna.

2.2.2.3 EXPERIMENTAL CONDITIONS OF OPERANDO FTIR MEASUREMENTS

All infrared spectra were collected in the 4,000–900 cm^{-1} range by averaging 256 scans to achieve good signal to noise ratios. A spectrum of the sample holder recorded in He atmosphere was used as a background for all spectra. Before each experiment, the catalyst was pretreated with synthetic air (50 mL min^{-1}) at 400 ^{o}C for 30 min (heating rate of 10 ^{o}C min^{-1}). The sample was then cooled to 30 ^{o}C under a flow of synthetic air and purged with helium for 10 min.

CO oxidation: the reaction mixture: a) 5 vol.% CO, 10 vol.% O_2 in He; b) 5 vol.% CO, 5 vol.% O_2 in He; b) 5 vol.% CO, 2.5 vol.% O_2 in He (total flow 25 mL min^{-1}) was continuously introduced into the cell and temperature resolved spectra were recorded while heating up to 250 °C with a heating rate of 2 ^{o}C min^{-1}. The products of the reaction were analyzed simultaneously with a gas chromatograph.

PROX: the reaction mixture of 1 vol.% CO, 1 vol.% O_2, 50 vol.% H_2 in He (total flow 50 mL min^{-1}) was continuously introduced into the cell and temperature-resolved spectra were recorded while heating up to 350 °C with a heating rate of 2 ^{o}C min^{-1}. Simultaneously the products of the reaction were analyzed with a quadrupole mass spectrometer (QMS) (PrismaPlus QMG 220, Pfeiffer Vacuum) equipped with a Faraday detector.

CO temperature programmed reduction followed by O_2 temperature programmed oxidation: 5 vol.% CO in He (25 mL min^{-1}) was continuously introduced into the cell and temperature-resolved spectra were recorded while heating up to 250 °C with a heating rate of 2 ^{o}C min^{-1}. Then the sample was

cooled down and 5 vol.% O_2 in He was introduced to the cell and temperature resolved spectra were recorded while heating up to 200 °C.

CO temperature programmed reduction followed by He temperature programmed desorption: 5 vol.% CO in He (25 mL min^{-1}) was continuously introduced into the cell and temperature resolved spectra were recorded while heating up to 250 °C with a heating rate of 2 °C min^{-1}. Then the sample was cooled down to RT and He was introduced into the cell and temperature resolved spectra were recorded while heating up to 200 °C.

CO vs O_2 switching experiments: CO (5 vol.% CO in He) was introduced and time resolved IR spectra were recorded for 10 min (5 spectra), then the atmosphere was changed to O_2 (5 vol.% O_2 in He) and time resolved IR spectra were recorded for 10 min (5 spectra). Such experiments were performed at RT, 50, 100, 150, 200, and 250 °C.

CO_2 adsorption: 5 vol.% CO_2 in He (25 mL min^{-1}) was continuously passed through the cell and temperature resolved spectra were recorded while heating up to 200 °C with a heating rate of 2 °C min^{-1}.

The spectra were evaluated with the OPUS 4.0 software. The background was subtracted from each absorption spectrum.

2.2.3 X-RAY ABSORPTION SPECTROSCOPY

2.2.3.1 FUNDAMENTALS OF X-RAY ABSORPTION SPECTROSCOPY

X-ray absorption is a powerful technique for studying the electronic and local geometric structure of materials. When a narrow parallel monochromatic X-ray beam with intensity I_o penetrates a sample of thickness **x**, it will be attenuated according to the equation:

$$\ln(I_0/I) = Mx \qquad (7)$$

I_0 is the intensity of the incident beam, **I** is the intensity after absorption, x is the thickness of the sample, and M is the linear absorption coefficient. M depends on the density of the investigated material and type of atoms. Often a mass absorption coefficient μ is used that is defined as M/ϱ. Normally μ decreases with decreasing wavelength. But when the energy of I_0 is high enough to cause the excitation of a core electron of the absorbing atom to the continuum (**Figure 10a**), a sudden increase in the X-ray absorption occurs giving rise to the absorption edge (**Figure 11**). The energy of the absorbed radiation at this edge is equal to the binding energy of electrons in e.g., K, L, M shells. When the photoelectron is ejected and a core-hole is created in the K, L, M etc. shell, the core-hole is filled by an electron from the next shell, causing photon emission or X-ray fluorescence (**Figure 10b**). The photon emission coresponds to the Kα emission lines of the absorbing atom. Alternatively, the emission of an Auger electron can occur (**Figure 10c**).
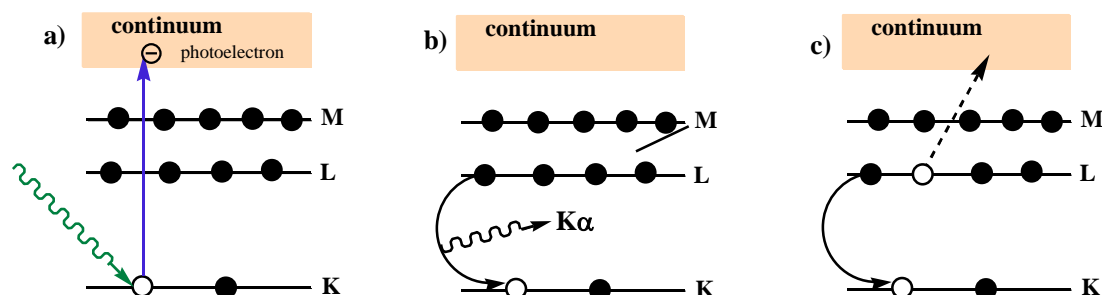
Figure 10. Excitation of an electron from the K edge (photoelectric effect) (a); decay of the excited state via: X-ray fluorescence (b) and the Auger process (c).

The information that can be obtained from a typical XAS spectrum depends on the energy range in the spectrum. Generally, three energy regions can be defined that provide different information about investigated materials. Classification of these regions is done with reference to a threshold energy of the absorption edge E_0 (i.e., the energy of the photoelectron ejection).

a) When $E<E_0$ (i.e., the pre-edge region), the only electronic transitions that might occur are the transitions within the atom to partially filled or unfilled energy levels.

b) When $E=E_0$ typically two cases must be considered: the edge region or X-ray Absorption Near Edge Spectroscopy (XANES) and Extended X-ray Absorption Fine Structure (EXAFS). For XANES, electronic transitions or excitation of core electrons occurs into unoccupied bound or continuum states, while for EXAFS excitation of core electrons occur into continuum states and photoelectrons are ejected. In the case of XANES, the core electron is excited into the continuum, but the photoelectron has a low kinetic energy; therefore, it is strongly backscattered by neighboring atoms. Although XANES is sensitive to the number, type, and coordination symmetry of atoms adjacent to the absorbing atom, it is still difficult to model the spectrum because of the multiple scattering events. In the case of EXAFS, the energy of the photoelectron is high. So the wavelength of the photoelectron becomes comparable to the distance to neighboring atoms, and the photoelectron wave is weakly backscattered by the neighboring atoms. Thus, the scattering is a single scattering event, and it is feasible to analyze this part of the spectrum and model the structure of the absorbing atom with respect to the number, type, and distances of neighboring atoms.
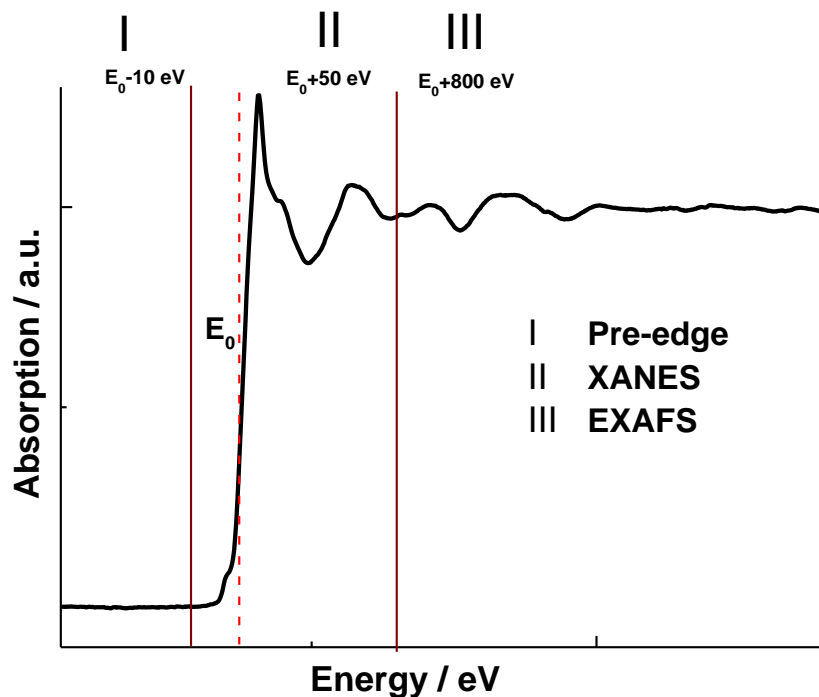
Figure 11. Spectrum of Co_3O_4 at the Co K edge indicating pre-edge, XANES, and EXAFS regions.

The schematic representation of a standard XAS station is given in **Figure 12**. The energy dependence of the absorption coefficient $\mu(E)$ can be measured either in the transmission mode or in the X-ray fluorescence mode. When the direct absorbance of the sample is measured, this is a transmission mode:

$$\mu(E) = \ln(I_0/I) \qquad (8)$$

In fluorescence mode, the X-ray fluorescence yield (i.e., the fluorescence X-rays emitted, when the core-hole is filled) is measured:

$$\mu(E) \sim I_f/I_0 \qquad (9)$$

I_f is the monitored intensity of a fluorescence line as the overall fluorescence yield.
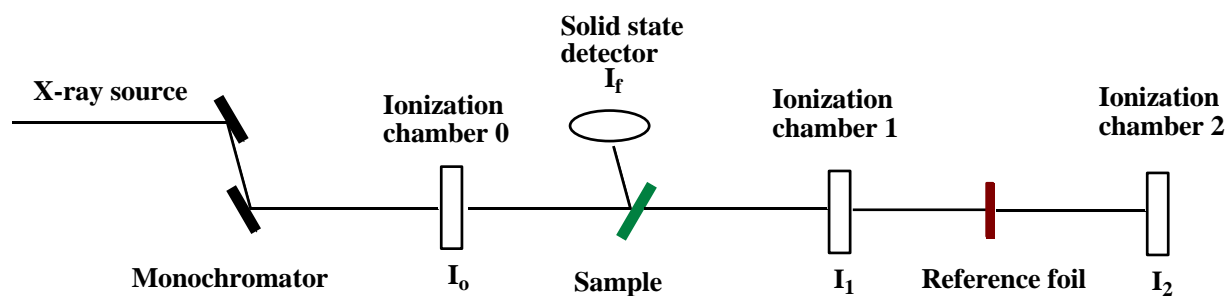
Figure 12. Schematic representation of a standard XAS station.

Usually for samples with a concentration of the investigated element above 2 wt% the transmission geometry is used and the intensity of the transmitted photons is measured with the ionization chamber **I_1**. For samples with a concentration below 2 wt% the fluorescence yield is measured with a solid state detector. For the detection of the fluorescence yield, the sample is usually mounted in 45 ° with respect to the solid state detector. After the ionization chamber 1 the reference metal foil of the investigated element is measured simultaneously with ionization chamber 2 in order to calibrate the E_0 energy of the investigated sample. Usually the measurements in transmission mode are preferred over fluorescence mode. For the data measured in fluorescence mode the self-absorption should be taken into consideration during the data treatment process.

2.2.3.2 EXPERIMENTAL SETUP FOR OPERANDO X-RAY ABSORPTION SPECTROSCOPY STUDIES

Operando X-ray absorption spectroscopy studies at the Co K (7709 eV) edge were carried out in transmission geometry at the I811 beamline at MAX-lab II in Lund, Sweden.[5] Co metal foil was used for energy calibration. Higher harmonics were rejected using a double crystal monochromator detuned to -50% of the maximum Bragg intensity. The picture of the experimental setup is presented in **Figure 13**.

A reaction cell for in situ XAS was supplied by MAX-lab II[6] and is presented in **Figure 14**. This is basically a flow-type cell very similar to that of a continuous-flow fixed-bed quartz reactor used in a laboratory for catalytic experiments. Moreover, the cell is designed in such a manner that the dead volume is minimized, thus, fast time-resolved measurements can be carried out in this cell. The cell consists of a heatable stainless steel holder, a plate with sealing/windows mounted onto the holder, the reaction cell compartment, and a plate with a sealing/window on top. The holder provides the heating plates system and a thermocouple. The type of the sealing/window materials depends on the absorption edge investigated. For our experiment at the Co K edge (7709 eV), Al foil (absorption edge 1562 eV) with a thickness of 15 microns was used that allows passing I_0 without tremendous loss of the intensity of incident photons. For our experiment, ca. 2.5 mg of the catalyst diluted with 10 mg of BN was loaded into

the cell. Quartz-wool plugs were inserted on both sides of the sample compartment. The gas inlet was directly connected to the cell from one side, whereas from the other side it was connected to a gas manifold system with calibrated mass flow controllers. The gas stream outlet of the cell was connected to theresi dual gas analyzer equipped with a SEM detector.
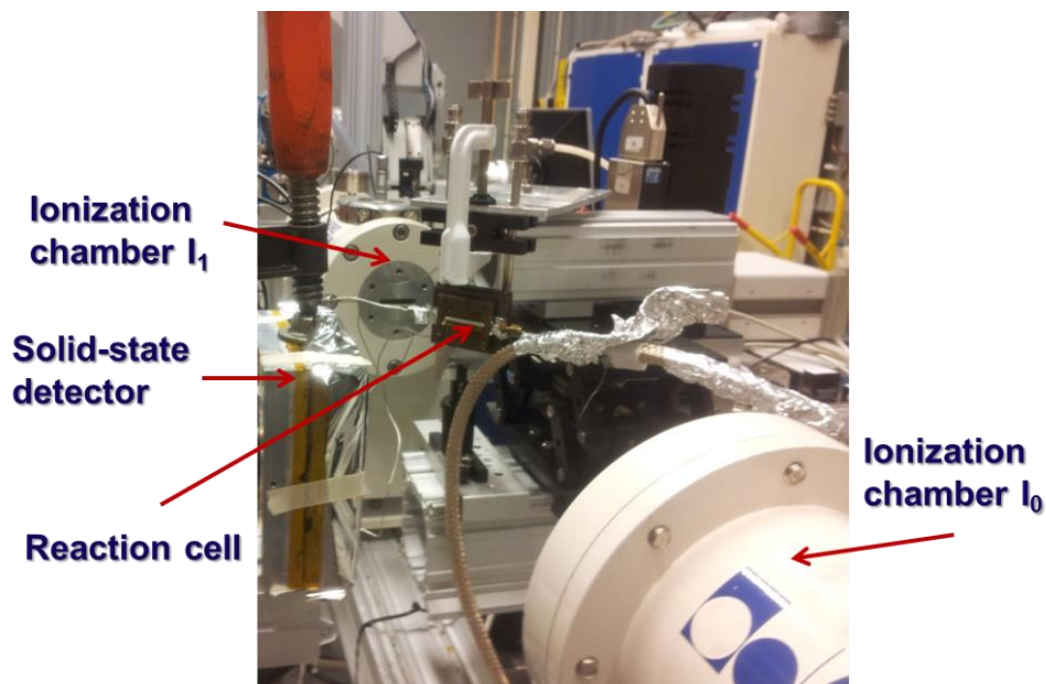
Figure 13. Picture of the XAS station for in situ experiments, I811 beamline, MAX-lab II.
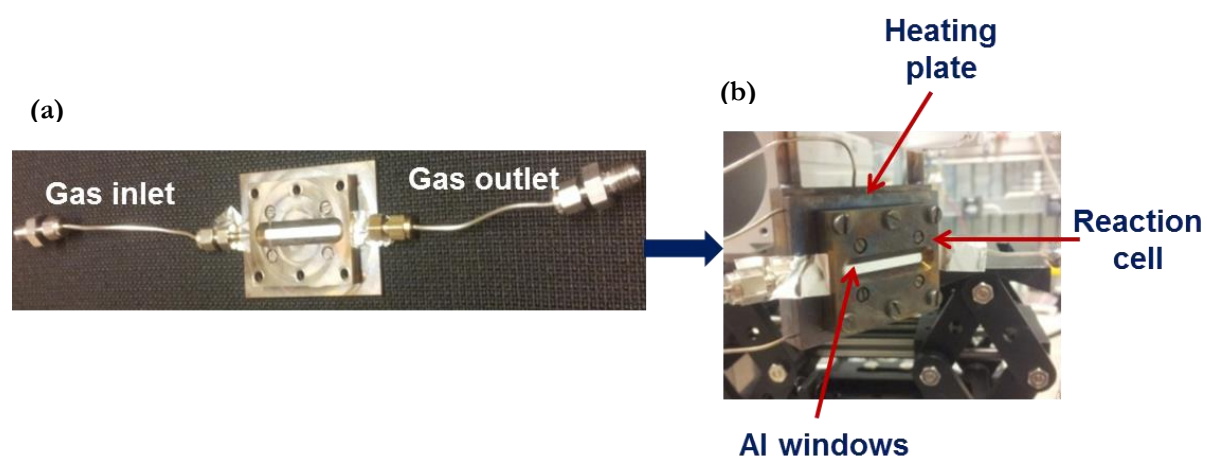
Figure 14. Picture of the reaction cell for in situ XAS (a); the reaction cell together with a heating plate during in situ XAS experiment (b) I811 beamline, MAX-lab II.

2.2.3.3 EXPERIMENTAL CONDITIONS OF OPERANDO X-RAY ABSORPTION SPECTROSCOPY MEASUREMENTS AND DATA ANALYSIS

The sample (Co_3O_4 or CeO_2-Co_3O_4) was pretreated in 20 vol.% O_2 in He at 400 °C for 30 min. Then it was cooled to RT and purged with He at RT for 15 min before the PROX reaction mixture of 1 vol.% CO, 1 vol.% O_2, 50 vol.% H_2 in He was introduced. The XAS spectra were recorded at RT and during subsequent heating to 350 °C. In addition to PROX, CO temperature programmed reduction (5 vol.% CO in He) followed by O_2 temperature programmed oxidation (20 vol.% O_2 in He) and H_2 temperature-programmed reduction (50 vol.% H_2 in He) experiments were performed. In case of CO oxidation on CoO, CoO was pretreated in He at 200 °C and cooled to RT, then the reaction mixture of 5 vol.% CO, 10 vol.% O_2 in He was introduced. The XAS spectra were recorded at RT and during subsequent heating to 360 °C in the reaction mixture. At 360 °C, CO was switched off and the sample was further heated in O_2 to 530 °C. All experiments were carried out at ambient pressure with a total flow of 50 mL min^{-1}. For Co K edge each XAS scan took 5 min.

Data reduction of all XAS spectra involved energy calibration using Co foil (7709 eV), background subtraction and normalization. Linear combination fitting (LCF) of normalized X-ray absorption near edge spectra (XANES $\mu(E)$) was performed with the Athena software using XANES spectra of Co_3O_4, CoO and Co foil as references, within an energy range of −20 eV below to +80 eV above the edge. The relative weights of the components of mixtures (Co_3O_4, CoO, and Co) under in situ conditions were constrained to be between 0 and 1, force weights were constrained to sum to 1, and all standards use the same E_0. The quality of the fits was examined using the R-factor and reduced χ^2 (R factor was not larger than 0.0008; reduced χ^2 was not larger than 0.0006).

2.2.4 X-RAY DIFFRACTION

2.2.4.1 FUNDAMENTALS OF X-RAY DIFFRACTION

X-ray powder diffraction is a standard analysis technique for studying crystal structures and atomic spacing of crystalline materials that relies on the dual wave/particle nature of X-rays. It is based on the scattering (diffraction) of an incident beam of monochromatic X-rays from atoms of the investigated material, when X-rays interact with that material. The scattered X-rays might undergo either constructive (in phase) or destructive (out of phase) interference. When the incident X-rays interact with the crystalline sample and conditions of Bragg's Law ($n\lambda = 2d \sin \theta$) are fulfilled this leads to the constructive interference of the X-ray reflected from the same atoms but from different layers/planes (**Figure 15**).
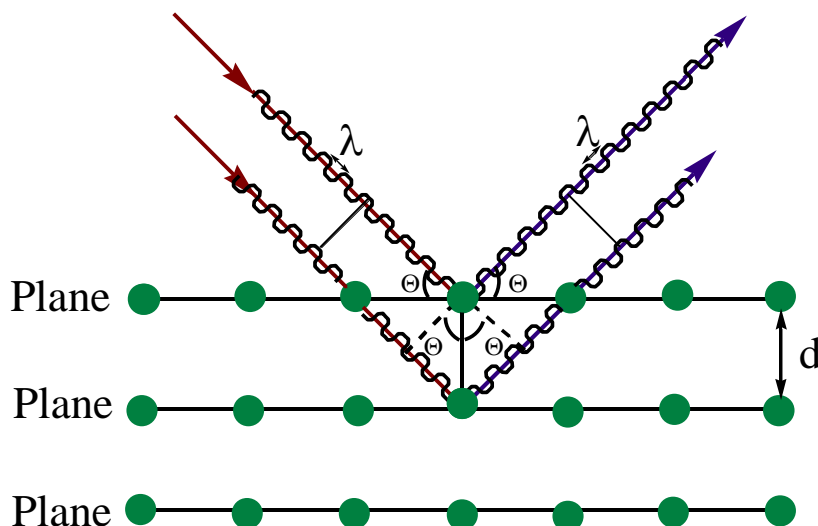
Figure 15. Schematic representation of Bragg's law.

Thus, the Bragg equation is a law that describes the diffraction/scattering of X-rays by a crystalline material. This law relates the wavelength λ of the incident electromagnetic radiation to the diffraction angle θ and the lattice spacing d in a crystalline sample:

$$n\lambda = 2d \sin\theta \tag{10}$$

The intensities of the scattered waves depend on the arrangement of atoms within the crystal structure. Typically, powder materials consist of many small randomly oriented crystallites. Because of the random orientation of the crystallites in powder materials, an investigated sample usually is scanned through a range of 2θ angles to detect all possible diffraction reflexes of the powder material. Thus, a powder diffractogram presents the scattered intensities as a function of a scattering angle θ.

Even though X-ray powder diffraction is regarded as one of the common standard techniques to investigate the structure of materials including catalysts, it can bring many new insights when X-ray powder diffraction studies are done in situ/operando, for instance for catalysts under realistic working conditions.

2.2.4.2 EXPERIMENTAL SETUP FOR IN SITU X-RAY DIFFRACTION STUDIES

In situ XRD experiments were performed in the laboratory on the XPERT III: PANalytical XPert Pro MPD diffractometer using Cu-Kα radiation (1.54 Å) (X-ray tube was operating at 40 kV and 40 mA)

operating in the Bragg-Brentano reflection geometry. The diffractometer is equipped with an Anton Paar XRK 900 high-temperature gas cell.[9] In situ diffraction patterns were recorded in the scanning range from 25-70° (2θ) using a step scan mode with the step of 0.05° (2θ) and a time per step of 2 s. The inlet of the Anton Paar XRK 900 high-temperature gas cell is connected to a gas manifold system with calibrated mass flow controllers; the outlet of the cell is connected to a quadrupole mass spectrometer (QMS) (PrismaPlus QMG 220, Pfeiffer Vacuum) equipped with a SEM detector. The sample (ca. 20 mg) was placed into a sample holder and inserted into the cell.

2.2.4.3 EXPERIMENTAL CONDITIONS OF IN SITU X-RAY DIFFRACTION MEASUREMENTS AND DATA ANALYSIS

For a lab source in situ XRD, a sample (ca. 20 mg) was pretreated in synthetic air at 400 °C (30 min) followed by treatment in 5 vol.% H_2 in He at 400 °C (30 min). Afterwards the reaction mixture of 5 vol.% CO, 10 vol.% O_2 and 85 vol.% was introduced and the XRD patterns were recorded at RT and at 100, 200, 300, and 400 °C. Also in situ XRD of CO oxidation over the Co_3O_4 pretreated only in in synthetic air at 400 °C (30 min) was carried out with a reaction mixture of 5 vol.% CO, 10 vol.% O_2 and 85 vol.% He. All experiments were performed at ambient pressure with a total flow of 50 mL min^{-1}.

XRD data were analyzed with the HighScore Plus program in order to identify XRD patterns. Crystal structure refinements were performed using the program package TOPAS 4.2.

2.3 DEVELOPMENT AND CONSTRUCTION OF A COMBINED XAS/XRD OPERANDO FLOW CELL

Both XRD and XAS are important techniques that are commonly employed for studying the geometric and electronic structure of catalysts. Moreover, these two techniques are widely exploited for investigation of catalysts under reaction conditions. However, the success of in situ/operando XRD and XAS experiments strongly depends on the design of the reaction cell. Therefore, a lot of attention is paid to the development and optimization of XRD and XAS reaction cells. Various sample-environment/reaction cells have been described for XRD and XAS experiments. [6 7 8 9 10 11] However, these designs are focused mainly on specific types of experiments and do not enable using the same cell for both XRD and XAS. As a great benefit, using the same cell, for instance for XRD and XAS, allows one to avoid discrepancies in results caused by different dead volumes of different cells, differences in local heating of the catalyst bed, etc. Therefore, further development and optimization of reaction cells that allow recording XAS spectra, both in the transmission and fluorescence mode, and X-ray diffraction/total scattering using the same cell is of great scientific interest.

We constructed a versatile capillary-flow cell that offers a greater capability to perform X-ray absorption and X-ray diffraction/total scattering studies of catalysts under operando conditions at different XAS and XRD beamline stations. Moreover, the cell is compatible with the in house laboratory source X-ray diffractometer operating in the Debey-Scherrer mode. The drawing of the cell is presented in **Figure 16**. The design of this cell is based on the design by Peter Chupas *et al.* [12] We made further modifications of the cell that allow for using this cell for both XAS and XRD experiments with capillaries in the range from 0.3 mm to 3 mm. The cell can be heated up to 600 ºC and allows a gas flow through the sample inside a quartz capillary at atmospheric pressure.

Generally, the cell is based on the capillary sample geometry. This implies that for XRD/scattering the transmission geometry of the diffractometer must be used, whereas XAS measurements can be carried out either in transmission mode or in fluorescence mode. For XRD experiments, the cell is fixed to the specially designed goniometer head by Huber that is compatible with a large number of diffractometers (**Figure 17a**). For XAS experiments, the cell is mounted into a metal block frame that can be fixed to the moving stage, as presented in **Figure 17b**. The construction of the cell is based on Swagelok fittings and allows one to change easily from 1/16 fittings to 1/8 fittings. This enables usage of capillaries with different sizes (from 0.3 mm to 3 mm) which makes this cell compatible for XRD (typical capillary size used 0.3-1 mm, thickness 10 microns) and XAS (typical capillary size used 1-3 mm, thickness 10 or 100 microns depending on the absorption edge of the investigated material). In a typical experiment, the sample is packed into the quartz capillaries, plugged with quartz wool, and inserted via the Swagelok fittings of the cell. Above and below the capillary, heating elements are inserted to the wall holes of the cell. As heating elements ceramic cylinders covered with Kanthal wires are used. For controlling the temperature, a thermocouple can be inserted inside the capillary.

The inlet of the cell is connected to a gas manifold system with calibrated mass flow controllers that allow variable feed gas compositions. The outlet of the cell can be connected either to a mass spectrometer or a gas chromatograph for monitoring the educts and products of the catalytic reaction.

The compact design of the cell and the low dead volume allow using this cell for fast time-resolved measurements, as well as for cycling experiments. To avoid a pressure drop and to be able to perform cycling experiments, the total flow should be 40 mL min^{-1} and higher. Therefore, the sample powder should be sieved and a fraction of particles of ~100 microns should be used. Moreover, the cell is compact, with no unnecessary components that minimize the background scattering. This is especially essential for X-ray total scattering experiments.
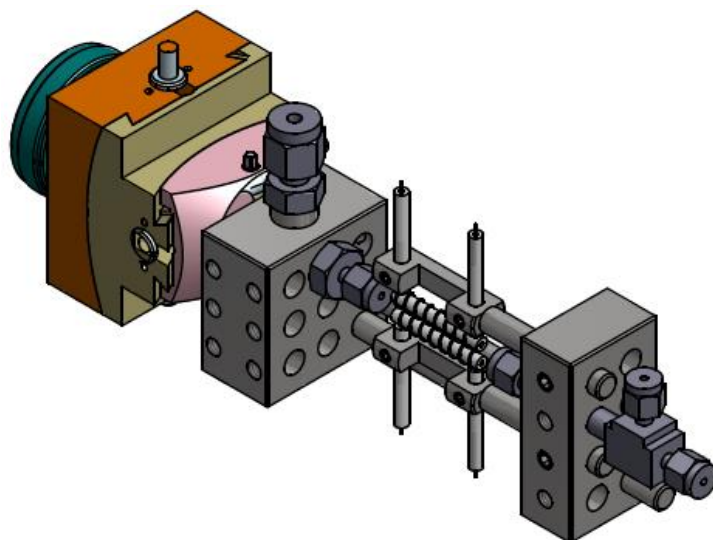
Figure 16. The flow cell for operando XRD and XAS experiments.

(a)   **(b)**
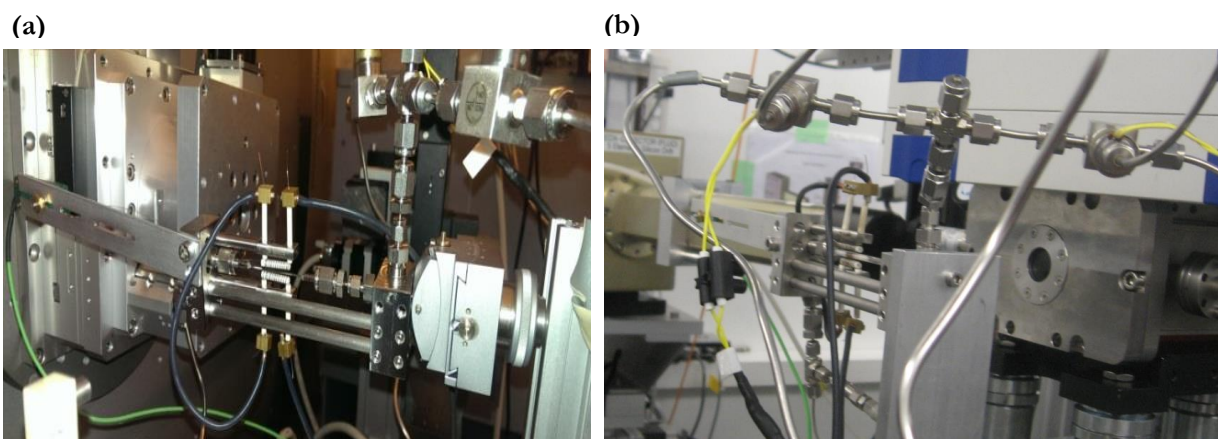
Figure 17. The flow cell during: in situ XRD at the P02.1 beamline, DESY, Hamburg, Germany (a): in situ XAS at the SuperXAS beamline, SLS, Villigen, Switzerland (b).

2.4 REFERENCES

1.   Tiefenthaller, R., Master thesis. *Institute of Materials Chemistry, Technische Universität Wien, Vienna, Austria* **October 2012**, 25.

2.   https://www.helmholtz-berlin.de/pubbin/igama_output?modus=einzel&sprache=en&gid=1671.

3.   Bluhm, H.; Hävecker, M.; Knop-Gericke, A.; Kiskinova, M.; Schlögl, R.; Salmeron, M., In Situ X-Ray Photoelectron Spectroscopy Studies of Gas-Solid Interfaces at Near-Ambient Conditions. *MRS Bulletin* **2007,** *32* (12), 1022-1030.

4.   http://www.specs.com/.

5.   https://www.maxlab.lu.se/node/677.

6.   Hannemann, S.; Casapu, M.; Grunwaldt, J.-D.; Haider, P.; Trussel, P.; Baiker, A.; Welter, E., A versatile in situ spectroscopic cell for fluorescence/transmission EXAFS and X-ray diffraction of heterogeneous catalysts in gas and liquid phase. *Journal of Synchrotron Radiation* **2007,** *14* (4), 345-354.

7.   Drake, I. J.; Liu, T. C. N.; Gilles, M.; Tyliszczak, T.; Kilcoyne, A. L. D.; Shuh, D. K.; Mathies, R. A.; Bell, A. T., An in situ cell for characterization of solids by soft x-ray absorption. *Review of Scientific Instruments* **2004,** *75* (10), 3242-3247.

8.   http://www.anton-paar.com/corp-en/products/group/xrd/.

9.   http://www.hysacatalysis.uct.ac.za/?page_id=1104.

10.   Jensen, T. R.; Nielsen, T. K.; Filinchuk, Y.; Jorgensen, J.-E.; Cerenius, Y.; Gray, E. M.; Webb, C. J., Versatile in situ powder X-ray diffraction cells for solid-gas investigations. *Journal of Applied Crystallography* **2010,** *43* (6), 1456-1463.

11.   Fischer, N.; Clapham, B.; Feltes, T.; van Steen, E.; Claeys, M., Size-Dependent Phase Transformation of Catalytically Active Nanoparticles Captured In Situ. *Angewandte Chemie International Edition* **2014,** *53* (5), 1342-1345.

12.   Chupas, P. J.; Chapman, K. W.; Kurtz, C.; Hanson, J. C.; Lee, P. L.; Grey, C. P., A versatile sample-environment cell for non-ambient X-ray scattering experiments. *Journal of Applied Crystallography* **2008,** *41* (4), 822-824.

CHAPTER 3

(NEAR)SURFACE ELECTRONIC AND
GEOMETRIC STRUCTURE MODIFICATIONS
OF Co_3O_4 UNDER REDUCING (CO) AND
OXIDIZING (O_2) ATMOSPHERES: IN SITU
NAP-XPS AND NEXAFS

ABSTRACT:

Despite the increasing interest in using cobalt-based materials for CO oxidation and CO hydrogenation reactions, the exact temperature-dependence of the (near)surface composition of cobalt oxide in reducing (CO) and oxidizing (O_2) atmospheres has not yet been studied in detail. Using synchrotron-based in situ near atmospheric pressure X-ray photoelectron spectroscopy (NAP-XPS), including depth profiling by photon energy variation, and near-edge X-ray absorption fine structure (NEXAFS) at the Co $L_{3,2}$ edge (total electron yield detection), the (near)surface electronic and structural changes of Co_3O_4, adsorbates and oxygen vacancies evolution during CO reduction and subsequent O_2 reoxidation were monitored. The results obtained by combining information from different information depths allowed distinguishing surface oxygen vacancy formation during reduction of Co_3O_4 in CO atmosphere (RT-150 °C) from the oxygen vacancies created by mobility of bulk lattice oxygen (200-250 °C). Additionally, formation of a mixed phase of rocksalt-type CoO and metastable wurtzite-type CoO in near-surface (~ 3-5 nm) during reduction of Co_3O_4 in CO atmosphere at 250 °C were identified. Moreover, the obtained data revealed that the temperatures for reduction of cobalt oxide and the reoxidation of metallic cobalt do not coincide. This provides new insights into the surface chemistry of Co_3O_4 and shed light on the CO oxidation mechanism on cobalt oxide, as well as the deactivation and regeneration of metallic cobalt Fischer-Tropsch catalysts under oxidizing conditions.

Keywords: in situ NAP-XPS, NEXAFS, valence band, reduction and reoxidation, cobalt oxide, CO oxidation

3.1 INTRODUCTION

Cobalt-based materials are widely used as gas sensors, cathode materials in Li ion rechargeable batteries, magnetic data storage systems, and catalysts in homogeneous and heterogeneous reactions.[1] [2] [3] [4] [5] [6] [7] [8] [9] [10] [11] In particular in the field of heterogeneous catalysis, metallic cobalt finds its potential application in numerous industrial processes, such as conversion of synthesis gas ($CO+H_2$) into liquid hydrocarbons by the Fischer-Tropsch (FT) synthesis, steam reforming of hydrocarbons for hydrogen production, and hydrodesulfurization of the refined petroleum products.[5] [6] [9] [12] Furthermore, in recent years cobalt oxide materials have attracted increasing attention as promising noble metal-free catalysts for oxidation reactions (i.e., CO oxidation, preferential CO oxidation (PROX), and hydrocarbon oxidation)[10] [11] [13] [14] [15] and for electrocatalytic oxygen reduction reactions.[7] [8] Therefore, many efforts are currently directed toward the development and commercialization of cobalt-based catalysts.

The correlation between the oxidation state of cobalt and its catalytic activity is a hot research topic in cobalt catalysis because the electronic structure of cobalt (i.e., oxidation state and interplay between Co^{3+}/Co^{2+} oxidation states) is one of the most important factors that governs the catalytic activity, selectivity, and stability of cobalt-based catalysts. For example, metallic cobalt is a well-known active phase of FT catalysts, whereas reoxidation of cobalt, formation of surface carbon species, and carbidization are the main reasons for FT catalysts deactivation.[16] [17] [18] [19] [20] Also for hydrocarbon steam reforming reactions most studies found that cobalt should be in the metallic form.[9] [21] [22] [23] In contrast, cobalt should preserve the oxide form for oxidation reactions (e.g., CO oxidation and PROX).[10] [11] [13] [14] [15]

To further develop and commercialize efficient cobalt-based catalysts, it is necessary to understand how the oxidation state of cobalt evolves under different chemical environments and temperatures. Furthermore, it is important to know how a specific oxidation state of cobalt can be preserved in order to improve the catalytic activity, selectivity and stability of the cobalt-based catalyst for a specific reaction. The reduction of Co_3O_4 in H_2 atmosphere has been extensively studied, especially with respect to the FT synthesis, using in situ/operando techniques (e.g., in situ X-ray diffraction (XRD), in situ X-ray absorption (XAS), and in situ transmission electron microscopy (TEM)) to monitor *bulk* structural and electronic changes.[24] [25] [26] [27] [28] [29] Yet in comparison, much less work has been done on Co_3O_4 reduction in CO atmosphere. [30] Very little is known about the evolution of the oxidation state and structure of cobalt under CO reducing atmosphere, despite the technological importance. Furthermore, the relative ease of lattice oxygen extraction, formation of oxygen vacancies ($V_O^{..}$) as well as the evolution of adsorbate species on cobalt oxide *surfaces* under CO are still not well understood although all this is crucial to explaining CO oxidation chemistry on cobalt oxide catalysts.

In addition, the investigation of the reoxidation of metallic cobalt is of particular interest. Regardless of the intensive studies, vague and contradictory results concerning the reoxidation behavior of metallic

cobalt and its deactivation are reported in the literature up to now,[19] [31] [32] [33] mainly because of the lack of information on the surface chemistry under reaction conditions. Further, the reoxidation of cobalt followed by re-reduction is one way in which FT catalysts are regenerated. Therefore, many investigations are currently directed toward fully understanding cobalt reoxidation at the molecular level.[34] [35] Although many studies of cobalt oxidation/reoxidation have been already performed using the in situ/operando approach, the techniques used were in situ XRD, in situ XAS, and in situ TEM, which allow the bulk structure changes to be monitored without keeping track of the surface composition.[36] [34] [37] The *surface* composition evolution is most relevant for catalytic events that take place on the *surface* of catalysts. Thus, it is highly desirable to develop an understanding of how cobalt oxide reduces under CO atmosphere and reoxidizes in O_2 atmosphere on the topmost surface layers as well as how the bulk structure is affected (different depths information).

Therefore, the objectives of the present work were threefold: (1) to investigate the *(near)surface* composition of cobalt oxide during inter-conversion between Co_3O_4, CoO and Co and vice versa upon variation in reaction atmospheres (CO, O_2) in a wide temperature range using synchrotron-based in situ NAP-XPS, including valence band, depth profiling and Near-Edge X-ray Absorption Fine Structure Spectroscopy (NEXAFS) at the Co $L_{3,2}$ edge (total electron yield (TEY) detection); (2) to compare the data obtained for different information depths (i.e., valence band Co 3d (the outermost surface layers), core level XPS for different information depth (~0.6 - 1.1 nm), and NEXAFS at the Co $L_{3,2}$ edge in the TEY (~2.5-5 nm);[38] [39] and (3) to provide a detailed discussion on the mechanistic insights of CO oxidation as well as metallic cobalt oxidation that is relevant to the FT catalysts deactivation and regeneration. A complete understanding of the *(near)surface* chemistry of cobalt oxide during reduction and reoxidation could add to our knowledge of the active sites and, as a result, to the development of more efficient catalysts for oxidation as well as for hydrogenation reactions.

3.2 EXPERIMENTAL

Co_3O_4 was used as received from Fluka, purity 99.5 %. The (average) crystallite size of Co_3O_4 determined by X-ray diffraction was 28 nm, the specific surface area was 38 m^2g^{-1}. The material is composed of nanospheres with sizes between 20 and 50 nm.

In situ NAP-XPS was performed at the ISISS beamline at BESSY II in Berlin, Germany. The setup consists of a reaction cell attached to a set of differentially pumped electrostatic lenses and a separately pumped analyzer (Phoibos 150 Plus, SPECS GmbH). The experimental conditions are presented in the experimental part of the thesis. Before the experiment, the Co_3O_4 sample was pretreated in the XPS reaction cell by oxidation (0.5 mbar O_2 at 400 ºC) until all residual surface carbon and carbonates disappeared.

3.3 RESULTS

3.3.1 Co₃O₄ UNDER CO ATMOSPHERE

3.3.1.1 CO-TPR: Co 2p AND C 1s CORE LEVELS

Co_3O_4 (normal spinel structure (Fd3m)) is the thermodynamically favored phase of cobalt oxide under ambient conditions with octahedrally coordinated (Oh) Co^{3+} and tetrahedrally coordinated (Td) Co^{2+} ions. Under reducing conditions (e.g., H_2, CO, or vacuum), Co_3O_4 undergoes first conversion into CoO (cobalt monoxide with rocksalt structure (fcc)) with Co^{2+} in Oh coordination environment, and then CoO can be further reduced to metallic cobalt. In this work, the evolution of the oxidation state and structure of cobalt in Co_3O_4 as well as the surface composition under 0.15 mbar CO were investigated using synchrotron-based NAP-XPS to understand oxygen vacancies formation, the reduction behavior of Co_3O_4 in CO atmosphere, and evolution of adsorbates. **Figure 1** shows the Co 2p and C 1s photoemission spectra during exposure of Co_3O_4 to CO upon heating from RT to 300 ᵒC for a kinetic energy (KE) of 200 eV. This KE corresponds to an inelastic-mean-free path (i.e., an information depth) of ca. 0.6 nm and probes mainly the two topmost surface layers. To quantitatively elucidate cobalt chemical state information, the Co 2p spectra were fitted by constraining the full width at half maximum (FWHM) and peak positions. The FWHM together with constraints are listed in **Table S1.** The identification of the cobalt oxidation state and the assignment of peaks were done based on data from the literature. Peak 1 at 779.4 eV was assigned to Co^{3+}, peak 2 at 780.9 eV to Co^{2+} in CoO, and peak 3 at 782.4 eV to Co^{2+} in $Co(OH)_2$.[40] Two shake-up satellites (i.e., 785.6 and 789.3 eV) of cobalt ions that are associated with the surface and bulk plasmons were also included in the fitting of the Co 2p region.[41] The intensities of these satellite peaks are very sensitive to the surface stoichiometry and help to identify the interconversion between Co_3O_4 and CoO. In the case of Co_3O_4, these satellite peaks are weak and broad, whereas for CoO they are much more pronounced in intensity. To describe the Co_3O_4 changes upon heating in CO, three temperature windows were defined that represent the main structural and electronic modifications that is in line with CO-temperature programed reduction data from a fixed-bed flow reactor (**Figure S1**):

1) RT-200 ᵒC - surface reduction of Co_3O_4 to CoO_x;

2) 200-250 ᵒC - reduction of CoO_x to CoO;

3) 250-300 ᵒC - reduction of CoO to metallic cobalt.

Previously in the literature it was reported that the reduction of Co_3O_4 in CO might already occur at RT. For example, the reduction of Co_3O_4 in CO oxidation mixture at RT was suggested by Jansson to be one of the reasons for the cobalt oxide catalyst deactivation at RT; [42] however, no experimental evidence of Co_3O_4 reduction was provided. In this work, evaluation of the Co 2p spectrum recorded at RT after exposing Co_3O_4 to 0.15 mbar CO does not firmly prove that surface reduction of Co_3O_4 (**Table1**). The decrease of the Co^{3+} fraction from 28% in O_2 atmosphere to 26% in CO atmosphere even after 1 h is rather small. Importantly to note that the measured fraction of Co^{3+} is 28% in O_2 atmosphere for Co_3O_4, while the theoretical value should be ~33 % of Co^{3+} in Co_3O_4 structure (1 Co^{3+} and 2 Co^{2+}). This might be explained by the fact that the top surface layers of Co_3O_4 are terminated by cobalt ions (i.e., coordinatively unsaturated oxygen surface). As the temperature increases, the satellite peaks become more pronounced and increase in intensity, a direct evidence of surface reduction. The fraction of Co^{3+} in Co_3O_4 decreases from 28% in O_2, to 24% at 100 °C and at 150 °C, and 23% at 200 °C in CO atmosphere (**Table 1**). These changes are attributed to the partial surface reduction of Co_3O_4 to CoO_x that is accompanied by the extraction of lattice oxygen and formation of surface oxygen vacancies (Vo·). Further increase in temperature from 200 to 250 °C leads to the complete reduction of CoO_x to CoO (**Figure 1a),** as seen by the drastic increase of the satellite features (i.e., peaks at 785.6 and 789.3 eV) and the shift of the peak position to 780.0 eV. These changes, as described in the literature, correspond to the phase transition from Co_3O_4 to CoO.[40] [43] When the temperature reaches 300 °C, CO reduces CoO partially to metallic cobalt (peak at 778.1 eV).

In the C 1s spectra (**Figure 1b**), three peaks were detected at 288.2, 286.1, and 284.7 eV upon exposure of Co_3O_4 to CO. The peak at 284.7 eV is attributed to elementary carbon,[44] whereas peaks at 288.2 and 286.1 eV are related to carbon-oxygen containing adsorbates. The peak at 288.2 eV can be assigned to adsorbed carbonates or carboxylate;[45] [46] [47] the assignment of carbonates is not trivial because their binding energy strongly depends on the type of metal and metal oxide.[47] In a recent XPS study of CO adsorption on a Co_3O_4 (111) thin film, carbonate species were formed with a binding energy of 288.5 eV.[46] Formation of carbonates was also detected by IR spectroscopy in studies of CO oxidation on cobalt oxide materials[11] as well as in our in situ IR study on Co_3O_4 (the results will be presented in **Chapter 4**). Considering this, the peak at 288.2 eV is assigned to adsorbed carbonates. The type of carbonates (e.g., monodentate, bidentate, or bicarbonates) can, however, not be determined based on the XPS data. The peak at 286.1 eV is ascribed to CO linearly adsorbed to cobalt cations (Co^{3+} or Co^{2+}) and to CO linearly adsorbed to metallic cobalt.[48]

The C 1s region was fitted in order to quantify carbon containing adsorbates and monitor changes in the ratios with temperature. The FWHM and peak positions are presented in **Table S2**. Surprisingly, already at RT elementary carbon is observed in the C 1s region in addition to carbonates and linearly adsorbed CO to cobalt cations. This suggests that CO undergoes either disproportionation (i.e., $2CO{\rightarrow}CO_2+C$) or dissociation (i.e., $CO{\rightarrow}C+O$) on the Co_3O_4 surface. Carbon accumulation was also detected by Jansson

on Co_3O_4/γ-Al_2O_3 by temperature programmed oxidation of a spent catalyst after low temperature CO oxidation. Jansson suggested that CO disproportionation might be either one of the reaction pathways of CO oxidation or causes catalyst deactivation.[42] [49] Raising the temperature to 200 °C leads to the increase of the fraction of elementary carbon (i.e., 51% carbon at RT and 78% at 200 °C), as seen from **Figure 1b.** Thus, the ratio between elementary carbon, carbonates, and CO linearly adsorbed to cobalt cations changes (**Table 1**). It should be noted that elementary carbon at 284.7 eV is attributed to adsorbed atomic carbon (C_{alfa}), as known from the literature; only above 250 °C C_{alfa} can be transformed to C_{beta} (i.e., polymeric carbon film).[50] At 300 °C the adsorbed atomic carbon is dominant whereas a small amount of carbonates is still present due to remaining CoO, as revealed by the Co 2p spectrum. Importantly, no cobalt carbide phase was observed in the C 1s region at 300 °C.
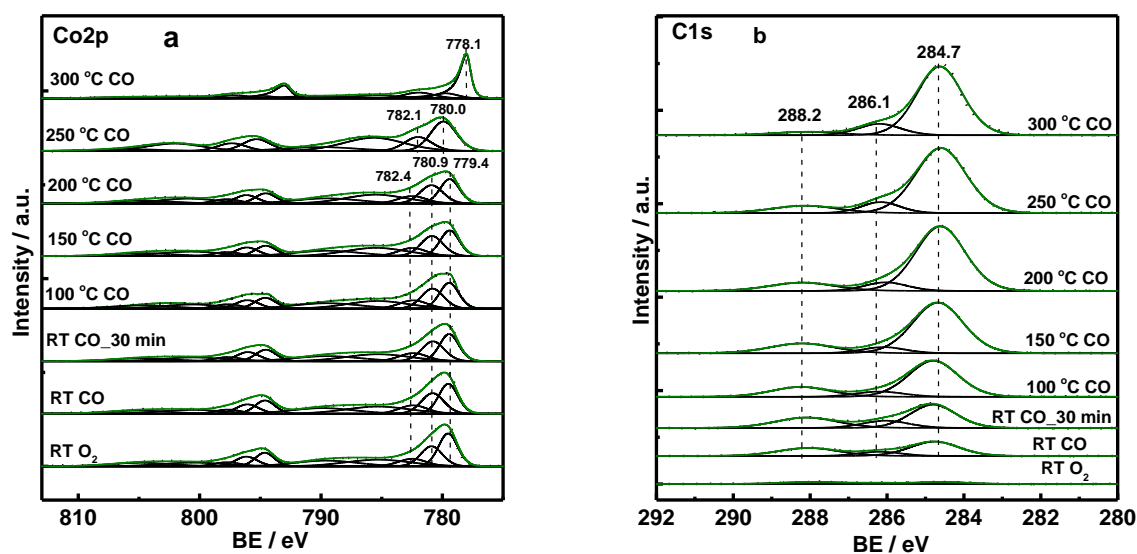
Figure 1. In situ NAP-XPS during CO-temperature programmed reduction of Co_3O_4 (0.15 mbar of CO): (a) Co 2p region (hv = 1015 eV); (b) C 1s region (hv = 465 eV).

Table 1. NAP-XPS CO-TPR on Co_3O_4: C 1s (hν = 465 eV) and Co 2p (hν = 1015 eV) regions.

Conditions	Elementary carbon, %	CO-$Co^{3+/2+/0}$, %	Carbonates, %	Co^{3+} in Co_3O_4,%	CoO	Metallic Co
CO RT	51	13	36	27	-	-
CO RT_30	52	16	32	26	-	-
CO 100 ᵒC	69	10	21	24	-	-
CO 150 ᵒC	74	8	18	24	-	-
CO 200 ᵒC	78	9	13	23	-	-
CO 250 ᵒC	79	10	11	-	100	-
CO 300 ᵒC	82	12	6	-	48	52

3.3.1.2 CO-TPR: DEPTH PROFILES

To monitor the extent of Co_3O_4 reduction during the CO-TPR experiment in the surface and subsurface regions, XPS spectra were recorded at varying photon energies to obtain photoelectron kinetic energies of 200, 400, and 600 eV, which result in probing depths of ~0.6 nm, 0.8 nm, and 1.1 nm, respectively. Higher kinetic energies were not used in our study because of a strong decrease of X-ray intensity above 1500 eV. The Co 2p and C 1s spectra from depth profiling were analyzed to determine the atomic percentage of species at different depths, and the results are summarized in **Figure 2** whereas the spectra are presented in **Figure S2** and **Figure S3**. Obvious changes of the Co^{3+} fraction between the top surface layers and the subsurface region during exposure of Co_3O_4 to CO are observed. The two top surface layers (0.6 nm) undergo reduction, whereas the deeper near-surface layers (~0.8-1.1 nm) exhibit a higher concentration of Co^{3+}. The fraction of Co^{3+} for 1.1.nm depth profile corresponds to the theoretical value ~33 % of Co^{3+} in a stoichiometric structure of Co_3O_4 (1 Co^{3+} and 2 Co^{2+}). Interestingly, increasing temperature to 150 ᵒC leads to the gradual decrease of the Co^{3+} concentration at the two top surface layers, while the concentration of Co^{3+} in the depth of 0.8 nm and 1.1 nm (i.e., subsurface) undergoes only minor change (i.e., 29 and 32% of Co^{3+} for 0.8 and 1.1 nm, respectively). When the temperature reaches 200 ᵒC, the deeper layers also undergo more severe reduction and the amount of Co^{3+} decreases (i.e., 26 and 29% of Co^{3+} for 0.8 and 1.1 nm, respectively).

Examination of the carbon containing species in the surface and subsurface regions shows that the amount of elementary carbon decreases with increasing kinetic energy from 200 to 600 eV, revealing that

carbon is present mostly at the surface of the catalyst, whereas the relative amount of carbonates and the CO linearly adsorbed to $Co^{3+/2+}$ species rises with increasing the kinetic energy. Thus, the amount of elementary carbon on the top surface layers correlates with the decrease of Co^{3+} fraction (i.e., the increased amount of oxygen vacancies on the top surface layers).
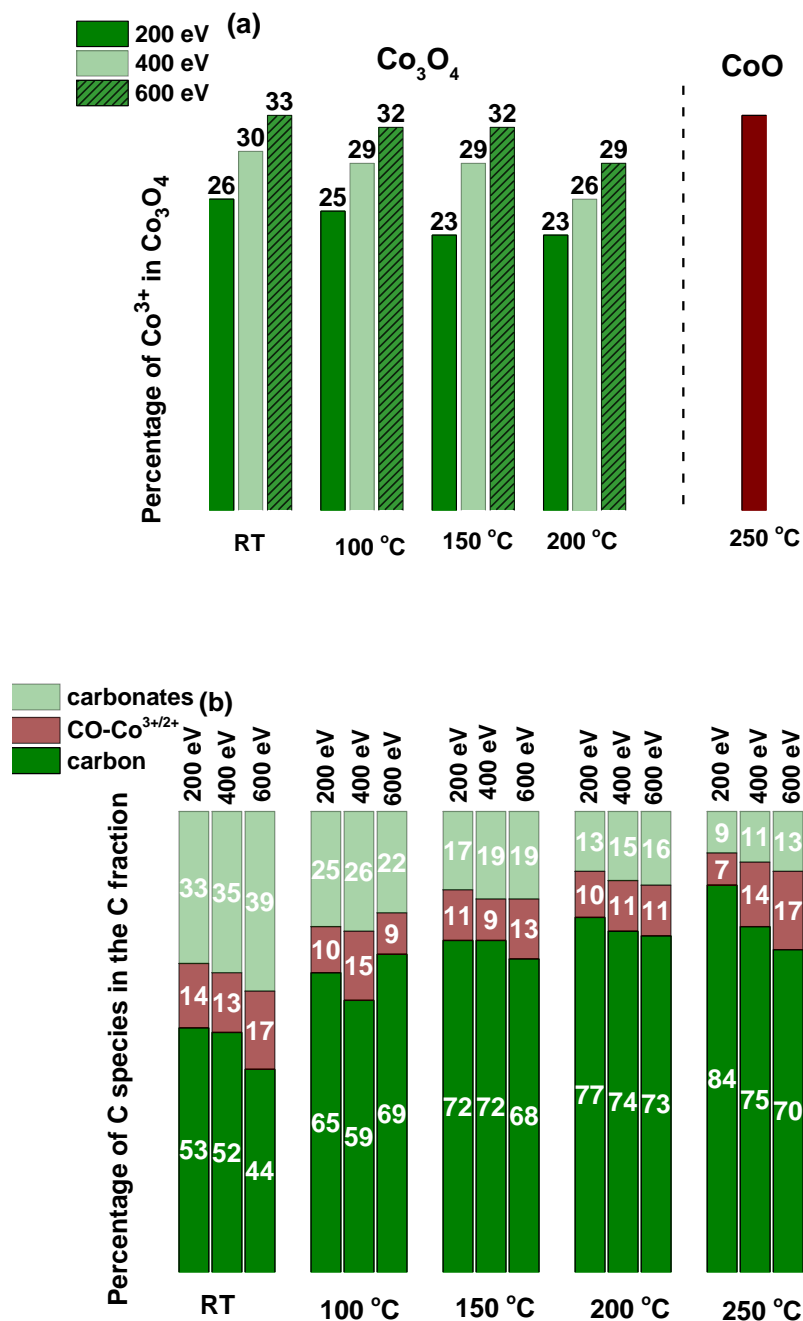
Figure 2. In situ depth profile NAP-XPS during CO-temperature programmed reduction of Co₃O₄ (0.15 mbar CO): (a) the Co 2p region with hν = 1015 eV, hν = 1215 eV, and hν = 1415 eV that results in 0.6.nm, 0.8 nm, and 1.1 nm inelastic-mean-free path for Co, respectively; (b) the C 1s region with hν = 465 eV, hν = 665 eV, and hν = 865 eV that results in ~0.6 nm, 0.8 nm, and 1.1 nm inelastic-mean-free path for C, respectively.

3.3.1.3 CO-TPR: VALENCE BAND SPECTRA

To complement core-level data, XPS valence band spectra of Co_3O_4 during CO-TPR were recorded at a primary beam energy of 200 eV to reveal surface sensitive information on the electronic and fine structure changes as valence band spectra have higher sensitivity than core-level spectra (**Figure 3**). Generally, XPS valence band data yield unique information on the density of state (DOS) near the Fermi level, electronic state in the band gap, and the binding energy of valence electrons of adsorbates. It should be noted that a contribution of deeper layers (i.e., bulk states) to the DOS of the outermost surface layers must be considered as well because of the delocalized nature of electrons in the valence band. Although the knowledge obtained for the valence band is very valuable, the interpretation of the valence band region is not as straightforward as the core level region. Moreover, the comparison of our data with the valence band spectra for Co_3O_4, CoO, and metallic cobalt from the literature is not feasible. This is because the spectral features in the VB strongly depend on both the incident energy, as shown by Langell *et al.* for Co_3O_4 grown on CoO(100),[51] and the type of radiation source (i.e., ultraviolet photoemission spectroscopy (UPS) or XPS) demonstrated by Hofmann *et al.* for metallic cobalt.[52] In addition, adsorption of CO or O_2 on the cobalt oxide surface contributes to the O 2p region of the valence band spectrum (i.e., a "charge-transfer") and complicates data interpretation. According to the UPS valence band study of Langell *et al.*, three main spectral features might be found in the valence band spectra of cobalt oxides obtained by irradiation with photons of 40 eV energy:[51]

- Co 3d-related features: the peak at ~1.7 eV for CoO, and this peak is shifted to a lower BE for Co_3O_4 (i.e., for 3d orbitals with t_{2g} (Co^{3+}) character); the peak at ~3.8 eV for 3d orbitals with e_g (Co^{2+}) character;
- O 2p-derived bands: at ~5.1 and 7.6 eV;
- Satellite feature at ~10.6 eV for CoO, lowering in intensity and shifting to a lower BE for Co_3O_4.

Although the spectral features of the VB strongly depend on the initial energy and the source of irradiation,[51] [52] we refer to the data of Langell *et al.* to find a general tendency in the interpretation of our data. However, it should be pointed out that the exact positions of our peaks are not in line with the peak position in the work of Langell *et al.* which might be because an electronic effect of the substrate used in their work. Furthermore, the interpretation of the O 2p is omitted here, as it strongly depends on the type of surface adsorbates (CO, O_2), and, therefore, further experimental and theoretical investigations should be carried out. This is beyond the scope of this chapter.
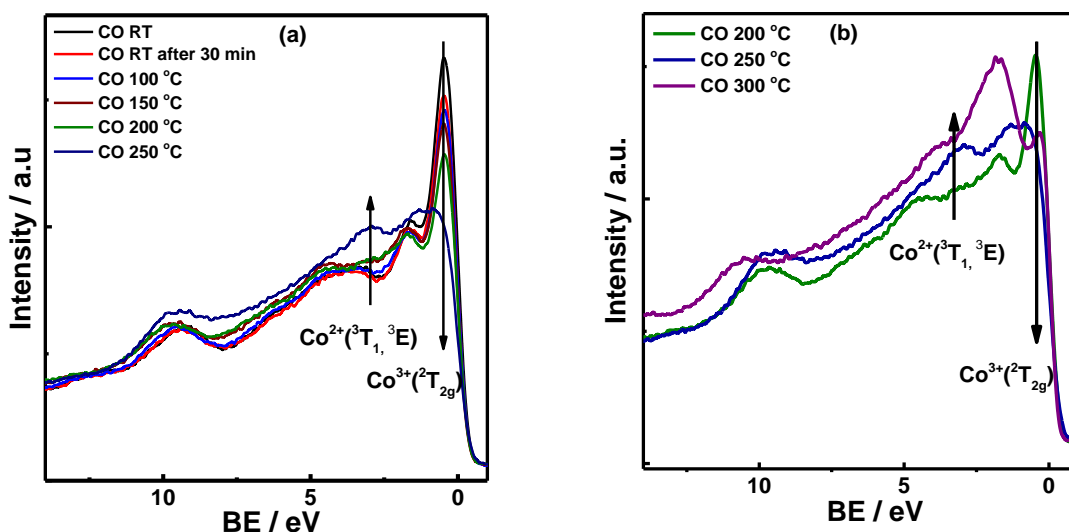
Figure 3. In situ NAP-XPS during CO-temperature programmed reduction of Co_3O_4 (0.15 mbar CO): (a) valence band region (hν = 200 eV) RT-250 °C; (b) valence band region (hν = 200 eV) 200-300 °C.

Herein, the main focus is on the Co 3d region and changes in the satellite features for monitoring Co_3O_4-CoO inter-conversion. Looking at the Co 3d valence band spectra, clear changes from spectrum to spectrum are seen. The feature that is characteristic of Co^{3+} (t_{2g}) decreases in intensity even at RT, suggesting RT reduction of Co_3O_4. This feature continues to decrease further upon heating. Starting from 150 °C, the feature characteristic of Co^{2+} (e_g) increases in intensity, indicating a stronger reduction. In addition, the satellite at ~ 10 eV becomes more pronounced and shifts to a higher energy, revealing a strong surface reduction at 150 °C. At 250 °C the shape of the valence band spectrum completely changes and the e_g feature strongly increases together with the satellite feature. This leads to the conclusion of severe electronic and structural changes of cobalt oxide (i.e., complete reduction of Co_3O_4 to CoO), as also revealed by core level XPS. Heating further in CO atmosphere causes more drastic spectral changes. However, interpreting the spectrum is not straightforward. When comparing our VB spectrum at 300 °C with the valence band spectra of a metallic cobalt film and crystal from the literature,[52] differences in the spectral features are observed. In our case, two peaks are present in the VB spectrum recorded at 300 °C (i.e., one narrow peak at 0.3 eV, and a broad peak at 1.7 eV). While the first peak might be attributed to the Fermi level, the second peak at ~1.7 eV might be attributed to CoO. According to our core level Co 2p XPS in addition to metallic cobalt, there is still a fraction of cobalt oxide at 300 °C.

3.3.1.4 CO-TPR: NEXAFS AT THE CoL$_{3,2}$

To reveal the geometric changes of cobalt oxide during heating in CO, NEXAFS spectra at the Co L$_{3,2}$ edge in the TEY, which probes approximately ∼5 nm of a sample depth, were recorded and are presented in **Figure 4**. Co$_3$O$_4$ has a spinel structure, which consists of (Oh) Co^{3+} and (Td) Co^{2+}, while rocksalt CoO consists of (Oh) Co^{2+}; both oxides have unique spectral features in the NEXAFS.[26][27][53] This enables the geometric structure changes of cobalt oxide to be examined and the coordination environment of cobalt to be ascribed. The analysis of NEXAFS spectra at the CoL$_{3,2}$ edge during exposure of Co$_3$O$_4$ to CO and heating to 200 ℃ reveals that the minor partial reduction of Co$_3$O$_4$ to CoO$_x$ starts already before 200 ℃, which is consistent with the information obtained from the core level Co 2p XPS spectra as well as valence band spectra. The feature at 778.0 eV gradually increases upon heating in CO, and at 200 ℃ the spectrum is broadened and shifted to a lower energy region. This shift is direct evidence of the Co$_3$O$_4$ reduction to CoO$_x$, but it is still not a complete CoO phase. It is interesting to note that even though the Co 2p XPS spectrum with KE = 200 eV taken at 200 ℃ points to the partial reduction of Co^{3+} to Co^{2+}, it is still difficult to estimate the extent of the reduction only based on the strong increase of the satellite feature in the Co 2p spectrum. Yet in comparison, the CoL$_{3,2}$ NEXAFS spectrum taken at 200 ℃ provides strong evidence of surface and near-surface reduction of Co$_3$O$_4$ to CoO$_x$. Further heating in CO atmosphere causes more severe structural changes, as seen in **Figure 4a**, and at 250 ℃ the CoO$_x$ transforms to CoO according to reference cobalt oxide spectra reported in the literature.[26][27][53]

Interestingly, CoO that is formed at 250 ℃ has a stronger feature at 778.8 than at 780.0 eV, which is a direct indication of Co^{2+} in a Td coordination environment present in addition to Co^{2+} in an Oh coordination environment. Although Co^{2+} in a Oh coordination environment is the most stable and common structure type for CoO, a few examples of CoO with a dominant Td coordination environment are also reported in the literature. For example, the Co^{2+} ion in Td coordination environment was documented for Zn$_{0.95}$Co$_{0.05}$O and was ascribed to the cobalt symmetry alternation/distortion because of the Co^{2+} ions substituting the Zn sites.[54] A similar effect was observed for cobalt oxide particles during reduction in H$_2$;[27] a Td coordination environment for CoO was stabilized by the preparation method using the PVP capping agent.[27] Also cobalt nanoparticles supported on amorphous carbon layers were found to contain a significant portion of metastable wurtzite-type CoO in a Td coordination environment in addition to rocksalt-type CoO in an Oh coordination environment in oxidative and reductive environment at 247 ℃.[55] When heating further to 300 ℃ in CO atmosphere, CoO is reduced to metallic cobalt, as seen from the spectral shape, but a small amount of CoO still remains, because the spectrum is still quite broad (**Figure 4b**).
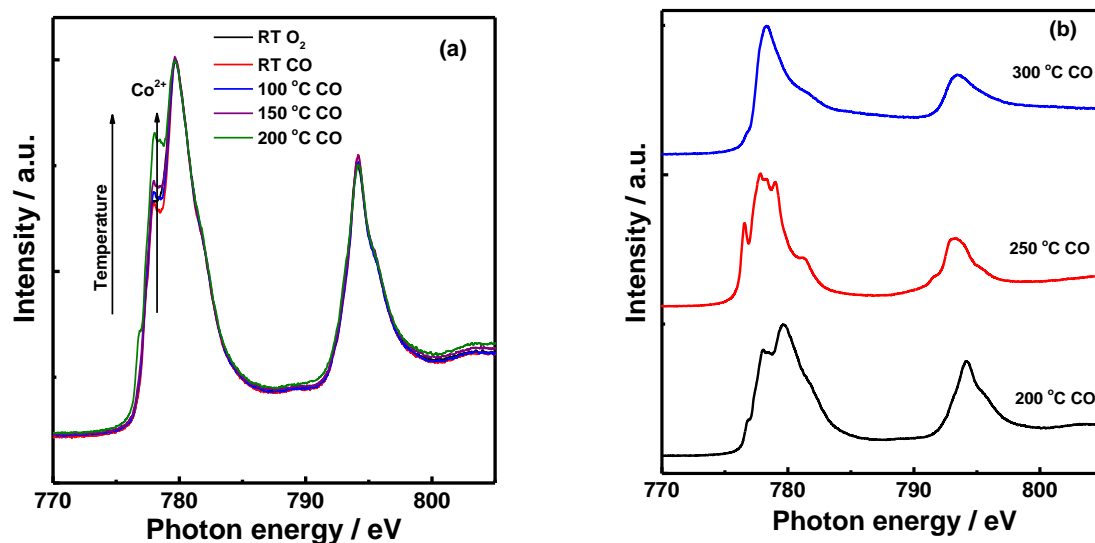
Figure 4. NEXAFS spectra at the Co $L_{3,2}$ edge during CO-temperature programmed reduction of Co_3O_4 (0.15 mbar CO): (a) RT-200 °C; (b) 200-300 °C.

3.3.2 Co under O₂ atmosphere

3.3.2.1 O₂-TPO: XPS Co 2p and C 1s core levels

In order to study the reoxidation behavior of cobalt, an O_2-TPO experiment was performed after CO-TPR. The reduced sample was cooled down to RT in CO atmosphere, CO was evacuated and O_2 (0.15 mbar) was introduced. The evolution of the Co 2p region and the C 1s region during heating in O_2 is presented in **Figure 5.** When O_2 (0.15 mbar) was introduced to the reaction chamber at RT, a broad peak at 780.1 eV corresponding to Co^{2+} in CoO together with the strong satellite feature become evident in the Co 2p region, indicating facile oxidation of metallic cobalt to CoO at RT even at very low pressures of O_2 (0.15 mbar O_2). Deconvolution of the Co 2p region clearly shows that CoO and metallic cobalt are present under these conditions at RT. As indicated in **Figure 5a** and **Table 2,** heating to 100 °C leads to the decrease of metallic cobalt. When the temperature reaches 150 °C, the two top most surface layers (~0.6 nm) are already completely reoxidized to Co_3O_4.
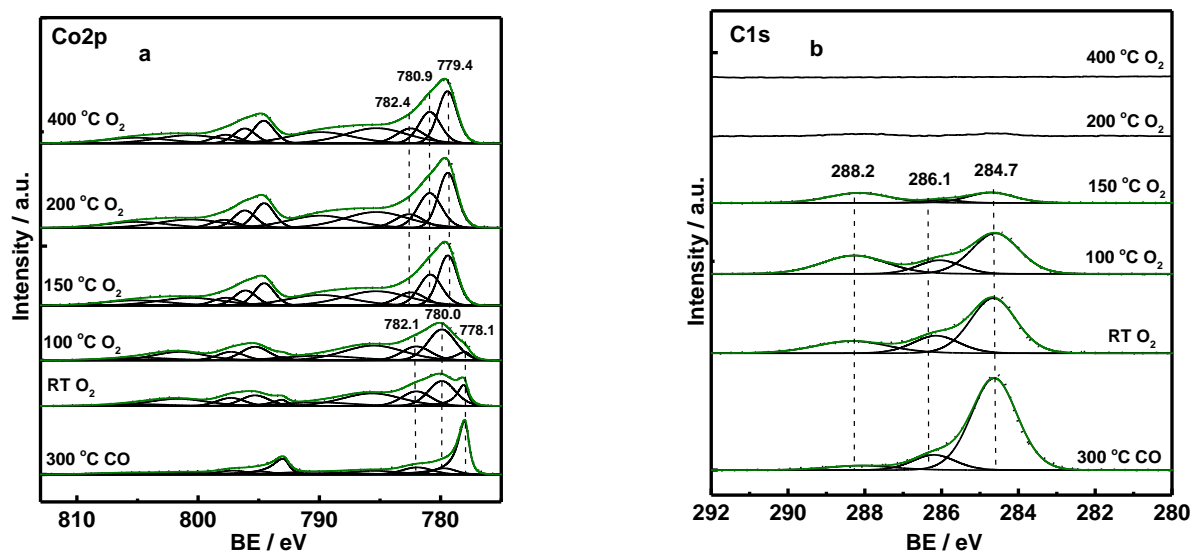
Figure 5. In situ NAP-XPS O₂-temperature programmed oxidation (0.15 mbar O₂): (a) Co 2p region (hν = 1015 eV); (b) C 1s region (hν = 465 eV).

Table 2. O₂-TPO on Co₃O₄ NAP-XPS: C 1s (hν = 465 eV) and Co 2p (hν = 1015 eV) regions.

Conditions	Elementary carbon, %	CO-Co$^{3+/2+/0}$, %	Carbonates, %	Co^{3+} in Co₃O₄,%	CoO	Metallic Co
RT O₂	60	19	21	-	88	12
O₂ 100 ºC	52	16	32	-	94	6
O₂ 150 ºC	40	9	51	26	-	-
O₂ 200 ºC	-	-	-	26	-	-
O₂ 400 ºC	-	-	-	26	-	-

By examining the C 1s region, the evolution of carbon-containing species was monitored during heating in O_2 atmosphere and corresponding data is given in **Table 2**, whereas spectra are presented in **Figure 5b**. Interestingly, in the C 1s region the peak attributed to atomic carbon (i.e., 284.7 eV) decreases in intensity and additionally a small amount of carbonates appeared as a product of atomic carbon oxidation to CO and readsorption on the cobalt oxide surface, revealing carbon oxidation by O_2 (i.e., $2C+O_2 \rightarrow 2CO$; $C+O_2 \rightarrow CO_2$) already at RT. It is clearly seen that the deposited carbon can be very easily oxidized upon heating in O_2 and its concentration decreases with temperature rise. At 200 °C the surface is almost clean. Moreover, the ratio between carbon and carbon-oxygen containing species changes towards the increase of carbonates upon heating in O_2 (i.e., 21% at RT and 51% at 150 °C).

3.3.2.2 O_2-TPO: XPS Co 2p and C 1s core level depth profiles

In order to assess the extent to which reoxidation proceeds, depth profiling was performed. The results are given in **Figure 6**, **Figure S4**, and **Figure S5**. As described before, the oxidation of metallic cobalt takes already place at RT and the CoO phase is present in addition to metallic cobalt. Evaluation of depth profile data shows that the deeper (near)surface layers (0.8-1.1 nm) have a higher concentration of metallic cobalt (i.e., 14 and 18% for 0.8 and 1.1 nm, respectively) than the top most surface layer (i.e., 11% for 0.6 nm), suggesting a gradient in oxidation of metallic cobalt with oxidation starting from the surface. Increasing temperature to 200 °C leads to further reoxidation of the outermost surface and subsurface layers, resulting in a decrease of metallic cobalt concentration and an increase of the CoO phase (i.e., 6, 8 and 11% of metallic cobalt for 0.6, 0.8 and 1.1 nm, respectively). At 150 °C the oxidation of metallic cobalt and CoO to Co_3O_4 occurs without significant differences of the Co^{3+} concentration within the probed information depths.

Turning to the results of depth profiling in the C 1s region, it can be seen that, unlike CO-TPR data, the ratio between elementary carbon, carbonates, and CO-Co (Co^{2+}/Co^{3+}) during O_2-TPO does not vary significantly at RT and at 100 °C when the KE changes from 200 eV to 600 eV. In contrast to the depth profiling data at RT and at 100 °C, the depth profiling data at 150 °C demonstrates that the ratio between carbon and carbonates and CO-Co (Co^{2+}/Co^{3+}) changes with depth. The relative amount of elementary carbon at 150 °C is higher at the top two surface layers (0.6 nm) (40%), whereas at 1.1 nm the relative concentration of carbon decreases to 34%, indicating possible segregation of elementary carbon toward the surface.
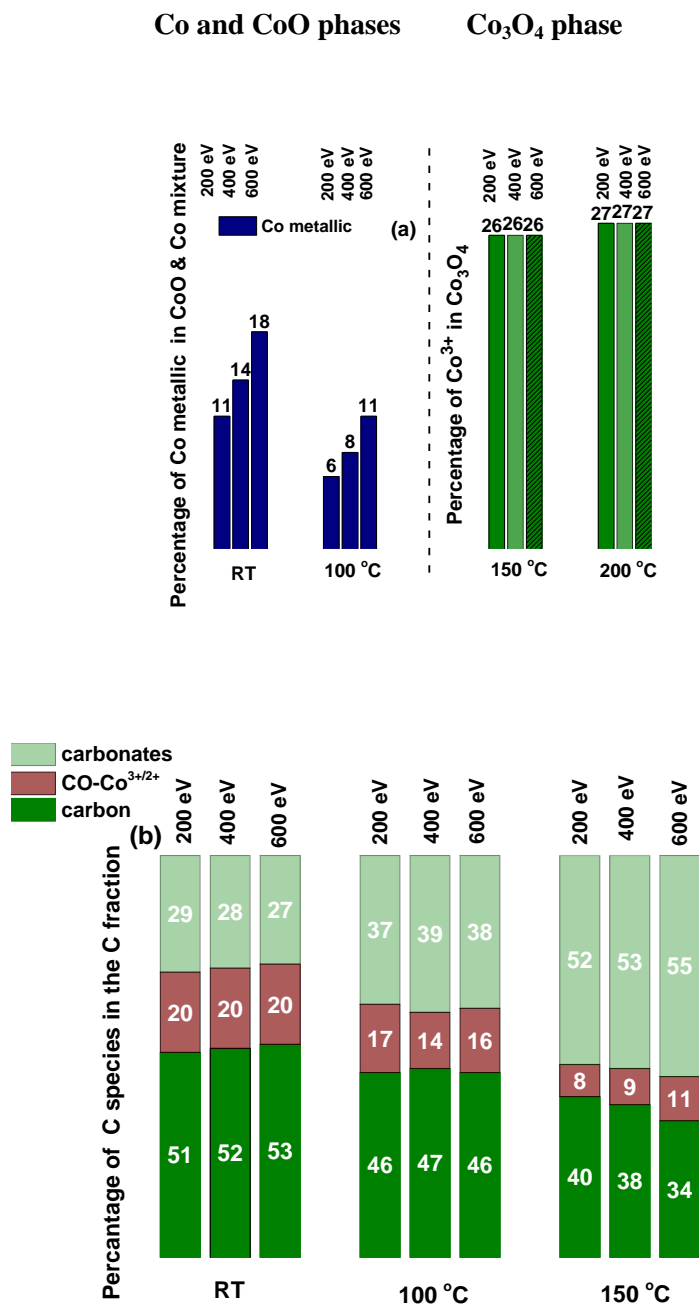
Figure 6. In situ depth profile NAP-XPS during O_2-temperature programmed oxidation (0.15 mbar O_2): (a) the Co 2p region with $h\nu = 1015$ eV, $h\nu = 1215$ eV, and $h\nu = 1415$ eV that results in ~0.6 nm, 0.8 nm, and 1.1 nm inelastic-mean-free path for Co, respectively: (b) the C 1s region with $h\nu = 465$ eV, $h\nu = 665$ eV, and $h\nu = 865$ eV that results in ~0.6 nm, 0.8 nm, and 1.1 nm inelastic-mean-free path for C, respectively.

3.3.2.3 O_2-TPO: VALENCE BAND SPECTRA

By examining the evolution of the valence band, the surface changes during reoxidation were monitored. The results, shown in **Figure 7**, indicate also the reoxidation of metallic cobalt already at RT (**Figure 7a**). The VB spectrum recorded at RT in O_2 is similar to the VB spectrum recorder at 250 °C in CO, where CoO was formed. The shape of VB spectra at RT and 100 °C in O_2 are similar to that at 250 °C in CO atmosphere when the main phase is CoO. This is to be expected and correlates well with the Co 2p core level results. At 150 °C the VB spectrum in O_2 changes the features and becomes typical for Co_3O_4; however, further heating to 200 °C in O_2 leads to the increase of the Co^{3+} t_{2g} feature, indicating a stronger oxidation. When comparing VB spectra at 150 °C in O_2 with spectra at 150 and 200 °C in CO, the differences in intensities are observed (**Figure 7b**) even though all three spectra are characteristic of Co_3O_4. Although the differences in the intensity of Co^{3+} t_{2g} also might account for the different atmospheres because of the different cross section effects, the relative ratio between Co^{3+} t_{2g} and the satellite peak at ~10 eV (see shaded areas in **Figure 7b**) is an indication of changes occurring under reducing and oxidizing atmosphere. The satellite feature at ~10 eV is much more pronounced with respect to Co^{3+} t_{2g} for the VB spectrum in CO atmosphere at 200 °C and 150 °C than for the spectrum in O_2 at 150 °C. On the basis of this observation, it can be concluded that the reduction of cobalt oxide and the reoxidation of metallic cobalt do not coincide in temperatures.
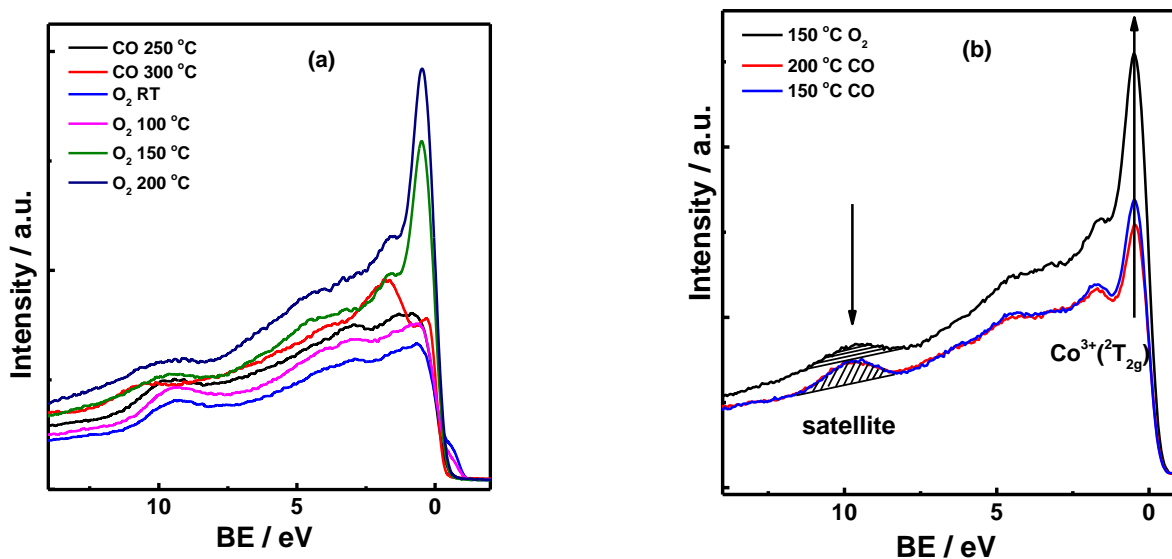
Figure 7. In situ NAP-XPS during O_2-temperature programmed oxidation (0.15 mbar O_2): (a) valence band (hν = 200 eV) RT-250 °C; (b) valence band (hν = 200 eV) spectra during O_2-TPO at 150 °C and CO-TPR at 200 °C and 150 °C.

3.3.2.4 O₂-TPO: NEXAFS AT THE CoL₃,₂

To monitor the structural changes upon O_2 reoxidation, the TEY CoL$_{3,2}$ spectra as a function of X-ray photon energy were taken and are shown in **Figure 8**.
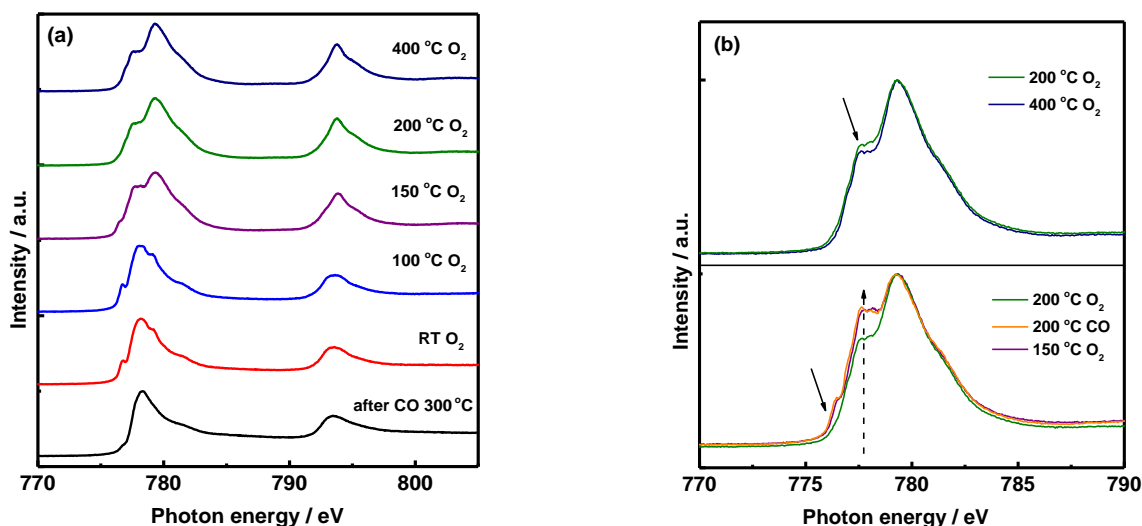
Figure 8. NEXAFS spectra at the Co L$_{3,2}$ edge: (a) during O$_2$-temperature programmed oxidation (0.15 mbar) RT-400 °C; (b) comparison of NEXAFS spectra at the Co L$_{3,2}$ edge during O$_2$-temperature programmed oxidation (0.15 mbar) at 150, 200, and 400 °C and during CO-temperature programmed reduction (0.15 mbar) at 200 °C.

The spectral shape as well as the energy peak position is changed when the atmosphere is switched from CO to O_2 even at RT, indicating oxidation of metallic cobalt not only at the surface but also on the subsurface, which is in agreement with the data from the Co 2p core level region. The shoulder at 777 eV that appears in the NEXAFS spectrum at RT is typical for Co^{2+} in an Oh coordination environment. This is a strong indication that the reoxidation evolves up to 5 nm in depth at RT. When comparing the CoL$_{3,2}$ spectrum at RT with that at 100 °C, no obvious changes can be observed at first glance. However, further heating in O_2 up to 150 °C causes the shift of the most intense peak to the higher photon energy (779 eV) and the spectral features become similar to that of Co₃O₄ (**Figure 8a**). It should be pointed out that the relative intensities between peaks at 779 eV and 778 eV for the spectrum at 150 °C are lower than those of the spectra at 200 or 400 °C (**Figure 8b**). This is a sign of the incomplete oxidation of cobalt oxide to Co₃O₄ at 150 °C. Moreover, the small shoulder at 777 eV, which is commonly associated with Co^{2+} in an Oh coordination environment for CoO, is still present, indicating the presence of Co^{2+} for the CoO

structure together with Co_3O_4. This provides direct and conclusive evidence that cobalt oxide is not yet fully oxidized at 150 °C, and only the top surface layers are oxidized to Co_3O_4, as revealed with the VB and the Co 2p spectra (KE = 200 eV). When the temperature reaches 200 °C, the feature characteristic of Co^{2+} in CoO disappears, and the shape of the spectrum is typical for Co_3O_4.

To reveal the structural changes, the NEXAFS spectra at 150, 200, and 400 °C in O_2 are plotted together with the spectrum at 200 °C in CO (**Figure 8b**). Firstly, by comparing the $CoL_{3,2}$ spectrum in CO atmosphere at 200 °C, where the cobalt phase is CoO_x, with spectra in O_2 at 150 °C and 200 °C, one can see that the NEXAFS $CoL_{3,2}$ spectrum in CO atmosphere at 200 °C is identical to one in O_2 at 150 °C. This reveals that subsurface reduction-reoxidation temperatures do not coincide. Furthermore, a comparison of $CoL_{3,2}$ spectra at 200 °C and 400 °C in O_2 shows the decrease in the feature at 778 eV with the increase of temperature, indicating further oxidation of cobalt oxide at 400 °C. Interestingly, when comparing the reduction at 200 °C and oxidation at 150 °C, the NEXAFS spectra are the same, but information obtained from the most top surface layers (i.e., valence band and the Co 2p XPS with KE of 200 eV) is different. At 150 °C in O_2 the two top surface layers are already reoxidized to Co_3O_4. Thus, the top surface layers are reoxidized, whereas there is a delay in the bulk oxidation, and higher temperatures are needed to oxidize also the bulk (i.e., gradual reoxdation).

3.4 DISCUSSION

The data obtained by combination of synchrotron-based photoemission core level, valence band, and NEXAFS spectra that correspond to the different information depths (i.e., valence band (the outermost surface layers), core level XPS together with depth profiling (~0.6 - 1.1 nm), NEXAFS at the Co $L_{3,2}$ edge in the total electron yield mode (~2.5-5 nm)) allows us to obtain valuable insights into surface and subsurface chemistry of cobalt oxide during CO-TPR and O_2-TPO. To simplify the discussion of obtained results, the following five ranges for CO-TPR and O_2-TPO are defined: 1) CO: RT-200 °C; 2) CO: 200-250 °C; 3) CO: 250-300 °C; 4) O_2: RT; 5) O_2: RT-200 °C (**Scheme 1**).

CO: RT-200 °C: Our core level Co 2p XPS data along with valence band spectra suggest that the surface reduction of Co_3O_4 in CO starts already at RT and progresses with temperature increase. NEXAFS spectra at the $CoL_{3,2}$ edge, which probes approximately ~5 nm of a sample depth, indicate minor structural changes of Co_3O_4 in CO starting at 100 °C, whereas more severe changes of the cobalt oxide structure are seen at 200 °C. Thus, the information obtained from XPS and complemented by NEXAFS demonstrates an ease of surface and near-surface Co_3O_4 reduction in CO atmosphere that is accompanied by the formation of oxygen vacancies: surface oxygen vacancies (RT-150 °C); oxygen vacancies created by mobility of bulk oxygen (starting from 200 °C).

The role of oxygen vacancies is widely discussed in the literature for CO oxidation on cobalt oxides, suggesting the lattice oxygen extraction to be one of the reaction steps.[10, 42] However, reported statements do not have solid experimental proves although numerous theoretical works support the oxygen vacancies formation and the redox Mars-van Krevelen mechanism on cobalt oxide catalysts.[56][57][58][59] Taking into account the results of this study, which reveal the formation of oxygen vacancies upon interaction of CO with Co_3O_4, it is assumed that the reduction of Co^{3+} to Co^{2+} might be one of the reaction steps of the CO oxidation reaction mechanism.

Apart from the role of oxygen vacancies, attention should be paid to the evolution of carbon containing species in the C 1s region, which can give a hint about reaction pathways involved in the CO oxidation mechanism. As it has already been noted, in the C 1s region carbonates, CO adsorption to cobalt cations (e.g., Co^{2+} or Co^{3+}), and atomic carbon at RT are observed. The later indicates that CO dissociation takes place. While carbonate formation is well documented in the literature for cobalt-based catalysts upon CO interaction with cobalt oxide or during CO oxidation reaction,[11][46][49] very little is reported on the elementary carbon formation and its role. Our XPS data in the C 1s region clearly indicates formation of carbon on the Co_3O_4 surface during CO exposure. Interestingly, this carbon is an amorphous carbon (C_{alfa}) that might easily be oxidized even without exposure to high temperatures. Notably, the correlation between the increase of carbon concentration and oxygen vacancies (i.e., concentration of Co^{2+}) is clearly seen from our XPS data. Further raise of temperature leads to an increase of elementary carbon as well as reduction of Co_3O_4 to CoO_x and further formation of oxygen vacancies. Thus, it is assumed that when CO interacts with the surface of cobalt oxide it forms first carbonates, extracting further lattice oxygen/forming surface oxygen vacancies. The vacancies that are formed might serve as active sites for further CO and O_2 adsorption and dissociation.

CO: 200-250 °C: The increase of temperature from 200 to 250 °C leads to drastic electronic and geometric changes of cobalt, as indicated by the Co 2p spectrum (i.e., the shift of XPS peak to 780.1 eV and an increase of the satellite feature). The valence band spectrum recorded at 250 °C is very different to the one recorded at 200 °C. Moreover, NEXAFS at the CoL$_{3,2}$ at 250 °C shows that the spectral shape changes entirely, the shift of the edge is seen, indicating clearly the transformation of Co_3O_4 to CoO. Thus, comparing valence band, XPS core level, and NEXAFS spectra at 250 °C, it can be concluded that the reduction of Co_3O_4 to CoO evolves up to 5 nm (i.e., surface and bulk reduction). As mentioned before, the structure of CoO is a mixture of Co^{2+} in two different coordination environments (i.e., Oh and Td), indicating a mixed structural phase of rock-salt-type CoO and metastable wurtzite-type CoO. Meyer *et al.* reported that nanosized CoO cannot be considered as a single structural phase.[60] They found that in CoO films of nanosized thickness two structures of cobalt oxide are present: rock-salt- and wurtzite-type CoO. In the bulk of the nanosized films a rocksalt Oh structure is dominant; while the top four layers are terminated by a thin slab of wurtzite-type Td CoO. The structure type of cobalt oxide and its correlation

with the CO adsorption affinity was discussed in the early work of Yao *et al.* [61] They revealed that CO chemisorption to the Oh coordinated cobalt sites is independent of the oxidation state (i.e., Co^{2+} or Co^{3+}), while the Td coordinated cobalt sites are inactive for CO adsorption.[61]

CO: 250-300 ᵒC: Examination of the Co 2p and C 1s regions at 300 ᵒC shows that cobalt oxide is reduced to metallic cobalt; but, in addition, a small amount of CoO is still present. This is also confirmed by the valence band spectrum and the CoL$_{3,2}$ NEXAFS. The surface is mainly covered with elementary carbon. This elementary carbon is often considered to be one of the causes of metallic cobalt FT catalyst deactivation. It should be noted that no carbide species were observed on the surface of metallic cobalt in our study. The absence of the cobalt carbide phase might be explained by a relatively short time of cobalt exposure to CO (~30 min) and much lower pressure of CO (i.e., 0.15 mbar of CO) compared to realistic FT synthesis conditions (i.e., 230 ᵒC, H_2/CO feed ratio = 2.1, 20 bar). The in situ XRD study of Karaca *et al.* on the evolution of alumina-supported cobalt catalysts under realistic FT conditions revealed formation of cobalt carbide and deactivation of a catalyst after 8-10 h of catalyst exposure to syngas.[20]

O₂: RT: Studying the reoxidation of metallic cobalt is of particular interest to FT catalysis. Firstly, reoxidation of cobalt is considered to be one of the reasons for the FT catalyst deactivation. Secondly, reoxidation of cobalt is one of the steps of FT catalysts regeneration. Deactivation of metallic cobalt during FT synthesis is discussed in the literature mainly with respect to the oxidation of metallic cobalt with water. Water that is generated under FT conditions might have a strong impact on the surface chemistry of FT catalysts and serves as an oxidation agent. Although FT catalysts under operation conditions are not exposed to O_2, the exposure of metallic cobalt to O_2 at RT, especially at very low pressure (i.e., 0.15 mbar O_2) and monitoring the evolution of its oxidation state could be useful in further understanding of cobalt reoxidation and deactivation of FT catalysts under realistic conditions.

Notwithstanding that many studies have already been performed to unravel the influence of H_2O on the oxidation of metallic cobalt, there are no consistent conclusions. For example, the in situ XAS study of Saib *et al.* on the oxidation of the planar Co/SiO₂/Si(100) model catalyst showed that there is no surface oxidation of metallic cobalt under model FT conditions (i.e., H_2/H_2O = 1, P_{total} = 0.4 mbar, 150-400 ᵒC), whereas the complete oxidation of metallic cobalt was observed at 450 ᵒC in the presence of H_2O.[18] Another study of FT catalyst deactivation on the powder CoRe/Al₂O₃ catalyst, employing temperature programmed reduction and thermogravimetric experiments, demonstrates only a small extent of bulk oxidation for cobalt at H_2O/H_2 = 10, whereas in sharp contrast, the XPS data revealed a significant surface oxidation of this catalyst even at H_2O/H_2 = 0.25.[32] This illustrates the importance of in situ surface studies when catalytic applications are considered. Also the theoretical study of Huo *et al.* on the oxidation of the Co(0001) surface under realistic FT synthesis conditions demonstrates that Co(0001) can be oxidized by water forming a ¼ monolayer oxygen-covered surface, whereas the subsurface oxidation (1/2 monolayers) is thermodynamically not possible.[33] As shown above, the surface oxidation of metallic

cobalt is markedly different from the bulk. Therefore, it is not surprising that a clear understanding of metallic cobalt reoxidation/deactivation of FT catalysts is still lacking because of the lack of data that reveal surface information.

O$_2$: RT-200 °C: Heating the catalyst in O$_2$ atmosphere results in the oxidation of metallic cobalt to cobalt oxide. The existence of two cobalt phases (i.e., CoO and metellic cobalt) at RT and at 100 °C is revealed by the Co 2p XPS as well as by NEXAFS at the Co L$_{3,2}$ edge. While the Co 2p and valence band spectra demonstrate that cobalt phase is Co$_3$O$_4$ at 150 °C, the NEXAFS that probes up to 5 nm reveals a coexistence of CoO and Co$_3$O$_4$ phases. The simultaneous presence of metallic cobalt and CoO at RT and 100 °C, as well as CoO and Co$_3$O$_4$ at 150 °C, might be evidence of a coexistence of different particle sizes of cobalt oxide that undergo oxidation differently. From the literature it is known that different particle sizes lead to different reduction and oxidation profiles; the smaller nanoparticles undergo oxidation more easily.[62] Also it might be the case that the oxidation of metallic cobalt is kinetically controlled and a longer time of exposure to O$_2$ is needed to obtain CoO phase at 100 °C. Interestingly, in the case of reduction in CO atmosphere, from Co$_3$O$_4$ to CoO no differences were observed in the reduction profile (i.e., no simultaneous presence of Co$_3$O$_4$ and CoO, indicating a possibility of different particle size). Moreover, the depth profile XPS on the Co 2p demonstrates an increase of metallic cobalt with an increase of the probing depth at RT in O$_2$ as well as at 100 °C. This might suggest that a core-shell structure (i.e., core-metallic cobalt, shell-cobalt oxide) is formed upon oxidation of metallic cobalt. Recently a spontaneous formation of hollow cobalt oxide nanoparticles/core-shell structure at RT at a water-air interface or in air atmosphere has been intensively discussed in the literature in terms of the metallic cobalt FT catalysts reoxidation/regeneration.[34 35 36 37 63] Such oxidation behavior of metallic cobalt was attributed to the Kirkendall effect that occurs as a result of different diffusion rates of oxygen and cobalt atoms.

At 200 °C the catalyst structure is completely recovered to Co$_3$O$_4$. Co$_3$O$_4$ is present on the surface and in the bulk, as confirmed by the combination of XPS, valence band and NEXAFS; moreover, no carbon and carbonates are present on the surface. The ease of elementary carbon reoxidation indicates that the reoxidation of carbon could be one of the reaction pathways of CO oxidation. Moreover, the ease of the cobalt oxide reoxidation hypothesizes the possibility of the Mars-van Krevelen mechanism for cobalt oxide materials for CO oxidation reaction. Further study on the CO oxidation (i.e., in the presence of CO and O$_2$) as well as cycling experiments together with the detailed FTIR spectroscopy studies that can help to clarify this hypothesis will be presented in **Chapter 4**.
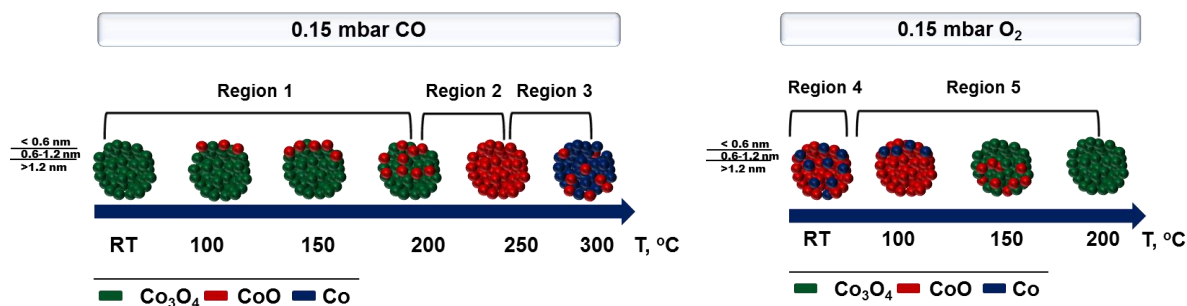
Scheme 1. Schematic representation of CO-TPR (0.15 mbar CO) for Co_3O_4 followed by O_2-TPO (0.15 mbar O_2).

Our study firmly demonstrates that upon interaction of CO with Co_3O_4, even at RT, carbonates and elementary carbon are formed, and Co_3O_4 undergoes minor reduction at the most top surface layers as it is seen from valence band spectra that have higher sensitivity than core-level spectra. During heating to 150 ^{o}C in CO, the amount of elementary carbon is increased, whereas Co_3O_4 is further reduced, indicating progressive oxygen vacancies formation mainly on the most top surface layers as revealed by valence band spectra and Co 2p core level XPS with KE = 200 eV. At 200 ^{o}C the mobility of lattice oxygen occurs/bulk reduction as it is seen from NEXAFS and Co 2p core level XPS with KE = 600 eV. At 250 ^{o}C the interconversion of Co_3O_4 to CoO takes place, and CoO that is formed has Co^{2+} in both Oh and Td coordination environments, indicating a coexistence of rock-salt-type CoO and metastable wurtzite-type CoO structures in nearsurface (~ 3-5 nm). At 300 ^{o}C the main phase is metallic cobalt covered with elementary carbon. Exposure of metallic cobalt at RT to O_2 causes its gradual reoxidation to CoO and the decrease of elementary carbon, whereas heating in O_2 atmosphere to 200 ^{o}C leads to the oxidation of cobalt phase (i.e., surface and subsurface) to Co_3O_4 and removal of carbon containing species from the surface. Combination of valence band spectra that have higher sensitivity than core-level spectra, with core level XPS including depth profiles and NEXAFS reveals that the reduction of cobalt oxide and the reoxidation of cobalt metallic do not coincide in temperatures.

3.5 CONCLUSIONS

Taking advantage of combined in situ NAP-XPS, including valence band, depth profile and NEXAFS at the Co $L_{3,2}$ edge, the reducibility of Co_3O_4 in CO and its reoxidation in O_2 atmospheres was investigated in terms of (near)surface electronic and structural changes of Co_3O_4, adsorbates and oxygen vacancies ($V_{O^{..}}$) evolution. The results obtained by combining information from different information depths allowed distinguishing surface oxygen vacancy formation during reduction of Co_3O_4 in CO atmosphere (RT-150 ^{o}C) from the oxygen vacancies created by mobility of bulk lattice oxygen (200-250 ^{o}C). Additionally formation of a mixed phase of rocksalt-type CoO and metastable wurtzite-type CoO in near-surface (~ 3-5 nm) during reduction of Co_3O_4 in CO atmosphere at 250 ^{o}C were identified. Combination of valence band spectra that have higher sensitivity than core-level spectra, with core level XPS including depth profiles and NEXAFS revealed that the reduction of cobalt oxide and the reoxidation of metallic cobalt do not coincide in temperatures. In summary, the results highlight a great potential of the combined in situ NAP-XPS and NAXAFS for studying the (near)surface changes of catalytic materials in terms of different depth profile information.

Based on the results obtained in this study it is suggested that CO adsorbs on Co_3O_4, extracting lattice oxygen and forming carbonates and surface oxygen vacancies that might serves as additional sites for CO and O_2 adsoption and dissociation. In addition, oxidation of elementary carbon and carbonates also might contribute to the CO oxidation reaction cycle. The ease of metallic cobalt reoxidation even at RT only in 0.15 mbar O_2 calls for further studies of FT catalyst deactivation under oxidation conditions using surface sensitive techniques. It is expected that these findings will enhance the fundamental understanding of CO oxidation on cobalt oxide catalysts as well as contribute to the research area of FT catalysts deactivation and regeneration under oxidizing conditions. Moreover, the approach used in the current study should stimulate researchers to investigate catalytic reactions using combined in situ NAP-XPS and NEXAFS for obtaining electronic and structural information on the different information depth.

3.6 REFERENCES

1.   Li, L.; Liu, M.; He, S.; Chen, W., Freestanding 3D Mesoporous Co₃O₄@Carbon Foam Nanostructures for Ethanol Gas Sensing. *Analytical Chemistry* **2014,** *86* (15), 7996-8002.
2.   Whittingham, M. S., Lithium Batteries and Cathode Materials. *Chemical Reviews* **2004,** *104* (10), 4271-4302.
3.   Qiu, W.; Chang, L.; Lee, D.; Dannangoda, C.; Martirosyan, K.; Litvinov, D., Patterning of Magnetic Thin Films and Multilayers Using Nanostructured Tantalum Gettering Templates. *ACS Applied Materials & Interfaces* **2015,** *7* (11), 6014-6018.
4.   László I. Simándi, Catalytic oxidations using cobalt(II) complexes Catalysis by Metal Complexes. *In Advances in Catalytic Activation of Dioxygen by Metal Complexes* **2002,** *26*, pp 265-328
5.   Khodakov, A. Y., Fischer-Tropsch synthesis: Relations between structure of cobalt catalysts and their catalytic performance. *Catalysis Today* **2009,** *144* (3), 251-257.
6.   den Breejen, J. P.; Sietsma, J. R. A.; Friedrich, H.; Bitter, J. H.; de Jong, K. P., Design of supported cobalt catalysts with maximum activity for the Fischer–Tropsch synthesis. *Journal of Catalysis* **2010,** *270* (1), 146-152.
7.   Liang, Y.; Wang, H.; Diao, P.; Chang, W.; Hong, G.; Li, Y.; Gong, M.; Xie, L.; Zhou, J.; Wang, J.; Regier, T. Z.; Wei, F.; Dai, H., Oxygen Reduction Electrocatalyst Based on Strongly Coupled Cobalt Oxide Nanocrystals and Carbon Nanotubes. *Journal of the American Chemical Society* **2012,** *134* (38), 15849-15857.
8.   Maiyalagan, T.; Jarvis, K. A.; Therese, S.; Ferreira, P. J.; Manthiram, A., Spinel-type lithium cobalt oxide as a bifunctional electrocatalyst for the oxygen evolution and oxygen reduction reactions. *Nat Commun* **2014,** *5*.
9.   Papadopoulou, E.; Ioannides, T., Steam reforming of methanol over cobalt catalysts: Effect of cobalt oxidation state. *International Journal of Hydrogen Energy* **2015,** *40* (15), 5251-5255.
10.   Xie, X.; Li, Y.; Liu, Z.-Q.; Haruta, M.; Shen, W., Low-temperature oxidation of CO catalysed by Co₃O₄ nanorods. *Nature* **2009,** *458* (7239), 746-749.
11.   Jia, C.-J.; Schwickardi, M.; Weidenthaler, C.; Schmidt, W.; Korhonen, S.; Weckhuysen, B. M.; Schüth, F., Co₃O₄–SiO₂ Nanocomposite: A Very Active Catalyst for CO Oxidation with Unusual Catalytic Behavior. *Journal of the American Chemical Society* **2011,** *133* (29), 11279-11288.
12.   Al-Zeghayer, Y. S.; Sunderland, P.; Al-Masry, W.; Al-Mubaddel, F.; Ibrahim, A. A.; Bhartiya, B. K.; Jibril, B. Y., Activity of CoMo/γ-Al₂O₃ as a catalyst in hydrodesulfurization: effects of Co/Mo ratio and drying condition. *Applied Catalysis A: General* **2005,** *282* (1–2), 163-171.
13.   Marbán, G.; López, I.; Valdés-Solís, T.; Fuertes, A. B., Highly active structured catalyst made up of mesoporous Co₃O₄ nanowires supported on a metal wire mesh for the preferential oxidation of CO. *International Journal of Hydrogen Energy* **2008,** *33* (22), 6687-6695.
14.   Teng, Y.; Sakurai, H.; Ueda, A.; Kobayashi, T., Oxidative removal of co contained in hydrogen by using metal oxide catalysts. *International Journal of Hydrogen Energy* **1999,** *24* (4), 355-358.
15.   Tian, Z.; Bahlawane, N.; Qi, F.; Kohse-Höinghaus, K., Catalytic oxidation of hydrocarbons over Co₃O₄ catalyst prepared by CVD. *Catalysis Communications* **2009,** *11* (2), 118-122.
16.   Rytter, E.; Holmen, A., Deactivation and Regeneration of Commercial Type Fischer-Tropsch Co-Catalysts—A Mini-Review. *Catalysts* **2015,** *5* (2), 478.
17.   Tsakoumis, N. E.; Rønning, M.; Borg, Ø.; Rytter, E.; Holmen, A., Deactivation of cobalt based Fischer–Tropsch catalysts: A review. *Catalysis Today* **2010,** *154* (3–4), 162-182.
18.   Saib, A. M.; Moodley, D. J.; Ciobîcă, I. M.; Hauman, M. M.; Sigwebela, B. H.; Weststrate, C. J.; Niemantsverdriet, J. W.; van de Loosdrecht, J., Fundamental understanding of deactivation and regeneration of cobalt Fischer–Tropsch synthesis catalysts. *Catalysis Today* **2010,** *154* (3–4), 271-282.
19.   Scalbert, J.; Legens, C.; Clemencon, I.; Taleb, A. L.; Sorbier, L.; Diehl, F., Multiple and antagonistic effects of water on intrinsic physical properties of model Fischer-Tropsch cobalt catalysts evidenced by in situ X-ray diffraction. *Chemical Communications* **2014,** *50* (58), 7866-7869.
20.   Karaca, H.; Hong, J.; Fongarland, P.; Roussel, P.; Griboval-Constant, A.; Lacroix, M.; Hortmann, K.; Safonova, O. V.; Khodakov, A. Y., In situ XRD investigation of the evolution of alumina-supported cobalt catalysts under realistic conditions of Fischer-Tropsch synthesis. *Chemical Communications* **2010,** *46* (5), 788-790.
21.   Passos, A. R.; Martins, L.; Pulcinelli, S. H.; Santilli, C. V.; Briois, V., Effect of the balance between Co(II) and Co(0) oxidation states on the catalytic activity of cobalt catalysts for Ethanol Steam Reforming. *Catalysis Today* **2014,** *229*, 88-94.
22.   Sun, J.; Karim, A. M.; Mei, D.; Engelhard, M.; Bao, X.; Wang, Y., New insights into reaction mechanisms of ethanol steam reforming on Co–ZrO₂. *Applied Catalysis B: Environmental* **2015,** *162*, 141-148.
23.   Wang, C.-B.; Lee, C.-C.; Bi, J.-L.; Siang, J.-Y.; Liu, J.-Y.; Yeh, C.-T., Study on the steam reforming of ethanol over cobalt oxides. *Catalysis Today* **2009,** *146* (1–2), 76-81.
24.   Garces, L. J.; Hincapie, B.; Zerger, R.; Suib, S. L., The Effect of Temperature and Support on the Reduction of Cobalt Oxide: An in Situ X-ray Diffraction Study. *The Journal of Physical Chemistry C* **2015,** *119* (10), 5484-5490.

25.   du Plessis, H. E.; Forbes, R. P.; Barnard, W.; Erasmus, W. J.; Steuwer, A., In situ reduction study of cobalt model Fischer-Tropsch synthesis catalysts. *Physical Chemistry Chemical Physics* **2013,** *15* (28), 11640-11645.

26.   Bazin, D.; Kovács, I.; Guczi, L.; Parent, P.; Laffon, C.; De Groot, F.; Ducreux, O.; Lynch, J., Genesis of Co/SiO₂ Catalysts: XAS Study at the Cobalt LIII,II Absorption Edges. *Journal of Catalysis* **2000,** *189* (2), 456-462.

27.   Zheng, F.; Alayoglu, S.; Guo, J.; Pushkarev, V.; Li, Y.; Glans, P.-A.; Chen, J.-l.; Somorjai, G., In-situ X-ray Absorption Study of Evolution of Oxidation States and Structure of Cobalt in Co and CoPt Bimetallic Nanoparticles (4 nm) under Reducing (H₂) and Oxidizing (O₂) Environments. *Nano Letters* **2011,** *11* (2), 847-853.

28.   Potoczna-Petru, D.; Kępiński, L., Reduction study of Co₃O₄ model catalyst by electron microscopy. *Catalysis Letters* **2001,** *73* (1), 41-46.

29.   Ward, M. R.; Boyes, E. D.; Gai, P. L., In Situ Aberration-Corrected Environmental TEM: Reduction of Model Co₃O₄ in H₂ at the Atomic Level. *ChemCatChem* **2013,** *5* (9), 2655-2661.

30.   Hu, L.; Sun, K.; Peng, Q.; Xu, B.; Li, Y., Surface active sites on Co₃O₄ nanobelt and nanocube model catalysts for CO oxidation. *Nano Res.* **2010,** *3* (5), 363-368.

31.   Saib, A. M.; Borgna, A.; van de Loosdrecht, J.; van Berge, P. J.; Niemantsverdriet, J. W., In Situ Surface Oxidation Study of a Planar Co/SiO₂/Si(100) Model Catalyst with Nanosized Cobalt Crystallites under Model Fischer–Tropsch Synthesis Conditions. *The Journal of Physical Chemistry B* **2006,** *110* (17), 8657-8664.

32.   Schanke, D.; Hilmen, A. M.; Bergene, E.; Kinnari, K.; Rytter, E.; Ådnanes, E.; Holmen, A., Reoxidation and Deactivation of Supported Cobalt Fischer–Tropsch Catalysts. *Energy & Fuels* **1996,** *10* (4), 867-872.

33.   Huo, C.-F.; Li, Y.-W.; Wang, J.; Jiao, H., Adsorption and Dissociation of CO as Well as CHx Coupling and Hydrogenation on the Clean and Oxygen Pre-covered Co(0001) Surfaces. *The Journal of Physical Chemistry C* **2008,** *112* (10), 3840-3848.

34.   Hauman, M. M.; Saib, A.; Moodley, D. J.; du Plessis, E.; Claeys, M.; van Steen, E., Re-dispersion of Cobalt on a Model Fischer–Tropsch Catalyst During Reduction–Oxidation–Reduction Cycles. *ChemCatChem* **2012,** *4* (9), 1411-1419.

35.   Saib, A. M.; Gauché, J. L.; Weststrate, C. J.; Gibson, P.; Boshoff, J. H.; Moodley, D. J., Fundamental Science of Cobalt Catalyst Oxidation and Reduction Applied to the Development of a Commercial Fischer–Tropsch Regeneration Process. *Industrial & Engineering Chemistry Research* **2014,** *53* (5), 1816-1824.

36.   Weststrate, C. J.; Hauman, M. M.; Moodley, D. J.; Saib, A. M.; van Steen, E.; Niemantsverdriet, J. W., Cobalt Fischer–Tropsch Catalyst Regeneration: The Crucial Role of the Kirkendall Effect for Cobalt Redispersion. *Top Catal* **2011,** *54* (13-15), 811-816.

37.   Ha, D.-H.; Moreau, L. M.; Honrao, S.; Hennig, R. G.; Robinson, R. D., The Oxidation of Cobalt Nanoparticles into Kirkendall-Hollowed CoO and Co₃O₄: The Diffusion Mechanisms and Atomic Structural Transformations. *The Journal of Physical Chemistry C* **2013,** *117* (27), 14303-14312.

38.   Akgül, G.; Aksoy, F.; Bozduman, A.; Ozkendir, O. M.; Ufuktepe, Y.; Lüning, J., Study of the L₂,₃ edges of 3d transition metals by X-ray absorption spectroscopy. *Thin Solid Films* **2008,** *517* (2), 1000-1004.

39.   Hahner, G., Near edge X-ray absorption fine structure spectroscopy as a tool to probe electronic and structural properties of thin organic films and liquids. *Chemical Society Reviews* **2006,** *35* (12), 1244-1255.

40.   Grosvenor, A. P.; Wik, S. D.; Cavell, R. G.; Mar, A., Examination of the Bonding in Binary Transition-Metal Monophosphides MP (M = Cr, Mn, Fe, Co) by X-Ray Photoelectron Spectroscopy. *Inorganic Chemistry* **2005,** *44* (24), 8988-8998.

41.   Biesinger, M. C.; Payne, B. P.; Grosvenor, A. P.; Lau, L. W. M.; Gerson, A. R.; Smart, R. S. C., Resolving surface chemical states in XPS analysis of first row transition metals, oxides and hydroxides: Cr, Mn, Fe, Co and Ni. *Applied Surface Science* **2011,** *257* (7), 2717-2730.

42.   Jansson, J., Low-Temperature CO Oxidation over Co₃O₄/Al₂O₃. *Journal of Catalysis* **2000,** *194* (1), 55-60.

43.   Zafeiratos, S.; Dintzer, T.; Teschner, D.; Blume, R.; Hävecker, M.; Knop-Gericke, A.; Schlögl, R., Methanol oxidation over model cobalt catalysts: Influence of the cobalt oxidation state on the reactivity. *Journal of Catalysis* **2010,** *269* (2), 309-317.

44.   Wolfbeisser, A.; Klotzer, B.; Mayr, L.; Rameshan, R.; Zemlyanov, D.; Bernardi, J.; Fottinger, K.; Rupprechter, G., Surface modification processes during methane decomposition on Cu-promoted Ni-ZrO₂ catalysts. *Catalysis Science & Technology* **2015,** *5* (2), 967-978.

45.   Feng, Z. A.; Machala, M. L.; Chueh, W. C., Surface electrochemistry of CO₂ reduction and CO oxidation on Sm-doped CeO₂₋ₓ: coupling between Ce³⁺ and carbonate adsorbates. *Physical Chemistry Chemical Physics* **2015,** *17* (18), 12273-12281.

46.   Ferstl, P.; Mehl, S.; Arman, M. A.; Schuler, M.; Toghan, A.; Laszlo, B.; Lykhach, Y.; Brummel, O.; Lundgren, E.; Knudsen, J.; Hammer, L.; Schneider, M. A.; Libuda, J., Adsorption and Activation of CO on Co₃O₄(111) Thin Films. *The Journal of Physical Chemistry C* **2015,** *119* (29), 16688-16699.

47.   Shchukarev, A. V.; Korolkov, D. V., XPS Study of group IA carbonates. *cent.eur.j.chem.* **2004,** *2* (2), 347-362.

48.   Ramsvik, T.; Borg, A.; Kildemo, M.; Raaen, S.; Matsuura, A.; Jaworowski, A. J.; Worren, T.; Leandersson, M., Molecular vibrations in core-ionised CO adsorbed on Co(0 0 0 1) and Rh(1 0 0). *Surface Science* **2001,** *492* (1–2), 152-160.

49.   Jansson, J.; Skoglundh, M.; Fridell, E.; Thormählen, P., A Mechanistic Study of Low Temperature CO Oxidation over Cobalt Oxide. *Topics in Catalysis* **2001,** *16-17* (1-4), 385-389.

50.   Argyle, M.; Bartholomew, C., Heterogeneous Catalyst Deactivation and Regeneration: A Review. *Catalysts* **2015,** *5* (1), 145.

51.   Langell, M. A.; Anderson, M. D.; Carson, G. A.; Peng, L.; Smith, S., Valence-band electronic structure of Co₃O₄ epitaxy on CoO(100). *Physical Review B* **1999,** *59* (7), 4791-4798.

52.   Hofmann, T.; Yu, T. H.; Folse, M.; Weinhardt, L.; Bär, M.; Zhang, Y.; Merinov, B. V.; Myers, D. J.; Goddard, W. A.; Heske, C., Using Photoelectron Spectroscopy and Quantum Mechanics to Determine d-Band Energies of Metals for Catalytic Applications. *The Journal of Physical Chemistry C* **2012,** *116* (45), 24016-24026.

53.   Morales, F.; de Groot, F. M. F.; Glatzel, P.; Kleimenov, E.; Bluhm, H.; Hävecker, M.; Knop-Gericke, A.; Weckhuysen, B. M., In Situ X-ray Absorption of Co/Mn/TiO₂ Catalysts for Fischer−Tropsch Synthesis. *The Journal of Physical Chemistry B* **2004,** *108* (41), 16201-16207.

54.   Kobayashi, M.; Ishida, Y.; Hwang, J. l.; Mizokawa, T.; Fujimori, A.; Mamiya, K.; Okamoto, J.; Takeda, Y.; Okane, T.; Saitoh, Y.; Muramatsu, Y.; Tanaka, A.; Saeki, H.; Tabata, H.; Kawai, T., Characterization of magnetic components in the diluted magnetic semiconductor Zn₁₋ₓCoₓO by x-ray magnetic circular dichroism. *Physical Review B* **2005,** *72* (20), 201201.

55.   Papaefthimiou, V.; Dintzer, T.; Dupuis, V.; Tamion, A.; Tournus, F.; Hillion, A.; Teschner, D.; Hävecker, M.; Knop-Gericke, A.; Schlögl, R.; Zafeiratos, S., Nontrivial Redox Behavior of Nanosized Cobalt: New Insights from Ambient Pressure X-ray Photoelectron and Absorption Spectroscopies. *ACS Nano* **2011,** *5* (3), 2182-2190.

56.   Wang, H.-F.; Kavanagh, R.; Guo, Y.-L.; Guo, Y.; Lu, G.; Hu, P., Origin of extraordinarily high catalytic activity of Co₃O₄ and its morphological chemistry for CO oxidation at low temperature. *Journal of Catalysis* **2012,** *296*, 110-119.

57.   Broqvist, P.; Panas, I.; Persson, H., A DFT Study on CO Oxidation over Co₃O₄. *Journal of Catalysis* **2002,** *210* (1), 198-206.

58.   Jiang, D.-e.; Dai, S., The role of low-coordinate oxygen on Co₃O₄(110) in catalyticCO oxidation. *Physical Chemistry Chemical Physics* **2011,** *13* (3), 978-984.

59.   Pang, X.-Y.; Liu, C.; Li, D.-C.; Lv, C.-Q.; Wang , G.-C., Structure Sensitivity of CO Oxidation on Co₃O₄: A DFT Study. *ChemPhysChem* **2013,** *14* (1), 204-212.

60.   Meyer, W.; Hock, D.; Biedermann, K.; Gubo, M.; Müller, S.; Hammer, L.; Heinz, K., Coexistence of Rocksalt and Wurtzite Structure in Nanosized CoO Films. *Physical Review Letters* **2008,** *101* (1), 016103.

61.   Yao, H. C.; Shelef, M., Nitric oxide and carbon monoxide chemisorption on cobalt-containing spinels. *The Journal of Physical Chemistry* **1974,** *78* (24), 2490-2496.

62.   Sadasivan, S.; Bellabarba, R. M.; Tooze, R. P., Size dependent reduction-oxidation-reduction behaviour of cobalt oxide nanocrystals. *Nanoscale* **2013,** *5* (22), 11139-11146.

63.   Varon, M.; Ojea-Jimenez, I.; Arbiol, J.; Balcells, L.; Martinez, B.; Puntes, V. F., Spontaneous formation of hollow cobalt oxide nanoparticles by the Kirkendall effect at room temperature at the water-air interface. *Nanoscale* **2013,** *5* (6), 2429-2436.

3.7 SUPPORTING INFORMATION

Table S1. Co 2p spectral fitting parameters: binding energy (eV), FWHM (eV)

Compound	Peak 1, eV	Peak 1 FWHM, eV	Peak 2, eV	Peak 2 FWHM, eV	Peak 3, eV	Peak 3 FWHM, eV	Peak 4, eV	Peak 4 FWHM, eV	Peak 5, eV	Peak 5 FWHM, eV
Co_3O_4	779.4±0.1	1.8±0.1	780.9±0.1	2.0±0.1	782.4±0.1	2.2±0.1	785.6±0.2	6.0±0.2	789.3±0.2	6.2±0.2
CoO	780.0±0.1	2.6±0.1	782.1±0.1	2.7±0.1	785.5±0.1	5.7±0.2	790.1±0.2	6.8±0.2		
Co	778.1±0.1	0.9±0.1	785.5±0.1	5.1±0.2						

The multiplets correspond to the spin-orbit splitting of $2p_{3/2}$ and $2p_{1/2}$ core holes. The spin-orbit splitting is 15.2 eV. The intensity ratio I $2p_{3/2}$/I $2p_{1/2}$ was fixed to 2.

Table S2. C 1s spectral fitting parameters: binding energy (eV), FWHM (eV)

Species	Peak, eV	FWHM, eV
Elementary carbon	284.7±0.1	1.5±0.1
C-O	286.1±0.1	1.1±0.1
Carbonates	288.2±0.1	1.8±0.1
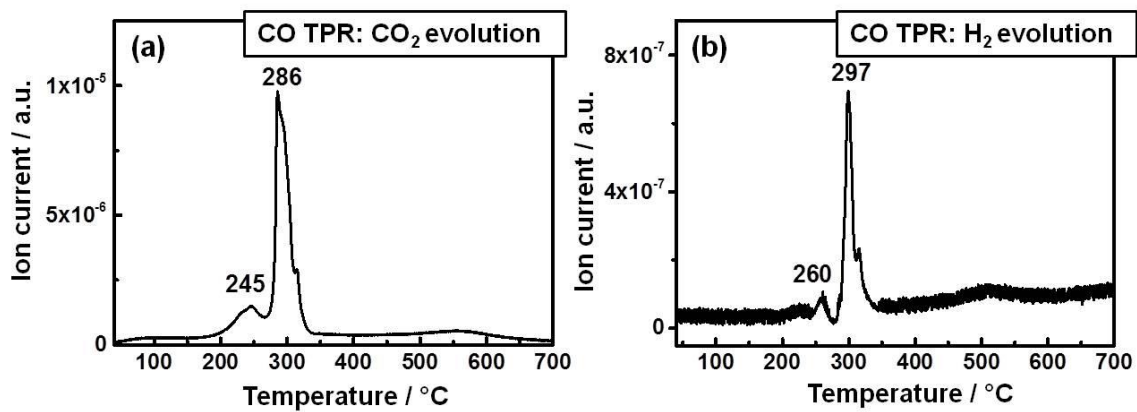
Figure S1. CO-TPR for Co_3O_4 5 vol.% CO in He, total flow 50 mL min^{-1}: (a) CO_2 evolution and (b) H_2 evolution.
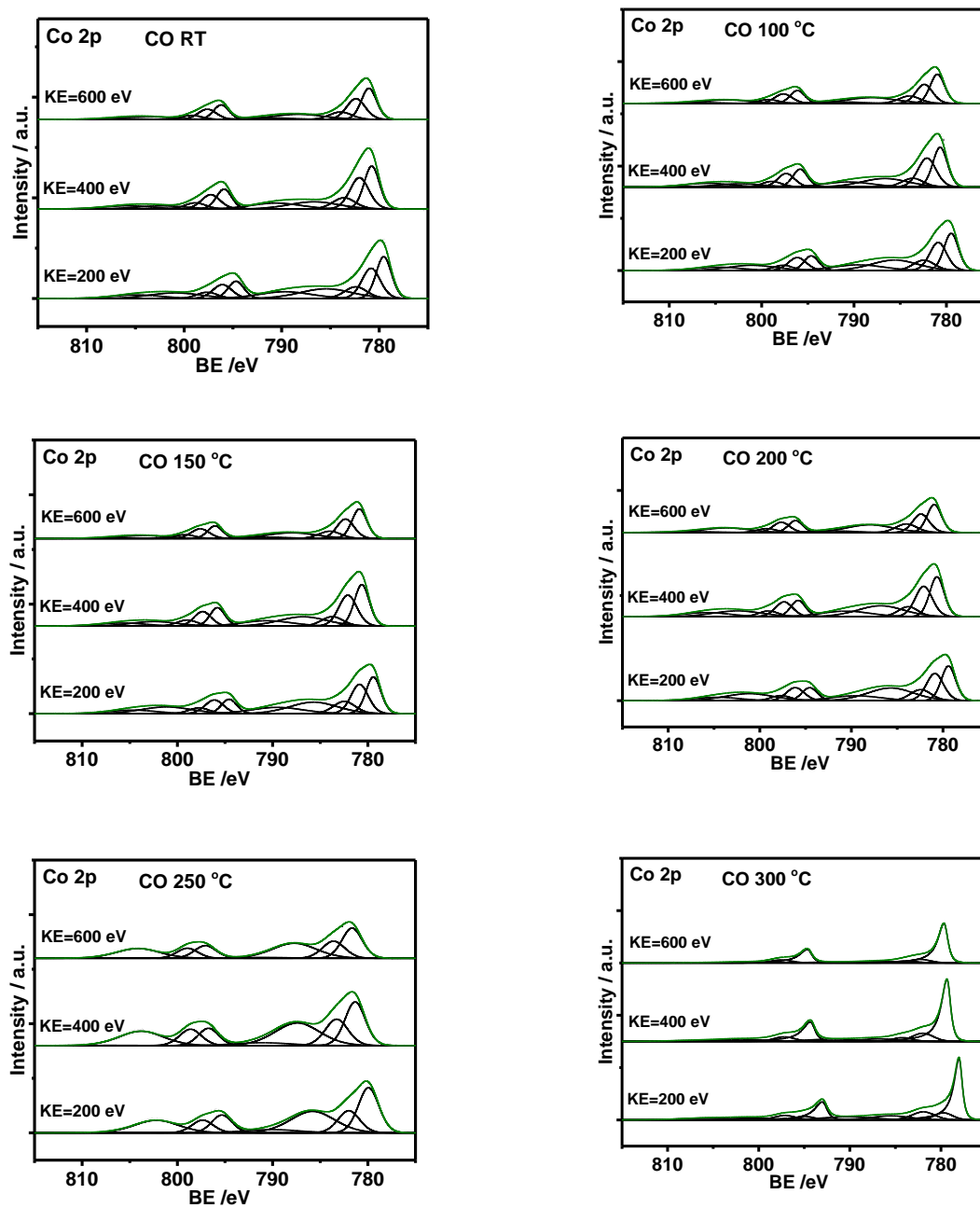
Figure S2. In situ depth profile NAP-XPS during CO-temperature programmed reduction for Co_3O_4 (0.15 mbar): Co 2p region with hν = 1015 eV, hν = 1215 eV, and hν = 1415 eV that results in 0.6.nm, 0.8 nm, and 1.1 nm inelastic-mean-free path for Co, respectively.
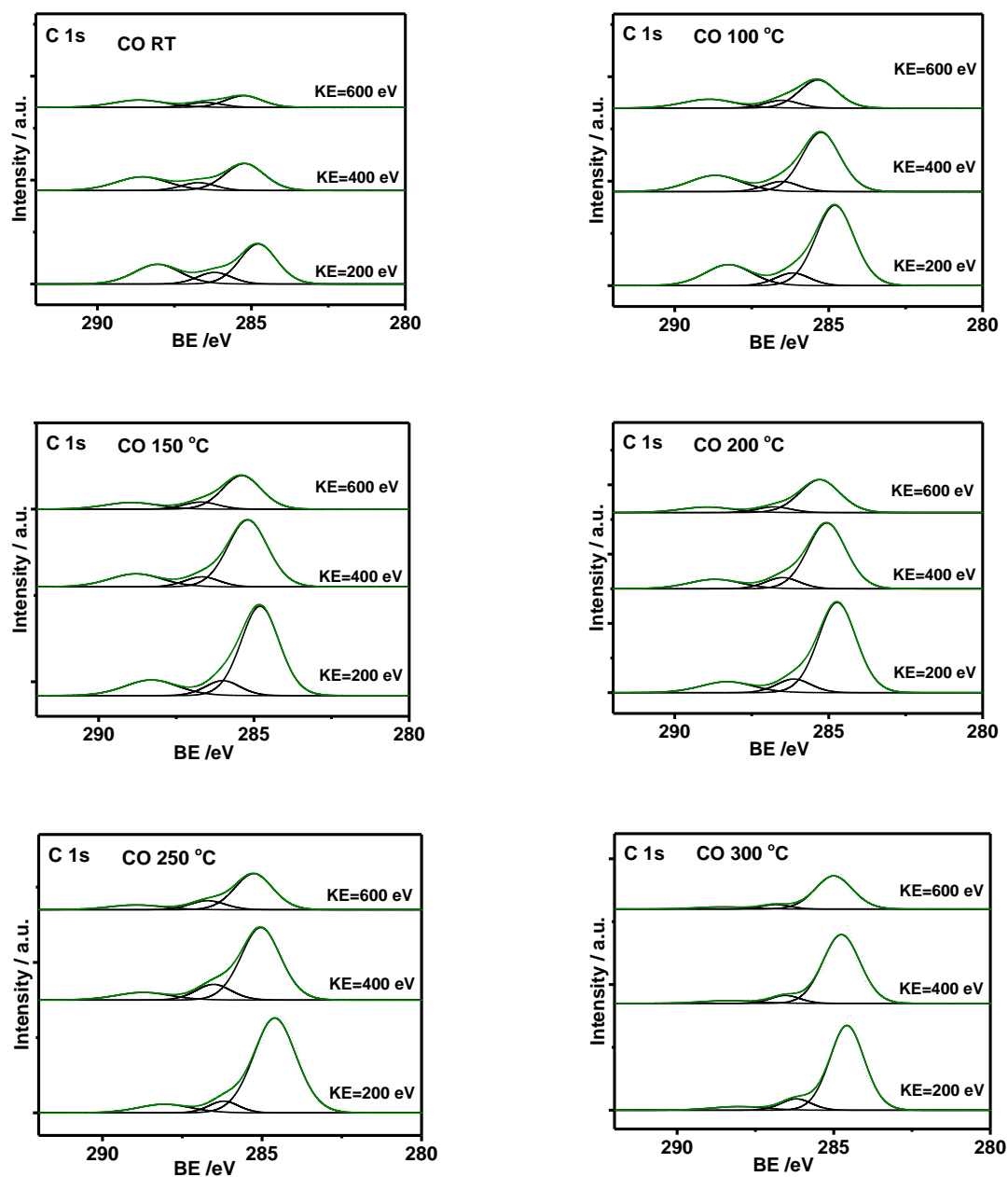
Figure S3. In situ depth profile NAP-XPS during CO-temperature programmed reduction for Co_3O_4 (0.15 mbar): C 1s region with $h\nu$ = 465 eV, $h\nu$ = 665 eV, and $h\nu$ = 865 eV that results in 0.6.nm, 0.8 nm, and 1.1 nm inelastic-mean-free path for C, respectively.
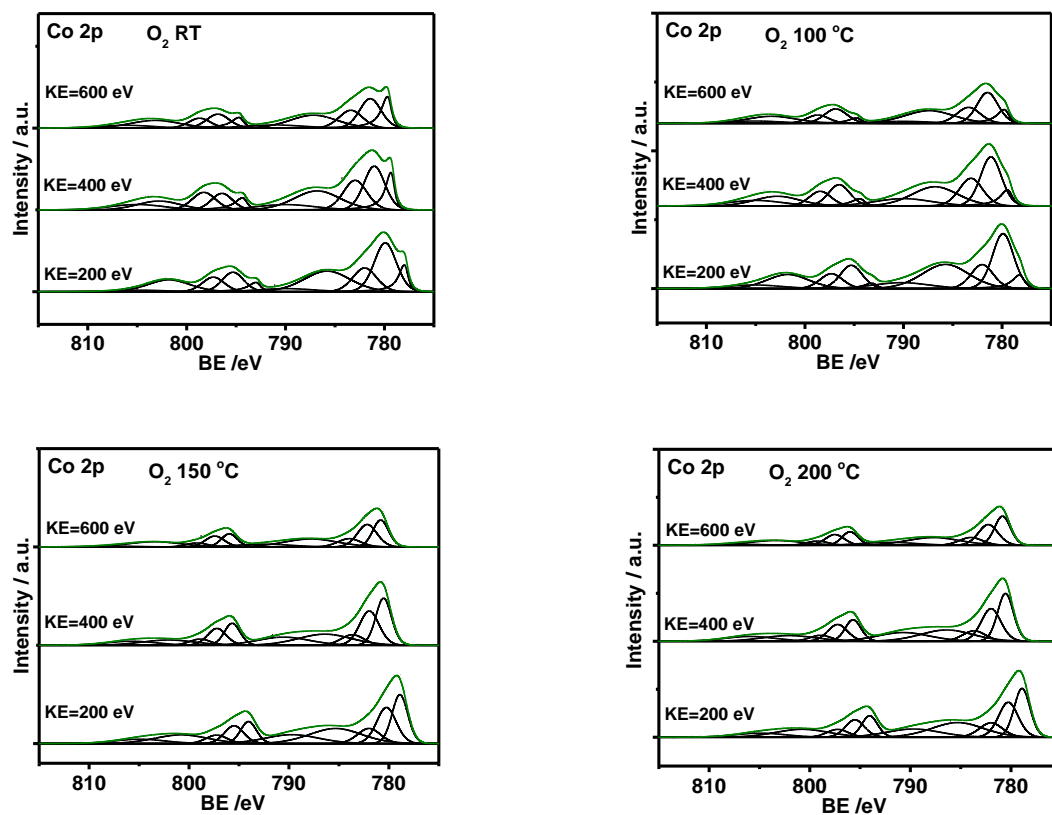
Figure S4. In situ depth profile NAP-XPS during O_2-temperature programmed oxidation (0.15 mbar): Co 2p region with $h\nu$ = 1015 eV, $h\nu$ = 1215 eV, and $h\nu$ = 1415 eV that results in 0.6.nm, 0.8 nm, and 1.1 nm inelastic-mean-free path for Co, respectively.
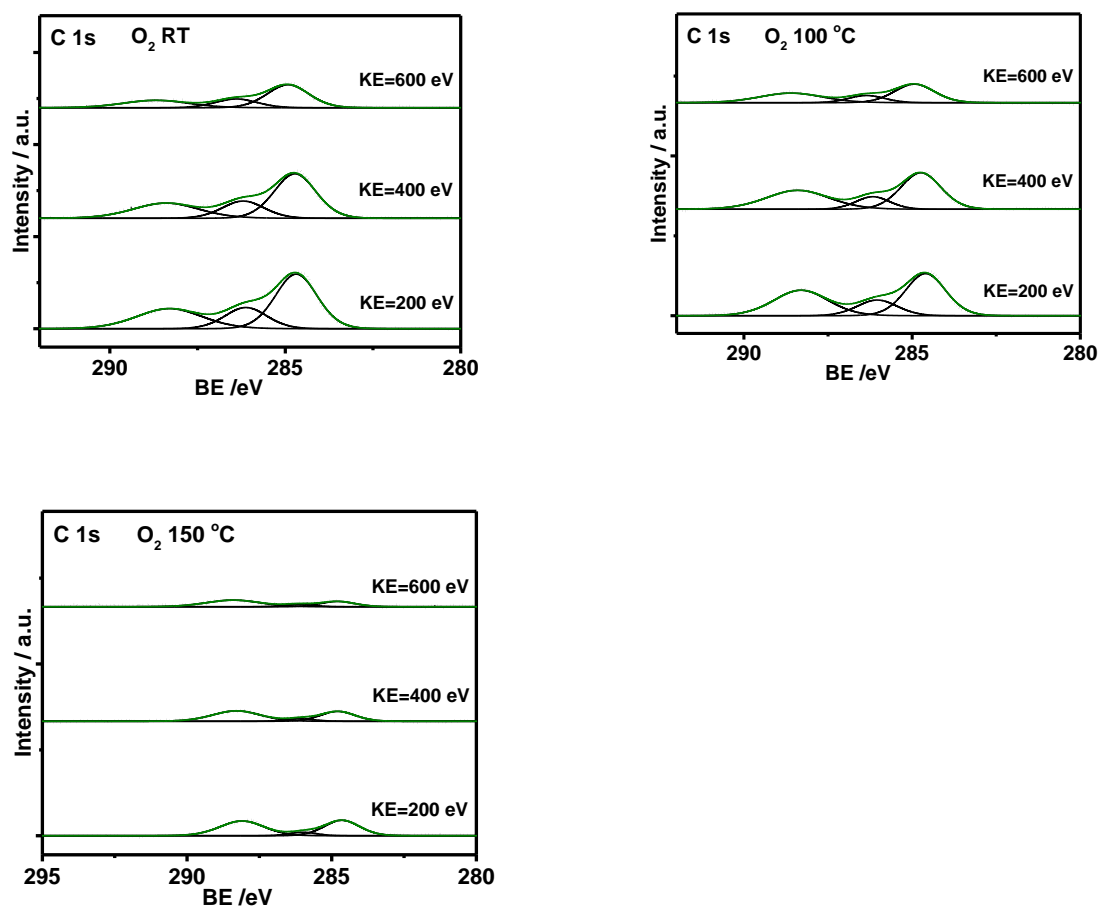
Figure S5. In situ depth profile NAP-XPS during O_2-temperature programmed oxidation (0.15 mbar): C 1s region with hν = 465 eV, hν = 665 eV, and hν = 865 eV that results in 0.6.nm, 0.8 nm, and 1.1 nm inelastic-mean-free path for C, respectively.

CHAPTER 4

MECHANISTIC INSIGHTS INTO CO OXIDATION ON COBALT OXIDE CATALYSTS BY MEANS OF OPERANDO TECHNIQUES

ABSTRACT:

To improve the understanding of cobalt oxide catalysts and to reveal the nature of active sites and the reaction mechanism of CO oxidation, a combined operando approach has been employed. Fourier transform infrared spectroscopy (FTIR), near atmospheric pressure X-ray photoelectron spectroscopy (NAP-XPS), X-ray diffraction (XRD), and X-ray absorption spectroscopy (XAS) were utilized to monitor surface and bulk changes under static reaction conditions (CO and O_2), in CO atmosphere and upon switching from CO to O_2. Operando NAP-XPS revealed fully oxidized Co_3O_4 during CO oxidation up to 200 ^{o}C, whereas in (pure) CO the surface reduction of Co_3O_4 started ~100 ^{o}C. Significant changes in the Co^{3+}/Co^{2+} fraction were observed upon switching from CO to O_2: 25% Co^{3+} in CO vs 28% Co^{3+} in O_2 at 150 ^{o}C; and 24% Co^{3+} in CO vs 28% Co^{3+} in O_2 atmosphere at 200 ^{o}C. In the C 1s region, carbonates, molecular CO adsorbed on cobalt cations, and elementary carbon were observed, the latter indicating CO dissociation during CO oxidation. FTIR spectroscopy clearly showed that CO formed surface carbonate species with Co_3O_4 (i.e., monodentate and at higher temperatures bidentate), while during reaction the amount of carbonates decreased. The combined results of operando NAP-XPS and operando FTIR spectroscopy (i.e., static steady state and dynamic switching experiments) indicate a redox Mars-van Krevelen mechanism of CO oxidation on Co_3O_4, involving the Co^{3+}/Co^{2+} cycle and oxygen vacancy formation at higher temperatures and likely the Langmuir–Hinshelwood mechanism at lower temperature. Moreover, the results point to reaction pathways such as: 1) carbonate formation followed by decomposition; 2) CO dissociation followed by elementary carbon reoxidation in the overall CO oxidation reaction mechanism on Co_3O_4.

An effect of the particle size of CoO materials on the catalytic activity was also revealed. For CoO with particles of 20-50 nm, (surface and near-surface) reoxidation of CoO to Co_3O_4 during CO oxidation was detected at 200 ^{o}C, causing high catalytic activity. In contrast, for macroscopic CoO (1 μm particle size) no bulk oxidation of CoO to Co_3O_4 was observed even during CO oxidation at 360 ^{o}C.

4.1 INTRODUCTION

Controlling automotive emissions during cold start of a car is still an unsolved issue because of the strong CO adsorption to noble metals at low temperatures (<200°C).[1] [2] The search for a catalyst that is able to lower the temperature of CO oxidation is ongoing. In this regard, transition metal oxides have attracted increased attention in recent years.[3] Among these oxides, cobalt oxide has emerged as a particularly promising catalyst for CO oxidation at low temperatures [4] [5] because of its unique redox properties such as the ease of lattice oxygen removal (i.e., formation of oxygen vacancies) and an interplay between Co^{3+}/Co^{2+} oxidation states. Interestingly, a strong dependence of the catalytic activity as well as catalyst stability on the structure and morphology of cobalt oxide materials has been observed. Co_3O_4 materials with defined nanoshapes such as rods (100 nm length and 10 nm width) show much higher CO oxidation activity compared to sphere-shaped nanoparticles.[5] [6] However, the origin of this structure-dependence as well as phase dependence (CoO vs Co_3O_4) is yet to be explained. This calls for detailed studies of the nature of active sites and the reaction mechanism for CO oxidation on cobalt oxide materials by operando methods.

The nature of active sites of cobalt oxide catalysts in the CO oxidation reaction is often associated with the abundance of cobalt cations. For example, in 2009 Haruta *et al.* found that Co_3O_4 nanorods predominately exposing (110) planes, and enriched in Co^{3+} cations, have very high activity in the low-temperature CO oxidation; therefore, the high catalytic activity has been ascribed to Co^{3+} cations (i.e., active sites).[5] However, no additional experimental evidence was provided to support this finding. Two years later Haruta *et al.* reported that Co_3O_4 nanosheets with (111) planes, enriched in Co^{2+} cations, were the most active among nanorods, nanocubes, and nanoparticles.[7] These results are surprising as they are not in line with previously reported data of the same group. Meanwhile, Jia *et al.* observed that a Co_3O_4-SiO_2 nanocomposite catalyst, enriched in Co^{2+} cations without regular planes, exhibited a very high activity for CO oxidation at low temperatures.[4] Interestingly, it has been recently reported that CoO with octahedrally coordinated Co^{2+} exhibited an unexpectedly high activity for CO oxidation that is due to the ease of CoO surface oxidation (i.e., oxidation of Co^{2+} to Co^{3+}) during the CO oxidation reaction.[8] However, these conclusions were primarily based on the catalytic experiments and no direct proof of the surface oxidation of Co^{2+} to Co^{3+} by surface sensitive techniques (e.g., in situ/operando XPS) was provided. Furthermore, the recent study of Iablokov *et al.* on CO oxidation on Co_3O_4 with different particle sizes (i.e., from 2 to 10 nm) has shown that the maximum rate of CO oxidation on Co_3O_4 was achieved for Co_3O_4 with particle sizes between 5-8 nm. This was related to the higher concentration of Co^{3+} 3d states revealed by XPS.[9] Another recent study of Ding *et al.* revealed the enhanced CO oxidation activity for flower-like Co_3O_4 with an increased number of surface Co^{3+} cations.[10] An increase in the number of surface Co^{3+} cations for Co_3O_4 was achieved by applying an optimized calcination process that

causes the redistribution of cobalt ions on the surface of cobalt oxide (i.e., decreasing the number of inactive Co^{2+} cations and simultaneously increasing the number of Co^{3+} active sites). Notably, not only the surface concentration of Co^{3+} cations but also the type of Co^{3+} cations might have a strong effect on the CO oxidation activity. As an example, Hu *et al.*, using Co_3O_4 nanobelts and nanocubes as model catalysts, found that the turnover frequency for Co^{3+} sites of (011) planes on Co_3O_4 nanobelts is far higher than that of (001) planes on Co_3O_4 nanocubes[11]. Therefore, they attributed differences in catalytic activity for these two nanoshapes to different locations of Co^{3+} sites on (011) and (001) planes (i.e., different types of Co^{3+} cations), suggesting that CO oxidation on Co_3O_4 is a structure-sensitive reaction driven by the type of Co^{3+} cations. All these findings highlight that there are still contradicting conclusions concerning the nature of active sites, the role of Co^{2+}/Co^{3+} and CoO/Co_3O_4 in the CO oxidation reaction.

A complete understanding of CO oxidation chemistry on cobalt oxide materials requires also knowledge of the CO oxidation reaction mechanism. This is not trivial although the stoichiometry of the overall CO oxidation reaction is simple. Proposed mechanisms in the literature for CO oxidation on cobalt oxide materials are diverse and are not firmly supported by experimental evidence. For example, based only on kinetic experiments, which show superior catalytic activity for Co_3O_4 nanorods enriched in Co^{3+} cations, it was concluded that CO adsorbs to Co^{3+} cations, while the oxidation of the adsorbed CO occurs by subtracting the surface lattice oxygen coordinated to three Co^{3+} cations.[5] Another example of indirect deduction of the CO oxidation mechanism on cobalt oxide is based on the study of the effect of pretreatment conditions (i.e., oxidation and reduction pretreatment) on the CO oxidation activity of Co_3O_4 by Yu *et al.*[12] The authors proposed that during pretreatment oxygen vacancies are formed and molecular oxygen adsorbs as O–O peroxo species on these vacancies, while a CO molecule adsorbs on the Co^{3+} site. Then a molecularly adsorbed CO attacks a molecularly adsorbed oxygen that leads to the breaking of the O–O peroxo bond, formation of CO_2, and filling the oxygen vacancy by the remaining oxygen from the gas phase.[12] However, Jia *et al.* in their study on low-temperature CO oxidation did not observe peroxo O–O species on the cobalt oxide catalyst with in situ Raman spectroscopy.[4] Further, Pollard *et al.* in their in situ IR study on CO oxidation[13] suggested that CO adsorbed on Co^{2+} sites interacts with an oxygen atom bonded to a neighboring Co^{3+} cation, forming CO_2; the lost oxygen atom (i.e., oxygen vacancy) is replaced by oxygen from the gas phase. As can be seen, oxygen vacancies formation is one of the key steps during CO_2 formation on cobalt oxides. This indicates that the Mars-van Krevelen mechanism of CO oxidation on cobalt oxide catalysts is dominant. Also Jansson in his early works on the mechanism of CO oxidation proposed lattice oxygen extraction to be the basis for the redox Mars-van Krevelen mechanism on cobalt oxide. Apart from a redox scenario of CO oxidation on cobalt oxides,[14] [15] [16] he found that CO disproportionation takes place during CO oxidation. While the Mars-van Krevelen mechanism for CO oxidation on cobalt oxide materials is widely discussed, the possibility of CO disproportionation/dissociation has been rarely considered. The CO oxidation mechanism on cobalt oxide materials is also explained widely on the basis of theoretical work.[17] [18] [19] [20] However, there are also

divergences in conclusions with respect to active sites and the CO reaction mechanism. For example, Jiang *et al.* in their study suggested that for $Co_3O_4(110)$ the CO molecule extracts lattice oxygen leading to CO_2 formation and an oxygen vacancy.[20] Afterwards, the O_2 molecule dissociates between two neighboring oxygen vacancies, replenishing the oxygen sites on the surface and enabling the catalytic cycle. Interestingly, Pang *et al.* proposed two scenarios for CO oxidation: 1) direct reaction of CO with surface lattice oxygen atoms (i.e., a Mars-van Krevelen reaction mechanism); 2) direct reaction of preadsorbed molecular O_2 with molecular CO from a gas phase.[19]

Thus, the proposed mechanism of CO oxidation and the nature of active sites for cobalt oxide catalysts are as of yet only hypothesized, because the current understanding of this reaction system is mostly based on ex situ analyses of catalysts and kinetic experiments. However, the cobalt oxidation state might undergo dynamic variations under reaction conditions. Furthermore, the question is to what extent the surface of the catalyst is changed under reaction conditions. The importance of surface variations was shown for a cobalt oxide model catalyst during methanol oxidation that was revealed with operando NAP-XPS.[21] Therefore, a deeper investigation of cobalt oxide catalysts by employing in situ/operando surface sensitive techniques is required in order to elucidate the nature of active sites and the CO oxidation reaction mechanism.

In **Chapter 3** on the reduction/oxidation behavior of Co_3O_4 (i.e., in situ NAP-XPS CO-TPR followed by O_2-TPO) mechanistic insights into the interaction of CO with Co_3O_4 were presented. Herein, CO oxidation on cobalt oxide catalysts is investigated further by operando NAP-XPS and FTIR spectroscopy, focusing on the fast change of reaction environments and understanding the role of carbonates. Furthermore, in the present chapter the effects of the cobalt oxide initial phase (i.e., Co_3O_4 and CoO) on the catalytic activity in CO oxidation is presented.

In the following, the structural properties of Co_3O_4 and CoO will be described in section 4.3.1. Next, in section 4.3.2, CO oxidation activity data will be presented for Co_3O_4 and the study on the effect of pretreatment conditions on the catalytic activity will be described, whereas in section 4.3.3, operando NAP-XPS and FTIR will be discussed. In section 4.3.4, the influence of the phase (i.e., Co_3O_4 vs CoO) on the catalytic activity will be outlined and the effect of particle size of CoO will be compared. Finally, section 4.4 will summarize results and discuss the CO oxidation mechanism for Co_3O_4.

4.2 EXPERIMENTAL

Co_3O_4 (20-50 nm particle size) was used as received from Fluka, purity 99.5%. Macroscopic CoO (1 μm particle size) was used as received from VWR, purity 99.5%. CoO of nanometer size was obtained by heating Co_3O_4 (Fluka, purity 99.5%) in the NAP-XPS chamber under vacuum to 615 °C. Catalytic activity measurements were performed in a fixed-bed flow reactor. Operando NAP-XPS was performed at the ISISS beamline at BESSY II in Berlin, Germany. The setup consists of a reaction cell attached to a set of differentially pumped electrostatic lenses and a separately pumped analyzer (Phoibos 150 Plus, SPECS GmbH). Operando XAS studies at the Co K (7709 eV) edge were carried out in transmission geometry at the I811 beamline at MAX-lab II in Lund, Sweden. Co metal foil was used for energy calibration. A reaction cell for in situ XAS was supplied by MAX-lab II. Operando FTIR studies were carried out in transmission mode using a Bruker Vertex 70 spectrometer (liquid N_2-cooled MCT detector, resolution of 4 cm^{-1}) with a stainless steel transmission flow cell equipped with CaF_2 windows. The detailed experimental conditions are presented in the experimental part of the thesis (**Chapter 2**).

4.3 RESULTS

4.3.1 STRUCTURAL PROPERTIES OF Co_3O_4 AND CoO

The structural properties of Co_3O_4 and CoO were investigated by X-ray diffraction (XRD) and Transmission Electron Microscopy (TEM). XRD patterns and TEM images of Co_3O_4 (Fluka) and CoO (VWR) are not shown here for brevity and are presented in the supporting information (**Figure S1, S2, S3**). The XRD pattern of Co_3O_4 was indexed to the cubic spinel Co_3O_4 structure. The diffraction pattern of CoO corresponds to the fcc-cubic rock salt structure. The average crystallite sizes calculated from XRD patterns using Rietveld refinement for Co_3O_4 and CoO were 28 and 33 nm, respectively. The BET surface areas of Co_3O_4 and CoO were measured to be 38.3 and 0.8 m^2 g^{-1}, respectively. TEM images of Co_3O_4 and CoO catalysts displayed in **Figure S2** and **Figure S3** show that particles of the Co_3O_4 material are around 20-50 nm and nanospheres-shaped (**Figure S2**), whereas CoO is a microscopic material with a particle size of ~ 0.5-1 micrometer interconnected into 2D structure (**Figure S3 (a, b)**). The HRTEM image of Co_3O_4 (**Figure S2 (b)**) reveals that the main lattice fringes of these materials are about 0.466 nm, corresponding to the (111) facet of Co_3O_4.

4.3.2 CO OXIDATION ACTIVITY OF Co₃O₄: INFLUENCE OF FEED GAS COMPOSITION AND PRETREATMENT

To study the influence of feed gas composition on the CO oxidation activity of Co_3O_4, the reaction was carried out with two reaction mixtures: 1) in excess of O_2 (5 vol.% CO, 10 vol.% O_2); 2) stoichiometric (5 vol.% CO, 2.5 vol.% O_2) (**Figure 1a**). The catalytic data demonstrate an increase of CO conversion for both mixtures with increasing temperature; however, the catalytic trends strongly depend on the concentration of O_2 in the reaction mixture. At 100 °C, a CO conversion of 35% is already reached for the O_2 excess oxidation mixture, while only ~ 20% of CO conversion is achieved for the stoichiometric conditions. A further increase of temperature leads to a sharp increase of CO oxidation for the O_2 excess oxidation mixture and at 110 °C ~ 90% of CO is converted to CO_2, whereas only 30% of CO conversion is observed for the stoichiometric mixture and heating to 140 °C is required to achieve 90% of CO conversion. This finding highlights a strong dependence of CO oxidation activity on the O_2 concentration for the Co_3O_4 catalyst. Also the early study of Perti on the kinetic of CO oxidation (steady state and dynamic experiments) on $Co_3O_4-Al_2O_3$ demonstrated a strong dependence of CO oxidation on the O_2 concentration (the reaction orders of CO and O_2 were 0 and 0.42, respectively).[22][23][24] Moreover, this study revealed that CO oxidation occurs via competitive mechanisms: reaction of CO with adsorbed and lattice oxygen.[22][23][24] It was suggested that the relative rates of reactions are influenced by temperature (i.e., a higher probability of CO reacting with a lattice oxygen at higher temperatures instead of an adsorbed oxygen).[24] In the recent study of Lou *et al.,* the reaction orders of CO and O_2 were found to be −0.64 and 0.88 for Co_3O_4.[25] The negative reaction order in CO indicated that the surface was saturated by CO. This might be explained by the fact that the reaction orders of O_2 and CO were measured in the temperature range of −55 to −95 °C.

In order to investigate the influence of the cobalt oxide oxidation state on the catalytic behavior in CO oxidation, the Co_3O_4 catalyst was pretreated differently: 1) synthetic air at 400 °C; 2) 5 vol.% H_2 in N_2 at 100 °C; 3) 5 vol.% H_2 in N_2 at 200 °C; 4) 5 vol.% H_2 in N_2 at 300 °C; 5) 5 vol.% H_2 in N_2 at 400 °C. After pretreatment, CO oxidation was carried out in the reaction mixture of 5 vol.% CO, 10 vol.% O_2 and 85 vol.% He (total flow 50 mL min^{-1}). The temperature-dependent conversion of CO for the differently pretreated Co_3O_4 is presented in **Figure 1b** and summarized in **Table 1.** The results show that the Co_3O_4 pretreated in H_2 at 100 and 200 °C and the Co_3O_4 pretreated in synthetic air demonstrate activity in CO oxidation already at ~ 80 °C. As the temperature rises, the CO conversion increases exponentially and 100% of CO conversion is reached at ~ 110-120 °C. Furthermore, it is noticeable that Co_3O_4 exposed to H_2 at 100 °C is even moderately more active than Co_3O_4 after oxidation in synthetic air and after reduction in H_2 at 200 °C. At 100 °C the difference in CO conversion for the Co_3O_4 pretreated in synthetic air and in H_2 at 100 °C is 10%, while catalysts reduced in H_2 at 100 °C and at 200 °C differ by ~ 25% in activity.

In contrast to the Co_3O_4 reduced at 100 and 200 °C, the CO conversion for the H_2 pretreated Co_3O_4 at 300 and 400 °C starts at higher temperature (i.e., ~ 120 °C) and reaches 100% of CO conversion only at 160 °C and 170 °C, respectively. The low catalytic activity of catalysts after reduction at 300 and 400 °C is due to the complete reduction of Co_3O_4 to the inactive metallic cobalt as revealed by an in situ XRD and in situ XAS at the Co K edge H_2-temperature programmed reduction experiments (**Figure S4**). We assume that upon heating in the CO/O_2 mixture to 140 °C, the catalyst initially being in the form of metallic cobalt is gradually reoxidised by O_2 from the reaction mixture and, as a result, CO conversion increases. This is confirmed by our in situ XRD experiments (**Figure 2a**) revealing that the exposure of metallic cobalt (i.e., metallic cobalt is prepared by reduction in H_2 at 400 °C) to the CO oxidation mixture (5 vol.% CO and 10 vol.% O_2 in He, total flow 50 mL min^{-1}) leads to oxidation of metallic cobalt to CoO and Co_3O_4 at 200 °C. At 250 °C the oxidation was still incomplete: in addition to CoO and Co_3O_4, metallic cobalt was still observed. Comparing these results with catalytic data, it might be concluded that the active phase is a mixed phase of CoO and Co_3O_4. However, keeping in mind that XRD is a bulk characterization technique, the surface composition of the catalyst might be different and has to be investigated further.
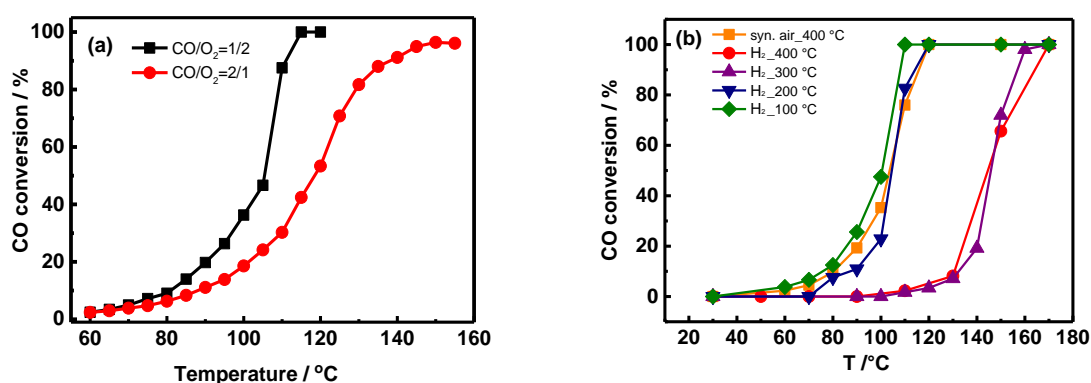
Figure 1. Temperature-dependence of the activity for CO oxidation: (a) for Co_3O_4 with a reaction mixture of 5 vol.% CO, 10 vol.% O_2 and 85 vol.% He, total flow 50 mL min^{-1} (black curve) and with a reaction mixture of 5 vol.% CO, 2.5 vol.% O_2 and 92.5 vol.% He, total flow 50 mL min^{-1} (red curve) (before reaction the catalyst was pretreated in synthetic air); (b) CO oxidation activity for a reaction mixture of 5 vol.% CO, 10 vol.% O_2 and 85 vol.% He (total flow 50 mL min^{-1}) for differently pretreated Co_3O_4.
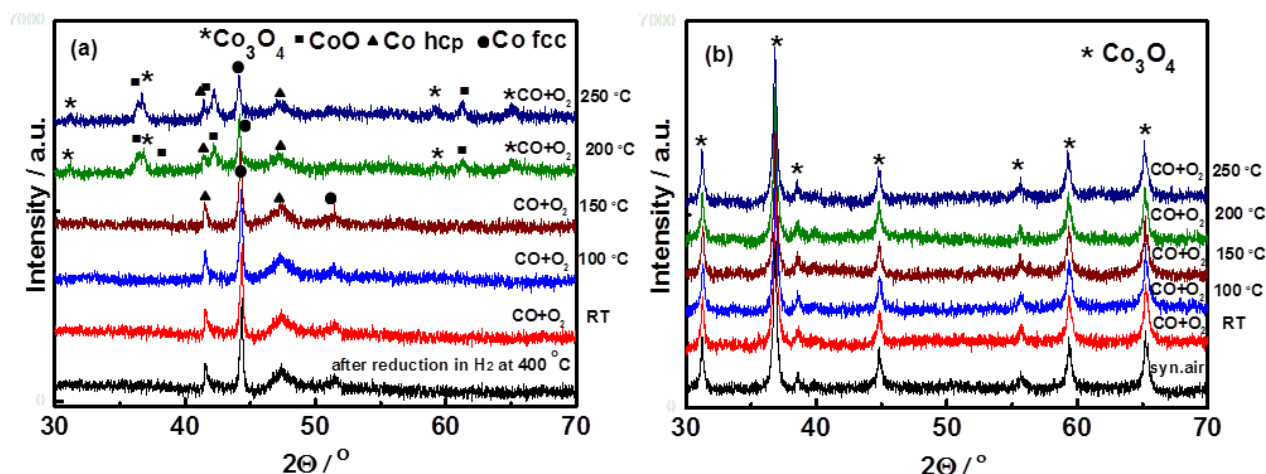
Figure 2. In situ XRD during CO oxidation (5 vol.% CO, 10 vol.% O_2 and 85 vol.% He, total flow 50 mL min^{-1}), (a) after reduction pretreatment of Co_3O_4 at 400 ^{o} C in 5 vol. % H_2; and (b) after oxidation pretreatment Co_3O_4 at 400 ^{o} C in synthetic air.

Table 1. Summary of CO conversion for the reaction mixture of 5 vol.% CO, 10 vol.% O_2 and 85 vol.% He (total flow 50 mL min^{-1}) for differently pretreated Co_3O_4.

Pretreatment	[a]$T_{10\%}$ (^oC)	[b]$T_{50\%}$ (^oC)	[c]$T_{90\%}$ (^oC)
Syn_air_400 ^oC	79	104	115
H₂_100 ^oC	76	101	108
H₂_200 ^oC	88	105	114
H₂_300 ^oC	132	146	157
H₂_400 ^oC	130	145	164

a Reaction temperature for 10% CO conversion; b Reaction temperature for 50% CO conversion; c Reaction temperature for 90% CO conversion.

Aiming at a better understanding of CO oxidation on Co_3O_4, in situ XRD during CO oxidation was also performed for Co_3O_4 pretreated in synthetic air (**Figure 2b**). The results of in situ XRD revealed that the Co_3O_4 oxidized in synthetic air remained Co_3O_4 under CO oxidation conditions (5 vol.% CO, 10 vol.% O_2 and 85 vol.% He, total flow 50 mL min^{-1}) at all temperatures investigated. This is in agreement with the in situ XRD study of Jansson on CO oxidation on Co_3O_4.[16] Jansson did not observe any changes in the diffractograms of the oxidized cobalt oxide sample during CO oxidation; the only phase present was Co_3O_4. Although the bulk structure of Co_3O_4 does not undergo any structural changes during CO

oxidation, the top surface layers of cobalt oxide might be affected by the CO oxidation reaction mixture. The *surface* state of cobalt oxide during CO oxidation still remains an open question and calls for surface sensitive techniques, such as X-ray photoelectron spectroscopy and infrared spectroscopy, in order to investigate the CO oxidation reaction mechanism on Co_3O_4.

4.3.3 OPERANDO STUDIES OF CO OXIDATION ON Co_3O_4

4.3.3.1 OPERANDO NAP-XPS

To gain insights into the mechanism of CO oxidation on the Co_3O_4 catalyst, it is imperative to investigate the surface state of the catalyst under reaction conditions, as reaction steps are driven primarily by changes of the surface of the catalyst. In this regard, operando NAP-XPS is seen as a most powerful tool that can provide information on the surface changes of cobalt (i.e., oxidation state and formation of oxygen vacancies when probing the Co 2p region) and also on the evolution of adsorbate species (e.g., carbonates and adsorbed CO when probing the C 1s region). In **Chapter 3** on the structural and electronic alterations of Co_3O_4 during CO-TPR and O_2-TPO, the strength of operando NAP-XPS for providing the detailed chemical structure information within different probing depths has been demonstrated. Such analysis undoubtedly facilitated the detailed characterization of the cobalt oxide catalyst and allowed us to gain insights into the interaction of CO with cobalt oxide. The main findings from **Chapter 3** with respect to the CO-TPR experiment show that when CO interacts with Co_3O_4 it reduces the top surface layers of cobalt oxide, forming oxygen vacancies, while elementary carbon, carbonates, and $CO-Co^{3+}/CO-Co^{2+}$ are seen in the C 1s region. The question arises whether the situation is the same when O_2 is present in the reaction mixture in addition to CO when the catalyst is active? To answer this question and advance the understanding of CO oxidation on cobalt oxide, it is important to know the surface state of cobalt oxide and the evolution of adsorbates in the CO oxidation mixture. Therefore, to study the surface composition of Co_3O_4 in the CO oxidation reaction mixture, operando NAP-XPS (KE = 200 eV, probing depth of 0.6 nm) during CO oxidation (0.15 mbar CO and 0.3 mbar O_2) was carried out, following the evolution of the Co 2p and the C 1s regions as a function of temperature (**Figure 3** and **Figure 4**).
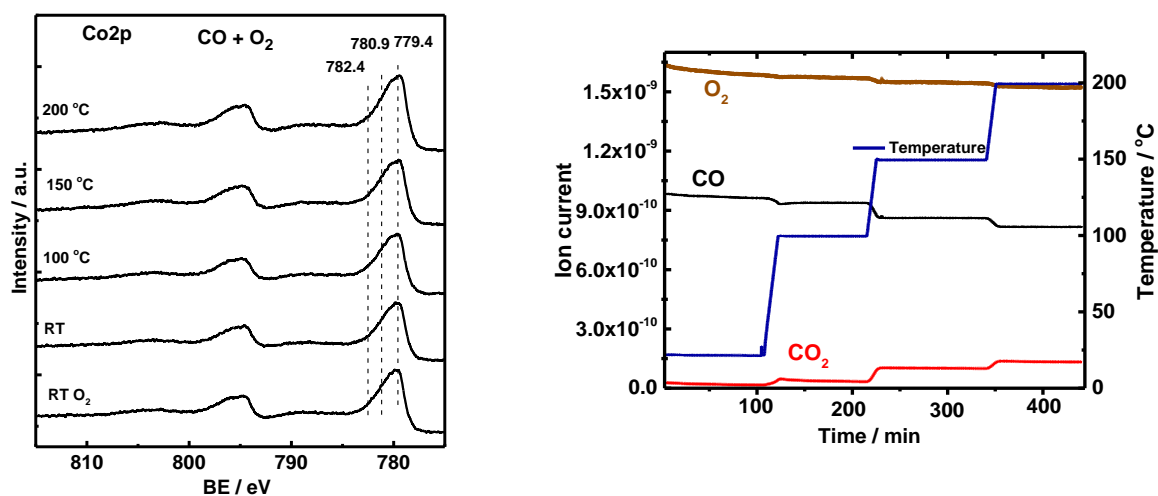
Figure 3. Operando NAP-XPS during CO oxidation from RT to 200 °C (0.15 mbar CO and 0.3 mbar O_2) for Co_3O_4: (a) the Co 2p region (hν = 1015 eV); (b) catalytic data recorded during NAP-XPS.

The assignment of peaks in Co 2p and C 1s regions has been presented in **Chapter 3**. The Co 2p XPS data do not indicate any obvious surface reduction of Co_3O_4 in the CO oxidation mixture neither at RT nor at higher temperatures (i.e., no satellite features are seen in the Co 2p region that would point to the partial surface reduction of Co_3O_4) (**Figure 3 (a)**). Note that in the CO-TPR experiment (pure CO), CO induces the surface reduction of cobalt oxide and formation of oxygen vacancies especially at higher temperatures (i.e., above 100 °C). Thus, under CO oxidation conditions (i.e., in an excess of O_2) no cobalt surface reduction occurs. This is probably because of: a) a fast and dynamic reduction/reoxidation of cobalt oxide surface in the CO-O_2 mixture that is impossible to monitor under steady state reaction conditions, or b) dissociative adsorption of O_2 on the cobalt oxide surface, lowering CO adsorption. Catalytic data recorded during the NAP-XPS experiment (**Figure 3 (b)**) are in agreement with data from a fixed-bed flow reactor and demonstrate an increase of CO conversion with temperature increase. A decrease in O_2 during CO oxidation concentration is better seen in **Figure S5**.

Examination of the C 1s region of Co_3O_4 during CO oxidation (**Figure 4a**) reveals three peaks that correspond to carbonates (288.2 eV), elementary carbon (284.7 eV), and CO weakly adsorbed to cobalt cations (i.e., CO-Co^{3+}/CO-Co^{2+}) (286.1 eV) similar to that of the CO-TPR experiment. The concentration of carbonates, elementary carbon, and CO-Co^{3+}/CO-Co^{2+} increases from RT to 100 °C, whereas between 100 and 150 °C the amount of carbon species remains constant (**Figure 4b**).
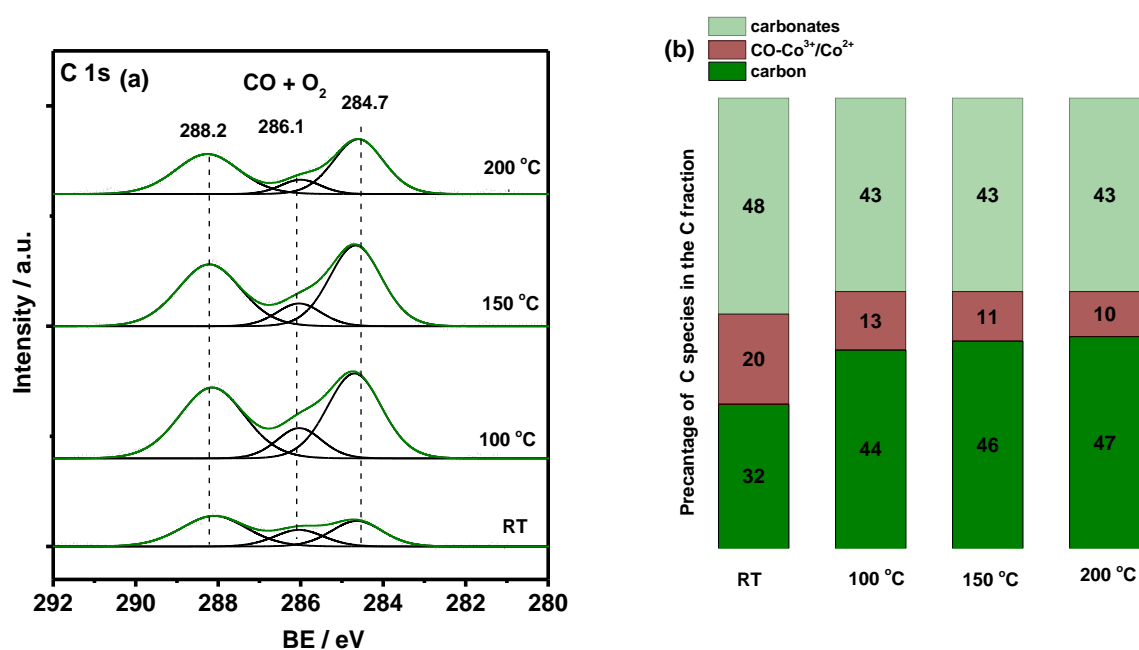
Figure 4. Operando NAP-XPS during CO oxidation from RT to 200 °C (0.15 mbar and 0.3 mbar O_2) for Co_3O_4: (a) the C 1s region (hν = 465 eV); (b) the amount of carbon species calculated from a linear peak fit.

Further increase of temperature from 150 to 200 °C leads to lowering the amount of carbon species. On the contrary to the CO oxidation reaction mixture, in the CO-TPR experiment the concentration of carbon species grows continuously with an increase of temperature (**Chapter 3, Figure 1**). It is also important to note that the relative concentration of elementary carbon, with respect to carbonates and weakly adsorbed CO, is smaller in the CO oxidation reaction mixture than in pure CO (i.e., CO-TPR experiment). In the CO oxidation reaction mixture the relative concentration of elementary carbon is 32% at RT and 44-47% between 100-200 °C with respect to other adsorbate species (**Figure 4b**). When O_2 is absent (i.e., in the CO-TPR experiment), the concentration of elementary carbon is 52% at RT and increases to 78% at 200 °C (**Chapter 3, Table 1**). This indicates that O_2 in the CO oxidation mixture either might suppress the growth of elementary carbon by preventing the CO dissociation reaction, or O_2 can (re-)oxidize the deposited elementary carbon, formed as a result of the CO dissociation reaction. On the basis of the experiments in the CO oxidation reaction mixture and the CO-TPR experiment, it is not yet possible to draw firm conclusions and explain why the concentration of elementary carbon is much smaller in the CO oxidation mixture than in pure CO.

To investigate the evolution of carbon species during the CO oxidation reaction in the surface and subsurface regions, XPS spectra were recorded by varying photon energies to obtain photoelectron kinetic

energies of 200, 400, and 600 eV, which result in probing depths of ~0.6 nm, 0.8 nm, and 1.1 nm, respectively. The results presented in **Figure 5** demonstrate that the relative amount of elementary carbon with respect to other adsorbates decreases with increasing kinetic energy from 200 to 400 eV, remaining similar at 400 and 600 eV. This evinces the presence of elementary carbon mainly at the surface of Co_3O_4.
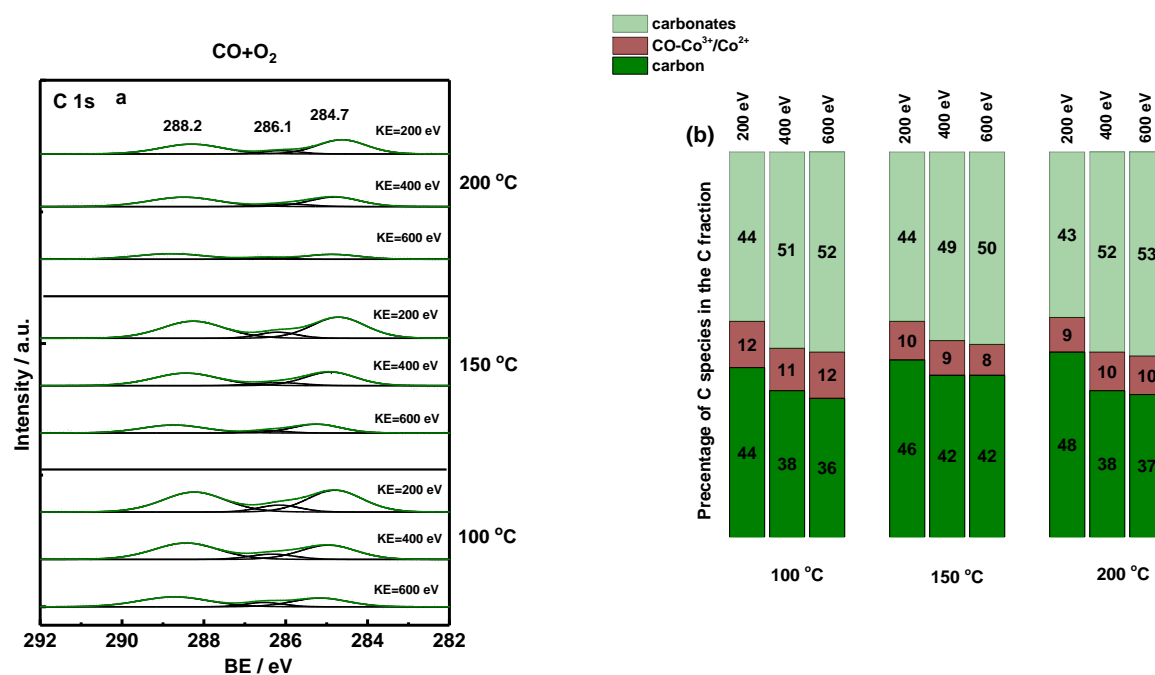

Figure 5. Operando depth profile NAP-XPS during CO oxidation from RT to 200 °C (0.15 mbar and 0.3 mbar O_2) for Co_3O_4: (a) the C 1s region with hν = 465 eV, hν = 665 eV, and hν = 865 eV that results in ~0.6.nm, 0.8 nm, and 1.1 nm inelastic-mean-free path for C, respectively; (b) the amount of carbon species calculated from a linear peak fit.

Being aware of the limited possibilities of steady state experiments for revealing the CO reaction mechanism and active sites, it was decided to perform dynamic operando NAP-XPS experiments to monitor the surface changes of cobalt oxide under cycling atmospheres of CO and O_2. Such experiments can help to understand the role of carbon species and redox properties of cobalt oxide in the CO oxidation reaction. For this purpose, CO-O_2 switching experiments (0.15 mbar CO followed by 0.15 mbar O_2) were performed at RT, 100, 150 and 200 °C, simultaneously recording XPS spectra at the Co 2p and the C 1s regions (KE = 200 eV) (**Figure 6**). Taking into account the attenuation of electrons in the gas phase, it was decided to keep the ratio between CO and O_2 at 1 to 1 (0.15 mbar CO vs 0.15 mbar O_2) in order to better compare spectral changes. **Figure 6** illustrates the Co 2p and C 1s spectra during CO-O_2 switching experiments (i.e., pure CO vs pure O_2). The results of operando NAP-XPS CO-O_2 switching

experiments show that the electronic structure of Co_3O_4 does not change at RT (i.e., no satellites appeared in the Co 2p region), whereas more significant changes in the Co^{3+}/Co^{2+} concentration are seen at higher temperatures: 25% Co^{3+} in a CO atmosphere vs 28% Co^{3+} in O_2 atmosphere at 150 ^{o}C, and 24% Co^{3+} in CO atmosphere vs 28% Co^{3+} in O_2 atmosphere at 200 ^{o}C. Such changes in the concentration of Co^{3+} upon a change from CO to O_2 point to the redox chemistry being involved into CO oxidation on Co_3O_4 (i.e., the Mars-van Krevelen mechanism).

In the C 1s region a switch from CO to O_2 leads to a decrease in the amount of carbon containing species. The most obvious changes upon CO-O_2 switching are seen for elementary carbon. Interestingly, O_2 oxidizes elementary carbon partially even at RT (42% of elementary carbon in CO atmosphere vs 33% in O_2 atmosphere). With an increase of temperature, in CO the concentration of elementary carbon increases with respect to carbonates and weakly adsorbed CO to cobalt cations. However, a switch to O_2 leads to a decrease of elementary carbon but an increase of carbonates, indicating the reoxidation of elementary carbon to CO and possible readsorption on the cobalt oxide surface. Thus, it is possible that a minor reaction pathway of CO oxidation on Co_3O_4 proceeds via CO dissociation followed by elementary carbon oxidation.

During NAP-XPS CO-O_2 switching experiments, changes of the feed gas composition (CO vs O_2) and evolution of CO_2 were monitored with a mass spectrometer. The results are presented in **Figure 7**. As it is seen from **Figure 7b**, evolution of CO_2 occurs already at RT when atmosphere was changed from O_2 to CO and increases with temperature increase. Importantly to note, before introducing reacting gas (e.g., CO) into the NAP-XPS chamber, other reacting gas (e.g., O_2) was vented form the chamber in order to keep the Co_3O_4 catalyst free form physisorbed molecules. A significant increase in CO_2 evolution at 200 ^{o}C and continuous production of CO_2 for ~30 min indicates that not only surface lattice oxygen takes part in CO_2 production (i.e., the Mars-van Krevelen mechanism). If only the Mars-van Krevelen mechanism took place or CO dissociation, then CO_2 production should have been dropped quickly. It is very likely that CO disproportionation ($2CO \rightarrow CO_2 + C$) takes place, as in the C 1s region an increase of elementary carbon is seen under these conditions. Deposition of elementary carbon on the catalyst surface causes deactivation/blockage of the catalyst surface; therefore, a gradual decrease in CO_2 evolution is seen at 200 ^{o}C. The amount of CO_2 produced at 200 ^{o}C during CO oxidation (0.15 mbar CO and 0.3 mbar O_2 **Figure 3b**), is $1.34*10^{-10}$ a.u. The amount of CO_2 produced at 200 ^{o}C in the presence of CO (0.15 mbar CO **Figure 7b**) is $6.10*10^{-12}$ a.u. (after ~5 min) and $3.61*10^{-12}$ a.u. (after ~30 min) that is 22-37 times lower than catalytic activity under CO and O_2 conditions (i.e., 0.15 mbar CO and 0.3 mbar O_2, $1.34*10^{-10}$ a.u.).
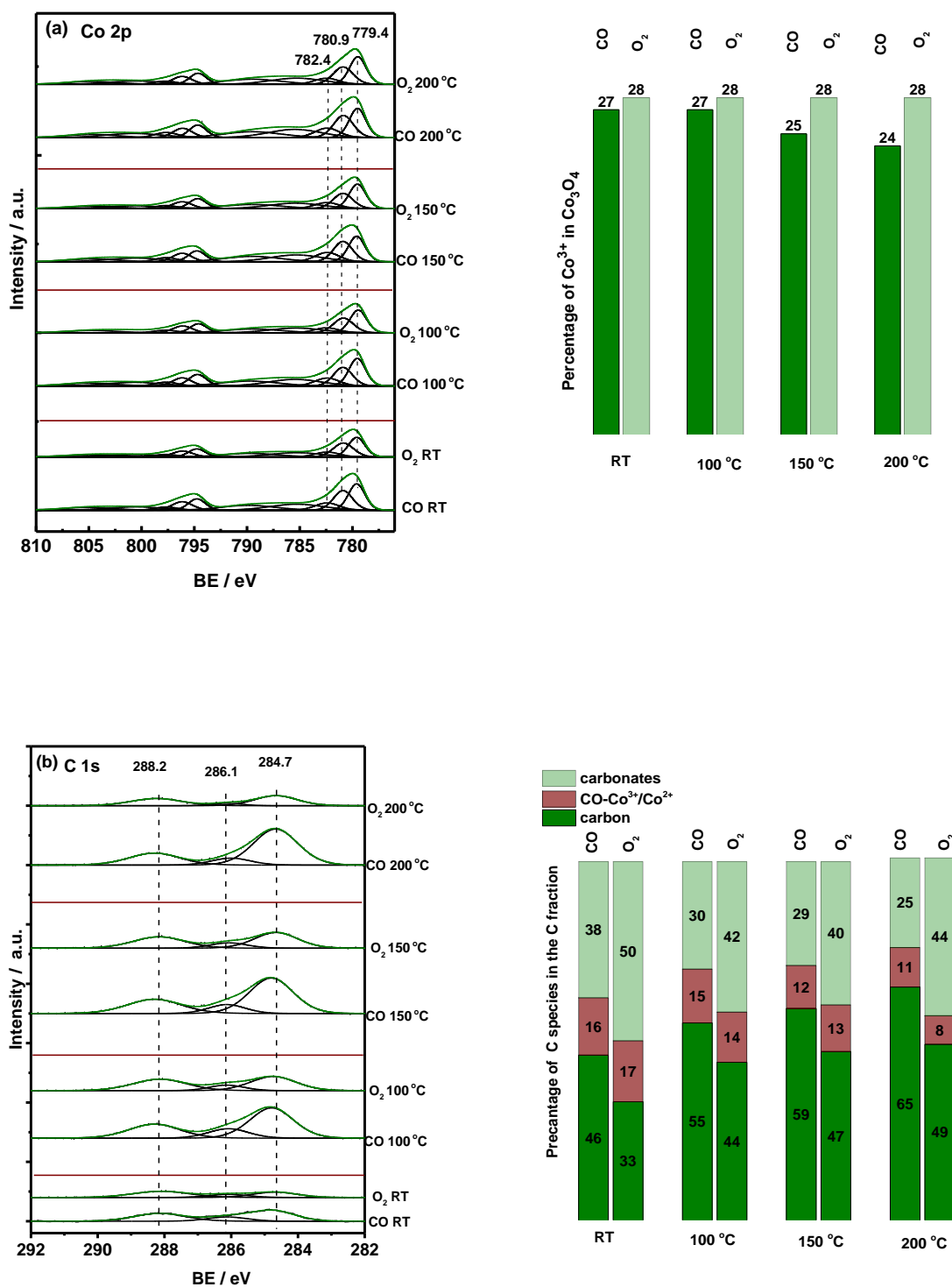
Figure 6. Operando NAP-XPS during CO/O₂ switching experiments (0.15 mbar CO vs 0.15 mbar O₂) for Co₃O₄: (a) the Co 2p region (hν = 1015 eV) with amount of reduced vs oxidized cobalt calculated from a linear peak fit; (b) the C 1s region (hν = 465 eV) with the amount of carbon species calculated from a linear peak fit.
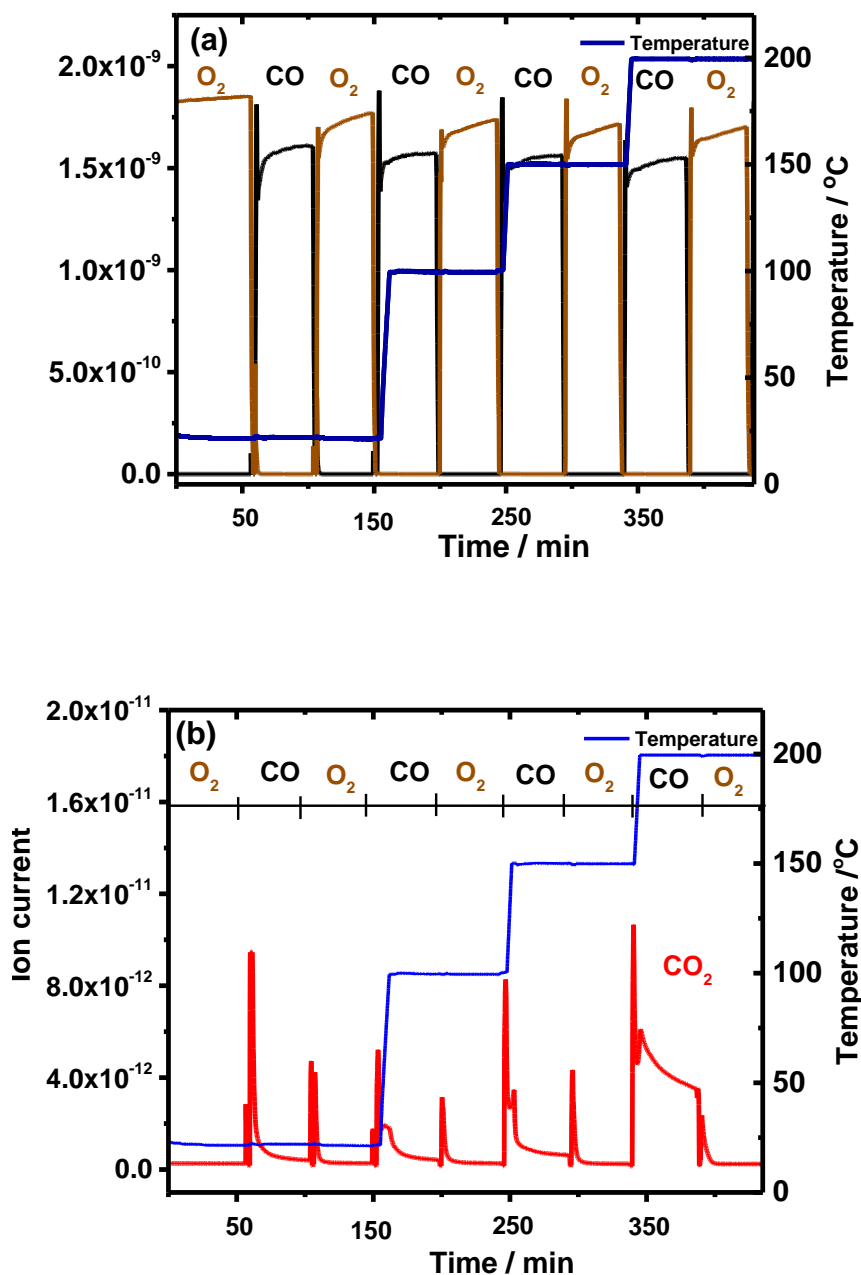
Figure 7. Catalytic data recorded during operando NAP-XPS CO/O_2 switching experiments (0.15 mbar CO vs 0.15 mbar O_2) for Co_3O_4: (a) switching of CO and O_2; (b) evolution of CO_2 during modulation of CO and O_2.

Thus, our operando NAP-XPS observations together with mass spectrometry data are indicative of the redox Mars-van Krevelen mechanism, involving the Co^{3+}/Co^{2+} reduction-reoxidation cycle, and point to a significant role of CO dissociation, elementary carbon deposition, and elementary carbon reoxidation in the reaction cycle of CO oxidation on Co_3O_4. However, from operando NAP-XPS experiments it is not straightforward to unravel the role of carbonates. It is not clear which of the carbonates are potential

reaction intermediates, spectators or might even lead to the poisoning of active sites. Thus, a detailed study for revealing the role of carbonates is needed in order to determine the type of carbonates and their reactivity. In this regard, operando FTIR spectroscopy is a suitable technique for revealing the role of carbonates and attaining deeper knowledge of the CO oxidation reaction mechanism on cobalt oxide.

4.3.3.2 OPERANDO FTIR SPECTROSCOPY

Operando IR spectroscopy is of great use for studying adsorbed species, probing active sites and gaining knowledge about reaction mechanisms. Although numerous in situ and operando IR spectroscopy studies have already been performed on Co_3O_4 under CO oxidation conditions and carbonate formation was detected before,[4] [15] [16] [26] the role of carbonates still remains unclear regarding their potential role as: a) reaction intermediates; b) spectators; c) poisons. To unravel the role of carbonates in the CO oxidation reaction on Co_3O_4, systematic operando IR spectroscopy studies are required. For this purpose, a set of operando FTIR spectroscopy experiments was designed and performed that include:
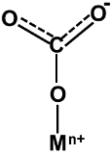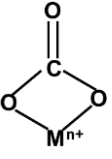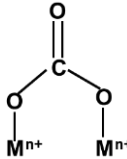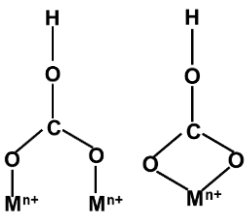
- Interaction of Co_3O_4 with carbon monoxide;
- Interaction of Co_3O_4 with carbon dioxide;
- CO oxidation reaction under different reaction atmospheres: a) CO to O_2 = 1 to 2; b) CO to O_2 = 1 to 1; c) CO to O_2 = 2 to 1);
- Investigation of carbonates stability under O_2 atmosphere and under He atmosphere;
- CO/O_2 switching experiments.

Interaction of Co_3O_4 with carbon monoxide

To gain information about the evolution of reaction adsorbates upon exposure of Co_3O_4 to CO, FTIR spectra were collected at RT and during heating in CO from RT to 200 ºC. The results are presented in **Figure 8a**. The spectra demonstrate the characteristic gas-phase bands of CO at 2110 and 2170 cm^{-1} and a set of bands in the 1000-1650 cm^{-1} region that are attributed to various vibrations of carbonates. On the contrary to NAP-XPS, the results of operando FTIR spectroscopy do not show any bands of CO linearly adsorbed to Co^{2+} or Co^{3+} neither at RT nor during heating. Typically, the CO stretching frequency for cobalt containing species is reported at 2023–2025 cm^{-1} on metallic cobalt, 2070–2110 cm^{-1} on Co^+, 2120–2170 cm^{-1} on Co^{2+}, and 2178–2180 cm^{-1} on Co^{3+}.[16] The 2120–2170 cm^{-1} on Co^{2+} and 2178–2180 cm^{-1} on Co^{3+} stretching frequencies overlap with the gas-phase CO; therefore, the identification of CO linearly adsorbed to cobalt cations by FTIR spectroscopy is not possible.

Although no strong IR adsorption of CO to cobalt cations is seen during CO exposure to Co_3O_4, it leads to formation of carbonates as seen in the 1650-1000 cm^{-1} region, in agreement with the NAP-XPS data. The assignment of surface carbonates is based on the literature [27] [28] and the spectral range of IR stretching vibrations for the assignment of surface carbonate is presented in **Table 2**. From our FTIR data it is seen that at RT mainly monodentate carbonates are formed on the surface of Co_3O_4. Interestingly, with an increase of temperature, intensity of carbonates increases. Moreover, in addition to monodentate carbonates bidentate carbonates start to emerge at 100 °C. This result suggests that upon increasing the temperature more reactive sites are formed (likely by reduction), enabling adsorption of the CO molecule to the Co_3O_4 catalyst surface and different carbonates formation (bidentate and monodentate).

Table 2. Spectral range of CO bond stretching vibrations (cm^{-1}) for the assignment of absorption bands in IR spectra of surface carbonates.[28]

Monodentate	Bidentate	Bridged	Bicarbonate
1530-1470	1620-1530	1670-1620	1700-1600
1370-1300	1270-1250	1270-1250	1397
1080-1040	1030-1020	1020-980	1222 (δOH)

Interaction of Co_3O_4 with carbon dioxide

CO_2 is a product of the CO oxidation reaction and its strong adsorption as carbonate species to the Co_3O_4 surface might lead to catalyst deactivation. Thus, Co_3O_4 was exposed to CO_2 at RT and heated to 200 °C (**Figure 8b**). Interestingly, neither at RT nor during heating any adsorption of CO_2 to the Co_3O_4 surface was observed; CO_2 remained mainly in the gas phase (2336 and 2360 cm^{-1}) and/or only weakly physisorbed (i.e., after evacuation no adsorption bands were seen). This is in contrary to the CO_2 adsorption to ZrO_2,[29] [27] where CO_2 forms carbonates with the ZrO_2 surface. The differences in the affinity to CO_2 between Co_3O_4 and ZrO_2 might be due to certain active sites or functional groups (i.e., OH, basic surface oxygen sites) that are missing in the case of Co_3O_4 which prevents binding/adsorption of CO_2 to Co_3O_4. Thus, all carbonates seen for Co_3O_4 are formed when CO interacts with Co_3O_4.
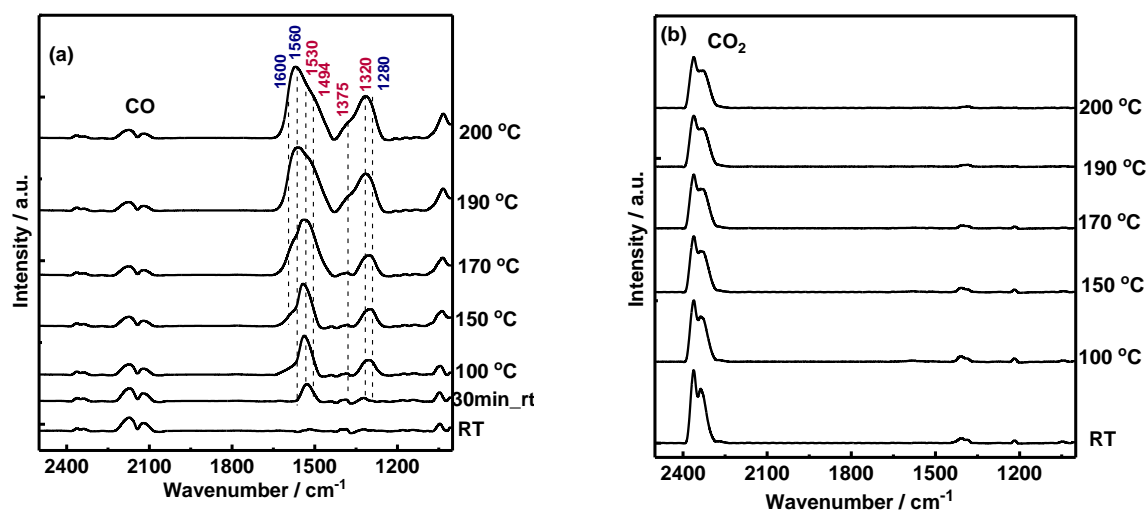
Figure 8. FTIR spectra for Co_3O_4 recorded during: (a) adsorption of CO (50 mbar) in flow mode (total flow 25 mL min^{-1}) from RT to 200 °C; (b) adsorption of CO_2 (50 mbar) in flow mode (total flow 25 mL min^{-1}) from RT to 200 °C.

CO oxidation under different reaction atmospheres: a) CO to O_2 = 1 to 2; b) CO to O_2 = 1 to 1; c) CO to O_2 = 2 to 1

The surface adsorbed species on Co_3O_4 were also studied during CO oxidation. Three cases were explored in order to find correlations between adsorbed species and catalytic activity: a) CO/O_2 = 1 to 2; b) CO/O_2 = 1 to 1; c) CO/O_2 = 2 to 1. The FTIR spectra together with simultaneously recorded catalytic data (using a gas chromatograph) are presented in **Figure 9**. Because of very different reactor designs and different amounts of catalyst loading in a fixed-bed flow reactor (20 mg of powder catalyst, flow through the catalyst bed without dead volume) in the FTIR cell (4-5 mg of the catalyst pressed into a pellet, dead volume of the cell) the actual conversion levels cannot be directly compared (i.e., **Figure 1a** and **Figure 9d**). Similarly to the CO-TPR experiment (**Figure 8a**), no strongly adsorbed CO on Co^{2+} and Co^{3+} was observed during CO oxidation and the only detectable surface species were carbonates. Note that formation of carbonates starts already at RT although the CO_2 production only begins after 150 °C and increases with an increase of temperature. Note also that similarly to the CO-TPR experiment (**Figure 8a**), carbonates that appear at RT are mainly monodentate carbonates. However, upon temperature increase bidentate carbonates evolve. The amount of carbonates in the CO oxidation mixture is smaller than in the case of the Co_3O_4 exposure to CO only. Comparison of the intensity of carbonate bands in the CO oxidation mixture and in pure CO is presented in supporting information (**Figure S5**). Importantly to note, all FTIR spectra were recorded on the same pellet of Co_3O_4 that allows us to compare quantitatively intensities of spectral bands and the amount of adsorbed species.
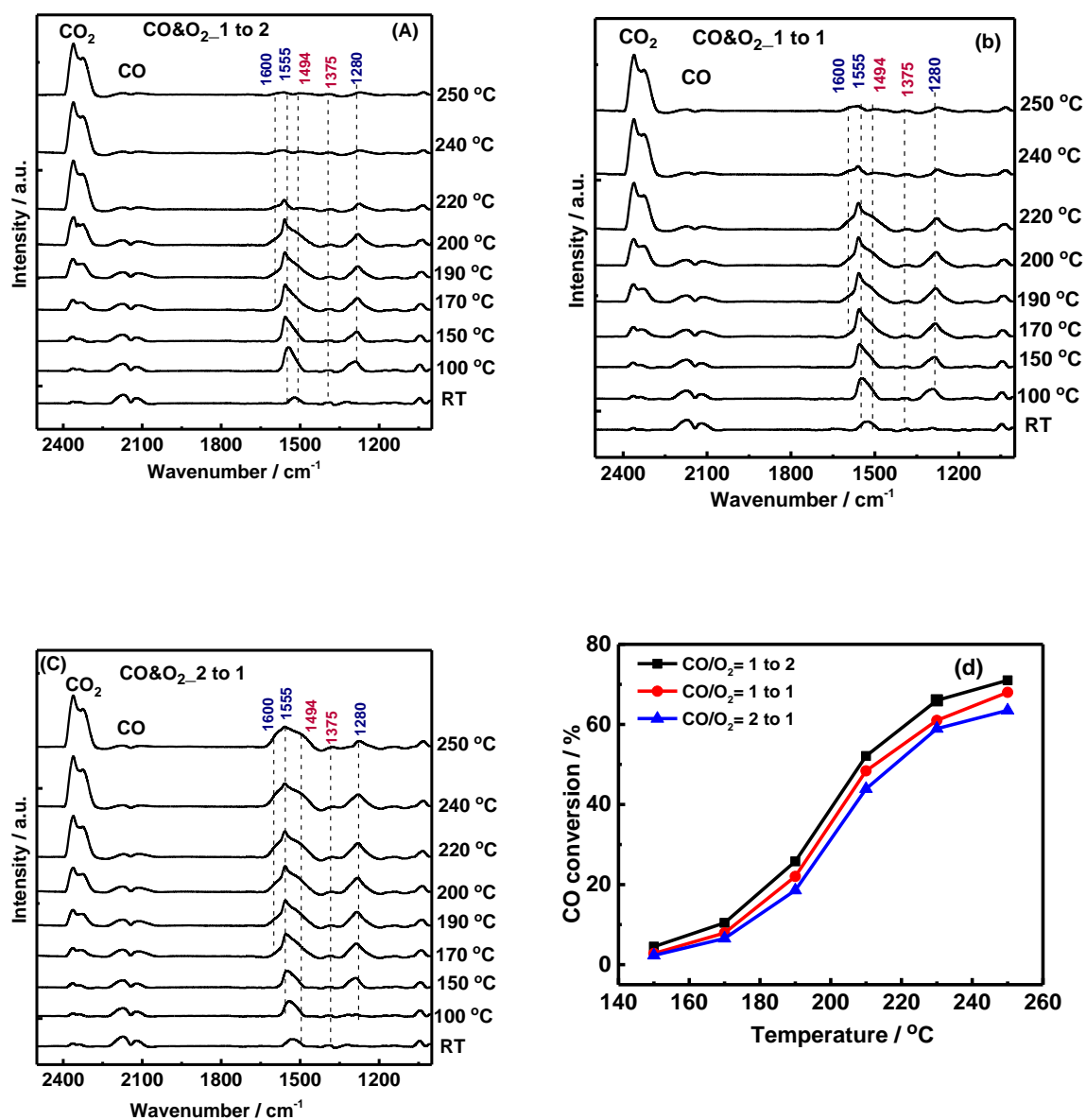
Figure 9. Operando FTIR spectra for Co_3O_4 recorded during CO oxidation reactions in flow mode (total flow 25 mL min^{-1}) from RT to 250 °C: (a) (CO = 50 mbar; O_2 = 100 mbar); (b) (CO = 50 mbar; O_2 = 50 mbar); (c) (CO = 50 mbar; O_2 = 25 mbar); (d) gas chromatography detection of CO conversion during FTIR experiments.

The main difference in the FTIR spectra for three CO oxidation mixtures is stability/decomposition affinity of carbonates under different O_2 concentrations. Under O_2-rich conditions (i.e., CO/O_2 = 1 to 2) the concentration of carbonates grows from RT up to 170 °C, between 170 and 200 °C additional bidentate carbonates are formed, whereas at 220 °C carbonates start to disappear and no carbonates are

present at 220 °C (**Figure 9a**). Importantly, at ~ 150 °C bidentate carbonates start to emerge (i.e., 1620-1530 cm^{-1}, 1270-1250 cm^{-1}) and the appearance of these peaks is accompanied by an increase of CO conversion, as shown by an increase in the gas-phase CO_2 peak in the FTIR spectra as well as in the catalytic data recorded simultaneously by GC (**Figure 9d**). The disappearance of carbonate peaks is accompanied by a further increase of the gas-phase CO_2 peak and an overall increase of CO conversion. The decreasing intensity of carbonates starting at 200 °C and their complete disappearance at 250 °C is likely due to a low thermal stability of carbonates under these conditions. In the CO oxidation mixture with CO/O_2 = 1 to 1 at 220 °C still a relatively high amount of carbonates remain on the surface of the catalyst and higher temperatures are needed to oxidize them as compared to the oxygen-rich conditions.

When the CO to O_2 ratio was adjusted to a stoichiometric ratio (i.e., CO-rich conditions with CO/O_2 = 2 to 1), the amount of carbonates was higher than in CO/O_2 with a 1 to 2 ratio and the concentration of carbonates grows continuously with temperature increase up to 250 °C. However, the concentration of carbonates formed under stoichiometric CO oxidation conditions is still lower than in pure CO (**Figure S 5b**). As seen from the catalytic activity curves (**Figure 9d**), O_2 rich conditions favors higher activity than stoichiometric. Comparing FTIR spectra for the O_2-rich and the stoichiometric mixture (**Figure 9a** and **Figure 9c**, respectively), it is seen that higher carbonates concentration on the surface of the catalyst decreases catalytic activity. However, based on these experiments it is not possible to assess the exact contribution of carbonates to the overall activity. The presence of an excess of O_2 in the reaction mixture either facilitates carbonates conversion to CO_2 or prevents a saturation of the surface by strongly adsorbed CO.

Investigation of carbonates stability under O_2 atmosphere and under He atmosphere

To further understand the role of carbonates in the CO oxidation reaction on Co_3O_4, their stability in O_2 atmosphere was investigated. Operando FTIR spectra for Co_3O_4 were recorded after exposing Co_3O_4 to CO at 200 °C and cooling down in CO atmosphere to RT (i.e., initial spectrum) and during heating in O_2 atmosphere (50 mbar O_2 bar in He, total flow 25 mL min^{-1}). As it is seen from **Figure 10a**, transformation of carbonates takes place already at RT upon introducing O_2. A broadening of the IR band is observed, due to the formation of additional monodentate carbonates appearing as a shoulder at ~1530-1470 cm^{-1}. Heating in O_2 leads to the decomposition or oxidation of carbonates, both into mono- and bidentate carbonates, starting already at 100 °C. At 130 °C the intensity of carbonate bands decreases to the 1/3 of their initial value. At 150 °C only a small amount of monodentate carbonates is left on the cobalt oxide surface, while at 200 °C the surface is completely clean. This is in agreement with the NAP-XPS O_2-TPO study presented in **Chapter 3**, where decomposition of carbonates as well as elementary carbon was observed at 200 °C.
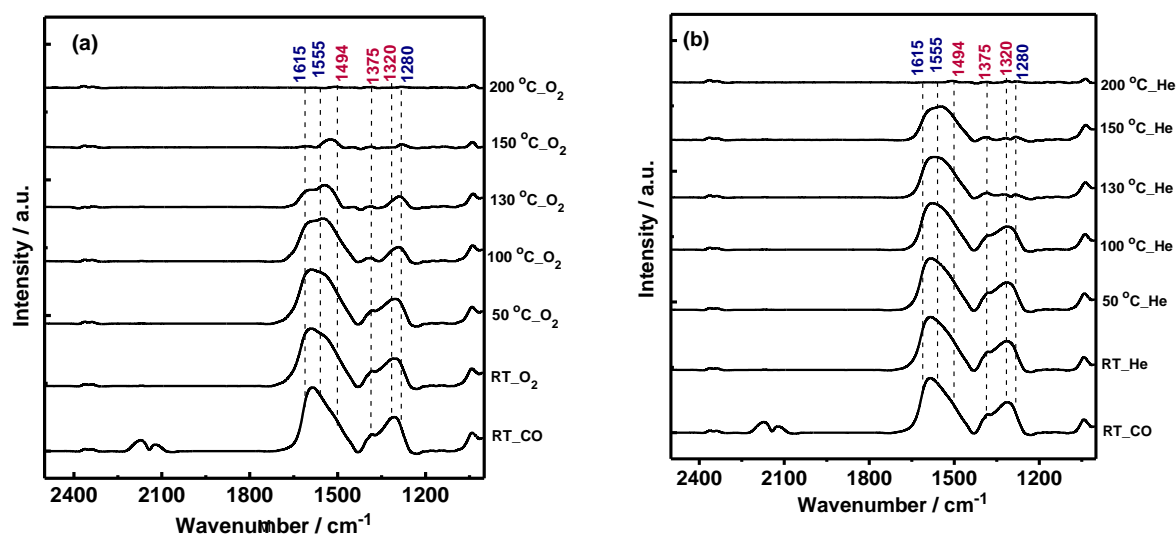
Figure 10. FTIR spectra for Co_3O_4 recorded after: (a) CO adsorption to Co_3O_4 at 200 °C, cooling down in CO atmosphere to RT and heating in O_2 atmosphere (100 O_2 mbar in He, total flow 25 mL min^{-1}); (b) CO adsorption to Co_3O_4 at 200 °C, cooling down in CO atmosphere to RT and heating in He atmosphere (total flow 25 mL min^{-1}).

To better understand the role of carbonates in the CO oxidation reaction, the thermal stability of carbonates was also investigated in He atmosphere (**Figure 10b**) and compared to the stability in O_2 described above (**Figure 10a**). FTIR spectra for Co_3O_4 were recorded after exposing Co_3O_4 to CO at 200 °C and cooling down in CO to RT and heating in He atmosphere. Up to 100 °C in He no significant carbonate decomposition is observed, whereas in O_2 atmosphere transformation of bidentate carbonates to monodentate takes place and lowering of the total intensity of the peak areas is seen. A further increase of temperature to 130 °C promotes decomposition of carbonates in He. However, the decrease is faster for the 1380-1280 cm^{-1} peaks than for the 1600-1430 cm^{-1} peaks, implying different thermal stability and reactivity of surface carbonates. Importantly at 150 °C a significant amount of carbonates is seen under He atmosphere, while under O_2 atmosphere only a small amount of carbonates is seen on the catalyst surface. The fact that carbonate peaks disappear at about 200 °C suggests that surface carbonates, which are formed during an exposure of Co_3O_4 to CO, are of low thermal stability. This is in agreement with the CO-temperature programmed experiment in He (CO-TPD) (**Figure S6**), where a peak of CO_2 desorption is seen at ~ 200 °C. In the CO-TPD experiment Co_3O_4 was exposed to CO at RT for 30 min and then the atmosphere was changed to He and the sample was heated in He to 500 °C. Under these conditions only CO_2 was evolved, demonstrating extraction of lattice oxygen from the cobalt oxide surface.

CO-O₂ switching experiments

In **Figure 11** operando FTIR CO-O$_2$ switching experiments (50 mbar CO vs 50 mbar O$_2$) for Co$_3$O$_4$ are presented: a) CO exposure recorded during the 10th min followed by exposure to O$_2$ recorded during the 2nd min; b) an exposure to CO recorded during the 10th min followed by exposure to O$_2$ recorded during the 10th min. In a typical experiment, firstly CO (5 vol.% CO in He) was introduced and time resolved IR spectra were recorded for 10 min (5 spectra), then the atmosphere was changed to O$_2$ (5 vol.% O$_2$ in He) and time resolved IR spectra were recorded for 10 min (5 spectra) and the Co$_3$O$_4$ sample was heated in O$_2$ to a next temperature before introducing CO. Such experiments were performed at RT, 50, 100, 150, 200, and 250 °C. The FTIR spectra show that neither at RT nor at 100 °C decomposition of carbonates by O$_2$ takes place even during 10 min of exposure to O$_2$. Under these conditions mainly monodentate carbonates are present. At 150 °C the area of carbonate peaks decreases during the first 2 min, and further heating facilitates the decrease of carbonates. The decrease is observed for both mono- and bidentate carbonates. At 200 and 250 °C further strong decrease in the intensity of carbonates is observed and already after 2 min and after 10 min no carbonates are present anymore on the catalyst surface. Importantly, an increase of temperature from 200 to 250 °C also leads to a lowering of carbonate peak areas already in the CO mixture which might be due to the low thermal stability of carbonates at higher temperatures (i.e., 350 °C) as presented in **Figure S7.**

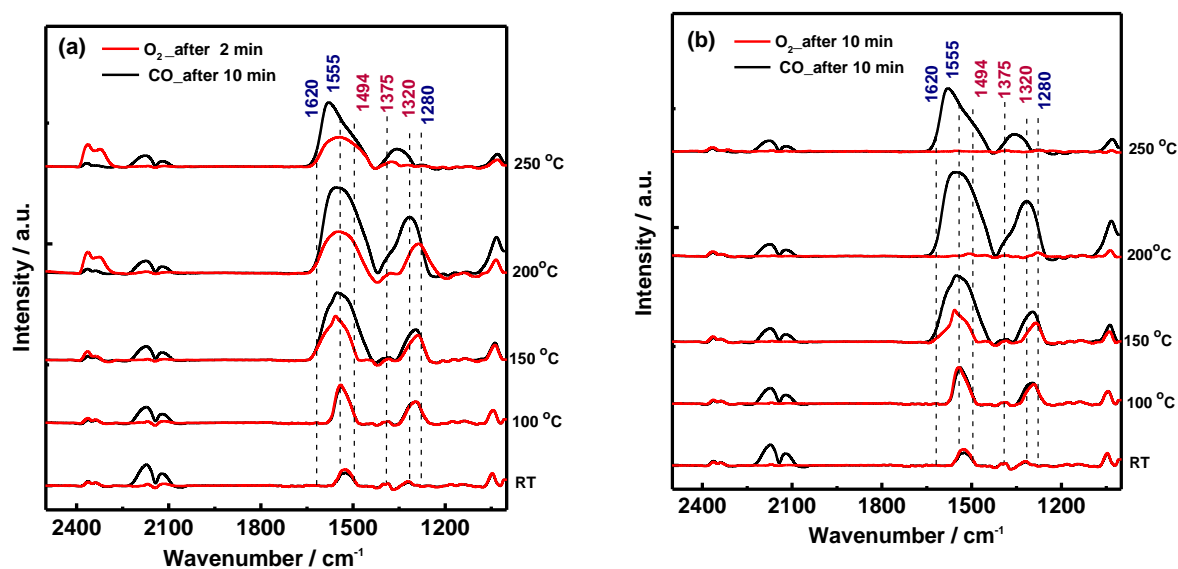**Figure 11.** Operando FTIR CO-O$_2$ switching experiments (50 mbar CO vs 50 mbar O$_2$) for Co$_3$O$_4$: (a) CO recorded during the 10th min followed by O$_2$ recorded during the 2nd min; (b) CO recorded during the 10th min followed by O$_2$ recorded during the 10th min.

4.3.4 CO OXIDATION ON CoO

Detailed operando NAP-XPS and FTIR spectroscopy allowed gaining mechanistic insights into CO oxidation on Co_3O_4. To further advance the understanding of CO oxidation chemistry on cobalt oxide materials, it is imperative to investigate also CoO (cobalt monoxide) with Co^{2+} and O^{2-} atoms in a stoichiometric relationship of Co:O = 1:1. Although under ambient conditions Co_3O_4 is the thermodynamically favored phase of cobalt oxide, CoO can be formed under certain CO oxidation reaction conditions. In contrary to Co_3O_4, much less is known in the literature about CO oxidation chemistry on CoO. The open questions that emerge are: what are the differences in the reactivity of Co_3O_4 and CoO? Does CoO undergo oxidation to Co_3O_4 under CO oxidation conditions? What is the mechanism of CO oxidation on CoO? To shed light on these questions and get mechanistic insights into CO oxidation on CoO, two different CoO were used: (1) commercial CoO (1 μm); (2) CoO prepared by controlled reduction of Co_3O_4 (20-50 nm) in vacuum.

4.3.4.1 CO OXIDATION ON MICROSCOPIC COMMERCIAL CoO (1 μM)

Commercial CoO was used in order to study CO oxidation. Although commercial CoO is structurally different to the Co_3O_4 discussed above – CoO is a microscopic material with very small SSA and big particle size – it might serve as a model catalyst for gaining understanding of CO oxidation chemistry on cobalt monoxide. CO oxidation experiments on commercial CoO were performed after different pretreatments of cobalt monoxide: 1) pretreatment in He at 200 °C; 2) pretreatment in synthetic air at 400 °C. Catalytic data is presented in **Figure 12**. Importantly, CO oxidation activities of differently pretreated CoO were monitored not only during heating but also during cooling. Comparing catalytic data, it is seen that the CoO pretreated in synthetic air at 400 °C is more active than that pretreated in He at 200 °C. For the CoO pretreated in synthetic air at 400 °C, the $T_{50\%}$ (i.e., temperature of 50% CO conversion) is 185 °C, whereas the $T_{90\%}$ (i.e., temperature of 90% CO conversion) is 206 °C. Note that heating and cooling curves almost coincide, indicating that the CoO catalyst does not undergo changes during the CO oxidation cycle. On the contrary, pretreatment of CoO in He at 200 °C leads to lower CO conversions: $T_{50\%}$ is 217 °C and $T_{90\%}$ is 270 °C. Moreover, heating and cooling curves do not coincide and follow the hysteresis loop (i.e., $T_{50\%}$ = 217 °C during heating and $T_{50\%}$ = 200 °C during cooling). This hysteresis provides direct evidence of changes occurring for the CoO catalyst in the CO oxidation reaction mixture, demonstrating that higher temperatures are needed in order to activate the CoO catalyst. From the results of catalytic data it might be assumed that in the CO oxidation mixture Co^{2+} adjusts to the reaction environment and oxidizes to Co^{3+}, facilitating CO oxidation activity. Whether bulk structural changes (i.e., oxidation of CoO to Co_3O_4) or only surface oxidation of CoO takes place during CO oxidation remains a question.
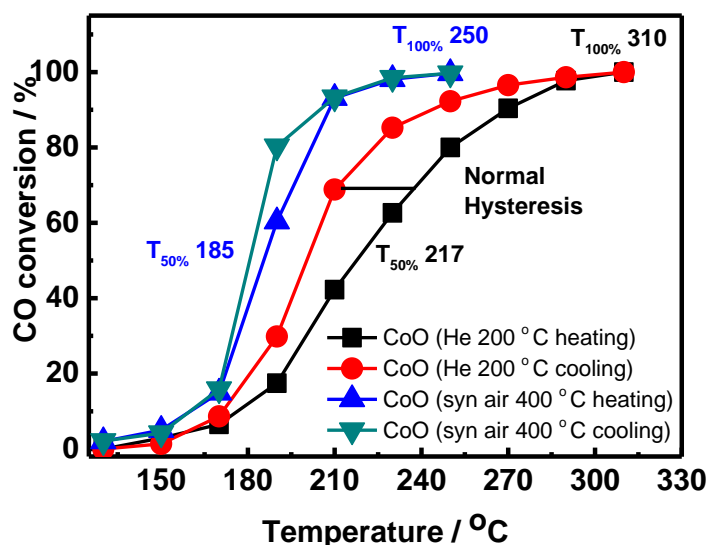
Figure 12. Temperature-dependence of the activity for CO oxidation for variously pretreated commercial CoO carried out with a reaction mixture of 5 vol.% CO, 10 vol.% O_2 in He (total flow 50 mL min^{-1}).

To explain the trends mentioned above for differently pretreated CoO and correlate them with the structural changes of CoO, operando XAS at the Co K edge was performed during CO oxidation. Prior to the CO oxidation reaction, CoO was pretreated in He at 200 °C for 30 min (i.e., in order to remove adsorbed water and any other gases but not to oxidize the surface), then cooled to RT. Afterwards the CO oxidation mixture (5 vol.% CO, 10 vol.% O_2, in He, 50 mL min^{-1}) was introduced and the catalyst was heated from RT to 360 °C. XANES spectra at the Co K edge for CoO during CO oxidation from RT to 360 °C are illustrated in **Figure S8** and **Figure 13**. Surprisingly, no clear changes indicating CoO oxidation to Co_3O_4 were observed in XANES spectra recorded from RT to 360 °C neither in the absorption threshold nor in the white line. However, taking a closer look and zooming in XANES spectra, a small decrease in the white line intensity between 300 and 360 °C is seen (**Figure 13c)**. Because no changes in the energy shift of the absorption threshold were observed between RT-360 °C, it can be assumed that no variations of the cobalt oxidation state take place and the slightly lower intensity of the white line is rather attributed to changes in coverage of the cobalt oxide surface with respect to CO and O_2. This raises the question whether: 1) the presence of CO hinders oxidation of CoO; or 2) particular structural properties of commercial CoO (very big particles) require higher temperatures for CoO oxidation to Co_3O_4.

To explore this, it was decided to switch off CO and leave cobalt oxide under O_2 atmosphere only (10 vol.% O_2 in He, 50 mL min^{-1}). After 30 min of oxidation in O_2 at 360 °C, the XANES spectrum at the Co K edge was taken and compared with the one recorded previously in the CO oxidation mixture at 360 °C. To our surprise the XANES spectrum for the cobalt oxide in O_2 was identical to the one at 360 °C in the

CO oxidation mixture (**Figure S9**). This leads to the conclusion that due to the large particle size of the microscopic CoO higher temperatures are required for oxidation to Co^{3+}.
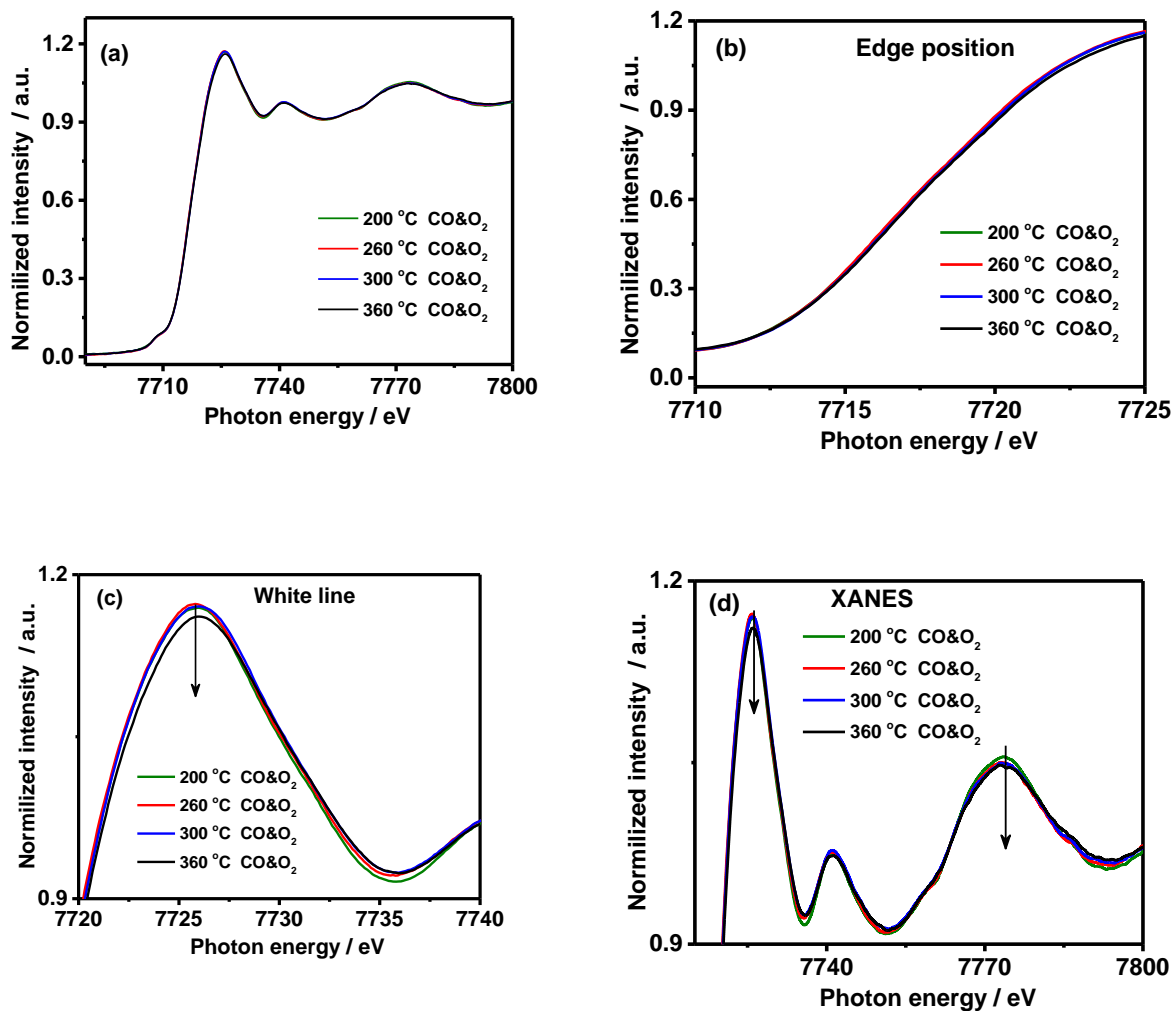
Figure 13. XANES at the Co K edge for CoO during CO oxidation with a reaction mixture of 5 vol.% CO, 10 vol.% O_2 and 85 vol.% He, total flow 50 mL min^{-1}: (a) overall spectra; (b) the edge position; (c) the white line; (d) the XANES region.

After this observation it was decided to heat the CoO further in O_2 and monitor how the oxidation state of cobalt undergoes changes (i.e., at which temperature CoO will be completely transformed to Co_3O_4). Surprisingly, even heating to 530 ºC (530 ºC is the upper limit of the reaction cell used in this study) did not result in a full oxidation of CoO to Co_3O_4 and severe structure alterations (**Figure 14a**). No shift in the absorption threshold/edge position is observed (**Figure 14b**), whereas the maximum of the white line is moved toward higher energy (i.e., a shift of approximately 1 eV (**Figure 14c**)) and moderate changes are

seen in the XANES region (**Figure 14d**), indicating only minor structural rearrangements in the coordination environment of cobalt atoms.
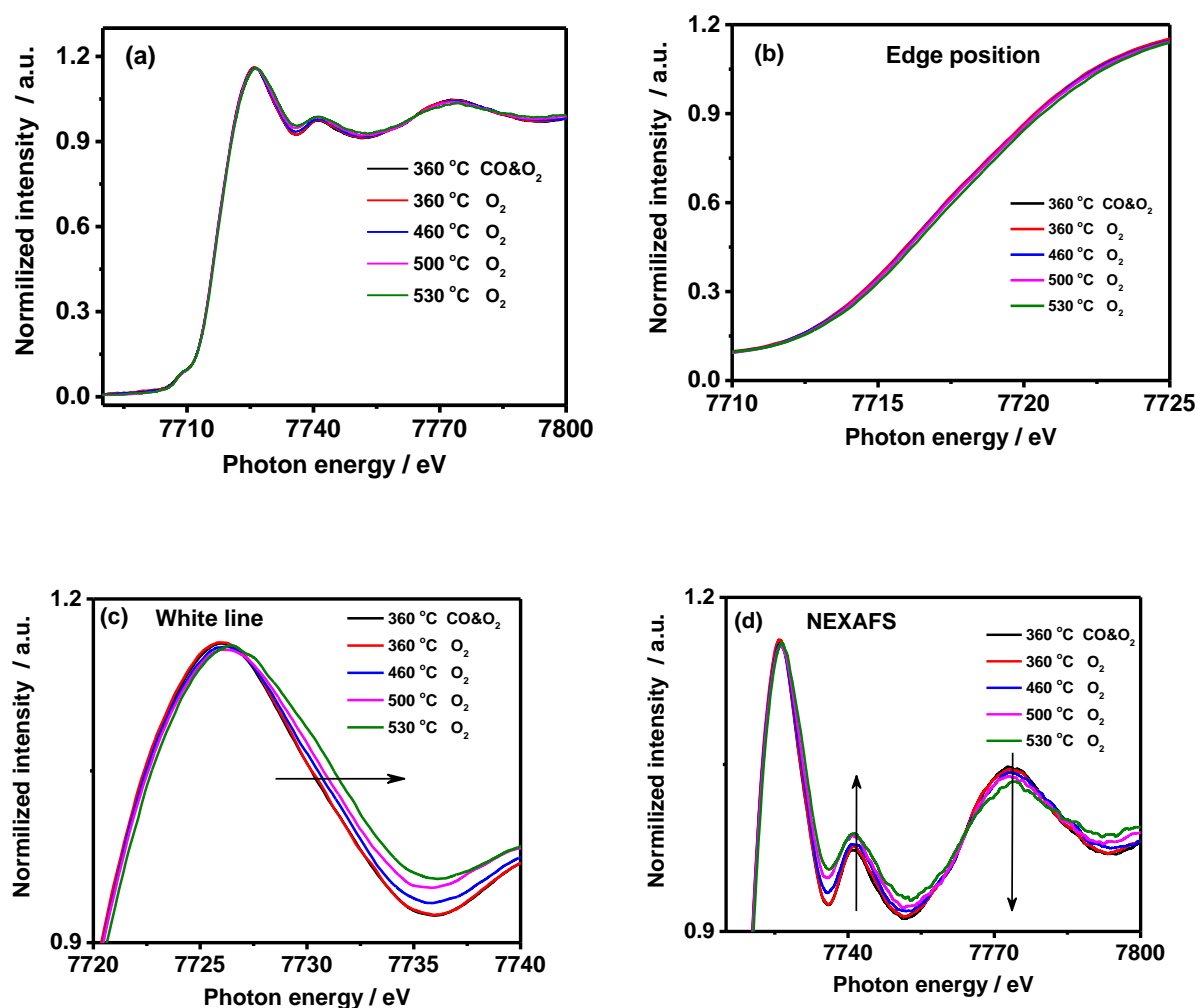
Figure 14. XANES at the Co K edge for CoO during exposure to O_2 (10 vol.% O_2 in He, total flow 50 mL min^{-1}) and heating to 530 °C: (a) overall spectra; (b) the edge position; (c) the white line; (d) the XANES region.

Typically, oxidation of CoO of nanometer size takes place already between 200-350 °C, as reported in the literature[8] and also found in our previous study for nanopowder cobalt (**Chapter 3, Figure 5**). However, the commercial CoO used in this study is of microscopic particle size. Thus, much higher temperatures are required to oxidize the material to Co_3O_4. Higher temperatures for oxidation of CoO single crystal was reported by Petitto *et al.,* where oxidation of CoO(100) to CoO(100)/Co_3O_4 was observed at 500 °C.[30] This demonstrates that oxidation of cobalt oxide strongly depends on the size of particles and explains why drastic structural changes did not occur on commercial CoO during CO oxidation. Even though

operando XANES at the Co K edge did not reveal any local structural changes for cobalt atoms, demonstrating that no bulk oxidation takes place for commercial CoO during CO oxidation, a partial surface oxidation of CoO to Co_xO_y or Co_3O_4 might have occurred. This would explain higher oxidation activity of CoO pretreated in synthetic air at 400 °C compared to CoO pretreated in He at 200 °C and the hysteresis loop for CO oxidation on CoO pretreated in He at 200 °C (**Figure 12**). In summary we cannot draw conclusions whether CoO is active or surface oxidation of CoO is required for catalytic activity due to the large particle size. In order to overcome this problem the second approach was used, as described in the following section.

4.3.4.2 CO OXIDATION ON NANOSCOPIC CoO OBTAINED BY CONTROLLED REDUCTION OF Co_3O_4

Because of limited information obtained from the study of CO oxidation on commercial CoO, different procedures were tried to obtain CoO from Co_3O_4. At first it was attempted to prepare CoO by controlled reduction of Co_3O_4 in H_2. With this aim, reducibility of Co_3O_4 in H_2 was studied by means of in situ XRD (5 vol.% H_2 in He, total flow 50 mL min^{-1}) to find an optimal temperature for CoO formation upon reduction of Co_3O_4 (**Figure S4**). The results of the in situ XRD H_2-temperature programmed reduction experiment show that up to 200 °C the bulk structure of Co_3O_4 remains intact; however, at 300 °C during the first 10-15 min of the experiment a mixture of Co_3O_4, CoO, and metallic cobalt (fcc and hcp phases) is observed as seen from the XRD pattern, whereas after 30 min only metallic cobalt is observed. Thus, the reduction of Co_3O_4 in H_2 does not allow obtaining the CoO phase. Because of the difficulties in direct reduction of Co_3O_4 to CoO in H_2 atmosphere, another attempt was made to prepare CoO via controlled reduction of Co_3O_4 in vacuum (base pressure was 10^{-12} mbar) in the XPS chamber (i.e., NAP-XPS chamber, the ISISS beamline, BESSY). The evolution of the Co 2p XPS and NEXAFS at the Co $L_{3,2}$ edge was monitored in order to control the formation of CoO in vacuum as illustrated in **Figure 14**. The NEXAFS at the Co $L_{3,2}$ edge complements the Co 2p XPS and provides additional information into bulk reduction (information depth ~3-5 nm), on the contrary to the Co 2p XPS with KE = 200 eV that probes ~0.6 nm of the catalyst surface (i.e., few surface layers). As seen from **Figure 15a** and **Figure 15b**, reduction of Co_3O_4 to CoO takes place at 625 °C and occurs at least down up to ~5 nm as revealed by NEXAFS at the Co $L_{3,2}$ edge. After obtaining CoO, the material was cooled to 100 °C in vacuum and the CO oxidation mixture (0.15 mbar CO and 0.3 mbar O_2) was introduced and Co 2p XPS as well as NEXAFS spectra at the Co $L_{3,2}$ edge were recorded (**Figure 15c** and **Figure 15d**). The results reveal that CoO preserves its electronic structure in the CO oxidation mixture up to 150 °C. No surface oxidation takes place at 100 and 150 °C, and the XPS spectra as well as NEXAXFS are very similar. Thus, CoO is present on the surface and in the bulk. Increasing the temperature to 200 °C leads to oxidation of CoO to Co_3O_4 as revealed by XPS in the Co 2p region. Interestingly, the oxidation is also observed in the NEXAFS spectra with an information depth of ~5 nm.
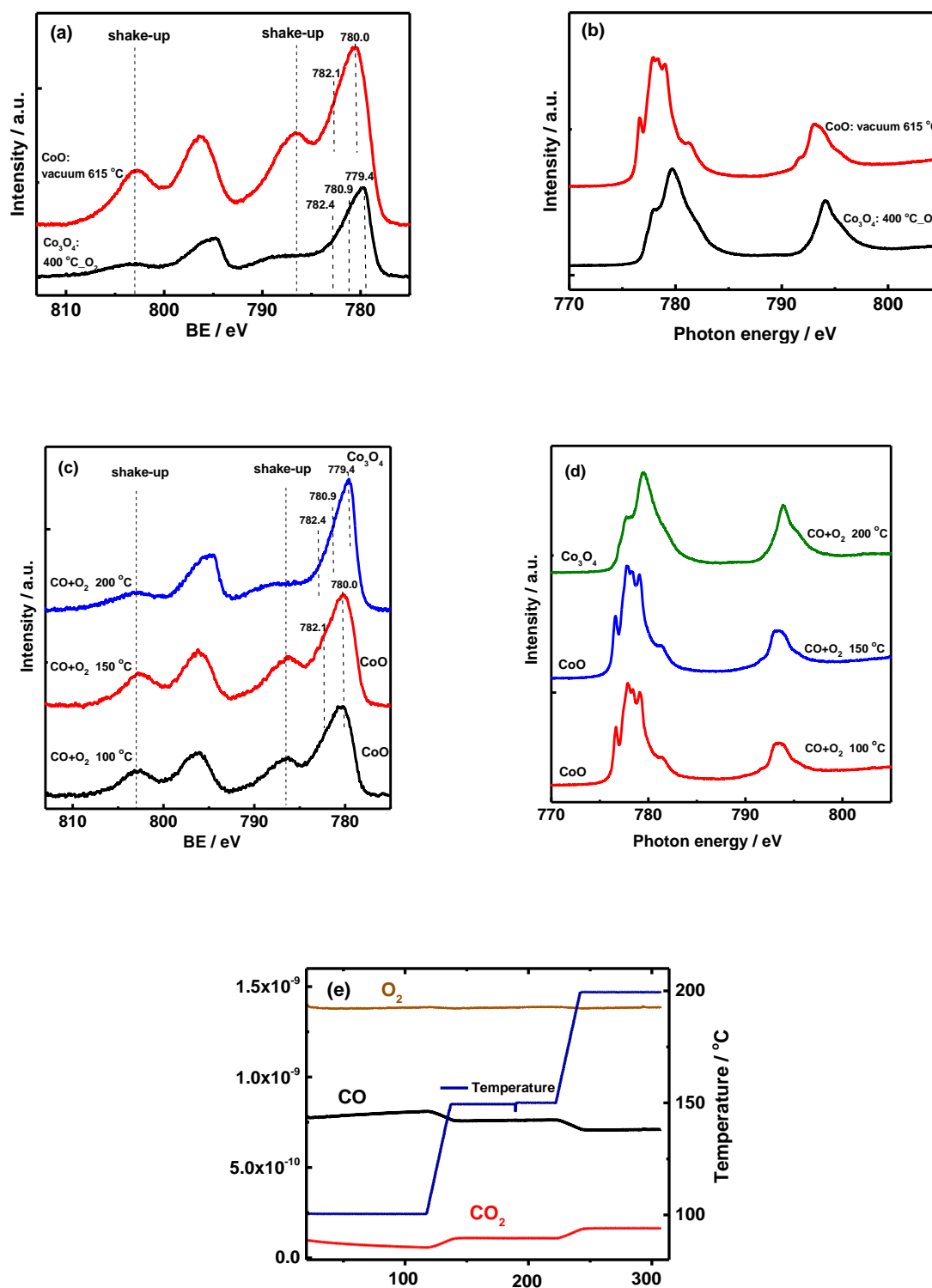
Figure 15. Operando NAP-XPS: (a) the Co 2p (hν = 1015 eV) during preparation of CoO from Co_3O_4 in vacuum; (b) NEXAFS spectra at the Co $L_{3,2}$ edge during preparation of CoO from Co_3O_4 in vacuum;(c) the Co 2p (hν = 1015 eV) during CO oxidation (0.15 mbar CO and 0.3 mbar O_2); (d) NEXAFS spectra at the Co $L_{3,2}$ edge during CO oxidation (0.15 mbar CO and 0.3 mbar O_2); (e) catalytic data recorded during NAP-XPS.

Comparing NAP-XPS combined with NEXAFS at the $CoL_{3,2}$ edge (**Figure 15 c, d**) with catalytic data recorded simultaneously (**Figure 15 e**) it is seen that oxidation of CO to CO_2 occurs already at 100 and 150 °C, when the surface of the catalyst is CoO. However, with an increase of temperature to 200 °C oxidation of CoO to Co_3O_4 during CO in CO oxidation mixture (surface and near-surface) takes place that causes the high activity. When comparing CO oxidation activity for Co_3O_4 (**Figure 3b**) and CoO obtained via reduction Co_3O_4 in vacuum (**Figure 15e**), similar trends/catalytic activity for both materials are observed.

It is important to note that in O_2 atmosphere the surface oxidation of CoO to Co_3O_4 takes place already at 150 °C (i.e., surface oxidation revealed by the Co 2p NAP-XPS), and bulk (revealed by NEXAFS at the Co $L_{3,2}$ edge) at 200 °C, as reported in **Chapter 3** (**Figure 5** and **Figure 8**). Thus, the presence of CO together with O_2 slows down CoO oxidation. However, when the temperature reaches 200 °C oxidation of CoO occurs. It is worth to mention that the nature of the cobalt oxide active phase for CO oxidation is mainly discussed in the literature in terms of bulk phase changes.[8] However, the possibility of dynamic surface and near-surface oxidation of CoO to Co_3O_4 is not taken into account and no study on surface changes of CoO is reported in the literature for CO oxidation. Our study is the first study demonstrating dynamic surface and near-surface changes of cobalt oxide. Although CoO by itself exhibits activity for CO oxidation, CoO is oxidized to Co_3O_4 in the CO oxidation mixture at 200 °C, leading to an increase in CO conversion. Thus, incontrast to the macroscopic CoO (1 μm) where no bulk oxidation of CoO to Co_3O_4 is observed during CO oxidation by operando XAS at the Co K edge at temperatures even of 360 °C, for CoO with particles of 20-50 nm, operando NAP-XPS combined with NEXAFS at the $CoL_{3,2}$ edge confirms reoxidation of CoO to Co_3O_4 during CO oxidation (surface and bulk).

4.4 DISCUSSION

Using operando FTIR spectroscopy and NAP-XPS, the surface of Co_3O_4 and the evolution of adsorbates in the CO oxidation reaction mixture has been examined and compared with those in pure CO and upon switching between CO and O_2. In particular, the comparison of static (steady state) and dynamic (switching) experiments provides valuable information on the reaction mechanism.

4.4.1 (SURFACE) OXIDATION STATE AND PHASE UNDER REACTION CONDITIONS

As described in section 4.3.2, the combination of catalytic tests after different pretreatment procedures and in situ XRD demonstrates a correlation between the appearance/presence of the Co_3O_4 phase and catalytic activity for CO oxidation. This observation is in agreement with the studies on the nanoscopic

CoO obtained by treatment Co_3O_4 in vacuum showing oxidation (surface and near-surface) of nanoscopic CoO to Co_3O_4 under CO oxidation conditions that is the cause of high catalytic activity.

NAP-XPS measurements provided important insights into the oxidation state of cobalt at the surface, which is most relevant for catalysis. During steady state CO oxidation (RT - 200°C) measurable/detectable surface reduction of Co_3O_4 in the Co 2p region (probing ca. 0.6 nm, i.e., the top surface layers) was not observed. On the contrary, in CO atmosphere the surface reduction of Co_3O_4 already starts at 100 °C, as demonstrated by operando NAP-XPS via the increase of the satellite peaks. This is a direct indication of oxygen vacancies formation by CO. The absence of detectable cobalt reduction under $CO+O_2$ is in agreement with the study of PROX on Co_3O_4 and is explained by a low amount of reduced surface species and a fast reoxidation by O_2 (the results are presented in **Chapter 5**).

Valuable insights were gained from the operando NAP-XPS $CO-O_2$ switching experiments showing significant changes in the Co^{3+}/Co^{2+} concentration at higher temperatures with 25% Co^{3+} in CO vs 28% Co^{3+} in O_2 at 150 °C; and 24% Co^{3+} in CO vs 28% Co^{3+} in O_2 atmosphere at 200 °C. This suggests reduction of some Co^{3+} species at the cobalt oxide surface with formation of oxygen vacancies in CO followed by oxidation in O_2. Such changes in the amount of Co^{3+} upon changes from CO to O_2 atmosphere support the Mars-van-Krevelen redox mechanism. The role of oxygen vacancies and the redox mechanism with respect to the CO oxidation reaction on cobalt oxide catalysts is widely discussed in the literature.[5] [14] [15] For instance, Jansson assumed that Co^{3+} is the active site and supplies oxygen to CO, forming Co^{2+} and consequently causing gradual catalyst deactivation at RT.[14] [15] This hypothesis was proven with isotope exchange studies.[14] [15] In a recent study of Zhou *et al.,* an enhancement of the catalytic activity of Co_3O_4 was achieved by substitution of the Co^{2+} ions in the lattice of Co_3O_4 by Cu^{2+}.[31] Using atomic modelling the authors found that the oxygen vacancy is more easily formed in the bonding of Co^{3+}-O-Cu^{2+} than in Co^{3+}-O-Co^{2+} and that Co^{3+} remains as the active site for CO adsorption for Cu-doped Co_3O_4. In addition, numerous theoretical works on CO oxidation on cobalt oxide catalysts support the formation of oxygen vacancies and the redox Mars-van Krevelen mechanism for cobalt oxide materials.[17] [18] [19] [20]

4.4.2 EVOLUTION OF ADSORBATES

For CO-TPR and CO oxidation reaction, carbonate formation, molecular CO adsorbed to cobalt cations, and elementary carbon deposition already at RT was observed in the C1s region by NAP-XPS. This indicates that CO dissociation takes place in CO as well as during CO oxidation. An increase of temperature leads to an increase of elementary carbon as well as reduction of Co_3O_4 to CoO_x and formation of oxygen vacancies in CO atmosphere. In the CO oxidation mixture the relative concentration of carbonates, elementary carbon, and CO-Co^{3+}/CO-Co^{2+} increases from RT to 100 °C, whereas between

100 and 150 °C the amount of carbon species remains constant. A further increase of temperature from 150 to 200 °C leads to a lower amount of carbon species. On the contrary, in the CO-TPR experiment the concentration of carbon species grows continuously with increasing temperature. Moreover, in pure CO the concentration of carbonates and carbon was higher than in the CO oxidation reaction mixture. Among the C-containing species, the relative concentration of elementary carbon, with respect to carbonates and weakly adsorbed CO, is smaller in the CO oxidation reaction mixture than in pure CO.

Carbonate formation is well documented for cobalt oxide catalysts in the literature upon the interaction of CO with cobalt oxide or during the CO oxidation reaction, even though the role of carbonates is not clear yet.[4] [15] [16] On the contrary, the carbon deposition during the interaction of CO with Co_3O_4 or during the CO oxidation reaction is much less discussed in the literature. The only studies that reported on carbon deposition on Co_3O_4 were indirect investigations by Jansson,[14] [15] which were based on CO oxidation over an isotope-labeled (^{18}O) cobalt oxide catalyst followed by temperature programmed desorption (TPD) and temperature programmed oxidation (TPO). Our NAP-XPS data in the C 1s region clearly indicates formation of carbon on Co_3O_4 during CO exposure as well as during CO oxidation. Moreover, the correlation between the increase of carbon concentration and oxygen vacancies is clearly seen from our data. Thus, it is reasonable to assume that CO forms carbonates with surface oxygen of cobalt oxide, extracting lattice oxygen and forming surface oxygen vacancies. The vacancies that are formed might serve as active sites for further CO adsorption and dissociation, depositing elementary carbon. When O_2 is present in the reaction mixture, the oxygen vacancies might serve as active sites for O_2 adsorption and dissociation.

Based on the binding energy it was found that amorphous carbon is formed at the Co_3O_4 surface that does not require higher temperatures to be oxidized. In order to probe its reactivity toward O_2, an operando NAP-XPS O_2-TPO experiment was performed after reduction of cobalt oxide in CO, the results of which are presented in the **Chapter 3, Figure 5b**. It was observed that the amount of elementary carbon already decreases at RT. This proves the ease of elementary/amorphous carbon oxidation. Heating in O_2 leads to decreasing of carbon and at 200 °C the catalyst surface and near-surface is completely recovered to Co_3O_4, and no carbon and carbonates are present on the surface. The reactivity of an amorphous/elementary carbon toward O_2 is confirmed by switching experiments followed operando by NAP-XPS. Similarly, a switch from CO to O_2 (**Figure 6**) leads to a decrease in the amount of carbon-containing species especially at higher temperatures. The most obvious changes upon CO-O_2 switching are seen for elementary carbon: a decrease of elementary carbon and an increase of carbonates upon switch to O_2, indicating the reoxidation of elementary carbon to CO and possible readsorption on the cobalt oxide surface. Thus, it is possible that one of the reaction pathways for CO oxidation on Co_3O_4 proceeds via CO dissociation followed by elementary carbon oxidation to CO/CO_2.

In agreement with NAP-XPS measurements, FTIR spectroscopy detects the formation of carbonates on the surface of Co_3O_4, when only CO is present. Our FTIR data demonstrate that at RT mainly monodentate carbonates are formed, while with an increase of temperature, in addition to monodentate carbonates bidentate carbonates start to emerge, and the overall intensity of carbonates increases. This result suggests that upon an increase of temperature more reactive sites are formed, enabling adsorption of CO as a carbonate. Binding of monodentate carbonates to the oxide surface requires only one oxygen atom, while two other oxygen atoms are not bound to the catalyst surface. Hence, the formation of monodentate carbonates upon interaction of CO with Co_3O_4 proceeds via an extraction of one of the lattice oxygen from the Co_3O_4, thus, reducing the surface when it is decomposed to CO_2. Our NAP-XPS results revealed the reduction of the Co_3O_4 surface and the formation of surface oxygen vacancies in CO especially when the temperature increases from 100 to 200 °C. In this way more defective sites/vacancies are created, where CO can strongly adsorb as carbonates. Therefore, upon heating in CO, which favors the lattice oxygen extraction, the concentration of carbonates also increases presumably as a result of progressive CO adsorption on/near the oxygen vacancies.

When CO and O_2 are present in the reaction mixture, both bidentate and monodentate carbonates are decomposed already at temperatures below 220 °C. As it is shown in **Figure 9**, an excess of O_2 in the reaction mixture facilitates decomposition of carbonates to CO_2 as well as the catalyst surface reoxidation and the oxidation of elementary carbon as revealed with NAP-XPS (**Chapter 3, Figure 5**). On the contrary, CO-rich conditions lead to a stronger reduction of the surface with CO, stronger binding of CO to the cobalt oxide surface as carbonate and more elementary carbon present. In summary, carbonates might play a minor role as intermediates in an additional pathway beside the fast direct CO oxidation according to the Mars-van Krevelen-type mechanism. The exact extent of this contribution is not known, but the carbonates seem to be rather stable surface species.

4.4.3 SUGGESTED REACTION MECHANISM

The following simplified reaction pathways likely play a role for CO oxidation on Co_3O_4:

1) **direct Mars–van-Krevelen pathway:**
   $CO_{ads} + O_{surf}/Co_3O_4 \rightarrow CO_2 + ox\ vac/\ CoO_x$ and $ox\ vac/\ CoO_x + O_2 \rightarrow O_{surf}/Co_3O_4$
2) **via CO dissociation and carbon oxidation** (*O_2 probably dissociated at vacancy*)
3) $CO_{ads} \rightarrow C + O$ and $C + O_{2(at\ ox\ vac)} \rightarrow CO_2$ or $C + 2O_{surf} \rightarrow CO_2$
4) **via carbonates as intermediates**
   $carbonate_{ads} \rightarrow CO_2 + ox\ vac\ /\ CoO_x$
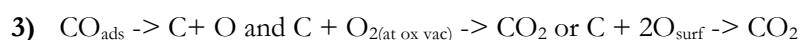
With the knowledge gained from operando NAP-XPS and FTIR spectroscopy – in particular from the dynamic switching experiments – it is proved that the fast CO oxidation reaction proceeds via the Mars-

van Krevelen-type mechanism (1) with an alternating reduction-oxidation of the Co_3O_4 surface by CO and O_2. However, the occurrence of the Langmuir–Hinshelwood mechanism in which the formation of CO_2 takes place in the presence of both CO and O_2 simultaneously adsorbed on the surface cannot be excluded. The oxidation of carbon monoxide adsorbed to cobalt cations involves oxygen from the catalyst surface. Furthermore, adsorbed CO undergoes dissociation, filling an oxygen vacancy with oxygen and depositing elementary carbon on the surface, which can then be oxidized by O_2. The CO dissociation likely occurs at oxygen vacancies as supported by the correlation between the amount of carbon and of oxygen vacancies. The carbon is quite reactive being oxidized even at RT, which suggests that the CO dissociation and carbon reoxidation to CO_2 is an additional pathway occurring during CO oxidation on Co_3O_4. Because of a sharp decrease in the concentration of the surface carbonates at higher temperatures (200-250 °C) in the CO oxidation mixture on the surface of Co_3O_4 (the surfaces of Co_3O_4 is almost free of carbonate) it might be suggested that carbonates play a role as intermediates of an additional minor pathway at higher temperatures (3). Decomposition of the carbonates to CO_2 appears to be facilitated by the presence/excess of O_2. In this study the possible reaction pathways/elementary steps for CO oxidation on Co_3O_4 are summarized in **Figure 16**. Clearly, surface reduction by CO, reoxidation by O_2, CO dissociation/disproportionation presumably at vacancies and carbonates are key players and processes. However, understanding the detailed contribution of all steps requires further studies of kinetics in order to determine the rate determining step for the CO oxidation reaction.

(1) Interaction of CO with Co_3O_4, formation of oxygen vacancies
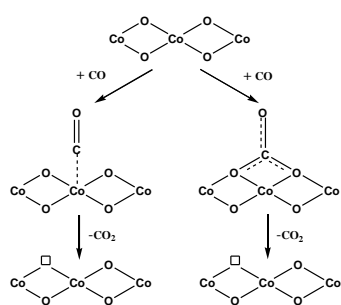
(2) Interaction of oxygen vacancies with O_2, CO dissociation
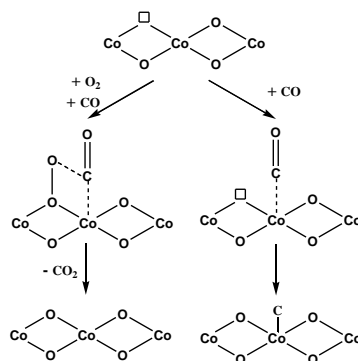
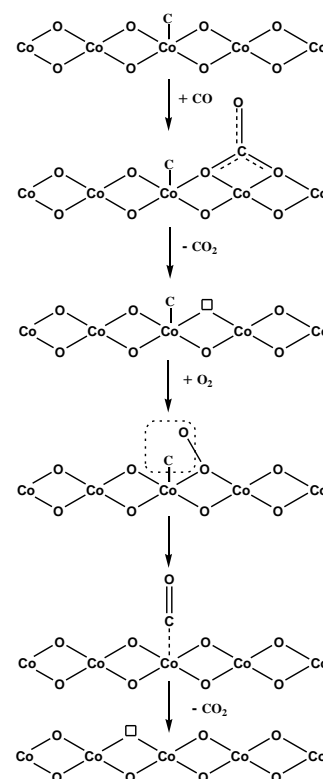**(3) Carbon decomposition**

Figure 16. Schematic representation of CO oxidation on Co_3O_4.

4.5 CONCLUSIONS

The combined results of operando NAP-XPS and operando FTIR spectroscopy (i.e., static steady state and dynamic switching experiments) are indicative of the redox Mars-van Krevelen mechanism for CO oxidation on Co_3O_4, involving the Co^{3+}/Co^{2+} couple and oxygen vacancies formation at higher temperatures. Moreover, results point to a role of reaction pathways such as carbonate formation followed by decomposition/reoxidation and CO dissociation followed by elementary carbon reoxidation in the overall CO oxidation reaction mechanism on Co_3O_4. It is suggested that upon an interaction of CO with Co_3O_4 in an excess of O_2, CO adsorbs linearly to cobalt cations and/or as carbonates, inducing vacancy formation by extracting lattice oxygen from the Co_3O_4 surface. Adsorbed oxygen on these vacancies can react with CO molecule adsorbed on the cobalt cation. CO adsorbed on a cobalt cation undergoes dissociation/disproportionation forming elementary carbon that is oxidized by an O_2 molecule likely activated on vacancies. Regarding carbonates, both bidentate and monodentate carbonates might be reaction intermediates at higher temperatures. An excess of O_2 in the reaction mixture facilitates decomposition/reoxidation of carbonates and their conversion to CO_2.

For CoO with particles of 20-50 nm, operando NAP-XPS combined with NEXAFS at the $CoL_{3,2}$ edge indicates oxidation of CoO to Co_3O_4 during CO oxidation (surface and near-surface) at 200 ^{o}C that causes the high activity. On the contrary, for the microscopic CoO (1 μm) no bulk oxidation of CoO to Co_3O_4 is observed during CO oxidation with operando XAS at the Co K edge at temperatures even of 360 ^{o}C that strongly points to an effect of the particle size on the catalytic activity of cobalt oxide materials.

This work clearly demonstrates the importance of combining several operando techniques in studying cobalt oxide catalysts under steady state as well as under dynamic conditions for revealing the reaction mechanism of CO oxidation.

4.6 REFERENCES

1. Ertl, G., Reactions at Surfaces: From Atoms to Complexity (Nobel Lecture). *Angewandte Chemie International Edition* **2008,** *47* (19), 3524-3535.

2. Zorn, K.; Giorgio, S.; Halwax, E.; Henry, C. R.; Gronbeck, H.; Rupprechter, G., CO Oxidation on Technological Pd-Al$_2$O$_3$ Catalysts: Oxidation State and Activity. *Journal of Physical Chemistry C* **2011,** *115* (4), 1103-1111.

3. Royer, S.; Duprez, D., Catalytic Oxidation of Carbon Monoxide over Transition Metal Oxides. *ChemCatChem* **2011,** *3* (1), 24-65.

4. Jia, C.-J.; Schwickardi, M.; Weidenthaler, C.; Schmidt, W.; Korhonen, S.; Weckhuysen, B. M.; Schüth, F., Co$_3$O$_4$–SiO$_2$ Nanocomposite: A Very Active Catalyst for CO Oxidation with Unusual Catalytic Behavior. *Journal of the American Chemical Society* **2011,** *133* (29), 11279-11288.

5. Xie, X.; Li, Y.; Liu, Z.-Q.; Haruta, M.; Shen, W., Low-temperature oxidation of CO catalysed by Co$_3$O$_4$ nanorods. *Nature* **2009,** *458* (7239), 746-749.

6. Alvarez, A.; Ivanova, S.; Centeno, M. A.; Odriozola, J. A., Sub-ambient CO oxidation over mesoporous Co$_3$O$_4$: Effect of morphology on its reduction behavior and catalytic performance. *Applied Catalysis A: General* **2012,** *431–432*, 9-17.

7. Teng, Y.; Kusano, Y.; Azuma, M.; Haruta, M.; Shimakawa, Y., Morphology effects of Co$_3$O$_4$ nanocrystals catalyzing CO oxidation in a dry reactant gas stream. *Catalysis Science & Technology* **2011,** *1* (6), 920-922.

8. Gu, D.; Jia, C.-J.; Weidenthaler, C.; Bongard, H.-J.; Spliethoff, B.; Schmidt, W.; Schüth, F., Highly Ordered Mesoporous Cobalt-Containing Oxides: Structure, Catalytic Properties, and Active Sites in Oxidation of Carbon Monoxide. *Journal of the American Chemical Society* **2015,** *137* (35), 11407-11418.

9. Iablokov, V.; Barbosa, R.; Pollefeyt, G.; Van Driessche, I.; Chenakin, S.; Kruse, N., Catalytic CO Oxidation over Well-Defined Cobalt Oxide Nanoparticles: Size-Reactivity Correlation. *ACS Catalysis* **2015,** *5* (10), 5714-5718.

10. Ding, K.; Wang, D.; Yang, P.; Hou, P.; Cheng, X., Enhanced CO catalytic oxidation of flower-like Co$_3$O$_4$ composed of small nanoparticles. *RSC Advances* **2016,** *6* (20), 16208-16214.

11. Hu, L.; Sun, K.; Peng, Q.; Xu, B.; Li, Y., Surface active sites on Co$_3$O$_4$ nanobelt and nanocube model catalysts for CO oxidation. *Nano Res.* **2010,** *3* (5), 363-368.

12. Yu, Y.; Takei, T.; Ohashi, H.; He, H.; Zhang, X.; Haruta, M., Pretreatments of Co$_3$O$_4$ at moderate temperature for CO oxidation at −80 °C. *Journal of Catalysis* **2009,** *267* (2), 121-128.

13. Pollard, M. J.; Weinstock, B. A.; Bitterwolf, T. E.; Griffiths, P. R.; Piers Newbery, A.; Paine Iii, J. B., A mechanistic study of the low-temperature conversion of carbon monoxide to carbon dioxide over a cobalt oxide catalyst. *Journal of Catalysis* **2008,** *254* (2), 218-225.

14. Jansson, J., Low-Temperature CO Oxidation over Co$_3$O$_4$/Al$_2$O$_3$. *Journal of Catalysis* **2000,** *194* (1), 55-60.

15. Jansson, J.; Skoglundh, M.; Fridell, E.; Thormählen, P., A Mechanistic Study of Low Temperature CO Oxidation over Cobalt Oxide. *Topics in Catalysis* **2001,** *16-17* (1-4), 385-389.

16. Jansson, J.; Palmqvist, A. E. C.; Fridell, E.; Skoglundh, M.; Österlund, L.; Thormählen, P.; Langer, V., On the Catalytic Activity of Co$_3$O$_4$ in Low-Temperature CO Oxidation. *Journal of Catalysis* **2002,** *211* (2), 387-397.

17. Broqvist, P.; Panas, I.; Persson, H., A DFT Study on CO Oxidation over Co$_3$O$_4$. *Journal of Catalysis* **2002,** *210* (1), 198-206.

18. Wang, H.-F.; Kavanagh, R.; Guo, Y.-L.; Guo, Y.; Lu, G.; Hu, P., Origin of extraordinarily high catalytic activity of Co$_3$O$_4$ and its morphological chemistry for CO oxidation at low temperature. *Journal of Catalysis* **2012,** *296*, 110-119.

19. Pang, X.-Y.; Liu, C.; Li, D.-C.; Lv, C.-Q.; Wang , G.-C., Structure Sensitivity of CO Oxidation on Co$_3$O$_4$: A DFT Study. *ChemPhysChem* **2013,** *14* (1), 204-212.

20. Jiang, D.-e.; Dai, S., The role of low-coordinate oxygen on Co$_3$O$_4$(110) in catalyticCO oxidation. *Physical Chemistry Chemical Physics* **2011,** *13* (3), 978-984.

21. Zafeiratos, S.; Dintzer, T.; Teschner, D.; Blume, R.; Hävecker, M.; Knop-Gericke, A.; Schlögl, R., Methanol oxidation over model cobalt catalysts: Influence of the cobalt oxidation state on the reactivity. *Journal of Catalysis* **2010,** *269* (2), 309-317.

22. Perti, D.; Kabel, R. L., Kinetics of CO oxidation over Co$_3$O$_4$/γ-Al$_2$O$_3$. Part I: Steady state. *AIChE Journal* **1985,** *31* (9), 1420-1426.

23. Perti, D.; Kabel, R. L., Kinetics of CO oxidation over Co$_3$O$_4$/γ-Al$_2$O$_3$. Part II: Reactor dynamics. *AIChE Journal* **1985,** *31* (9), 1427-1434.

24. Perti, D.; Kabel, R. L.; McCarthy, G. J., Kinetics of CO oxidation over Co$_3$O$_4$/γ-Al$_2$O$_3$. Part III: Mechanism. *AIChE Journal* **1985,** *31* (9), 1435-1440.

25. Lou, Y.; Ma, J.; Cao, X.; Wang, L.; Dai, Q.; Zhao, Z.; Cai, Y.; Zhan, W.; Guo, Y.; Hu, P.; Lu, G.; Guo, Y., Promoting Effects of In$_2$O$_3$ on Co$_3$O$_4$ for CO Oxidation: Tuning O2 Activation and CO Adsorption Strength Simultaneously. *ACS Catalysis* **2014,** *4* (11), 4143-4152.

26.   Ferstl, P.; Mehl, S.; Arman, M. A.; Schuler, M.; Toghan, A.; Laszlo, B.; Lykhach, Y.; Brummel, O.; Lundgren, E.; Knudsen, J.; Hammer, L.; Schneider, M. A.; Libuda, J., Adsorption and Activation of CO on Co_3O_4(111) Thin Films. *The Journal of Physical Chemistry C* **2015,** *119* (29), 16688-16699.

27.   Köck, E.-M.; Kogler, M.; Bielz, T.; Klötzer, B.; Penner, S., In Situ FT-IR Spectroscopic Study of CO_2 and CO Adsorption on Y_2O_3, ZrO_2, and Yttria-Stabilized ZrO_2. *The Journal of Physical Chemistry C* **2013,** *117* (34), 17666-17673.

28.   Davydov, A., *MOLECULAR SPECTROSCOPY OF OXIDE CATALYST SURFACES*. John Wiley & Sons Ltd: The Atrium, Southern Gate, Chichester, West Sussex PO19 8SQ, England, 2003; p 684.

29.   Pokrovski, K.; Jung, K. T.; Bell, A. T., Investigation of CO and CO_2 Adsorption on Tetragonal and Monoclinic Zirconia. *Langmuir* **2001,** *17* (14), 4297-4303.

30.   Petitto, S. C.; Marsh, E. M.; Carson, G. A.; Langell, M. A., Cobalt oxide surface chemistry: The interaction of CoO(1 0 0), Co_3O_4(1 1 0) and Co_3O_4(1 1 1) with oxygen and water. *Journal of Molecular Catalysis A: Chemical* **2008,** *281* (1–2), 49-58.

31.   Zhou, M.; Cai, L.; Bajdich, M.; García-Melchor, M.; Li, H.; He, J.; Wilcox, J.; Wu, W.; Vojvodic, A.; Zheng, X., Enhancing Catalytic CO Oxidation over Co_3O_4 Nanowires by Substituting Co^{2+} with Cu^{2+}. *ACS Catalysis* **2015,** *5* (8), 4485-4491.

4.7 SUPPORTING INFORMATION
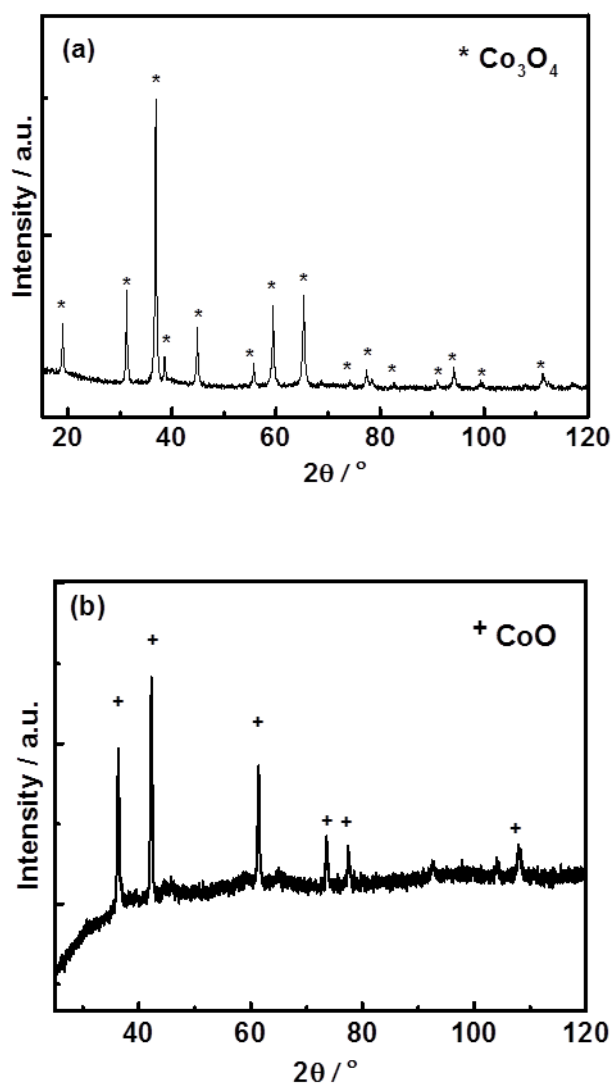
Figure S1. X-ray diffraction patterns for Co_3O_4 (a) and commercial microscopic CoO (b).
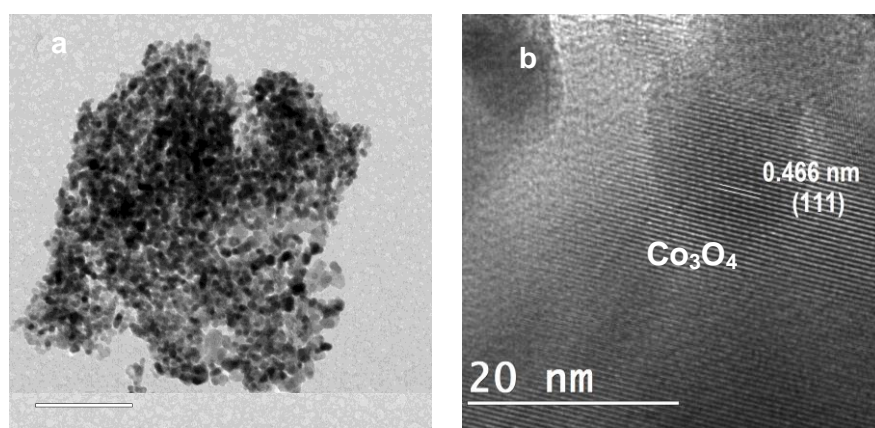
Figure S2. (HR)TEM of Co_3O_4 (a, b).
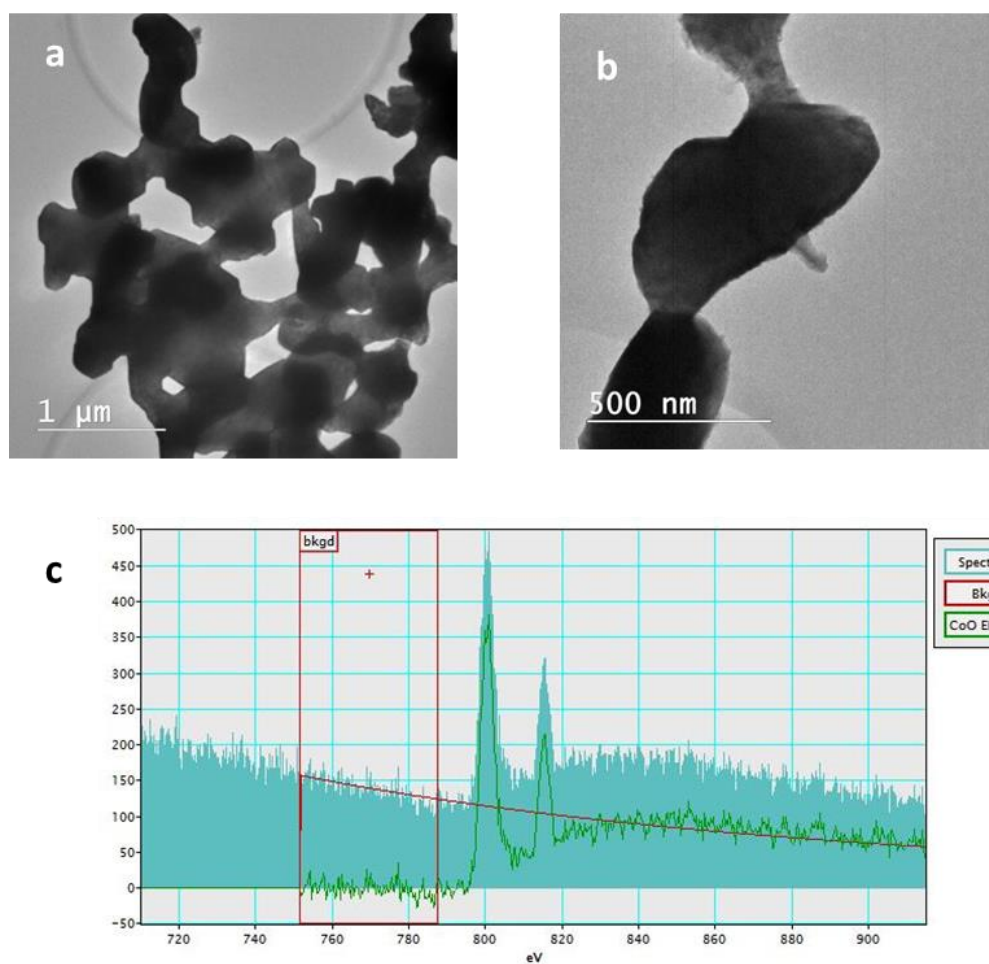
Figure S3. TEM (a, b) and EELS (c) of commercial microscopic CoO.
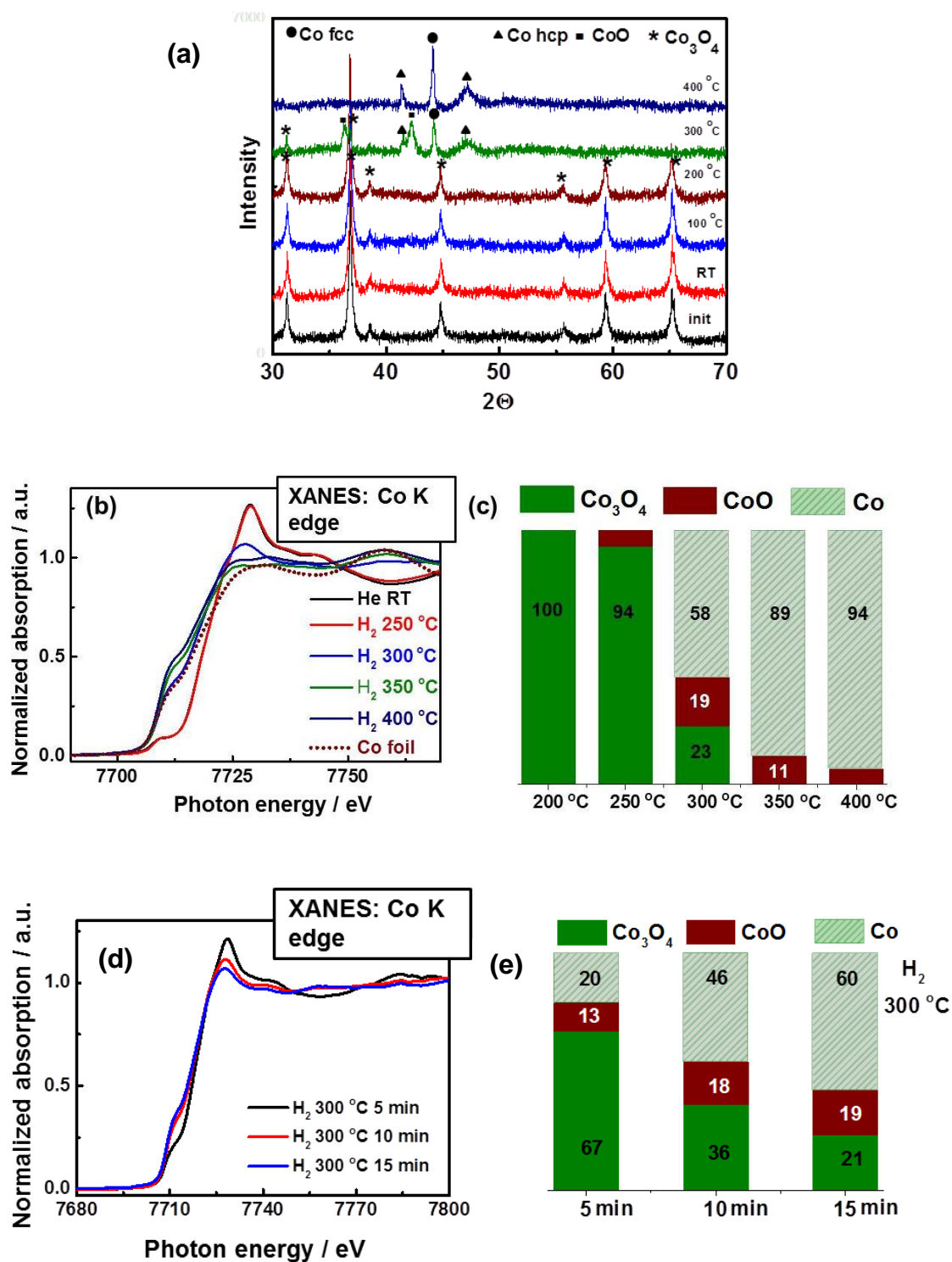
Figure S4. In situ XRD during H_2-temperature programmed reduction (TPR) of Co_3O_4 (a); in situ XAS H_2-TPR at the Co K edge (b, c); in situ XAS H_2-TPR at the Co K edge at 300 °C over (d, e); in all cases (5 vol.% H_2 in He, total flow 50 mL min^{-1}, heating rate 10 °C min^{-1})
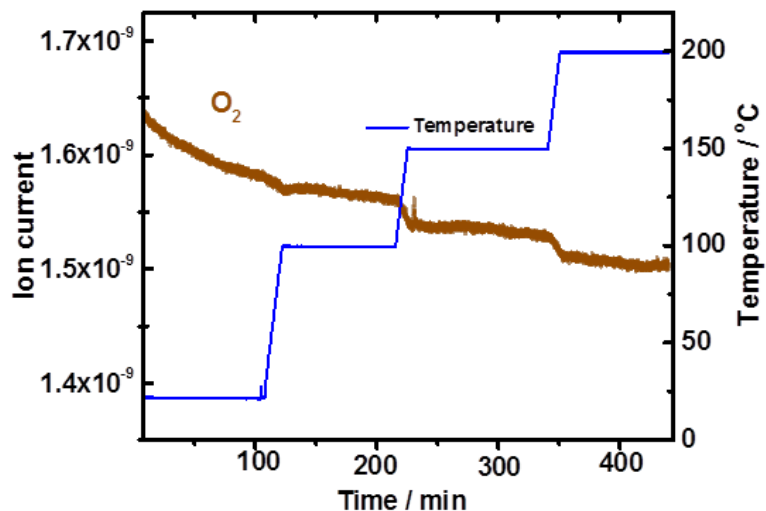
Figure S5. O_2 region for catalytic data recorded during NAP-XPS CO oxidation from RT to 200 ^{o}C (0.15 mbar CO and 0.3 mbar O_2) on Co_3O_4.
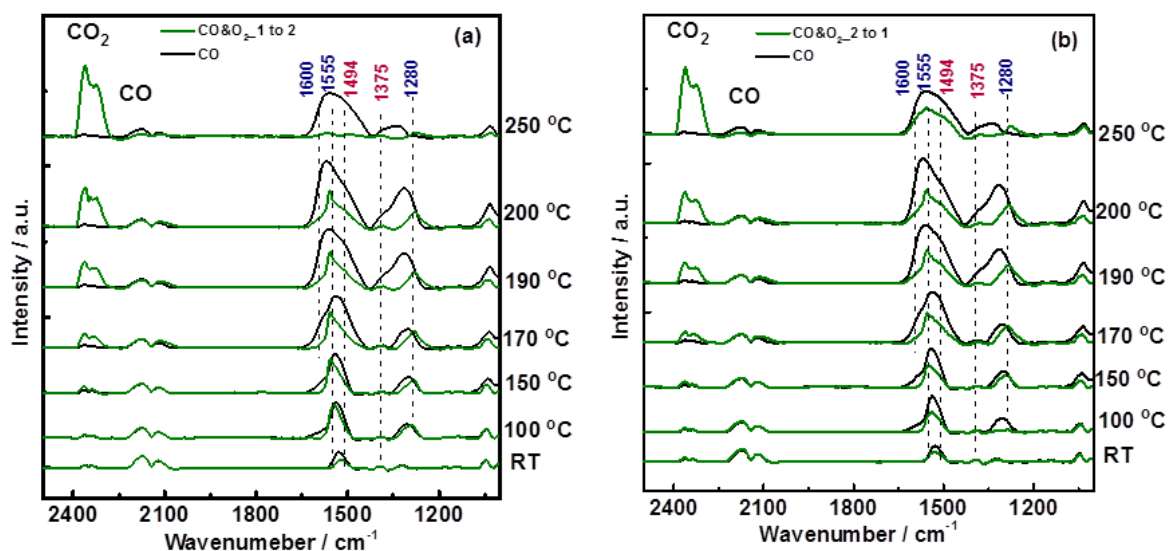
Figure S5. FTIR spectra for Co_3O_4 recorded during: (a) adsorption of CO (50 mbar) and during CO oxidation (50 mbar and 100 mbar O_2) in flow mode from RT to 250 ^{o}C (total flow 25 mL min^{-1}); (b) adsorption of CO (50 mbar) and during CO oxidation (50 mbar and 25 mbar O_2) in flow mode from RT to 250 ^{o}C (total flow 25 mL min^{-1}).
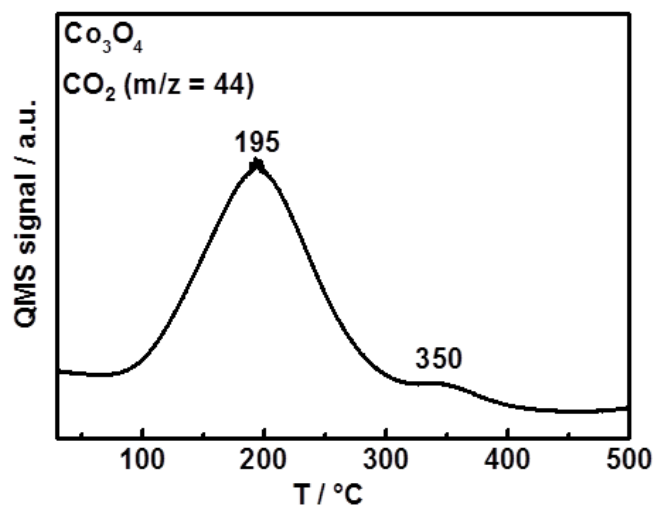
Figure S6. CO-temperature programmed desorption on Co_3O_4.
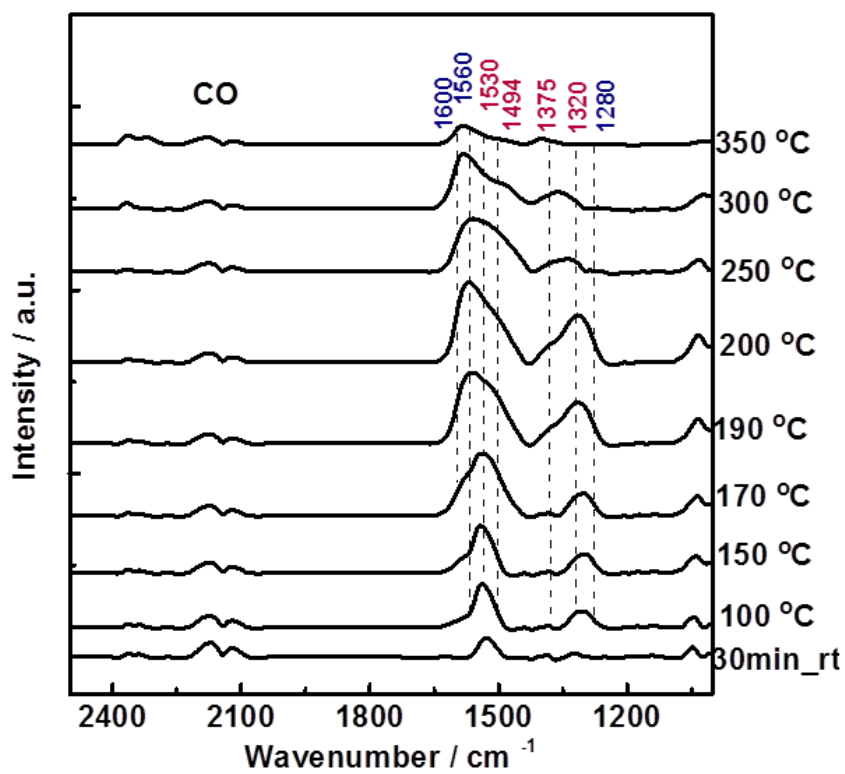
Figure S7. FTIR spectra for Co_3O_4 recorded during adsorption of CO (50 mbar) in flow mode (total flow 25 mL min^{-1}) from RT to 350 ^{o}C.
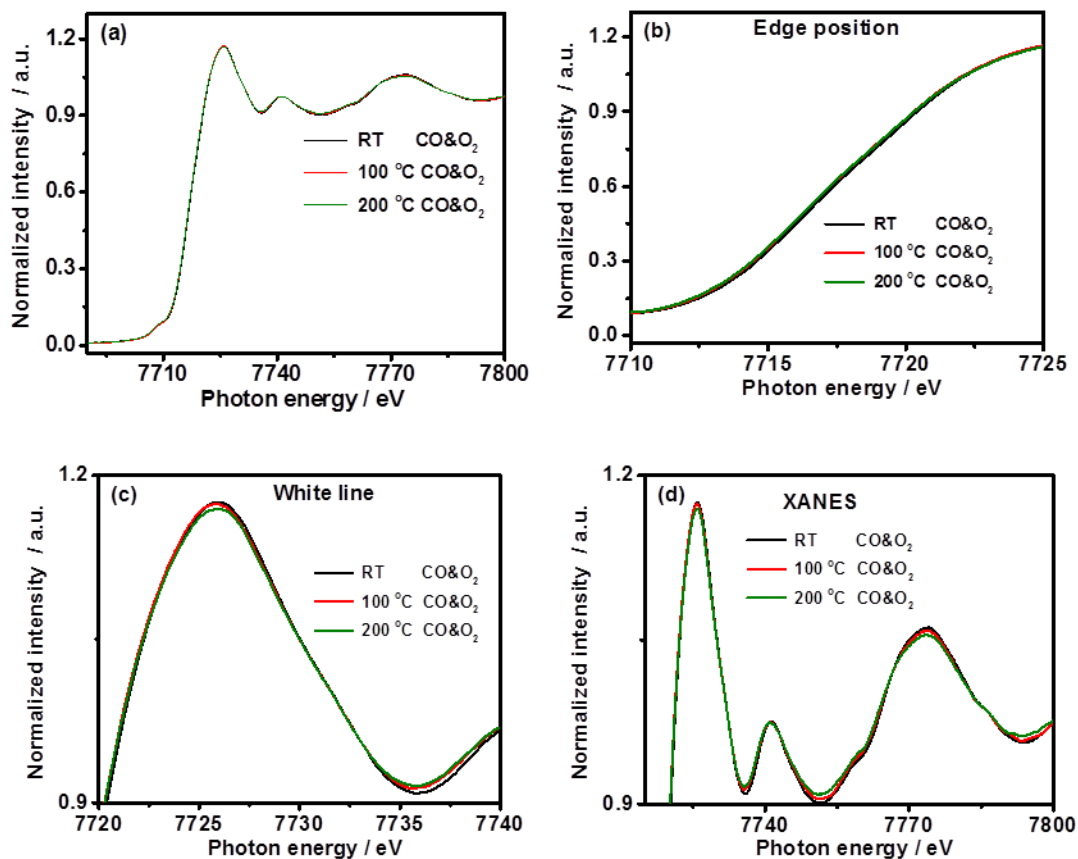
Figure S8. XANES at the Co K edge for CoO during CO oxidation with a reaction mixture of 5 vol.% CO, 10 vol.% O_2 and 85 vol.% He, total flow 50 mL min^{-1} from RT to 200 ^{o}C: (a) overall spectra; (b) the edge position; (c) the white line; (d) the XANES region.
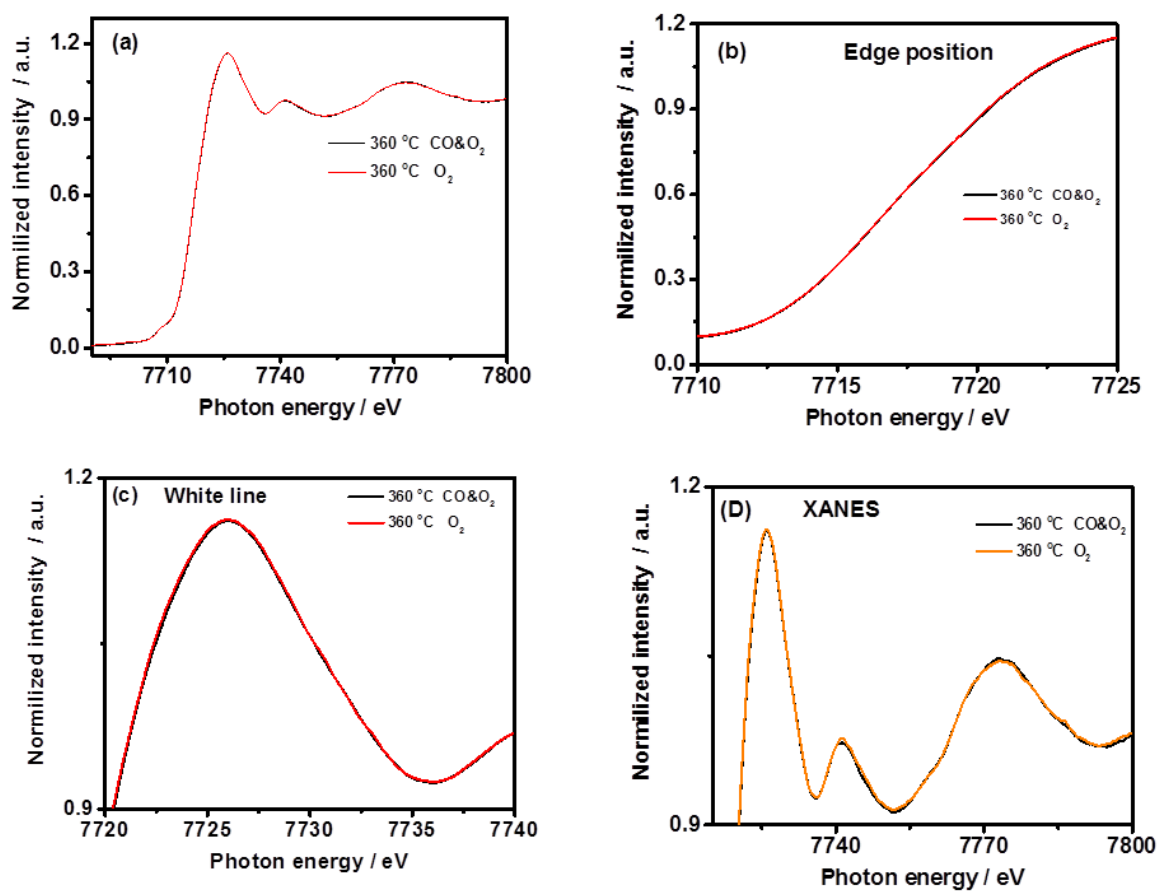
Figure S9. Comparison of XANES at the Co K edge for CoO after CO oxidation with a reaction mixture of 5 vol.% CO, 10 vol.% O_2 and 85 vol.% He, total flow 50 mL min^{-1} at 360 °C and after O_2 oxidation with 10 vol.% O_2 and 90 vol.% He, total flow 50 mL min^{-1} at 360 °C: (a) overall spectra; (b) the edge position; (c) the white line; (d) the XANES region.

CHAPTER 5

OPERANDO XAS AND NAP-XPS STUDIES OF PREFERENTIAL CO OXIDATION ON Co_3O_4 AND CeO_2-Co_3O_4 CATALYSTS

ABSTRACT:

Co_3O_4 is a promising catalyst for removing CO from H_2 streams via the preferential CO oxidation (PROX). A Mars-van Krevelen redox mechanism is often suggested but a detailed knowledge especially of the oxidation state of the catalytically active surface under reaction conditions is typically missing. We have thus utilized operando X-ray absorption spectroscopy to examine structure and oxidation state during PROX, and near atmospheric pressure-XPS at low photoelectron kinetic energies and thus high surface sensitivity to monitor surface composition changes. The rather easy surface reduction in pure CO (starting already at ~100 °C) and the easy reoxidation by O_2 suggest that molecularly adsorbed CO reacts with lattice oxygen, which is replenished by gas phase O_2. Nevertheless, the steady state concentration of oxygen vacancies under reaction conditions is too low even for XPS detection so that both the bulk and surface of Co_3O_4 appear fully oxidized during PROX. Furthermore, the effect of adding CeO_2 (a less active material) to Co_3O_4 was studied. Promotion of Co_3O_4 with 10 wt% CeO_2 increases the reduction temperatures in CO and H_2 and enhances the PROX activity. Since CeO_2 is a less active material, this can only be explained by a higher activity of the Co-O-Ce interface.

5.1 INTRODUCTION

The hydrogen-fueled proton exchange membrane fuel cell (PEMFC) is an attractive pollution-free power source for portable and stationary applications, but it requires hydrogen of high purity. The current hydrogen production is mainly based on methane steam reforming, oil/naphtha reforming, and coal gasification to syngas (CO + H_2), followed by the water-gas shift reaction (WGSR) (i.e., $CO+H_2O{\rightarrow}CO_2+H_2$), and separation processes [1]. However, even after these processes the hydrogen produced still contains CO traces, typically 1-100 ppm, which bind strongly to the Pt/C anode and reduce the number of Pt surface sites available for H_2 adsorption/dissociation and oxidation, thus lowering the overall efficiency of PEMFC [2]. For long-term PEMFC operation, a very deep purification of hydrogen for obtaining CO-free H_2 is thus crucial. Purification of H_2 can be achieved through Pd membrane separation, catalytic methanation (i.e., $CO+3H_2{\rightarrow}CH_4+H_2O$) or preferential oxidation of CO (PROX) (2) [3].

$$\text{PROX}: CO+H_2+0.5O_2{\rightarrow}CO_2+H_2 \quad \Delta H_{298} = -283 \text{ kJ/mol} \quad (1)$$
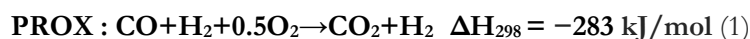
During catalytic methanation there is an apparent loss of H_2 which can be avoided for PROX, provided this reaction runs selective. However, the competitive adsorption of CO and H_2 on the catalyst surface and similar enthalpies of CO oxidation (2) and H_2 oxidation (3) facilitate their parallel occurrence:

$$CO+0.5O_2{\rightarrow}CO_2 \quad \Delta H_{298} = -283 \text{ kJ/mol} \quad (2)$$

$$H_2+0.5O_2{\rightarrow}H_2O \quad \Delta H_{298} = -242 \text{ kJ/mol} \quad (3)$$

The challenge of PROX is thus to achieve a high CO oxidation rate at moderate temperature and with high selectivity, thereby avoiding H_2 oxidation and methanation, accompanied by resistance towards deactivation (e.g., by coking).

The PROX catalysts most frequently investigated are supported noble metals (e.g., Pt, Rh, Ru, Ir) [1c], but none of them meets all requirements. In recent years, due to their price and limited availability, increasing attention has been directed toward non-noble-metal alternatives, such as transition metal oxides. Especially copper-based and cobalt-based catalysts show potential for PROX [4]. While copper-based PROX catalysts exhibit high activity even at low temperature, they operate in a rather narrow temperature window (50-160 °C) and show limited stability at higher temperatures [5].

In contrast, cobalt-based catalysts operate in a wider temperature window, offering a higher stability with regard to hot spots induced by the exothermicity of both CO oxidation and H_2 oxidation. However, the onset temperature of CO oxidation of current catalysts needs to be lowered, and the ideal catalyst should start working already at room temperature (RT) and have high activity and selectivity around 80-100 °C. Thus, research has been directed toward the improvement of the catalytic performance of cobalt oxide catalysts via addition of other reducible metal oxides (e.g., MnO_2, CeO_2) [4h, 4i, 6]. Nevertheless, the improvement of effective cobalt-based catalysts requires a fundamental understanding of the active catalyst.

Previous studies of PROX on cobalt-based catalysts have demonstrated that the oxidation state of cobalt is the most important factor. For example, a study of the active cobalt species using substituted cobalt spinel oxides, such as $Zn_xCo_{3-x}O_4$ (x = 0 - 1), $Al_xCo_{3-x}O_4$ (x = 0 - 2.5), and $Fe_xCo_{3-x}O_4$ (x = 0 - 2.5), has shown that octahedrally coordinated Co^{3+} surface ions are crucial for high oxidation activity and selectivity in the presence of H_2 [7]. However, another investigation of PROX over Co_3O_4 and CoO has demonstrated that CoO shows higher activity than Co_3O_4, while the metallic Co phase induces methane formation, resulting in a decrease of selectivity [4e]. Thus, the current understanding of PROX over cobalt-based catalysts remains ambiguous with contradicting results concerning the role of Co^{2+} and Co^{3+}. This is due to the fact that the investigations of PROX on cobalt-based catalysts were mostly based on ex situ analyses of the catalysts. A recent in situ X-ray absorption (XAS) study of Gewade et al. on Co_3O_4-CeO_2 catalyst has revealed that the catalyst (bulk) is Co_3O_4 under the reducing PROX reaction environment at 175 °C when CO oxidation is dominant [4h]. But it is still unclear whether the surface is also composed of Co_3O_4 or is partially reduced. Furthermore, the structure of ceria is unknown.

As outlined, the correlation between the cobalt (surface) oxidation state and its catalytic activity is an important topic of cobalt oxide PROX catalysis. This encompasses also fundamental questions of how Co_3O_4 undergoes reduction in (pure) H_2 or CO atmospheres and how to preserve the ideal cobalt oxide over a wide temperature range, thereby preventing reduction to metallic cobalt e.g. on hot spots, which promotes side reactions. Several studies have already been performed to obtain an understanding of Co_3O_4 reduction in H_2 that include primary structural investigations by in situ X-ray diffraction (XRD), in situ environmental electron microscopy, and temperature programmed reduction (TPR) [8]. In contrast to H_2 reduction, Co_3O_4 reduction in CO atmosphere has been much less investigated and very little is known on a fundamental level [9].

In this study, we aim to improve the understanding of PROX over cobalt oxide catalysts by applying in situ (operando) methodology, in particular to shed light on the correlation of the surface and bulk oxidation state with the specific activity/selectivity [10]. While the Mars-van Krevelen mechanism is widely accepted for CO oxidation on Co_3O_4, the oxidation state and structure of the catalyst under PROX

conditions and whether (surface) reduction of Co_3O_4 by CO or reoxidation by O_2 proceed faster is unknown. This applies particularly for the surface. Thus, we combined advanced operando methods, i.e. in situ XAS at the Co K edge to reveal bulk structural changes, , whereas for surface composition changes (information depth around 0.5 nm) in situ near atmospheric pressure X-ray photoelectron spectroscopy (NAP-XPS) was applied. Along these lines, cobalt oxide reduction in H_2 or CO were also examined, because none of the previous studies examined, for the same material, the oxidation state in H_2, CO, and in the PROX reaction mixture. We also investigated the promotional role of CeO_2 on the improvement of Co_3O_4 reactivity.

5.2 EXPERIMENTAL

5.2.1 CATALYST SYNTHESIS

Co_3O_4 was used as received from Fluka (purity 99.5 %). CeO_2-Co_3O_4 with 10 wt% CeO_2 loading was prepared via wet impregnation of Co_3O_4. In a typical synthesis, 0.504 g of $Ce(NO_3)_3 \cdot 6H_2O$ was dissolved in 7 mL of distilled water, added to 1.8 g of Co_3O_4, and stirred over night. After that, the catalyst was dried at 110 °C for 3 h and further calcined at 400 °C for 2 h.

CeO_2 powder catalyst has been prepared via surfactant-assisted precipitation method. In a typical synthesis, 6 mmol of surfactant Pluronic F-127 (Sigma-Aldrich, used as received) was dissolved in 200 mL distilled water at room temperature and 10 mmol of $Ce(NO_3)_3 \cdot 6H_2O$ was added to it. After that, an aqueous solution of NaOH (0.3 mol L^{-1}) was added to the solution under vigorous stirring until pH 10 was reached. Then the obtained mixture was aged at 90 °C for 3 h. The precipitate was filtered, washed 3 times with deionized water, and dried at 110°C for 12 h. Afterwards, the powder was calcined at 500 °C for 4h.

Basic characterization of the materials was done by N_2 physisorption, X-ray powder diffraction (XRD) and high resolution transmission electron microscopy (HRTEM). Experimental details are provided as supplementary material.

5.2.2 TEMPERATURE PROGRAMMED REDUCTION (CO-TPR, H_2-TPR)

CO-temperature programmed reduction (CO-TPR) and H_2-temperature programmed reduction (H_2-TPR) experiments on catalysts (ca. 20 mg) were performed in a continuous-flow fixed-bed quartz reactor under atmospheric pressure. Before each experiment, the catalysts were pretreated with synthetic air (50 mL min^{-1}) at 400 °C for 30 min (heating rate 10 °C min^{-1}) to remove contaminants. The samples were then cooled to 30 °C under a flow of synthetic air and purged with helium for 5-10 min.

For CO-TPR and H_2-TPR, the pretreated samples were exposed either to a mixture of 5 vol.% CO and 95 vol.% He (CO-TPR) at RT or to 5 vol.% H_2 or 50 vol.% H_2 in He (H_2-TPR). The total flow was always adjusted to 50 mL min^{-1}. Then, the system was heated to 700 °C with a heating rate of 10 °C min^{-1}. The gas stream was analyzed by an online quadrupole mass spectrometer (Prisma Plus QMG 220, Pfeiffer Vacuum) equipped with a Faraday detector.

5.2.3 CATALYTIC PREFERENTIAL CO OXIDATION

Preferential CO oxidation on Co_3O_4 and CeO_2-Co_3O_4 catalysts was performed in a continuous-flow fixed-bed quartz reactor under atmospheric pressure. The sample (ca. 20 mg), mixed with quartz powder to avoid mass and heat transfer limitations, was loaded into the reactor and pretreated with synthetic air (50 mL min^{-1}) at 400 °C for 30 min (heating rate 10 °C min^{-1}). The sample was then cooled to 30 °C under a flow of synthetic air, before a 1 vol.% CO, 1 vol.% O_2, 50 vol.% H_2 and 48 vol.% He mixture (total flow 50 mL min^{-1}) was introduced. Then, the system was heated to 200 °C with a heating rate of 2 °C min^{-1}. The concentrations of CO and CO_2 in the outlet stream were monitored by gas chromatography using a HP-PLOT Q column and a flame-ionization detector with a methanizer.

In addition, the following temperature programmed reaction experiments were carried out in the same setup as PROX: PROX (1 vol.% CO, 1 vol.% O_2, 50 vol.% H_2), CO oxidation (1 vol.% CO, 1 vol.% O_2), hydrogen oxidation (1 vol.% O_2, 50 vol.% H_2), CO methanation (1 vol.% CO, 50 vol.% H_2), CO_2 hydrogenation (1 vol.% CO_2, 50 vol.% H_2), and water gas shift (1 vol.% CO, 3 vol.% H_2O), reactions (total flow 50 mL min^{-1}). The gas stream was analyzed by an online quadrupole mass spectrometer (PrismaPlus QMG 220, Pfeiffer Vacuum, equipped with a Faraday detector) during heating the catalyst in the reaction mixtures from RT to 350 °C with a heating rate of 2 °C min^{-1}.

5.2.4 OPERANDO XAS

Operando X-ray absorption spectroscopy studies at the Co K edge (7709 eV) were carried out in transmission geometry at the I811 beamline at the MAX-lab synchrotron radiation source, Lund University, Sweden, in a reaction cell supplied by MAX-lab II [11]. Co metal foil was used for energy calibration. Higher harmonics were rejected using a double crystal monochromator detuned by -50% of the maximum Bragg intensity. Typically, ca. 2.5 mg of the catalyst diluted with 10 mg of BN was loaded into the cell and pretreated in 20 vol.% O_2 in He at 400 °C for 30 min. The sample was then cooled to RT and purged with He at RT for 15 min, before the PROX reaction mixture of 1 vol.% CO, 1 vol.% O_2, 50 vol.% H_2 and 48 vol.% He was introduced. XAS spectra were recorded at RT and during subsequent heating to 350 °C. The gas stream outlet was controlled by an MKS mass spectrometer equipped with a

SEM detector. In addition to PROX, CO-temperature programmed reduction (5 vol.% CO in He) followed by O_2-temperature programmed oxidation (20 vol.% O_2 in He) and H_2-temperature programmed reduction (50 vol.% H_2 in He) experiments were performed. All experiments were carried out at ambient pressure with a total flow of 50 mL min^{-1}. The duration of each Co K edge XAS scan was 5 min. Details on data analysis are provided as supplementary material.

5.2.5 OPERANDO NAP-XPS

Operando near atmospheric pressure X-ray photoelectron spectroscopy was performed at the ISISS beamline at the synchrotron radiation facility BESSY II of the Helmholtz-Zentrum Berlin, Germany. The setup consists of a reaction cell attached to a set of differentially pumped electrostatic lenses and a separately pumped analyzer (Phoibos 150 Plus, SPECS GmbH), as described elsewhere [12]. Typically, the powder sample (ca. 30 mg) was pressed into a Tantalum grid (to minimize potential charging effects) together with a K-type thermocouple, fixed to a sapphire sample holder and mounted inside the XPS reaction cell in front of the first aperture of the differentially pumped electrostatic lens system. The heating of the samples was done from the back using an infrared laser. Before the experiments, the sample was pretreated in the XPS reaction cell by oxidation (0.5 mbar O_2 at 400 °C) until all residual surface carbon and carbonates disappeared. After cooling the sample to RT, either CO (0.15 mbar), H_2 (0.4 mbar) or the CO+O_2+H_2 PROX mixture (1/1/12 ratio at 0.5 mbar) were introduced with the partial pressure of the gasses controlled by calibrated mass flow controllers, and photoemission spectra were recorded. Then, the sample was heated to 100, 150, 200, 250 and 300 °C with a heating rate of 5 °C min^{-1}, and photoemission spectra were acquired at these temperatures. To ensure surface specificity, the Co 2p, Ce 3d, and C 1s core-level regions were recorded using selected photon energies that resulted in photoelectrons with 200 eV kinetic energy and a 0.6 nm inelastic mean free path for cobalt. The gas phase composition was monitored on-line by an electron impact Quadrupole mass spectrometer and multichannel gas chromatograph, which were connected to the XPS cell via a gas dosing valve. Details on data analysis are described in the supplementary material.

5.3 RESULTS AND DISCUSSION

5.3.1 STRUCTURAL CHARACTERIZATION OF Co_3O_4 AND CeO_2-Co_3O_4 CATALYSTS

The structural and textural properties of Co_3O_4 and CeO_2-Co_3O_4 catalysts were studied by X-ray diffraction (XRD) (**Figure S1)** and N_2 adsorption (**Figure S2**). For Co_3O_4 the (average) crystallite size was 28 nm, for CeO_2-Co_3O_4 it was again 28 nm for Co_3O_4 but 4 nm for CeO_2, as determined from XRD. The specific surface area, average pore diameter, and pore volume for Co_3O_4 and CeO_2-Co_3O_4 were similar:

38.3 m²/g, 14.2 nm, 0.15 cm³/g for Co_3O_4 and 36.2 m²/g, 13.0 nm, 0.15 cm³/g for CeO_2-Co_3O_4. Thus, wet impregnation of Co_3O_4 with 10 wt% CeO_2 did not alter the textural properties of Co_3O_4 and led to a homogeneous distribution of CeO_2 on Co_3O_4. The structure and morphology of the catalysts were further investigated by high resolution transmission electron microscopy (HR-TEM). The low magnification TEM image of Co_3O_4 (**Figure 1a**) illustrates that Co_3O_4 is present as nanospheres with sizes between 20 and 50 nm. The HRTEM image (**Figure 1b**) shows lattice fringes with a 0.466 nm spacing that corresponds to (111) planes of Co_3O_4. (HR)TEM images were also taken for CeO_2-Co_3O_4 (**Figures 1c, d**). The lattice fringes of 0.311 nm with slightly darker contrast correspond to CeO_2 (111), indicating CeO_2 particles with diameters of 5 to 10 nm supported on Co_3O_4. Elemental mapping by EELS and HAADF-STEM confirmed that the small CeO_2 particles were homogeneously distributed throughout the sample (**Figure S3**).
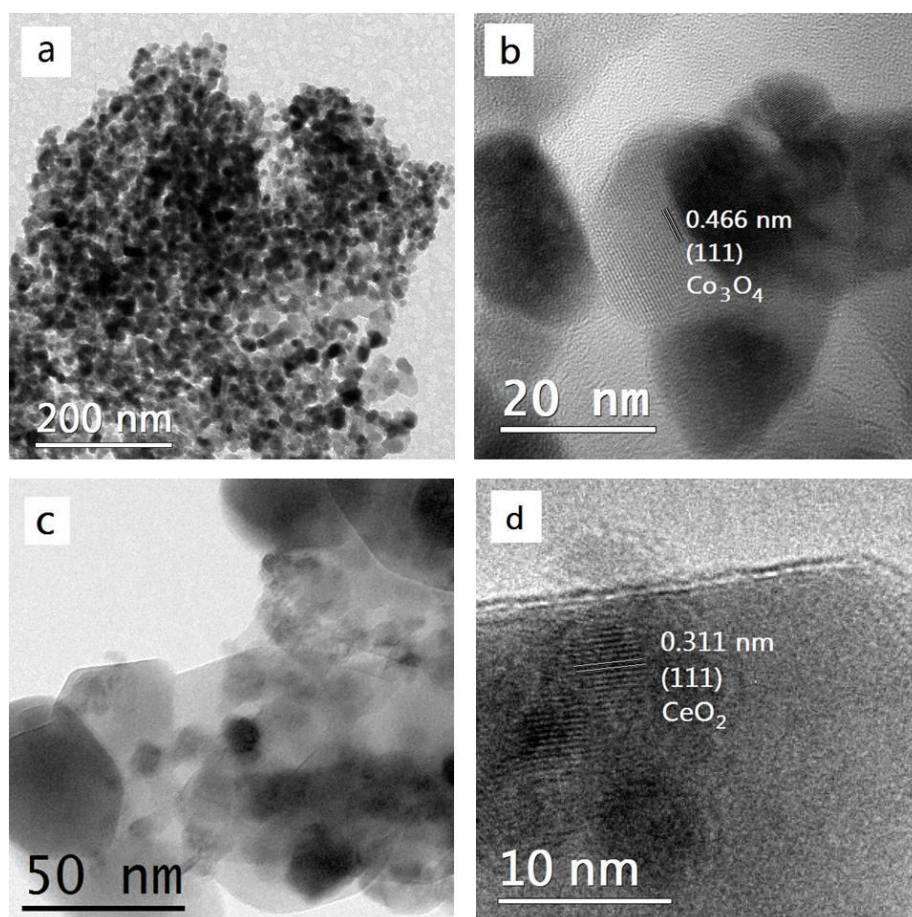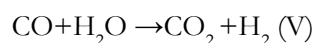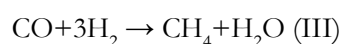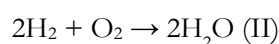

Figure 1. (HR)TEM of Co_3O_4 (a,b), and CeO_2-Co_3O_4 (c, d).

5.3.2 PROX ACTIVITY OF Co_3O_4

To examine PROX reaction profiles, temperature programmed reaction experiments were performed over Co_3O_4 catalyst (**Figure 2a**). Following the concentration of the educts (CO, O_2) and products (CO_2, H_2O, CH_4), three temperature windows were identified. On Co_3O_4, CO oxidation is the dominant reaction from 50 to 175 °C, with only negligible amounts of H_2O being produced above 100 °C (**Figure 2a**). Above 175 °C the concentration of CO and H_2O increased, while that of CO_2 decreased. At 230 °C methane formation started and water production strongly increased. The H_2O peak at 260 °C is due to reduction of Co_3O_4 (see below).

To better understand the temperature-dependence of the PROX reaction profile, the corresponding individual reactions were examined as well. This holds for reactions of the educts (CO oxidation (I), H_2 oxidation (II), CO hydrogenation (III)), as well as for reactions of products with reactants (CO_2 hydrogenation (IV), H_2O + CO (water gas shift reaction) (V)).

$$2CO + O_2 \rightarrow 2CO_2 \text{ (I)}$$
$$2H_2 + O_2 \rightarrow 2H_2O \text{ (II)}$$
$$CO+3H_2 \rightarrow CH_4+H_2O \text{ (III)}$$
$$CO_2+4H_2 \rightarrow CH_4+2H_2O \text{ (IVa)}$$
$$CO_2 +H_2 \rightarrow CO+H_2O \text{ (IVb)}$$
$$CO+H_2O \rightarrow CO_2 +H_2 \text{ (V)}$$
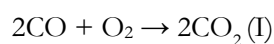
CO oxidation (I) starts around 75 °C and reaches a maximum at 150 °C, when 100 % conversion is reached. For H_2 oxidation (II), a similar pattern is observed with the water peak at 260 °C being due to Co_3O_4 reduction (**Figure S4**). For CO hydrogenation (III), methanation was observed above 225 °C with the water again peaking at 255 °C due to Co_3O_4 reduction. For CO_2 hydrogenation (IVa; Sabatier reaction), formation of CH_4 and H_2O was observed above 220 °C when the CO_2 concentration strongly decreases, whereas there was no activity for reverse water gas shift reaction (IVb; RWGS). However, the Sabatier reaction runs via CO. It might be that CO that is formed via RWGS immediately undergoes CO methanation, because CO methanation on Co_3O_4 starts in the same temperature range at around 225-230 °C (III). Note that the water peak at around 255°C is not so pronounced because of the high concentration of water that is formed. For CO + H_2O (water gas shift reaction) (V), it was observed that the conversion of CO to CO_2 starts only above 350 °C. Apparently, the presence of water hinders Co_3O_4 reduction by CO. Only a small peak of CO_2 was observed at around 250°C.
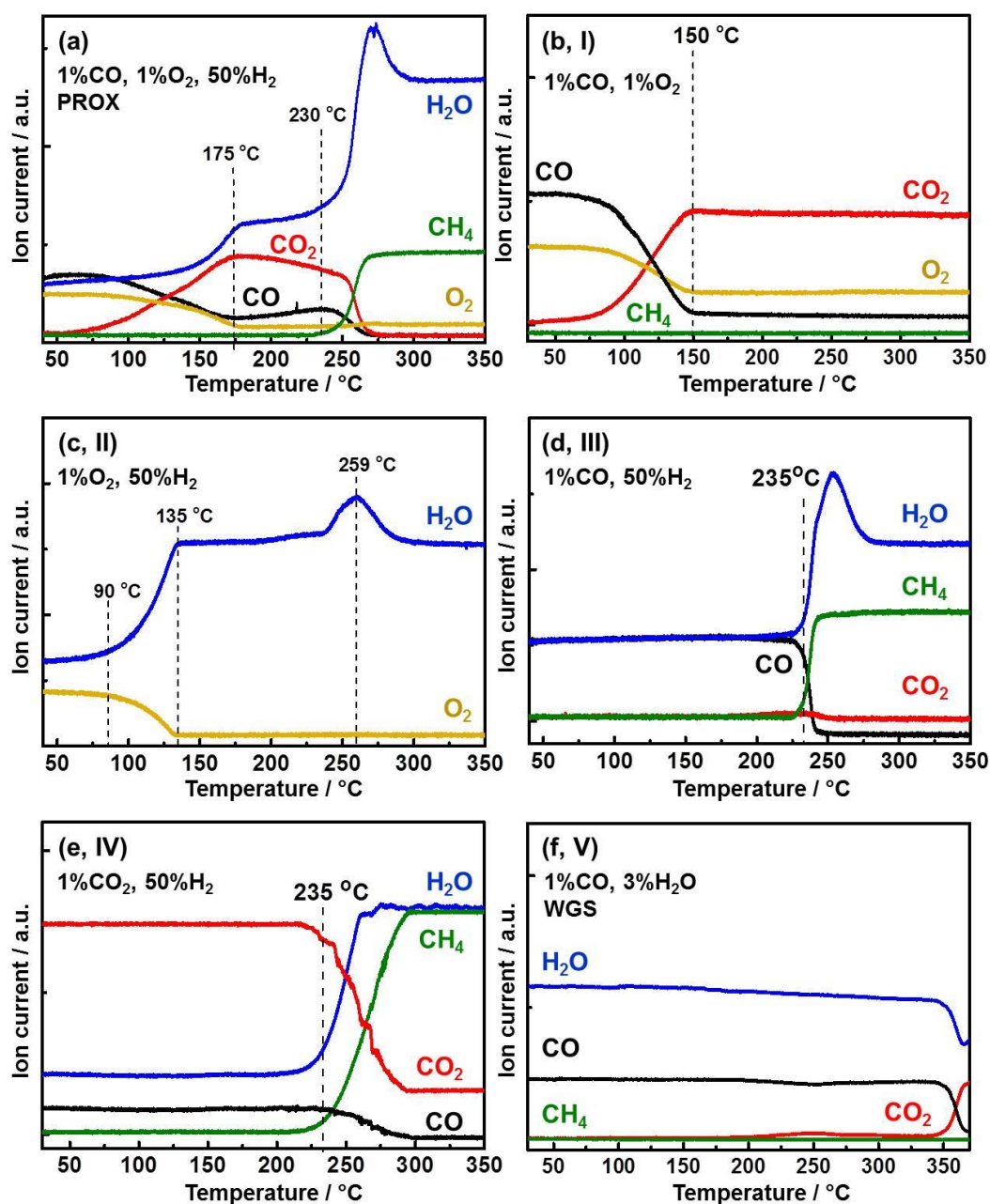
Figure 2. Temperature programmed reactions on Co_3O_4: **(a)** PROX reaction (1 vol.% CO, 1 vol.% O_2, 50 vol.% H_2); **(b, I)** CO oxidation (1 vol.% CO, 1 vol.% O_2); **(c, II)** H_2 oxidation (1 vol.% O_2, 50 vol.% H_2); **(d, III)** CO hydrogenation (1 vol.% CO, 50 vol.% H_2) ; **(e, IV)** CO_2 hydrogenation (1 vol.% CO_2, 50 vol.% H_2); **(f, V)** H_2O + CO (water gas shift reaction) (1 vol.% CO, 3 vol.% H_2O), total flow 50 mL min^{-1} . I-V refer to the reaction equations given below.

Based on these reactivity patterns one can conclude that CO oxidation dominates up to 175 °C, between 175 and 230 °C there is both CO oxidation and H_2 oxidation occurring, and above 230 °C methane formation prevails. Secondary reactions of CO_2 with H_2 do not occur below 230 °C, above 230 °C CO_2

and CO hydrogenation are identical (RWGS and CO methanation (II) may occur sequentially). The water gas shift does not take place below 350 ^{o}C and is thus not relevant for CO_2 formation. In order to better understand the temperature-dependent changes in selectivity we have examined the reduction behavior of Co_3O_4 in pure H_2 and pure CO. In both cases reaction with lattice oxygen creates oxygen vacancies (and water or CO_2, respectively). We will start with H_2-TPR because its behavior is somewhat simpler than that of reduction by CO. Under PROX conditions the oxygen vacancies will be replenished by gas phase oxygen but the oxidation state will depend on whether reduction or (re)oxidation dominates. Thus, the catalyst oxidation state during PROX was examined as well.

5.3.3 H_2-TEMPERATURE PROGRAMMED REDUCTION OF Co_3O_4: IN SITU XAS AND IN SITU NAP-XPS

The reducibility of Co_3O_4 in H_2 was studied in a continuous-flow fixed-bed reactor with different concentrations of H_2 (5 and 50 vol.% H_2) to reveal the influence of H_2 concentration/pressure on the TPR profile (**Figure 3a**). This is crucial for comparison with operando experiments (e.g., XAS and XPS), which mimic experimental conditions but cannot be carried out in exactly the same reaction environment as in a continuous-flow fixed-bed reactor. For both H_2 concentrations, two rather broad peaks were observed that can be attributed to $Co_3O_4{\rightarrow}CoO$ and $CoO{\rightarrow}Co$ reduction (at lower and higher temperature, respectively). The absence of a larger, narrow TPR peak characteristic of the reduction of Co_3O_4 to CoO on the low-temperature side suggests that in the present case the H_2 reduction of Co_3O_4 is not a well-defined two-step reduction process consisting of two clearly separated steps (i.e., Co_3O_4 to CoO and CoO to Co, involving CoO as an thermodynamically stable intermediate). The reduction of Co_3O_4 is rather a one-step process that occurs around 290°C. A similar effect for Co_3O_4 reduction in H_2 was observed by Kuznetsov et al. [13]. Based on isothermal investigations, they concluded that CoO is thermodynamically unstable below 291 °C. Therefore, Co_3O_4 undergoes reduction "directly" to metallic cobalt. On the contrary, CoO is stable above 291 °C; thus, Co_3O_4 reduction becomes a two-step process.
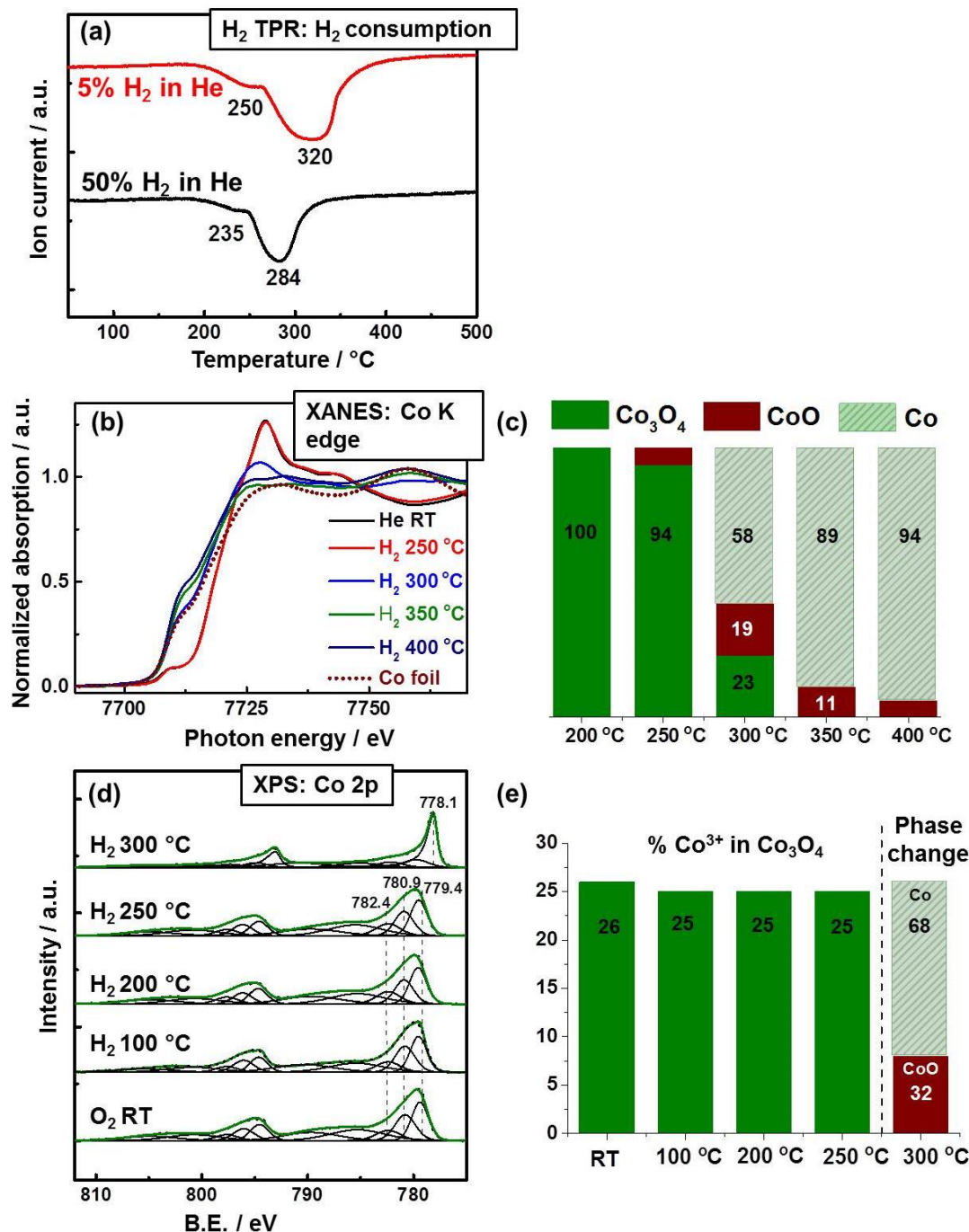
Figure 3. (a) H_2-TPR for Co_3O_4: 50 vol.% H_2 in He (black) and 5 vol.% H_2 in He (red), total flow 50 mL min^{-1}. (b) XANES spectra at the Co K edge of Co_3O_4 during H_2-temperature-programmed reduction (50 vol.% H_2 in He, total flow 50 mL min^{-1}) and (c) amount of reduced versus oxidized cobalt calculated by linear combination of reference spectra. (d) Operando NAP-XPS H_2-temperature-programmed reduction of Co_3O_4: Co 2p region (hν = 1015 eV), 0.4 mbar H_2 and (e) amount of reduced versus oxidized cobalt calculated from linear peak fit.

The bulk electronic structure during H_2 reduction of Co_3O_4 was studied by in situ XAS while heating from RT to 400 °C in 50 vol.% H_2 in He. XANES spectra at the Co K edge, acquired during H_2-TPR of

Co_3O_4 with Co foil as a reference, are shown in **Figure 3b**. To quantify the extent of cobalt reduction, the H_2-TPR XANES spectra were fitted with a linear combination of reference spectra (i.e., Co_3O_4, CoO, and Co), and the result is presented in **Figure 3c**. Analysis of the XANES spectra reveals that the bulk structure of Co_3O_4 remains intact up to 200 °C in H_2; at 250 °C reduction begins, and at 300 °C formation of CoO and Co (in addition to Co_3O_4) was observed. From the time-dependent in situ XANES spectra at 300 °C (**Figure S5a**) it can been seen that Co_3O_4 undergoes reduction from Co_3O_4 to metallic cobalt very fast. The linear combination analysis indicates that during the first 5 min only 20 % of metallic Co is present but after 15 min ~60 % of cobalt atoms are metallic (**Figure S5b**). At 350 °C the main phase is metallic cobalt (~90 %). Based on the in situ XANES data it can be concluded that the reduction of Co_3O_4 to metallic Co proceeds via intermediate formation of CoO, but it is not a slow two-step reduction process with a well-defined CoO intermediate phase. Similar effects have been observed by Potoczna-Petru et al. and Garces et al. using TEM and in situ XRD, respectively [8a, 8c]. The study of Potoczna-Petru et al. on Co_3O_4 particles reduction (~ 12 nm and 20 nm) suggests that two effects are responsible for such unusual reduction behavior: diffusion limitations and differences in surface defects [8c]. However, a simple consecutive two-step reduction mechanism of Co_3O_4 (i.e., 1. $Co_3O_4 \rightarrow$ CoO; 2. CoO$\rightarrow$Co) has been more frequently discussed in the literature [8b, 8d]. In contrast, our in situ study rather points to the simultaneous presence of Co_3O_4, CoO, and Co under H_2 reduction conditions, in agreement with Garces and Potoczna-Petru [8a, 8c].

According to in situ XAS, the *bulk* of Co_3O_4 remains intact up to 200 °C. Nevertheless, the *surface* of Co_3O_4 may already be partially reduced at 200 °C in H_2 and may already exhibit oxygen vacancies or defects (as indicated by the H_2 oxidation activity in **Figure 2 (II)**). To address this question and to examine surface changes of Co_3O_4, NAP-XPS H_2-TPR was performed from RT to 300 °C in 0.4 mbar H_2. The Co 2p spectra are presented in **Figure 3d** for a kinetic energy of 200 eV, corresponding to an inelastic mean free path of 0.6 nm (i.e., probing mainly the two topmost layers). To quantitatively elucidate the extent of Co_3O_4 reduction, the Co 2p region was fitted. The peak positions, full width at half maximum (FWHM), and constraints are presented in **Table S1**. According to the literature [14], the peak at 779.4 eV corresponds to Co^{3+}, the peak at 780.0 eV to Co^{2+} in CoO, and the signal at 782.4 eV to Co^{2+} in $Co(OH)_2$. For the fitting also the two shake-up satellites (surface and bulk plasmons) of cobalt ions were included [15], in addition to Co^{3+}, Co^{2+} in CoO and Co^{2+} in $Co(OH)_2$. In situ NAP-XPS data in the Co 2p region indicate that at temperatures up to 250 °C no significant surface reduction of Co_3O_4 to CoO took place (i.e. there was no growth of satellite peaks and the area fraction of the peak at 779.4 eV representative of Co^{3+} were 26 % at RT, 25 % at 100 ºC, 25 % at 200 °C, and 25 % at 250 °C). Only above 250 °C the surface started to be reduced. At 300 °C, metallic cobalt (peak at 778.1 eV) was formed, while a small fraction of CoO was still present. The difference in the reduction temperature for Co_3O_4 in XAS and NAP-XPS experiments is likely related to the different H_2 pressures, which influence the reduction temperature of cobalt oxide, as demonstrated in **Figure 3a**.

5.3.4 CO-TEMPERATURE PROGRAMMED REDUCTION OF Co_3O_4: IN SITU XAS AND IN SITU NAP-XPS
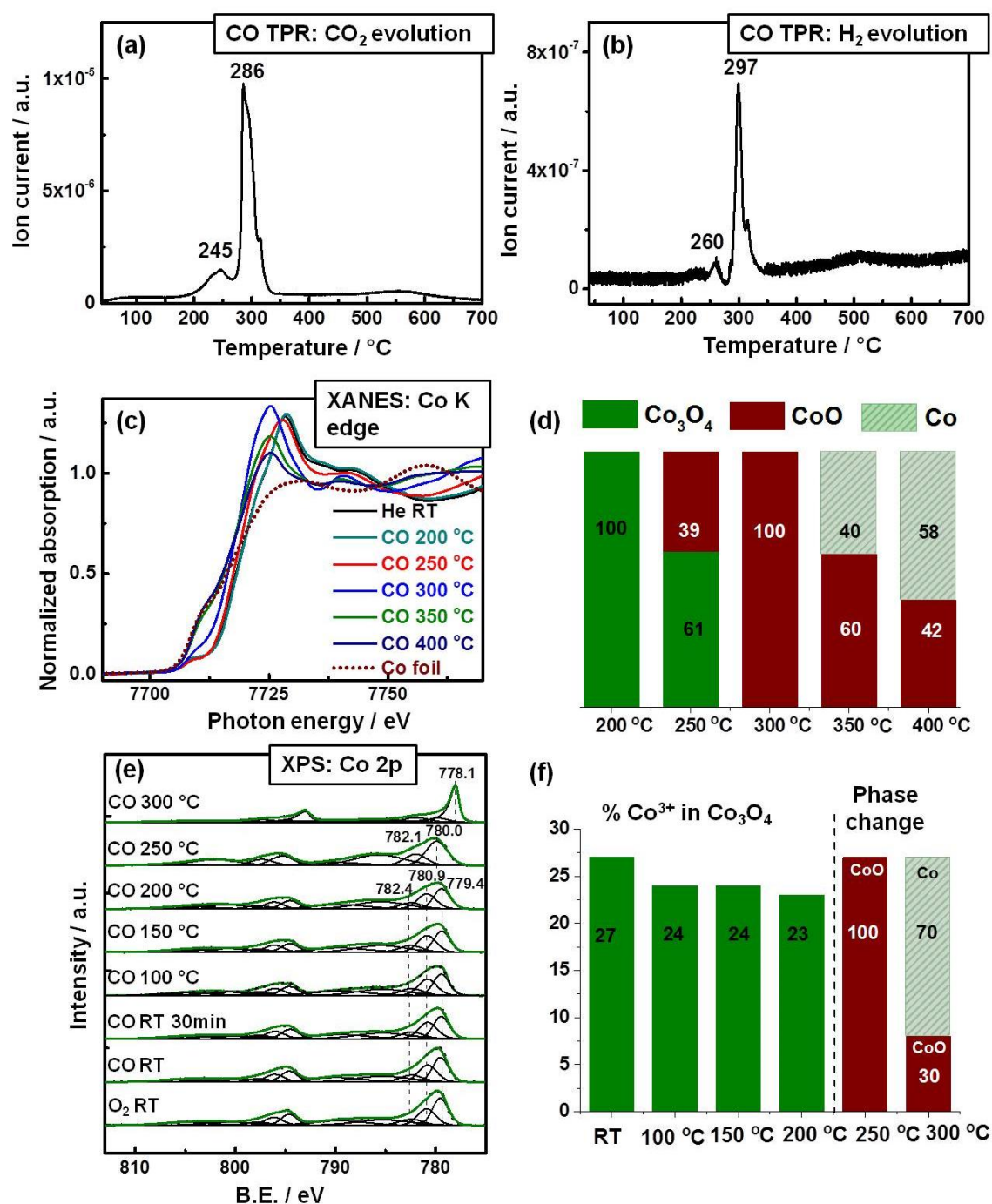
Figure 4. (a) CO-TPR for Co_3O_4 5 vol.% CO in He, total flow 50 mL min^{-1}: CO_2 evolution and (b) H_2 evolution. (c) XANES spectra at the Co K edge of Co_3O_4 during CO-temperature-programmed reduction (5 vol.% CO in He, total flow 50 mL min^{-1}) and (d) amount of reduced versus oxidized cobalt calculated by linear combination of reference spectra. (e) Operando NAP-XPS CO-temperature-programmed reduction (0.15 mbar): Co 2p region (hν = 1015 eV); (f) amount of reduced versus oxidized cobalt calculated from linear peak fit.
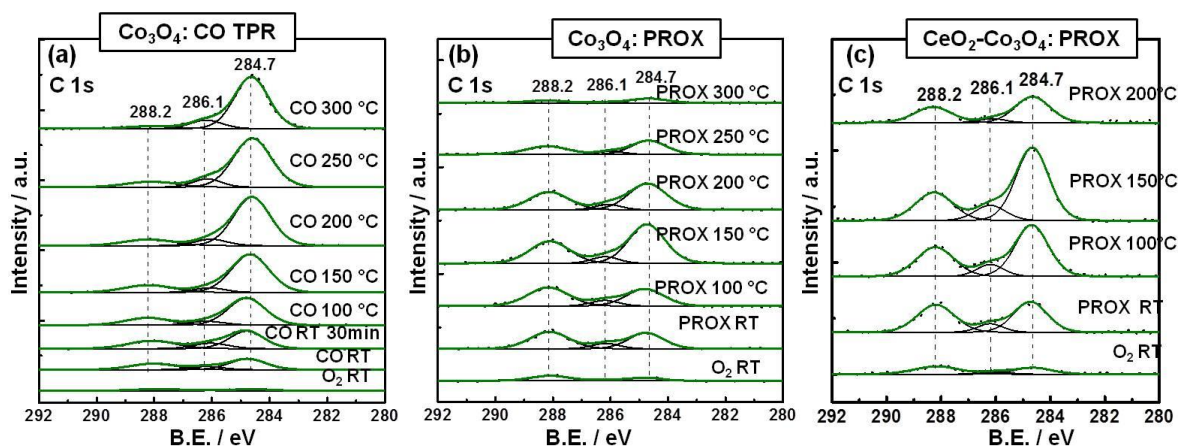
Figure 5. C 1s region (hν = 465 eV) for operando NAP-XPS during (a) CO-TPR of Co_3O_4 (0.15 mbar CO); (b) PROX over Co_3O_4 (1.5 ml/min O_2 + 1.5 ml/min CO + 17 ml/min H_2, 0.5 mbar); (c) PROX over CeO_2-Co_3O_4 (1.5 ml/min O_2 + 1.5 ml/min CO + 17 ml/min H_2, 0.5 mbar).

During PROX, based on previously suggested mechanisms, CO is assumed to react with surface lattice oxygen and to reduce the surface. For a better understanding of the resulting oxidation state we have thus examined the interaction of Co_3O_4 with CO in a wide temperature range, performing CO-TPR in a continuous-flow fixed-bed reactor (**Figure 4a).** The CO_2 profile (**Figure 4a)** shows a small broader peak around 245 °C which is attributed to the reduction of Co_3O_4 to CoO. Note that the low temperature peak is much more pronounced than that in H_2-TPR (**Figure 3a**). The sharp peak at 286 °C is assigned to the reduction of CoO to metallic Co, as previously reported in the literature [9]. The second peak exhibits a shoulder at higher temperature (~315°C), which could be explained by the potential presence of intermediate wurtzite CoO beside the rocksalt CoO being reduced at somewhat shifted temperatures or by Co_3O_4 with different particles sizes. XRD, however, shows only the presence of the cubic CoO phase. Overall, the CO-TPR profile of Co_3O_4 indicates a two-step reduction with (the expected) ratio of ~ 1:3 between the intensities of the 1st and the 2nd peaks. Above 450 °C, small amounts of CO_2 further evolve up to 650 °C due to CO disproportionation (2CO→CO_2+C) or CO dissociation (CO→C+O) on metallic Co [16].

Interestingly, during CO-TPR, H_2 evolution (**Figure 4b**) was observed at 260 °C and 300 °C. It most likely originates from a surface reaction of CO with OH groups of the catalyst via a WGSR (2CO+2OH→2CO_2+H_2) [17]. The amount of CO_2 evolved from WGSR was estimated to be 10 % of the total CO_2 production (i.e., most of the CO_2 is due to the cobalt oxide reduction). For CeO_2 materials WGSR is well known to be one of the mechanisms of CO_2 production [18]. The (nearly) parallel formation of CO_2 and H_2 suggests that the onset of reduction by CO creates active sites for the reaction of CO with

surface OH groups. However, according to our reactivity data presented in **Figure 2**, in the presence of gaseous H_2O WGSR only occurs above 350 °C.

To monitor changes in oxidation state during CO interaction with Co_3O_4, in situ XAS (50 mbar CO in He) and in situ NAP-XPS (0.15 mbar CO) were performed. XANES spectra at the Co K edge, acquired during CO-TPR of Co_3O_4, are presented in **Figure 4c,** while linear combination fitting results displayed in **Figure 4d.** As expected, the reduction profile of Co_3O_4 in CO atmosphere is different from that in H_2 atmosphere. No bulk reduction of Co_3O_4 was observed up to 200 °C; however, at 250 °C nearly 40 % of CoO was present, whereas at 250 °C in H_2 the major phase was still Co_3O_4 for bulk and surface. Further heating to 300 °C in CO reduced Co_3O_4 completely to CoO, but no metallic Co was formed, and no significant time dependent reduction was observed **(Figure S6)**. In contrast, in H_2 atmosphere at 300 °C Co_3O_4, CoO, and Co were present. At 350 °C in CO atmosphere CoO and metallic Co were present; whereas in H_2 Co was mainly metallic. Thus, XAS suggests that the reduction of Co_3O_4 in CO atmosphere started at lower temperature and proceeded faster at 250 °C but, in contrast to reduction in H_2, it was rather a well-defined two-step reduction (with only one or two phases coexisting, but not three).

To investigate the re-oxidation of the catalyst *after* CO-TPR, O_2-temperature-programmed oxidation was performed and the results are presented in **Figure S7.** From the XANES spectra it is seen that the oxidation of (metallic) cobalt starts above 200 °C, and at 300 °C the edge shifts to higher energy due to the oxidation of Co to CoO and Co_3O_4. At 400 °C, the sample was fully (re)oxidized to Co_3O_4.

It is possible that CO undergoes dissociation (CO→C+O) at higher temperatures and that the carbon deposited on the surface slows down reduction. Thus, the evolution of Co 2p and C 1s upon heating from RT to 300 °C were also studied by NAP-XPS (CO 0.15 mbar) (**Figure 4** and **5**). Contrary to Co_3O_4 reduction in H_2, partial reduction of Co_3O_4 started already at RT and proceeded as the temperature increased **(Figure 4e)**. The area fraction of the peak representative of Co^{3+} decreased from 28 % (RT in O_2) to 23 % at 200 °C, and an increase of the satellite peaks was observed. At 250 °C, the surface was completely reduced to CoO, as observed by the strong increase of the satellite features and shift of the peak to 780.0 eV. Thus, NAP-XPS also indicates the intermediate formation of CoO, in good agreement with operando XAS data. At 300 °C, the surface was partially reduced to metallic Co (peak at 778.1 eV), and, in addition, a small fraction of CoO was still present.

In **Figure 5a** the C 1s core level region is presented, acquired during exposure of Co_3O_4 to CO from RT to 300 °C. Three carbon species were detected, at 288.2 eV, 286.1 eV, and 284.7 eV. The peak at 288.2 eV can be attributed to carbonates/carboxylates [19]. We assign this peak to carbonates, as observed by Jansson et al. [20] by FTIR spectroscopy. The peak at 286.1 eV may be assigned to C-O (i.e., molecularly adsorbed CO on Co^{3+} and/or Co^{2+}) or C-OH species [21]. In a recent study of CO adsorption on Co_3O_4 (111) thin

films, Ferstl et al. reported formation of surface carbonate species (C 1s 288.5 eV) that form at defects of the film and are stable up to 127 °C, whereas molecular adsorption of CO to Co^{2+} was observed only at temperatures below -73 °C [19c]. In our case, elementary carbon (C 1s binding energy at 284.7 eV) was detected in addition to carbonates and C-O, C-OH, indicating that CO dissociates on Co_3O_4 already at RT (CO → C + O), depositing carbon at the surface. From the C 1s region **(Figure 5a, Table S3)** it is clearly seen that the amount of elementary carbon increases at higher temperature, indicating progressive CO dissociation, while the carbonates decrease above 150 °C and the C-O species rather increase.

Based on these results, we suggest that CO adsorbs on the Co_3O_4 surface as a carbonate or molecularly, which both subsequently desorb as CO_2, extracting part of the surface lattice oxygen from Co_3O_4. The oxygen vacancies, which are formed by lattice oxygen removal, may then serve as sites for O_2 adsorption/dissociation and the neighboring Co^{x+} sites serve for CO adsorption. Also CO dissociation likely occurs on oxygen vacancies. In any case, the two-step reduction of Co_3O_4 is more pronounced under CO than under H_2 atmosphere, in agreement with in situ XAS experiments.

Thus, XAS, NAP-XPS, and MS analysis of Co_3O_4 during CO-TPR proves three pathways: lattice oxygen removal by CO, surface water-gas shift reaction, and CO dissociation. On the contrary, interaction of H_2 with cobalt oxides proceeds via extraction of lattice oxygen from cobalt oxide only.

5.3.5 PROX on Co₃O₄: operando XAS and operando NAP-XPS

Based on the H_2- and CO-TPR experiments, we are now able to understand the differences in Co_3O_4 reduction in H_2 and CO atmospheres. Nevertheless, it is essential to determine the catalyst state in the PROX reaction mixture when both reducing gases (1 vol.% CO and 50 vol.% H_2) are simultaneously present and, in addition, there is an oxidative (1 vol.% O_2) gas. The oxidation state of Co_3O_4 was thus studied during PROX employing (again) operando XAS, while the surface changes were studied by operando NAP-XPS. The reaction conditions and reaction environment for operando XAS were very similar to those of a continuous-flow fixed-bed reactor in the laboratory. The operando MS data are shown in **Figure 7**.

The operando Co K edge XANES spectra of Co_3O_4 during heating from RT to 350 °C in the PROX reaction mixture are displayed in **Figure 6a**, and linear combination fitting results are shown in **Figure 6b**. The analysis of XANES reveals that from RT to 250 °C the phase of the catalyst did not change and that solely Co_3O_4 was present. As shown in **Figure 2a**, starting around 70 °C CO oxidation took place and around 150-170 °C water production set in. Interestingly, methane production started at 230 °C and increased with temperature, even though the bulk structure of the catalyst was still Co_3O_4. However, the

catalyst surface may have already exhibited defective/reduced structure (see below). Only at 300 °C Co_3O_4 was partially reduced to CoO (14%) and metallic Co (11 %). At 300 °C, CO and O_2 were fully consumed via hydrogenation and the excess H_2 reduced the catalyst, as in pure H_2. Heating Co_3O_4 in the PROX reaction mixture to 350 °C induced further reduction of cobalt oxide to metallic Co (around 70 %).

A comparison of operando XANES spectra during PROX with H_2-TPR and CO-TPR spectra demonstrates that the reduction of Co_3O_4 in the PROX reaction mixture sets in at least 50 °C higher than those in H_2/He or CO/He atmospheres. Reduction of cobalt oxide in H_2/He started directly above 250 °C, and at 300 °C 60 % of the catalyst was already metallic Co, whereas in CO/He atmosphere the reduction started at 250 °C, but at 300 °C CoO was the major single phase.

It seems apparent that the comparably lower reduction state of Co_3O_4 in the PROX reaction mixture, in comparison with H_2/He or CO/He atmospheres, is due to the reoxidation of the catalyst surface by gas phase oxygen. At lower temperature up to 170 °C, CO reaction dominates over H_2 reaction, between 170 and 230 °C H_2 reaction increases, and above 230 °C the reactants CO and H_2 rather react with each other than to reduce the catalyst. At high temperature the gas phase oxygen, together with produced water and the oxygen supplied by CO dissociation, reoxidize the surface. Clearly, above 250 °C the excess of hydrogen leads to increasing Co_3O_4 reduction, as demonstrated by the O_2-H_2 TPR (**Figure S4**), since even in 1 vol.% O_2, 50 vol.% H_2 (in He) Co_3O_4 reduction starts at 260 °C.
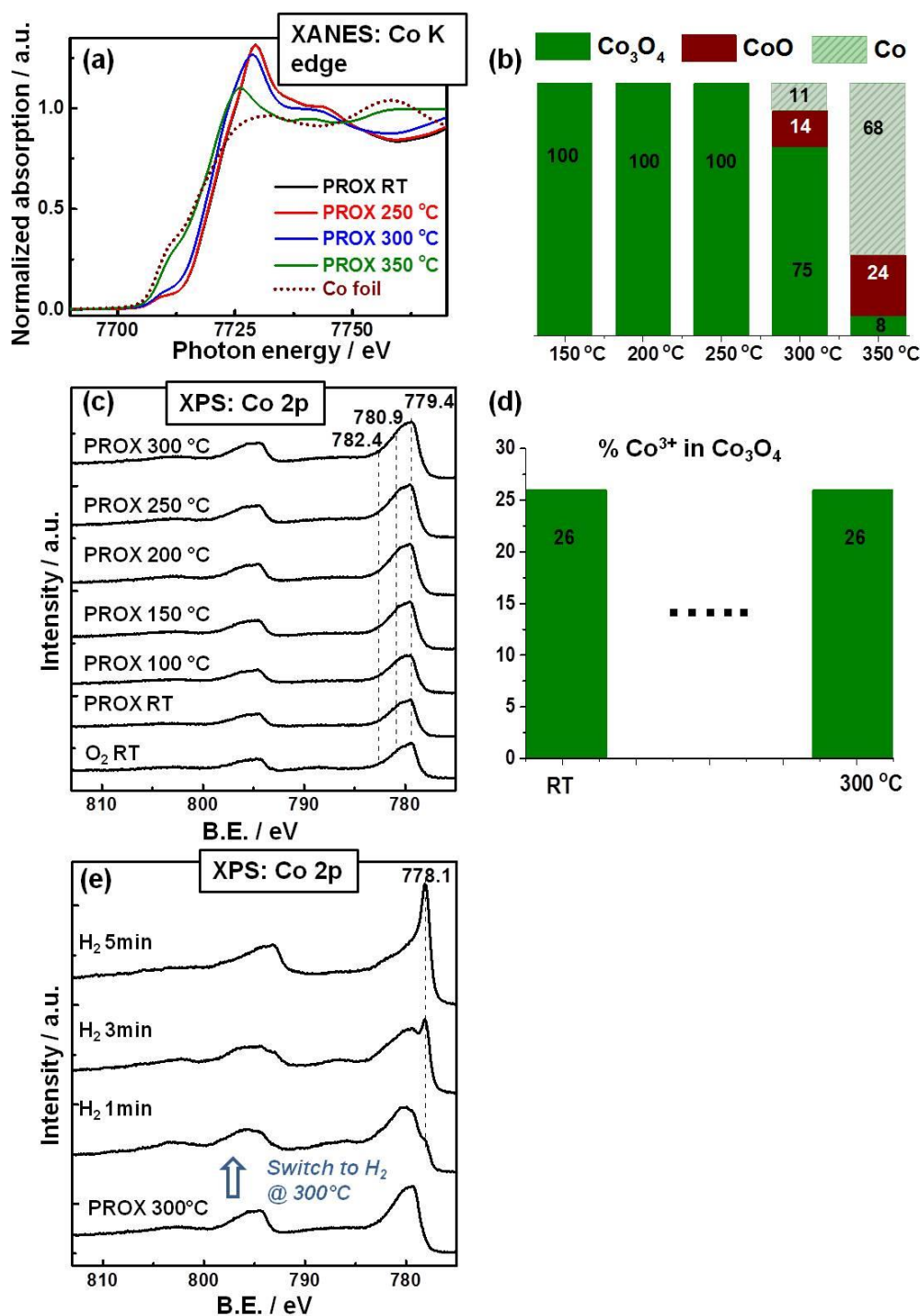
Figure 6. (a) XANES spectra at Co K edge of Co_3O_4 PROX (1 vol.% CO, 1 vol.% O_2 50 % H_2 in He, total flow 50 mL min^{-1}) and (b) amount of reduced versus oxidized cobalt calculated by linear combination of reference spectra. (c) Operando NAP-XPS during PROX over Co_3O_4 (1.5 ml/min O_2 + 1.5 ml/min CO + 17 ml/min H_2, 0.5 mbar): Co 2p region (hν = 1015 eV); (d) amount of oxidized cobalt calculated from linear peak fit; (e) operando NAP-XPS after switching the gas flow from the PROX reaction mixture to H_2 only at 300°C over Co_3O_4, 17 ml/min H_2, 0.5 mbar: Co 2p region (hν = 1015 eV).

According to operando XANES, it was evident that the (bulk) oxidation state of Co_3O_4 did not change in the selective PROX temperature window, in which CO oxidation was the dominant reaction. However, it remains to be answered whether the *surface* of Co_3O_4 was partially reduced during PROX, and if surface carbon was also present when O_2 was one of the reactants. Therefore, operando NAP-XPS was also performed during PROX. It should be mentioned that the ratio between CO, O_2 and H_2 was 1/1/12 due to the total pressure limitation (0.5 mbar) of NAP-XPS. Although the reaction conditions are somewhat different from those of a continuous-flow fixed-bed reactor and operando XAS, NAP-XPS may still help to gain further insights. The catalytic data obtained by mass spectrometry during NAP-XPS and XAS experiments are included for comparison in **Figure 7**.

The evolution of Co 2p and C 1s under PROX conditions was studied from RT to 300 °C. **Figure 6c** shows Co 2p spectra that clearly demonstrate the stability of the Co_3O_4 phase up to 250 °C. Even at 300 °C no Co_3O_4 reduction to CoO was detected during PROX. Thus, in contrast to H_2- and CO-TPR, for which the surface of Co_3O_4 started to reduce at lower temperature and for which a mixture of CoO and metallic Co was present at 300 °C, Co_3O_4 did not undergo surface reduction at 300 °C (even after 30 min) when O_2 was present during PROX and available for surface re-oxidation. To confirm this, CO and O_2 were switched off from the PROX reaction mixture at 300 °C and in H_2 Co_3O_4 was rapidly reduced to CoO and Co (after 5 min the surface was mainly metallic) (**Figure 6e**). Thus, the presence of O_2 prevents reduction of the catalyst and its deactivation. The presence of a minor amount of reduced Co species observed at 300°C in the corresponding operando XAS experiments, which are not found in the XPS experiments at this temperature, can be attributed to a slight shift of the reduction to higher temperatures due to the different cell characteristics.

In the C 1s region (**Figure 5b, Table S4)** the formation of carbonates, C-O species and elementary carbon were detected. The presence of O_2 apparently does not fully remove elementary carbon but lowers its concentration, as compared to that observed during CO-TPR. This is true especially above 150 °C, when carbon oxidation takes place. For the CO-TPR experiment carbon increased continuously with increasing temperature. This confirms that elementary carbon originates from CO dissociation (and is clearly not an impurity). The carbonates and C-O species also decreased at higher temperature.
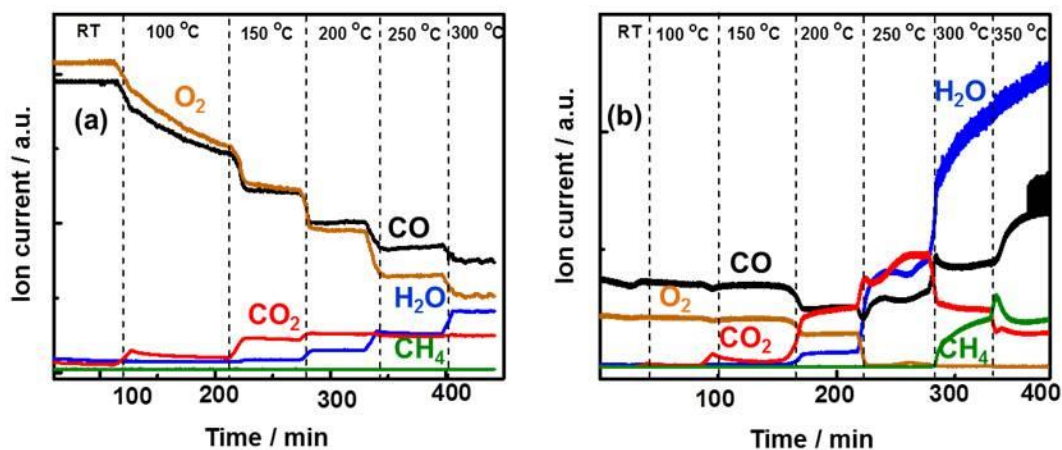
Figure 7. MS data of PROX on Co_3O_4 recorded during (a) operando NAP-XPS; (b) operando XAS at the Co K edge.

5.3.6 CORRELATION OF OXIDATION STATE AND CATALYTIC PERFORMANCE IN PROX

Because of differences in the design of the cells/reactors and the conditions applied (i.e., dead volumes, pressures, pellet in XPS vs sieve fraction of the catalyst used in the reactor and XAS cell, total flows, contact time between catalyst and reacting molecules), the temperature onset for the PROX reaction as well as for reduction in H_2 and CO differs for the NAP-XPS cell, the XAS cell, and the fixed-bed flow reactor in the lab. This applies in particular and necessarily for NAP-XPS measurements, while the conditions are much more similar for XAS and lab reactor experiments. Nevertheless, the trends observed for operando NAP-XPS, operando XAS and fixed bed flow reactor data are in good agreement which allows us to correlate the oxidation state of cobalt and the catalytic performance in PROX.

Therefore, based on the operando information of the surface and bulk oxidation state of Co_3O_4 we can now try to understand its temperature-dependent selectivity. Up to 250 °C, both the surface and bulk remain fully oxidized, only above 250 °C XANES indicates partial reduction of Co_3O_4 to CoO (14%) and Co (11%). It is thus reasonable (and in agreement with previous knowledge) to conclude that this "metallization" around 250 °C switches the selectivity from PROX to CO hydrogenation to methane. NAP-XPS detected minor surface reduction at 300 °C but this offset may be due to different flow conditions (and a smaller fraction of H_2). The amount of elementary C, C-O and carbonate species is rather low at 250 °C and even lower at 300 °C.

The situation is more complex below 250 °C, for which both methods indicate a fully oxidized Co_3O_4 surface and bulk, despite the change in selectivity around 170 °C. According to the reactivity patterns in **Figure 2**, the decrease in CO_2 concentration and increase in CO concentration starting at 175 °C is clearly

due to competitive hydrogen oxidation, whereas RWGS can be excluded. A likely explanation for the increase in the competitive H_2 oxidation is that H_2 oxidation has been reported to have a larger apparent activation energy than CO oxidation (52 and 74 kJ/mol for CO oxidation and H_2 oxidationon Co_3O_4/CeO_2, respectively) [4i], which explains the stronger increase of the H_2 oxidation rate with temperature as compared to the CO oxidation rate, even though the reaction onset temperature is very similar (**Figure 2 (I) and (II)**). Due to the competition of H_2 and CO for the limited amount of O_2 available under PROX conditions, the low concentration of CO at high conversions, the differences in activation energies and the fact that H_2 is present in large excess, the selectivity to CO_2 decreases as H_2 oxidation speeds up.

Another potential contribution to the decreasing CO oxidation selectivity could be the onset of CO desorption between 150-220 °C, as indicated by the CO-TPD profile (**Figure S8**), providing more available sites for H_2 oxidation (assuming site blocking by adsorbed CO which could prevent the coadsorption of hydrogen). Thus, H_2 oxidation activity would increase in the 150-220 °C temperature range, whereas CO oxidation selectivity decreases. This suggestion is also confirmed by the hydrogen oxidation temperature programmed experiment (**Figure 2(II) and S4**), in which the hydrogen oxidation on Co_3O_4 catalysts started already at 90 °C and increased rapidly to 135 °C, whereas during PROX H_2 oxidation started only around 150 °C). Interestingly, (in the absence of CO) H_2 oxidation takes place already above 90 °C, despite measurable Co_3O_4 reduction in H_2 started only around 250 °C. Similar to PROX conditions, we suggest that the concentration of oxygen vacancies serving as O_2 activation sites is apparently too low to be detected by XPS and bulk-sensitive techniques like XAS.

Referring to the operando C 1s spectra, the amount of elementary C, C-O and carbonate species is increasing up to 150 °C and decreasing above 150 °C, indicating effective carbon oxidation.

With respect to the detailed reaction mechanism, the current steady-state experiments provide only limited information, however. We assume that during PROX CO adsorbs on Co_3O_4 molecularly (linearly adsorbed to cobalt cations) and also as a carbonate. Both species eventually (have) extract(ed) lattice oxygen from the Co_3O_4 surface, inducing vacancy formation. The vacancies that are formed then serve as sites for O_2 adsorption/dissociation and for reaction with another CO molecule adsorbed on the cobalt cation. However, despite this Mars-van Krevelen mechanism the steady state concentration of oxygen vacancies is even below our NAP-XPS detection level so that the catalyst appears "fully oxidized". Furthermore, CO adsorbed on a cobalt cation might undergo dissociation, thereby depositing elementary carbon and creating oxygen that either fills an oxygen vacancy or reacts with another CO molecule (CO disproportionation). Depending on temperature, elementary carbon may be re-oxidized to CO_2.

Further details and, in particular, the contribution of the individual reaction paths can, however, not be exploited based on the current measurements. For example, we are currently unable to evaluate whether the observed carbonate species are intermediates to CO_2 formation or rather spectators. Studies involving isotopes and concentration modulation are planned for the near future.

5.3.7 PROX on CeO_2-Co_3O_4: operando XAS, operando NAP-XPS

Previous studies have reported that modification of Co_3O_4 with CeO_2 enhanced the activity for CO oxidation, preferential CO oxidation, hydrocarbon oxidation, and diesel soot oxidation [4i, 22]. However, the exact nature of the promotional role of CeO_2, especially in PROX, is unknown and calls for operando XAS and NAP-XPS studies. We modified Co_3O_4 by wet impregnation with an aqueous solution of $Ce(NO_3)_3$. This resulted in homogeneously distributed CeO_2 particles on Co_3O_4 (**Figures S2, S3**) and enhanced the catalytic activity for PROX (**Figure 8a**). Already at 150 °C, CO oxidation reached its maximum and the temperature window for CO oxidation was widened by ~25 °C (i.e., methane production started at around 255 °C).

The promotional effect is even more clear from the reaction rates and CO conversion data during catalytic PROX between 40 and 180 °C, presented in **Table 1** and **Figure 8b**. The $T_{50\%}$ temperature (i.e., the temperature at which 50 % CO conversion is reached) for Co_3O_4 is 139 °C, whereas for CeO_2-Co_3O_4 $T_{50\%}$ is 108 °C. The $T_{90\%}$ temperature of Co_3O_4 is 170 °C, and for CeO_2-Co_3O_4 it is 142 °C. This promotional effect (~30 °C shift) is remarkable, because the onset temperature for (pure) CeO_2 prepared as a reference catalyst is ~275 °C (**Figure S9**).

Table 1: Reaction rates of CO conversion and turnover frequencies (TOF) for Co_3O_4 and CeO_2-Co_3O_4 in 1 vol.% CO, 1 vol.% O_2, 50 vol.% H_2 at a total flow of 50 mL min^{-1}.

	S_{BET}[a]	$T_{10\%}$[b]	$T_{90\%}$[c]	$r_{70°C}$[d]	$R_{70°C}$[e]	$R_{Co3O4\_70°C}$[f]	[g]$TOF_{70°C}$	[h]$TOF^{ll}_{70°C}$
	(m²/g)	(°C)	(°C)	(mol/s·g)	(mol/s·m²)	(mol/s·g)	(s^{-1})	(s^{-1})
Co₃O₄	38.3	80	170	1.02×10^{-6}	2.66×10^{-8}	1.02×10^{-6}	$0.12\text{-}0.24\times10^{-2}$	3.3×10^{-3}
CeO₂-Co₃O₄	36.2	60	142	2.65×10^{-6}	7.32×10^{-8}	2.94×10^{-6}	$0.35\text{-}0.70\times10^{-2}$	9.0×10^{-3}

a BET surface area from N_2 sorption

b Reaction temperature for 10% CO conversion

c Reaction temperature for 90% CO conversion

d Reaction rate of CO oxidation at 70°C per gram of a catalyst

e Normalized specific reaction rates of CO oxidation on a unit surface area at 70°C

f Reaction rates on the basis of amount of Co_3O_4 at 70°C

g Turnover frequency of Co^{3+} sites at 70°C assuming 5-10% of Co^{3+} in surface defects as active sites according to [23]

h Alternative calculation of turnover frequency at 70°C based on all surface Co atoms (ll…lower limit)
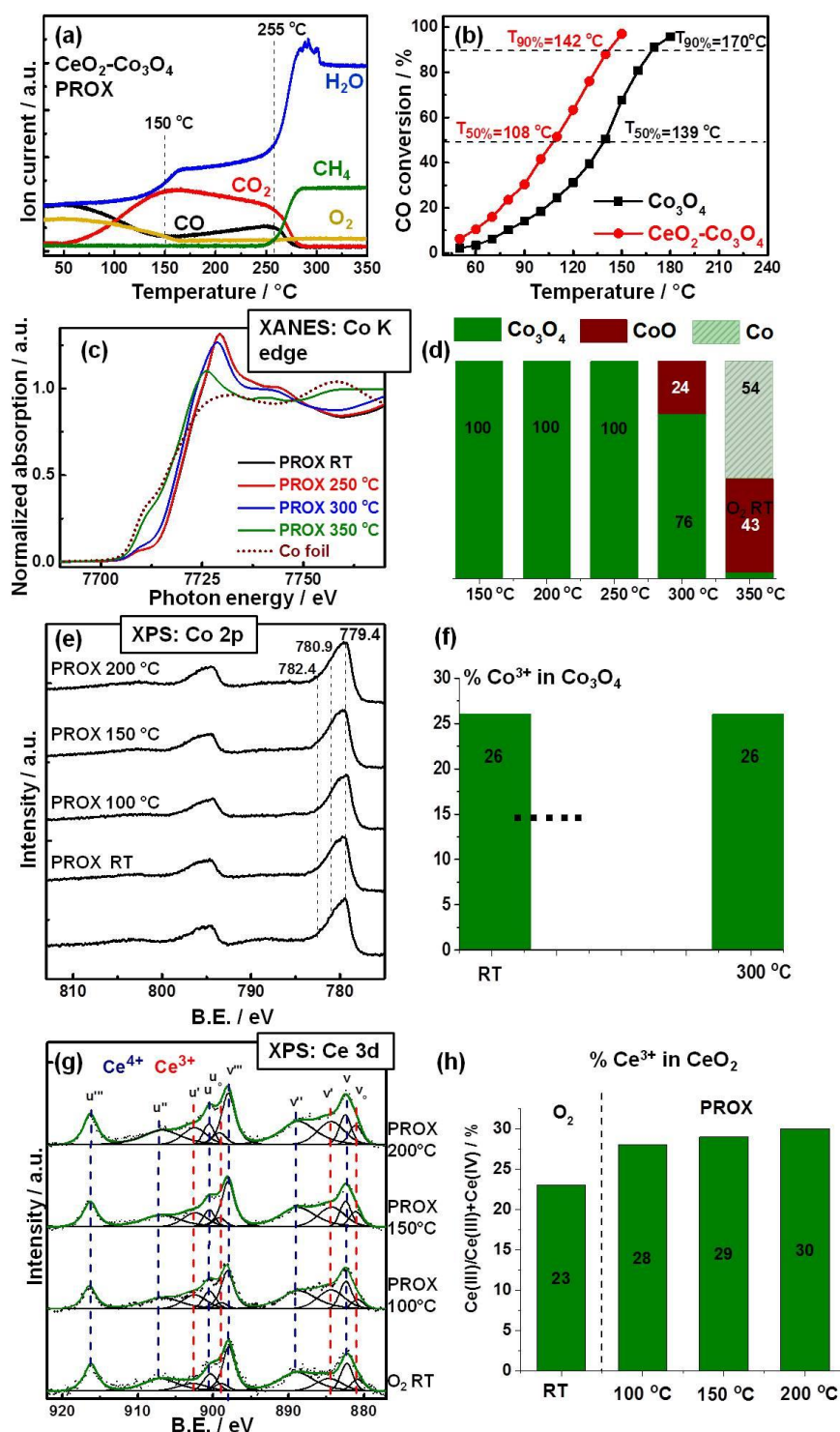
Figure 8. (a) Temperature programmed PROX reaction on CeO_2-Co_3O_4; (b) CO conversion for Co_3O_4 and CeO_2-Co_3O_4 in the presence of 1 vol.% CO, 1 vol.% O_2, 50 vol.% H_2, total flow 50 mL min^{-1}. (c) XANES spectra at the Co K edge of CeO_2-Co_3O_4 under PROX conditions (1 vol.% CO, 1 vol.% O_2 50 % H_2 in He, total flow 50 mL min^{-1}) and (d) amount of reduced versus oxidized cobalt calculated by linear combination of reference spectra. (e) Operando NAP-XPS during PROX over CeO_2-Co_3O_4 (1.5 ml/min O_2 + 1.5 ml/min CO + 17 ml/min H_2, 0.5 mbar): Co 2p region (hν = 1015 eV); (f) amount of oxidized cobalt calculated from linear peak fit; (g) Ce 3d region (hν = 1110 eV) and (h) concentration of Ce^{3+} determined by XPS.

TOF values were estimated assuming that Co^{3+} cations are the active sites in analogy to the work of Haruta´s group. Co_3O_4 nanoparticles possess mainly (111) facets as revealed with HRTEM, in agreement with Xie et al. [23] who described the morphology of the nanoparticles as truncated octahedra, surrounded by eight (111) and six (001) planes. (111) and (001) facets do not contain octahedrally coordinated Co^{3+}, only in the sub-layers. Thus, Xie et al. [23] suggested that the active sites for CO oxidation are surface defects located in the corners and edges of the spherical particles, with the Co^{3+} being exposed in these defects. They proposed a fraction of surface defects of around 5-10% of Co^{3+} for Co_3O_4 nanoparticles with a mean size of 20 nm. In alternative approach we estimated the turnover frequencies based on the total number of surface Co atoms per m^2 Co_3O_4 thus avoiding an assumption on the nature of active sites. Again we assumed a certain distribution of low index planes from the shape of the nanoparticles ((111) and (001) planes as described above) and calculated the number of surface Co atoms per m^2. In this way we obtain the lowest (theoretical) limit of TOF values (TOF^{ll}) assuming all Co surface atoms are active.

Figure 8c shows the operando Co K edge XANES spectra of the CeO_2-Co_3O_4 catalyst during PROX, upon increasing the temperature from RT to 350 °C. Similar to Co_3O_4, XANES of CeO_2-Co_3O_4 reveals that up to 250 °C the Co_3O_4 oxidation state did not change. This agrees with the study of CeO_2-Co_3O_4 by Gawade et al. who reported that Co did not change its electronic structure at 175 °C in the active and selective PROX region [4h]. A further increase of temperature led to the reduction of the catalyst, as evident from the shift of the absorption edge to lower energy (**Figure 8c**), explaining the selectivity change to methanation. When comparing operando XANES of CeO_2-Co_3O_4 and Co_3O_4, differences in the extent of cobalt oxide reduction for CeO_2-Co_3O_4 and Co_3O_4 are observed. It seems that the first is more difficult to reduce to metallic cobalt. At 300 °C no metallic cobalt was formed in the case of CeO_2-Co_3O_4, whereas 11 % of cobalt was metallic for the unpromoted catalyst.

Moreover, an increase of the reduction temperature of cobalt oxide for CeO_2-Co_3O_4 compared with Co_3O_4 catalyst was found by means of CO- (~11 °C) and H_2-TPR (~35 °C for 5 vol. % H_2 and 16 °C for 50 vol. % H_2) performed in a continuous-flow fixed-bed reactor (**Figure S10, S11**). All this might account for the broadening of the temperature window for CO oxidation on CeO_2-Co_3O_4.

The Co and Ce surface changes and the evolution of adsorbates during PROX were also examined by operando NAP-XPS, with Co 2p for CeO_2-Co_3O_4 presented in **Figure 8e.** Again, we compare the catalytic data obtained by mass spectrometry during NAP-XPS and XAS experiments in **Figure 9**. Similar to Co_3O_4, there are no significant changes of the Co 2p spectra. In the C 1s region, the formation of carbonates and elementary carbon were again detected and they also decreased above 150 °C (**Figure 5c**). Interestingly, the concentration of elementary carbon with respect to carbonate and C-O, C-O-H species during PROX was higher on CeO_2-Co_3O_4 than on Co_3O_4 (**Tables S5**).

To monitor the Ce^{4+}/Ce^{3+} evolution, Ce 3d spectra were recorded for CeO_2-Co_3O_4 during PROX, and the representative spectra are presented in **Figure 8g**. The signal of the Ce 3d level has a complex satellite structure reflecting hybridization between the Ce 4f and O 2p states. This results in two sets of spin-orbital multiplets u and v that are associated with $3d_{3/2}$ and $3d_{5/2}$ contributions, respectively [24]. The peaks of v, v'' and v''' correspond to a mixing configuration of Ce(IV) $(3d^9 4f^2)$ $O(2p^4)$, Ce(IV) $(3d^9 4f^1)$ $O(2p^5)$ and Ce(IV) $(3d^9 4f^0)$ $O(2p^6)$, respectively. The peaks v_o and v' are assigned to a mixture of Ce(III) $(3d^9 4f^2)$ $O(2p^5)$ and Ce(III) $(3d^9 4f^1)$ $O(2p^6)$, respectively [24]. The same assignments are also valid for the u series of peaks. In case of our Ce 3d spectra, Ce(IV) has six peaks at binding energies of 916.5, 907.5, 900.9, 897.7, 889.3, and 882.4 eV; whereas Ce(III) peaks labeled v_o, v', u_o, and u' are found to appear at binding energies ranging from 880.4 to 903.9 eV, in line with the literature. [24] To reduce the error in the curve fitting procedure, constraints were applied. The FWHM values together with the peak positions and constraints are listed in **Table S6**. To estimate the (near) surface ratios of Ce(III) to the total amount of Ce species (i.e., Ce(III)/(Ce(III)+Ce(IV)) ratio), the relative areas under the fitted XPS peaks of the u_0, v_0, u' and v_0' with respect to the area of the entire Ce 3d region were used. It should be mentioned that reduction of Ce(IV) to Ce(III) may occur simply due to X-ray photons. Revoy et al. [25] reported reduction of the surface with monochromatic Al Kα (1486.7 eV) X-ray radiation for CeO_2. Therefore, in order to avoid beam-induced reduction, every Ce 3d spectrum was recorded from a new sample spot.

From the Ce(III)/(Ce(III)+Ce(IV)) ratios, the degree of CeO_2 reduction was determined for CeO_2-Co_3O_4 during PROX from RT to 200 °C. The Ce(III) content of the freshly oxidized sample in O_2 was 23 %. Upon heating in the PROX reaction mixture (1.5 ml/min O_2 + 1.5 ml/min CO + 17 ml/min, H_2, 0.5 mbar) the Ce(IV) undergoes reduction to Ce(III), and Ce(III) concentrations are 28 % at 100 °C, 29 % at 150 °C, and 30 % at 200 °C. Selective oxidation of CO to CO_2 starts at 50 °C and proceeds selectively up to about 125 °C. The results indicate that the relative Ce(III) concentration remains relatively constant during PROX between 100 and 200 °C.
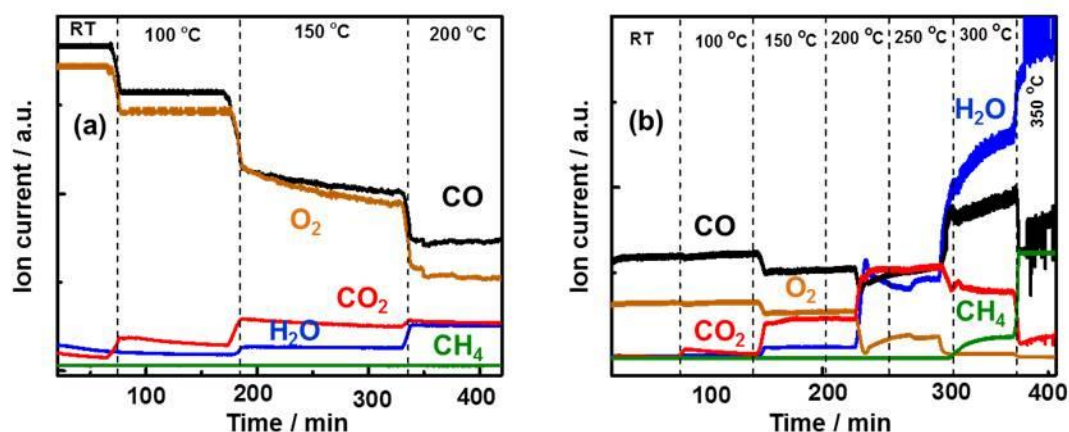
Figure 9. MS data of PROX on CeO_2-Co_3O_4 recorded during (a) operando NAP-XPS; (b) operando XAS at the Co K edge.

How can the promotional effect be explained? Clearly, upon adding CeO_2 both Ce^{3+} ions and (additional) oxygen vacancies are present. However, CeO_2 by itself, with reaction onset temperatures around 275 °C, is much less active than Co_3O_4 (**Figure S9**). We observed a similar trend in our previous study on CO oxidation [18a, 22d]. The CeO_2 nanoparticles alone can thus not account for the enhanced activity. It is apparent that the addition of CeO_2 to Co_3O_4 must create Co-O-Co-O-Ce-O- Ce interfacial active sites that exhibit easier oxygen activation and/or oxygen vacancy formation. Moreover, incorporation of cerium (atoms) into the cobalt oxide surface (i.e., formation of local Co-O-Co-O-Ce-O-Co ensembles) and distortion of the cobalt oxide structure, forming additional vacancies, may also contribute to the catalytic improvement. The role of Ce^{3+} (e.g., for CO adsorption) remains an open question.

PROX on CeO_2-Co_3O_4 likely follows a similar reaction mechanism as on Co_3O_4, but, in addition, specific ensembles such as Co-O-Ce must play an important role, due to lower activation barriers at the interfacial sites. Further experimental and theoretical work is clearly needed to fully understand the reaction pathways of PROX on Co_3O_4 and CeO_2-Co_3O_4.

5.4 CONCLUSIONS

We have shown that during PROX on Co_3O_4 the catalyst appears fully oxidized (i.e., both the surface and bulk oxidation state do not change up to 250 °C). However, as revealed by reference measurements in (pure) CO, CO reduces the catalyst (surface) starting around 100 °C via reaction with lattice oxygen. However, the reoxidation by O_2 during PROX is fast enough to prevent overall reduction. Hence, despite this Mars-van Krevelen mechanism the steady state concentration of oxygen vacancies is so low - even below our NAP-XPS detection level - that the catalyst appears "fully oxidized".

In (pure) H_2, surface and bulk reduction both start above 250 °C. While the Co_3O_4 reduction to CoO and Co around 250 °C explains the selectivity change to methanation, the change in selectivity around 170 °C from PROX (with predominantly CO oxidation) to both CO and H_2 oxidation cannot be explained by a change in (surface) oxidation state. Rather, upon increasing the temperature the difference in the increase of H_2 oxidation rate vs CO oxidation rate (higher apparent activation energy for H_2 oxidation), as well as the competition for the limited amount of O_2, are responsible for the decreasing CO oxidation selectivity. During PROX, elementary carbon, C-O species and carbonates were observed on the catalyst surface, but it is currently unclear to which extent they contribute to the overall reaction.

Adding CeO_2 to Co_3O_4 promoted the PROX activity despite that CeO_2 is much less active than Co_3O_4. This suggests that interfacial sites and/or Co-O-Ce ensembles account for the increased activity. Operando experiments did not detect differences to unpromoted Co_3O_4, apart from the presence of Ce^{3+}. The current results encourage further dynamic studies of PROX over cobalt-based catalysts in order to reveal the exact reaction pathways.

5.5 REFERENCES

1.   (a) http://energy.gov/eere/fuelcells/hydrogen-resources; (b) Liu, K.; Cui, Z.; Fletcher, T. H., Coal Gasification. In *Hydrogen and Syngas Production and Purification Technologies*, Liu, K.; Song, C.; Subramani, V., Eds. John Wiley and Sons, Inc., Hoboken: New Jersey, pp 156-168; (c) Liu, K.; Wang, A.; Zhang, T., Recent Advances in Preferential Oxidation of CO Reaction over Platinum Group Metal Catalysts. *ACS Catal.* **2012,** *2* (6), 1165-1178.

2.   Jiménez, S.; Soler, J.; Valenzuela, R. X.; Daza, L., Assessment of the performance of a PEMFC in the presence of CO. *J. Power Sources* **2005,** *151*, 69-73.

3.   (a) Tosti, S., Overview of Pd-based membranes for producing pure hydrogen and state of art at ENEA laboratories. *Int. J. Hydrogen Energy* **2010,** *35* (22), 12650-12659; (b) Park, E. D.; Lee, D.; Lee, H. C., Recent progress in selective CO removal in a H_2-rich stream. *Catal. Today* **2009,** *139* (4), 280-290.

4.   (a) Arango-Díaz, A.; Moretti, E.; Talon, A.; Storaro, L.; Lenarda, M.; Núñez, P.; Marrero-Jerez, J.; Jiménez-Jiménez, J.; Jiménez-López, A.; Rodríguez-Castellón, E., Preferential CO oxidation (CO-PROX) catalyzed by CuO supported on nanocrystalline CeO_2 prepared by a freeze-drying method. *Applied Catalysis A: General* **2014,** *477*, 54-63; (b) Arango-Díaz, A.; Cecilia, J. A.; Moretti, E.; Talon, A.; Núñez, P.; Marrero-Jerez, J.; Jiménez-Jiménez, J.; Jiménez-López, A.; Rodríguez-Castellón, E., Comparative study of CuO supported on CeO_2, $Ce_{0.8}Zr_{0.2}O_2$ and $Ce_{0.8}Al_{0.2}O_2$ based catalysts in the CO-PROX reaction. *Int. J. Hydrogen Energy* **2014,** *39* (8), 4102-4108; (c) Gamarra, D.; Cámara, A. L.; Monte, M.; Rasmussen, S. B.; Chinchilla, L. E.; Hungría, A. B.; Munuera, G.; Gyorffy, N.; Schay, Z.; Corberán, V. C.; Conesa, J. C.; Martínez-Arias, A., Preferential oxidation of CO in excess H_2 over CuO/CeO_2 catalysts: Characterization and performance as a function of the exposed face present in the CeO_2 support. *Applied Catalysis B: Environmental* **2013,** *130–131*, 224-238; (d) Marbán, G.; López, I.; Valdés-Solís, T.; Fuertes, A. B., Highly active structured catalyst made up of mesoporous Co_3O_4 nanowires supported on a metal wire mesh for the preferential oxidation of CO. *International Journal of Hydrogen Energy* **2008,** *33* (22), 6687-6695; (e) Teng, Y.; Sakurai, H.; Ueda, A.; Kobayashi, T., Oxidative removal of co contained in hydrogen by using metal oxide catalysts. *International Journal of Hydrogen Energy* **1999,** *24* (4), 355-358; (f) Yung, M. M.; Zhao, Z.; Woods, M. P.; Ozkan, U. S., Preferential oxidation of carbon monoxide on CoO_x/ZrO_2. *J. Mol. Cat. A* **2008,** *279* (1), 1-9; (g) Zhao, Z.; Yung, M. M.; Ozkan, U. S., Effect of support on the preferential oxidation of CO over cobalt catalysts. *Catal. Commun.* **2008,** *9* (6), 1465-1471; (h) Gawade, P.; Bayram, B.; Alexander, A.-M. C.; Ozkan, U. S., Preferential oxidation of CO (PROX) over CoO_x/CeO_2 in hydrogen-rich streams: Effect of cobalt loading. *Applied Catalysis B: Environmental* **2012,** *128*, 21-30; (i) Woods, M. P.; Gawade, P.; Tan, B.; Ozkan, U. S., Preferential oxidation of carbon monoxide on Co/CeO_2 nanoparticles. *Applied Catalysis B: Environmental* **2010,** *97* (1–2), 28-35.

5.   (a) Martínez-Arias, A.; Gamarra, D.; Fernández-García, M.; Hornés, A.; Bera, P.; Koppány, Z.; Schay, Z., Redox-catalytic correlations in oxidised copper-ceria CO-PROX catalysts. *Catal. Today* **2009,** *143* (3–4), 211-217; (b) Gamarra, D.; Martínez-Arias, A., Preferential oxidation of CO in rich H_2 over CuO/CeO_2: Operando-DRIFTS analysis of deactivating effect of CO_2 and H_2O. *J. Catal.* **2009,** *263* (1), 189-195; (c) Martínez-Arias, A.; Hungría, A. B.; Munuera, G.; Gamarra, D., Preferential oxidation of CO in rich H_2 over CuO/CeO_2: Details of selectivity and deactivation under the reactant stream. *Applied Catalysis B: Environmental* **2006,** *65* (3–4), 207-216.

6.   (a) Zhang, Q.; Liu, X.; Fan, W.; Wang, Y., Manganese-promoted cobalt oxide as efficient and stable non-noble metal catalyst for preferential oxidation of CO in H_2 stream. *Applied Catalysis B: Environmental* **2011,** *102* (1–2), 207-214; (b) Zhao, Z.; Bao, T.; Li, Y.; Min, X.; Zhao, D.; Muhammad, T., The supported CeO_2/Co_3O_4–MnO_2/CeO_2 catalyst on activated carbon prepared by a successive-loading approach with superior catalytic activity and selectivity for CO preferential oxidation in H_2-rich stream. *Catal. Commun.* **2014,** *48*, 24-28; (c) Zhao, Z.; Bao, T.; Zeng, Y.; Wang, G.; Muhammad, T., Efficient cobalt–manganese oxide catalyst deposited on modified AC with unprecedented catalytic performance in CO preferential oxidation. *Catal. Commun.* **2013,** *32*, 47-51.

7.   Omata, K.; Takada, T.; Kasahara, S.; Yamada, M., Active site of substituted cobalt spinel oxide for selective oxidation of COH_2. Part II. *Applied Catalysis A: General* **1996,** *146* (2), 255-267.

8.   (a) Garces, L. J.; Hincapie, B.; Zerger, R.; Suib, S. L., The Effect of Temperature and Support on the Reduction of Cobalt Oxide: An in Situ X-ray Diffraction Study. *The Journal of Physical Chemistry C* **2015,** *119* (10), 5484-5490; (b) Lin, H.-Y.; Chen, Y.-W., The mechanism of reduction of cobalt by hydrogen. *Materials Chemistry and Physics* **2004,** *85* (1), 171-175; (c) Potoczna-Petru, D.; Kępiński, L., Reduction study of Co_3O_4 model catalyst by electron microscopy. *Catalysis Letters* **2001,** *73* (1), 41-46; (d) Ward, M. R.; Boyes, E. D.; Gai, P. L., In Situ Aberration-Corrected Environmental TEM: Reduction of Model Co_3O_4 in H_2 at the Atomic Level. *ChemCatChem* **2013,** *5* (9), 2655-2661.

9.   Hu, L.; Sun, K.; Peng, Q.; Xu, B.; Li, Y., Surface active sites on Co_3O_4 nanobelt and nanocube model catalysts for CO oxidation. *Nano Res.* **2010,** *3* (5), 363-368.

10.   (a) Demoulin, O.; Rupprechter, G.; Seunier, I.; Le Clef, B.; Navez, M.; Ruiz, P., Investigation of Parameters Influencing the Activation of a Pd/γ-Alumina Catalyst during Methane Combustion. *The Journal of Physical Chemistry B* **2005,** *109* (43), 20454-20462; (b) Rupprechter, G.; Weilach, C., Mind the gap! Spectroscopy of catalytically active phases. *Nano Today* **2007,** *2* (4), 20-29; (c) Föttinger, K.; Rupprechter, G., In Situ Spectroscopy of Complex Surface

Reactions on Supported Pd–Zn, Pd–Ga, and Pd(Pt)–Cu Nanoparticles. *Accounts of Chemical Research* **2014,** *47* (10), 3071-3079.

11.   Hannemann, S.; Casapu, M.; Grunwaldt, J.-D.; Haider, P.; Trussel, P.; Baiker, A.; Welter, E., A versatile in situ spectroscopic cell for fluorescence/transmission EXAFS and X-ray diffraction of heterogeneous catalysts in gas and liquid phase. *Journal of Synchrotron Radiation* **2007,** *14* (4), 345-354.

12.   Knop - Gericke, A.; Kleimenov, E.; Hävecker, M.; Blume, R.; Teschner, D.; Zafeiratos, S.; Schlögl, R.; Bukhtiyarov, V. I.; Kaichev, V. V.; Prosvirin, I. P.; Nizovskii, A. I.; Bluhm, H.; Barinov, A.; Dudin, P.; Kiskinova, M., Chapter 4 X - Ray Photoelectron Spectroscopy for Investigation of Heterogeneous Catalytic Processes. *Adv. Catal.* **2009,** *52*, 213-272.

13.   N.F., K. A. N. K., Certain characteristics of the kinetics and mechanisms of processes of reducing Co₃O₄ with H2. *Izvestiya Akademii Nauk SSSR, Otdelenie Tekhnicheskikh Nauk, Metallurgiya i Toplivo* **1959,** *4*, 52–58.

14.   Biesinger, M. C.; Payne, B. P.; Grosvenor, A. P.; Lau, L. W. M.; Gerson, A. R.; Smart, R. S. C., Resolving surface chemical states in XPS analysis of first row transition metals, oxides and hydroxides: Cr, Mn, Fe, Co and Ni. *Applied Surface Science* **2011,** *257* (7), 2717-2730.

15.   Grosvenor, A. P.; Wik, S. D.; Cavell, R. G.; Mar, A., Examination of the Bonding in Binary Transition-Metal Monophosphides MP (M = Cr, Mn, Fe, Co) by X-Ray Photoelectron Spectroscopy. *Inorganic Chemistry* **2005,** *44* (24), 8988-8998.

16.   (a) Khassin, A. A.; Yurieva, T. M.; Zaikovskii, V. I.; Parmon, V. N., Effect of metallic cobalt particles size on occurrence of CO disproportionation. Role of fluidized metallic cobalt-carbon solution in carbon nanotube formation. *React Kinet Catal Lett* **1998,** *64* (1), 63-71; (b) Chen, Y.; Ciuparu, D.; Lim, S.; Yang, Y.; Haller, G. L.; Pfefferle, L., Synthesis of uniform diameter single wall carbon nanotubes in Co-MCM-41: effects of CO pressure and reaction time. *Journal of Catalysis* **2004,** *226* (2), 351-362; (c) Herrera, J. E.; Balzano, L.; Borgna, A.; Alvarez, W. E.; Resasco, D. E., Relationship between the Structure/Composition of Co–Mo Catalysts and Their Ability to Produce Single-Walled Carbon Nanotubes by CO Disproportionation. *Journal of Catalysis* **2001,** *204* (1), 129-145.

17.   Fottinger, K.; Schlogl, R.; Rupprechter, G., The mechanism of carbonate formation on Pd-Al₂O₃ catalysts. *Chemical Communications* **2008,** (3), 320-322.

18.   (a) Yang, J.; Lukashuk, L.; Li, H.; Föttinger, K.; Rupprechter, G.; Schubert, U., High Surface Area Ceria for CO Oxidation Prepared from Cerium t-Butoxide by Combined Sol–Gel and Solvothermal Processing. *Catal. Lett.* **2014,** *144* (3), 403-412; (b) Wu, Z.; Li, M.; Overbury, S. H., On the structure dependence of CO oxidation over CeO₂ nanocrystals with well-defined surface planes. *Journal of Catalysis* **2012,** *285* (1), 61-73.

19.   (a) Shchukarev, A. V.; Korolkov, D. V., XPS Study of group IA carbonates. *cent.eur.j.chem.* **2004,** *2* (2), 347-362; (b) Feng, Z. A.; Machala, M. L.; Chueh, W. C., Surface electrochemistry of CO₂ reduction and CO oxidation on Sm-doped CeO₂₋ₓ: coupling between Ce³⁺ and carbonate adsorbates. *Physical Chemistry Chemical Physics* **2015,** *17* (18), 12273-12281; (c) Ferstl, P.; Mehl, S.; Arman, M. A.; Schuler, M.; Toghan, A.; Laszlo, B.; Lykhach, Y.; Brummel, O.; Lundgren, E.; Knudsen, J.; Hammer, L.; Schneider, M. A.; Libuda, J., Adsorption and Activation of CO on Co₃O₄(111) Thin Films. *The Journal of Physical Chemistry C* **2015,** *119* (29), 16688-16699.

20.   Jansson, J.; Skoglundh, M.; Fridell, E.; Thormählen, P., A Mechanistic Study of Low Temperature CO Oxidation over Cobalt Oxide. *Topics in Catalysis* **2001,** *16-17* (1-4), 385-389.

21.   (a) Ramsvik, T.; Borg, A.; Kildemo, M.; Raaen, S.; Matsuura, A.; Jaworowski, A. J.; Worren, T.; Leandersson, M., Molecular vibrations in core-ionised CO adsorbed on Co(0 0 0 1) and Rh(1 0 0). *Surface Science* **2001,** *492* (1–2), 152-160; (b) Wolfbeisser, A.; Klotzer, B.; Mayr, L.; Rameshan, R.; Zemlyanov, D.; Bernardi, J.; Fottinger, K.; Rupprechter, G., Surface modification processes during methane decomposition on Cu-promoted Ni-ZrO₂ catalysts. *Catalysis Science & Technology* **2015,** *5* (2), 967-978.

22.   (a) Dhakad, M.; Mitshuhashi, T.; Rayalu, S.; Doggali, P.; Bakardjiva, S.; Subrt, J.; Fino, D.; Haneda, H.; Labhsetwar, N., Co₃O₄–CeO₂ mixed oxide-based catalytic materials for diesel soot oxidation. *Catal. Today* **2008,** *132* (1–4), 188-193; (b) Liotta, L. F.; Di Carlo, G.; Pantaleo, G.; Deganello, G., Catalytic performance of Co₃O₄/CeO₂ and Co₃O₄/CeO₂–ZrO₂ composite oxides for methane combustion: Influence of catalyst pretreatment temperature and oxygen concentration in the reaction mixture. *Applied Catalysis B: Environmental* **2007,** *70* (1–4), 314-322; (c) Tang, C.-W.; Wang, C.-B.; Chien, S.-H., Abatement of Carbon Monoxide over CeO₂–CoOₓ Catalysts: Effect of Preparation Method. *Catal. Lett.* **2009,** *131* (1-2), 76-83; (d) Yang, J.; Lukashuk, L.; Akbarzadeh, J.; Stöger-Pollach, M.; Peterlik, H.; Föttinger, K.; Rupprechter, G.; Schubert, U., Different Synthesis Protocols for Co₃O₄–CeO₂ Catalysts—Part 1: Influence on the Morphology on the Nanoscale. *Chemistry – A European Journal* **2015,** *21* (2), 885-892.

23.   Xie, X.; Li, Y.; Liu, Z.-Q.; Haruta, M.; Shen, W., Low-temperature oxidation of CO catalysed by Co₃O₄ nanorods. *Nature* **2009,** *458* (7239), 746-749.

24.   (a) Bêche, E.; Charvin, P.; Perarnau, D.; Abanades, S.; Flamant, G., Ce 3d XPS investigation of cerium oxides and mixed cerium oxide (CeₓTiᵧOᵤ). *Surf. Interface Anal.* **2008,** *40* (3-4), 264-267; (b) Burroughs, P.; Hamnett, A.; Orchard, A. F.; Thornton, G., Satellite structure in the X-ray photoelectron spectra of some binary and mixed oxides of lanthanum and cerium. *J. Chem. Soc. Dalton Trans.* **1976,** (17), 1686-1698.

25.   Revoy, M. N.; Scott, R. W. J.; Grosvenor, A. P., Ceria Nanocubes: Dependence of the Electronic Structure on Synthetic and Experimental Conditions. *J.Phys. Chem. C* **2013,** *117* (19), 10095-10105.

5.6 SUPPORTING INFORMATION

Experimental details on basic characterization of the catalysts

N_2 adsorption-desorption isotherms were recorded at -196 °C using an ASAP 2020 instrument from Micrometrics. Before each run, a known mass of sample (ca. 0.12 g) was heated to 80 °C under vacuum for 3 h. Specific surface areas (SSAs) were calculated from the linear part of the Brunauer-Emmett-Teller line. Pore size distributions were obtained applying the Barrett-Joyner-Halenda (BJH) equation to the desorption branch of the isotherm. Total pore volume was estimated from the N_2 uptake at a P/P_0 value of 0.99.

X-ray powder diffraction (XRD) measurements were performed on a Philips X'Pert diffractometer using Cu-Kα radiation (0.154 nm) (X-ray tube was operated at 40 kV and 40 mA) operating in Bragg-Brentano reflection geometry. The scanning range was 5-120° (2θ) in step scan mode of 0.05° (2θ), with 4.5 s per step.

High resolution transmission electron microscopy (HRTEM) was performed on a TECNAI F20 operated at 200 kV. High-angle annular dark-field scanning TEM (HAADF-STEM) and electron energy loss spectroscopy (EELS) were employed to determine the elemental distribution in CeO_2-Co_3O_4 and the particle size of CeO_2. Samples were ultrasonically dispersed in ethanol for 10 min and then deposited onto holey carbon copper grids.

Temperature programmed desorption (CO-TPD, O_2-TPD)

CO-temperature programmed desorption (CO-TPD), and O_2-temperature programmed desorption (O_2-TPD) experiments on the catalysts (ca. 20 mg) were performed in a continuous-flow fixed-bed quartz reactor under atmospheric pressure. Before the CO-TPD, the Co_3O_4 was pretreated with synthetic air (50 mL min⁻¹) at 400 °C for 30 min (heating rate 10 °C min⁻¹), then cooled to 30 °C under a flow of synthetic air and purged with helium for 5-10 min. Then, the pretreated sample was exposed to 5 vol.% CO and 95 vol.% He mixture (total flow 50 mL min⁻¹) at RT followed by purging in He for 30 min. For desorption, the catalyst was heated to 700 °C with 10 °C min⁻¹.

For O_2-TPD, the sample was exposed to 5 vol.% O_2 and 95 vol.% He mixture (total flow 50 mL min⁻¹) at 500 °C for 30 min followed by cooling down to RT. At RT pure He (total flow 50 mL min⁻¹) was purged through the catalyst for 30 min. Then the system was heated up in He (total flow 50 mL min⁻¹) to 700 °C with a heating rate of 10 °C min⁻¹.

The gas stream was analyzed by an online quadrupole mass spectrometer (OmniStar GSD320 O, Pfeiffer Vacuum) equipped with a secondary electron multiplier detector.

Data analysis

Evaluation of XRD

XRD data were analyzed with the HighScore Plus program in order to identify XRD patterns (JCPDS data base). Crystal structure refinement was performed using the TOPAS 4.2 program package.

Evaluation of XAS

All XAS spectra were energy aligned using the Co foil (7709 eV) as a reference, background subtracted, and normalized with the Athena software package. Linear combination fitting (LCF) of normalized X-ray absorption near edge spectra (XANES μ(E)) was performed also with the Athena software using XANES spectra of Co_3O_4, CoO (commercial), and Co foil as references, within an energy range of -20 eV below to $+80$ eV above the edge. The relative weights of the components of mixtures (Co_3O_4, CoO, and Co) under in situ conditions were constrained to be between 0 and 1, force weights were constrained to sum to 1, and all standards use the same threshold energy E_0. The quality of each fit was examined using the R-factor and reduced χ^2 (R factor $<$ 0.0008; reduced $\chi^2 <$ 0.0006).

Evaluation of XPS

All XPS spectra were analyzed using the CasaXPS package. All binding energies (BE) were calibrated using the second-order O 1s peak. The accuracy of the BE calibration was estimated to be around 0.05 eV. To fit the high-resolution spectra, a Shirley-type function was first used to remove the background arising from energy loss for Co 2p, while a linear-type function was used in the case of Ce 3d, because it sits on the slope of the O_{KLL} Auger peak and the Co 2p core level peaks. Either a Shirley-type function or a linear-type function was used in the case of C 1s. The extracted spectra were then fitted with a combined Gaussian and Lorentzian line profile that takes into account both spectrometer and lifetime broadening.

Supporting results and data
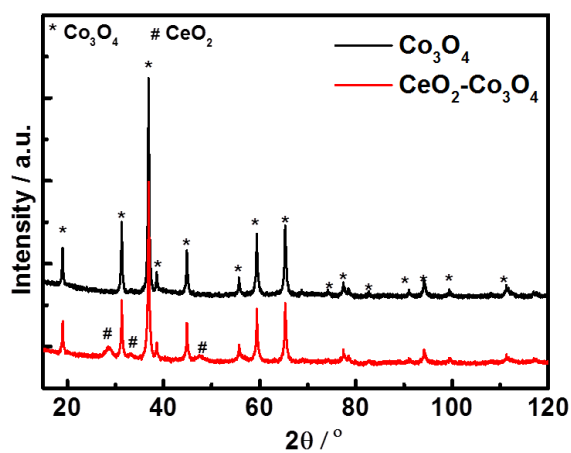
Figure S1. X-ray diffraction patterns for Co_3O_4 and CeO_2-Co_3O_4
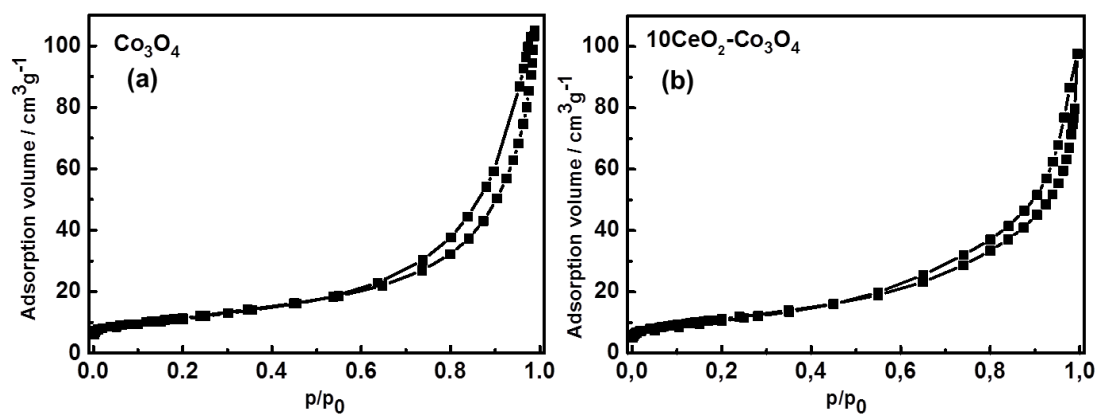
Figure S2. N_2 adsorption isotherms for Co_3O_4 (a) and CeO_2-Co_3O_4 (b)
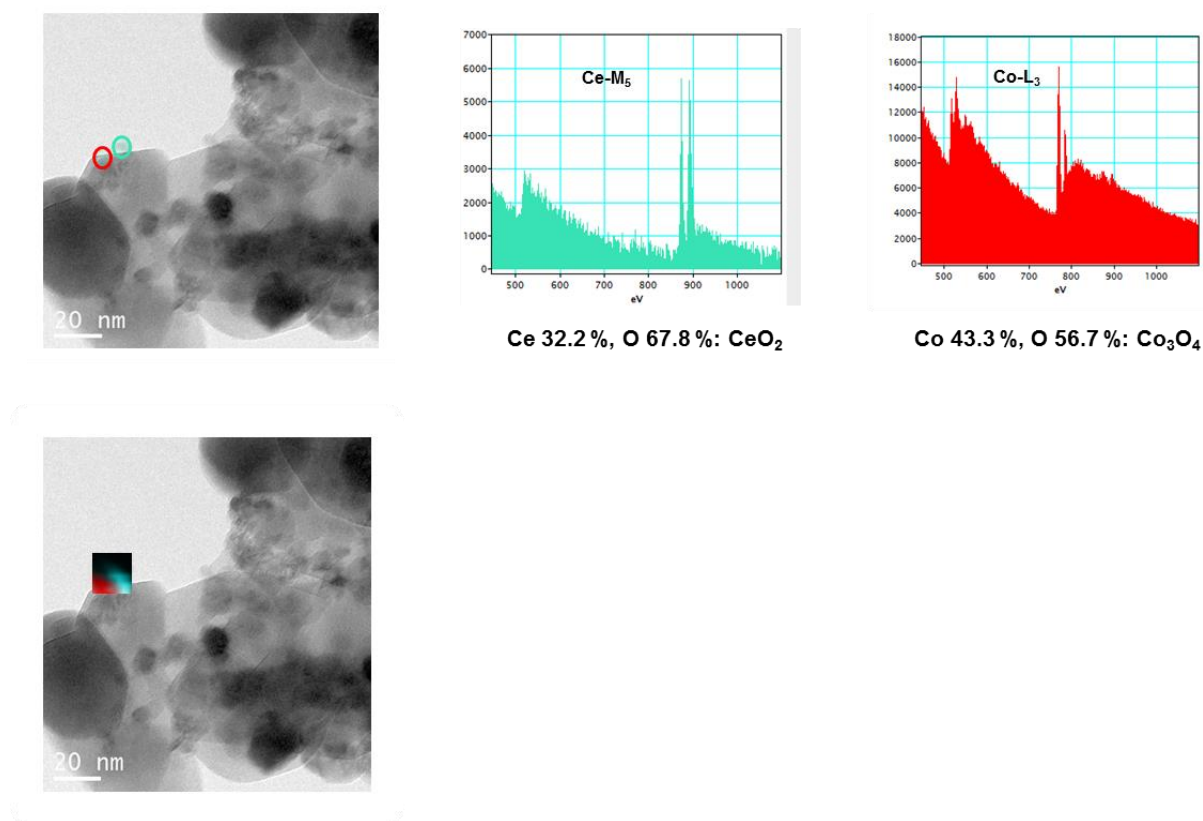
Figure S3. STEM mapping and subsequent EELS fitting of the spectra for CeO_2-Co_3O_4
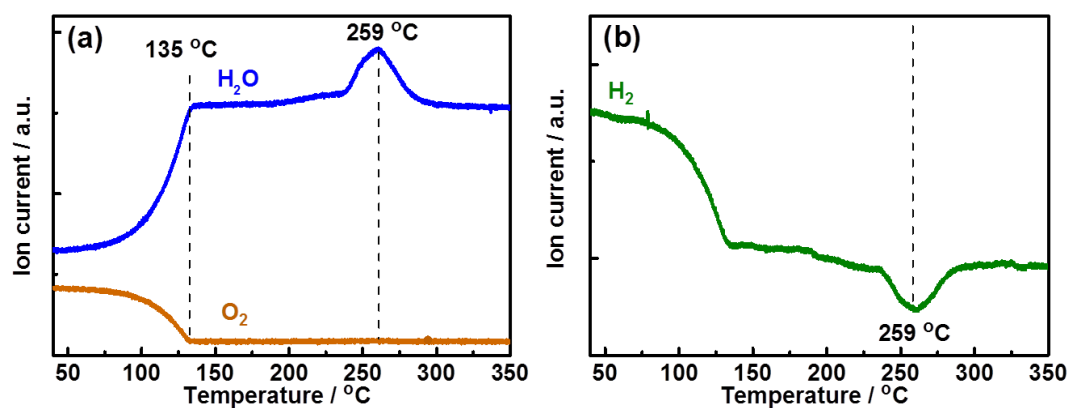
Figure S4. O_2-H_2-TPR for Co_3O_4: 1vol.% O_2, 50 vol.% H_2 in He, total flow 50 mL min^{-1}. O_2 and H_2O evolution (a), H_2 evolution (b)
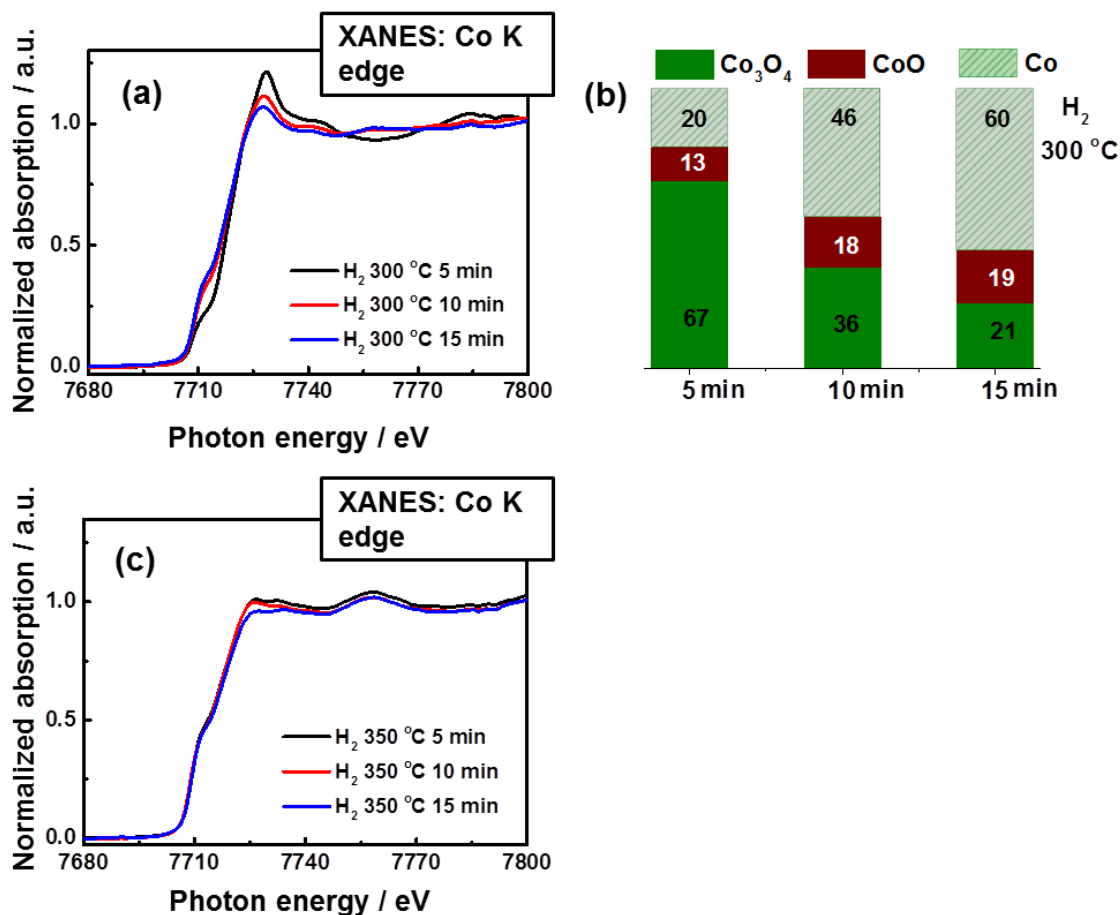
Figure S5. Operando XAS H_2-temperature-programmed reduction at the Co K edge (50 vol.% H_2 in He, total flow 50 mL min^{-1}) at 300 °C over time for Co_3O_4 (a); amount of reduced versus oxidized cobalt calculated by linear combination of reference spectra at 300 °C (b); XAS H_2-temperature-programmed reduction at the Co K edge at 350 °C over time for Co_3O_4 (c)
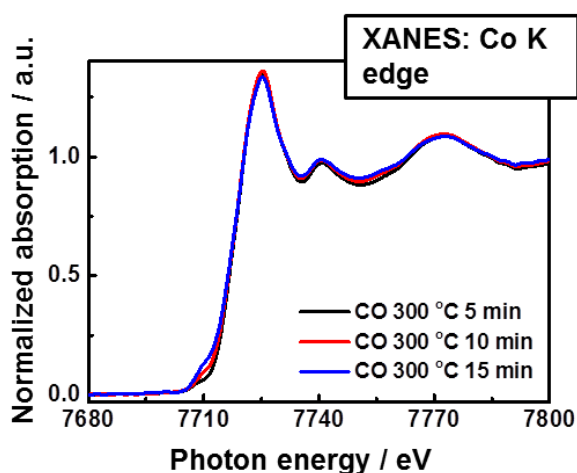
Figure S6. Operando XAS CO-temperature-programmed reduction at the Co K edge (5 vol.% CO in He, total flow 50 mL min^{-1}) at 300 °C over time for Co_3O_4
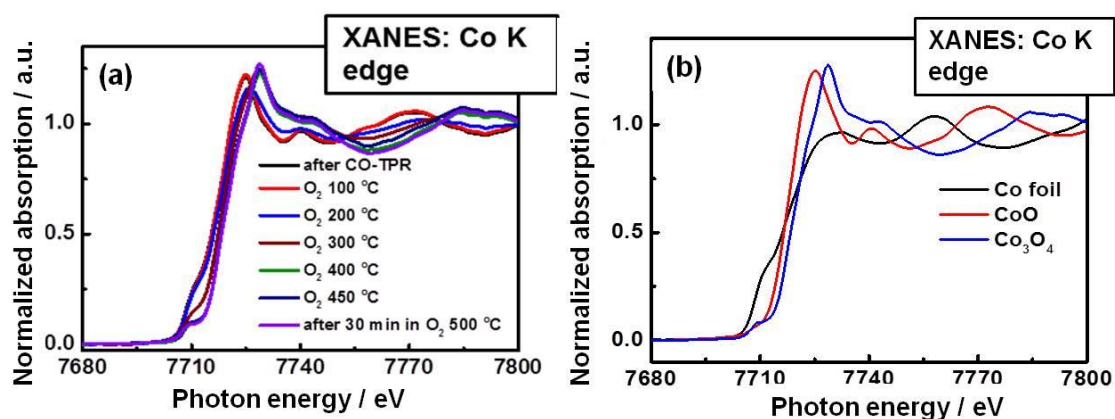
Figure S7. Operando XAS O_2-temperature-programmed oxidation at the Co K edge (20 vol.% O_2 in He, total flow 50 mL min^{-1}) at 300 °C over time for Co_3O_4 (a); Co K edge spectra of the reference compounds Co_3O_4, CoO and Co foil
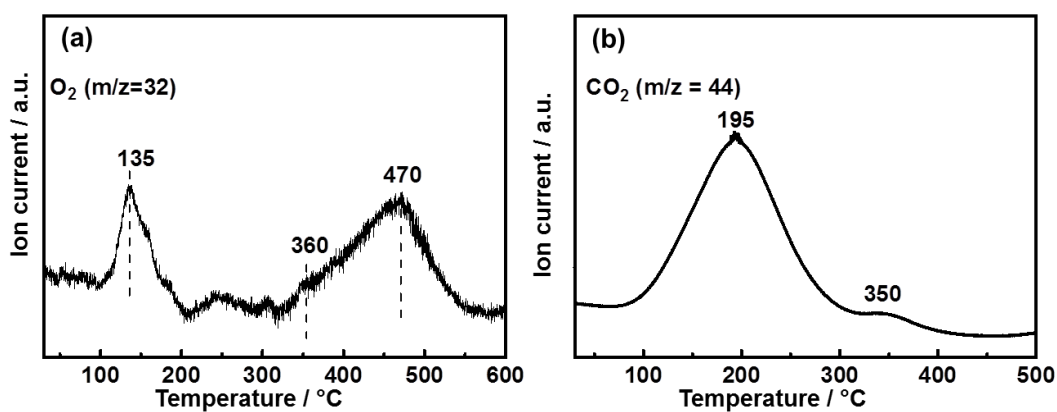
Figure S8. O_2-temperature programmed desorption (a) and CO-temperature programmed desorption (b) on Co_3O_4
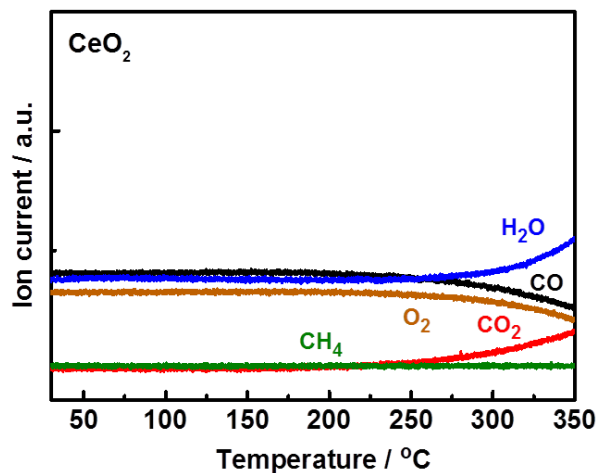
Figure S9. PROX-temperature programmed reaction for CeO_2 (1 vol.% CO, 1 vol. % O_2, 50 vol. % H_2 in He, total flow 50 ml min^{-1})
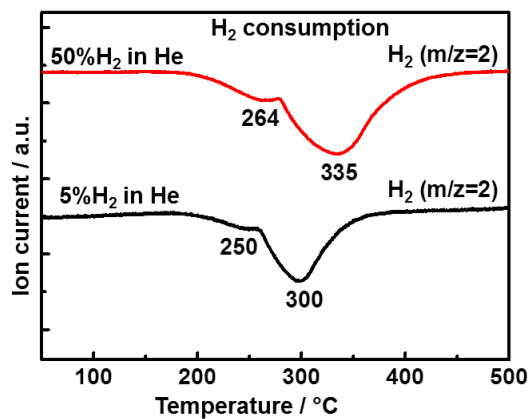
Figure S10. H_2-TPR for CeO_2-Co_3O_4: 50 vol.% H_2 in He (black); 5 vol.% H_2 in He (red), total flow 50 mL min^{-1}
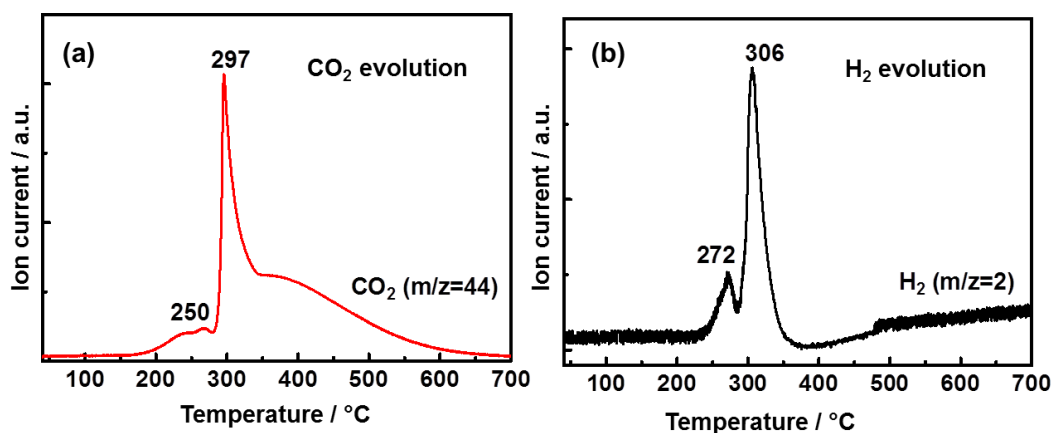
Figure S11. CO-TPR for CeO_2-Co_3O_4 5 vol.% CO in He, total flow 50 mL min^{-1}: CO_2 evolution (a); H_2 evolution (b)

Table S1. Co 2p spectral fitting parameters: binding energy (eV), FWHM (eV)

Compound	Peak 1, eV	Peak 1 FWHM, eV	Peak 2, eV	Peak 2 FWHM, eV	Peak 3, eV	Peak 3 FWHM, eV	Peak 4, eV	Peak 4 FWHM, eV	Peak 5, eV	Peak 5 FWHM, eV
Co_3O_4	779.4±0.1	1.8±0.1	780.9±0.1	2.0±0.1	782.4±0.1	2.2±0.1	785.6±0.2	6.0±0.2	789.3±0.2	6.2±0.2
CoO	780.0±0.1	2.6±0.1	782.1±0.1	2.7±0.1	785.5	5.7±0.2	790.1±0.2	6.8±0.2		
Co	778.1±0.1	0.9±0.1	785.5±0.1	5.1±02						

The multiplets correspond to the spin-orbit splitting of $2p_{3/2}$ and $2p_{1/2}$ core holes. The spin-orbit splitting is 15.2 eV. The intensity ratio I $2p_{3/2}$/I $2p_{1/2}$ was fixed to 2.

Table S2. C 1s spectral fitting parameters: binding energy (eV), FWHM (eV)

Species	Peak, eV	FWHM, eV
Elementary carbon	284.7±0.1	1.5±0.1
C-O or C-OH	286.1±0.1	1.1±0.1
Carbonates	288.2±0.1	1.8±0.1

Table S3. CO-TPR on Co_3O_4 NAP-XPS, C 1s and Co 2p regions

Conditions	Elementary carbon, %	C-O or C-OH, %	Carbonates, %	Co^{3+} ,%
CO RT	51	13	36	27
CO RT_30	52	16	32	26
CO 100 ºC	69	10	21	24
CO 150 ºC	74	8	18	24
CO 200 ºC	78	9	13	23
CO 250 ºC	79	10	11	CoO
CO 300 ºC	82	12	6	CoO and Co metallic

Table S4. PROX on Co_3O_4 NAP-XPS, C 1s region

Conditions	Elementary carbon, %	C-O or C-OH, %	Carbonates, %
CO RT	41	11	48
CO 100 ºC	41	10	49
CO 150 ºC	58	7	36
CO 200 ºC	54	8	39
CO 250 ºC	53	9	38
CO 300 ºC	57	7	36

Table S5. PROX on Co_3O_4 NAP-XPS, C 1s region

Conditions	Elementary carbon, %	C-O or C-OH, %	Carbonates, %
CO RT	45	10	45
CO 100 ºC	55	10	35
CO 150 ºC	62	12	26
CO 200 ºC	56	7	37

Table S6. Ce 3d spectra fitting parameters for CeO_2: binding energy (eV), FWHM (eV)

	v_0	v	v'	v''	v'''
Peak position, eV	880.9±0.1	882.3±0.	884.5±0.2	888.9±0.2	898.1±0.2
FWHM, eV	2.1±0.1	1.9±0.1	4±0.2	5.6±0.2	2.1±0.1

The multiplets correspond to the spin-orbit splitting $3d_{5/2}$ and $3d_{3/2}$ core holes. The spin-orbit splitting is 18.1 eV. The intensity ratio I $3d_{5/2}$/I $3d_{3/2}$ was fixed to 1.5.

CHAPTER 6

SUMMARY

SUMMARY

The objective of the research described in this doctoral thesis was to improve the fundamental understanding of CO oxidation and preferential CO oxidation on cobalt oxide catalysts (i.e., the nature of active sites and reaction mechanism) and to reveal the role of CeO_2 in enhancing the catalytic activity of cobalt oxide catalysts. To reach the objectives of the thesis, an integrated approach was applied that is based on the combination of: 1) preparation, characterization of catalysts and correlating structural and reduction properties of catalysts with their catalytic performance; 2) kinetic studies; 3) application of in situ/operando techniques for studying catalysts under working conditions. To study catalysts under working conditions, a set of operando/in situ techniques was employed: FTIR spectroscopy and NAP-XPS to monitor surface changes of catalysts, while XRD and XAS were applied to examine bulk changes of catalysts.

Having combined in situ NAP-XPS, including valence band, depth profile and NEXAFS at the Co $L_{3,2}$ edge, the reducibility of Co_3O_4 in CO and its reoxidation in O_2 atmospheres was investigated in terms of (near)surface electronic and structural changes of Co_3O_4, adsorbates and oxygen vacancies ($V_{O^{..}}$) evolution. The results obtained by combining information from different information depths allowed to distinguish surface vacancy formation during reduction of Co_3O_4 in CO atmosphere (RT-150 ^oC) from the oxygen vacancies created by mobility of bulk lattice oxygen (200-250 ^oC) and to identify formation of a mixed structural phase of rocksalt-type CoO and metastable wurtzite-type CoO in near-surface (~ 3-5 nm) during reduction of Co_3O_4 in CO atmosphere at 250 ^oC. Valence band spectra, together with core level XPS including depth profiles and NEXAFS revealed that the temperatures for reduction of Co_3O_4 to metallic cobalt and the reoxidation of metallic cobalt to Co_3O_4 did not coincide.

The results of in situ NAP-XPS CO-TPR followed by O_2-TPO suggest that CO adsorbs on Co_3O_4, extracting lattice oxygen and forming surface oxygen vacancies that might serve as additional sites for CO adsoption, O_2 adsoption and dissociation, while oxidation of elementary carbon formed as a result of CO dissociation and oxidation of carbonates also contributes to the CO oxidation reaction cycle. To gain deeper understanding of CO oxidation, operando NAP-XPS and FTIR spectroscopy during CO oxidation (i.e., static steady state and dynamic switching experiments) were performed. The results are indicative of the redox Mars-van Krevelen mechanism for CO oxidation on Co_3O_4, involving the Co^{3+}/Co^{2+} cycle and oxygen vacancies formation at higher temperatures and likely the Langmuir–Hinshelwood mechanism at lower temperatures. In addition, results point to a significant role of reaction pathways such as carbonate formation followed by decomposition/reoxidation and CO dissociation followed by elementary carbon reoxidation in the overall CO oxidation reaction mechanism on Co_3O_4. It is suggested that upon an interaction of CO with Co_3O_4 in an excess of O_2, CO adsorbs linearly to cobalt cations and/or as carbonates, inducing vacancy formation by extracting lattice oxygen from the Co_3O_4 surface. Adsorbed

oxygen on these vacancies can react with CO molecule adsorbed on the cobalt cation. CO adsorbed on a cobalt cation undergoes dissociation/disproportionation forming elementary carbon that is oxidized by an O_2 molecule likely activated on vacancies. Both bidentate and monodentate carbonates might be reaction intermediates at higher temperatures and an excess of O_2 in the reaction mixture facilitates decomposition/reoxidation of carbonates and their conversion to CO_2.

To get insights into CO oxidation on CoO, two different CoO were used: (1) commercial CoO (1 μm); (2) CoO prepared by controlled reduction of Co_3O_4 (20-50 nm) in vacuum. This study revealed a strong effect of the particle size of CoO materials on the catalytic activity in CO oxidation. For CoO with particles of 20-50 nm, reoxidation of CoO to Co_3O_4 during CO oxidation (surface and near-surface) was observed at 200 ºC. On the contrary, for the microscopic CoO (1 μm) no bulk oxidation of CoO to Co_3O_4 is observed during CO oxidation at temperatures even of 360 ºC.

After gaining insights into CO oxidation, oxidation of CO in the presence of H_2 (i.e., preferential CO oxidation) was studied because selective oxidation/removal of CO is of great importance for purification of H_2. Many applications, such as hydrogen fuel cell technology and ammonia synthesis, require the use of clean hydrogen. The Co_3O_4 catalyst oxidation state in the PROX reaction mixture (CO, O_2, H_2) was investigated. In addition, Co_3O_4 reduction in pure CO or H_2 atmospheres was examined. The operando XAS and NAP-XPS results indicated that during PROX both the bulk and surface of Co_3O_4 were fully oxidized up to 250 ºC, while in CO the surface reduction of Co_3O_4 occurs starting from 100 ºC. Similarly to CO oxidation, in the C 1s region NAP-XPS detected adsorbed carbonates, molecular CO and elementary carbon on the surface during PROX. In pure hydrogen Co_3O_4 remains fully oxidized up to 250 °C. Taking into consideration the information obtained from CO-O_2 switching experiments, it is suggested that selective oxidation of CO to CO_2 in an excess of H_2 follows predominantly the Mars-van Krevelen mechanism. While the Co_3O_4 reduction to CoO and Co around 250 °C explains the selectivity change to methanation, the change in selectivity around 170 °C from PROX (with predominantly CO oxidation) to both CO and H_2 oxidation cannot be explained by a change in (surface) oxidation state. The difference in the increase of H_2 oxidation rate vs CO oxidation rate (higher apparent activation energy for H_2 oxidation) as well as the competition for the limited amount of O_2 account for the decreasing CO oxidation selectivity when the temperature increases. Promotion of Co_3O_4 with 10 wt% CeO_2 increases the reduction temperatures in CO and H_2 and enhances the PROX activity. Since CeO_2 is a less active material, this can only be explained by a higher activity of the Co-O-Ce ensembles.

This work clearly demonstrates the importance of combining several operando techniques in studying catalysts under steady state as well as under dynamic conditions for revealing reaction mechanisms and for finding a correlation between structure/surface and activity/selectivity of catalysts. Moreover, presented results highlight a great potential of in situ NAP-XPS for obtaining electronic and structural information

on the (near)surface changes of catalytic materials for different information depths. It is expected that the results of this thesis will make a strong contribution to fundamental and applied research in catalytic CO oxidation and advance the future development of novel catalysts for oxidation reactions.

PUBLICATIONS

PUBLICATIONS

REVIEWED

Liliana Lukashuk, Karin Föttinger, Elisabeth Kolar, Christoph Rameshan, Detre Teschner, Michael Hävecker, Axel Knop-Gericke, Nevzat Yigit, Hao Li, Eamon McDermott, Michael Stöger-Pollach, Günther Rupprechter, Operando XAS and NAP-XPS studies of preferential CO oxidation on Co_3O_4 and CeO_2-Co_3O_4 catalysts, Journal of Catalysis, 334 (2016) pp. 1-15.

M. Sommariva, N. Dadivanyan, M. Gateshki, M. Rayner, **L. Lukashuk**, K. Föttinger, G. Rupprechter, Application of differential PDF (d-PDF) and SAXS to the structural characterization of supported catalysts; Acta Physica Polonica A, 130 (2016) pp. 884-885.

Andrey B Lysenko, Ganna A Senchyk, **Liliana V Lukashuk**, Konstantin V Domasevitch, Marcel Handke, Jörg Lincke, Harald Krautscheid, Eduard B Rusanov, Karl W Krämer, Silvio Decurtins, Shi-Xia Liu, Composition Space Analysis in the Development of Copper Molybdate Hybrids Decorated by a Bifunctional Pyrazolyl/1,2,4-Triazole Ligand, Inorg. Chem*.,* 55, 1 (2016) pp. 239-250.

J. Yang, **L. Lukashuk**, J. Akbarzadeh, M. Stöger-Pollach, H. Peterlik, K. Föttinger, G. Rupprechter, U. Schubert, Different synthesis protocols for Co_3O_4-CeO_2 catalysts. Part 1: Influence on the morphology on the nanoscale, Chem. Eur. J., 21, 2 (2015) pp. 885-892.

J. Yang, **L. Lukashuk,** H. Li, K. Föttinger, G. Rupprechter, U. Schubert, High surface area ceria for CO oxidation prepared from cerium t-butoxide by combined sol-gel and solvothermal processing, Catal. Lett. 144 (2014) pp. 403-412.

L. V. Lukashuk, A. B. Lysenko, H. Krautscheid, K. V. Domasevitch, New organic–inorganic frameworks incorporating iso- and heteropolymolybdate units and a 3,3',5,5'-tetramethyl-4,4'-bi-1H-pyrazole-2,2'-diium multiple hydrogen-bond donor, Acta Cryst. C67 (2011) pp. 378-383.

Liliana Lukashuk, Andrey Lysenko, Konstantin Domasevitch, New heterometallic Cu(I,II)/Mo(VI) oxide coordination polymers, Acta Cryst. A66 (2010), p. 268.

O. A. Bondar, **L. V. Lukashuk**, A. B. Lysenko, H. Krautscheid, E. B. Rusanov, A. N. Chernega, K. V. Domasevitch, New microporous copper(II) coordination polymers based upon bifunctional 1,2,4-triazole/tetrazolate bridges, CrystEngComm, 10 (2008) pp. 1216-1226.

L. V. Lukashuk, A. B. Lysenko, E. B. Rusanov, A. N. Chernega, K. V. Domasevitch, Diaquabis[4-(4H-1,2,4-triazol-4-yl)benzoato-2O,O']cobalt(II), and the cadmium(II) and copper(II) analogues: new self-complementary hydrogen-bond donor/acceptor modules for designing hydrogen-bonded frameworks, Acta Cryst. C63 (2007) pp. 140-143.

IN PREPARATION

Liliana Lukashuk, Raffael Rameshan, Detre Teschner, Michael Hävecker, Axel Knop-Gericke, Karin Föttinger, Günther Rupprechter, (Near)surface electronic and geometric structure modifications of Co_3O_4 under reducing (CO) and oxidizing (O_2) atmospheres: in situ NAP-XPS and NEXAFS, in preparation.

Liliana Lukashuk, Jingxia Yang, Karin Föttinger, Ulrich Schubert, Günther Rupprechter, Different synthesis protocols for Co_3O_4-CeO_2 catalysts. Part 2: Influence on the catalytic properties, in preparation.

Liliana Lukashuk, Raffael Rameshan, Nevzat Yigit, Elisabeth Kolar, Detre Teschner, Michael Hävecker, Axel Knop-Gericke, Karin Föttinger, Karin Föttinger, Günther Rupprechter, Mechanistic insights into CO oxidation on cobalt oxide catalysts by means of operando techniques, in preparation.

TALKS AND POSTER PRESENTATIONS WITH PROCEEDINGS-ENTRY

N. Yigit, **L. Lukashuk**, K. Föttinger, G. Rupprechter, Operando spectroscopy studies: revealing of preferential CO oxidation (PROX) on Co_3O_4 and $LaCoO_3$ catalysts; Talk: The 13th Pannonian International Symposium on Catalysis, Siofok, Hungary, September 19-23 (2016), O52.

M. Sommariva, N. Dadivanya, M. Gateshki, **L. Lukashuk**, G. Rupprechter, K. Föttinger, Structural Characterization of Supported Catalysts by X-ray Scattering Techniques; Talk: 8th International Conference on Materials Science and Condensed Matter Physics (MSCMP 2016), Chisinau, Rep. of Moldova, September 12-16 (2016), p. 362.

M. Sommariva, N. Dadivanyan, M. Gateshki, C. Reiss, E. Casini, **L. Lukashuk**, K. Föttinger, G. Rupprechter, Application of X-ray total scattering for the structural characterization of supported catalysts; Talk; EPDIC15, Bari, Italy, June 12-15 (2016), p. 37.

Nevzat Yigit, **Liliana Lukashuk**, Karin Föttinger, Günther Rupprechter, Operando Spectroscopy Studies of Co_3O_4 and $LaCoO_3$ Catalysts during Preferential CO Oxidation; Poster: International FOXSI Conference, Vienna, Austria, May 23-25, (2016), p.38.

M. Sommariva, N. Dadivanyan, M. Gateshki, C. Reiss, **L. Lukashuk**, K. Föttinger, G. Rupprechter, PDF and SAXS for the structural characterization of supported catalysts; Poster: The 17th Netherlands' Catalysis and Chemistry Conference, Noordwijkerhout, Netherlands, March 7-9 (2016).

Liliana Lukashuk, Karin Föttinger, Günther Rupprechter, Natalia Dadivanyan, Marco Sommariva, Detlef Opper, Structural Characterization of Noble Metal Catalysts Supported on Reducible Oxides by a Laboratory X-ray Diffractometer, DECHEMA, Frankfurt am Main, February 25-26 (2016), p. 36.

M. Sommariva, N. Dadivanyan, M. Gateshki, M. Rayner, **L. Lukashuk**, K. Föttinger, Application of differential PDF (d-PDF) and SAXS to the structural characterization of supported catalysts; Talk: XXIII Conference on Applied Crystallography, Krynica Zdroj, Poland, September 20-24 (2015), pp. 103-104.

Lukashuk L., Kolar E., Rameshan C., Teschner D., Knop-Gericke A., Föttinger K., Rupprechter G., Mechanistic Insights into CO Oxidation and Preferential CO Oxidation over Cobalt Oxide and Promoted Cobalt Oxide Catalysts; Talk & Poster: XII European Congress on Catalysis, Kazan, Russia, August 30-September 4 (2015), p. 381.

Lukashuk L., Li H., Yigit N., McDermott E., Carlson S., Föttinger K., Rupprechter G., Operando X-ray Absorption Spectroscopy Studies of Co_3O_4 and CeO_2-Co_3O_4 Catalysts during Preferential CO Oxidation; Poster: XII European Congress on Catalysis, Kazan, Russia, August 30-September 4 (2015), p. 389.

G. Rupprechter, **L. Lukashuk**, K. Föttinger, Operando FTIR, NAP-XPS and XAS studies of Co_3O_4 and CeO_2-Co_3O_4 Catalysts during Preferential CO Oxidation; Oral: The 250th ACS National Meeting & Exposition, Boston, Massachusetts, USA, August 16-20 (2015), p. 107.

Natalia Dadivanyan, **Liliana Lukashuk**, Karin Föttinger, Marco Sommariva, Structural Characterization of Supported Noble Metal Catalysts by in-situ X-ray Diffraction; Talk: 18. Tagung Festkörperanalytik, Vienna, Austria, July 6-8 (2015), p. 25.

Liliana Lukashuk, Elisabeth Kolar, Michael Stöger-Pollach, Günther Rupprechter, Karin Föttinger, Operando Studies of Palladium on Cobalt Oxide and Iron Oxide Catalysts during CO Oxidation; Poster: The 5th International Conference on Operando Spectroscopy, Deauville, France, May 17-21 (2015), p.97.

G. Rupprechter, Ch. Rameshan, K. Föttinger, Y. Suchorski, A. Bukhtiyarov, H. Li, K. Anic, A. Wolfbeisser, **L. Lukashuk**, Operando Studies on PdZn, Co_3O_4/CoO and Ni-ZrO_2: Synergies of Surface Science Based Model Systems and Technological Catalysts; Talk: The 5th International Conference on Operando Spectroscopy, Deauville, France, May 17-21 (2015), p.40.

L. Lukashuk, K. Föttinger, G. Rupprechter, CO Oxidation and Preferential CO Oxidation over Cobalt Oxide and Promoted Cobalt Oxide Catalysts: Operando XAS and NAP-XPS Studies; Talk: 9th European NESY Winterschool & Symposium on Neutron and Synchrotron Radiation, Altaussee, Austria, March 9-13 (2015), p.27.

Natalia Dadivanyan, Marco Sommariva, **Liliana Lukashuk**, Karin Föttinger, On the Structural Characterization of Noble Metal Catalysts Supported on Reducible Oxides by a Laboratory X-ray Diffractometer; Talk: The 16th Netherlands' Catalysis and Chemistry Conference, Noordwijkerhout, Netherlands, March 2-4 (2015), p. 91.

L. Lukashuk, K. Föttinger, G. Rupprechter, In situ studies of CO oxidation and preferential CO oxidation on Co_3O_4 nanostructured catalysts; Talk: The 12th Pannonian International Symposium on Catalysis, Castle Trest, Czech Republic, September 16-20 (2014), p. 30.

E. Kolar, **L. Lukashuk,** M. Stöger-Pollach, K. Föttinger, G. Rupprechter, In situ studies on the synergetic effect between Pd species and Co_3O_4 and Fe_2O_3 in CO oxidation; Talk: The 12th Pannonian International Symposium on Catalysis, Castle Trest, Czech Republic, September 16-20 (2014), p. 33.

G. Rupprechter, Ch. Rameshan, H. Li, A. Bukhtiyarov, K. Anic, K. Föttinger, **L. Lukashuk**, Ultrathin Films of Zirconium Oxide and Cobalt Oxide as Model Catalyst; Talk: The 12th Pannonian International Symposium on Catalysis, Castle Trest, Czech Republic, September 16-20 (2014), p. 1.

Liliana Lukashuk, Karin Föttinger and Günther Rupprechter, Co_3O_4 modified with CeO_2: the effect of cerium precursor salts on the structure and catalytic performance for CO oxidation; Talk: The 15th Netherlands' Catalysis and Chemistry Conference, Noordwijkerhout, Netherlands, March 10-12 (2014), p. 74.

Liliana Lukashuk, Karin Föttinger and Günther Rupprechter, Morphology effect of Co_3O_4 nanostructures on the reducibility and catalytic performance for CO oxidation; Poster: Symposium "Research at European Neutron and Synchrotron facilities by Austrian researchers", Vienna, Austria, November 11-12 (2013), p. 77.

Liliana Lukashuk, Andrey Bukhtiyarov, Karin Föttinger and Günther Rupprechter, Understanding the catalytic activity of cobalt oxide nanocrystals by means of in situ techniques; Talk: 15. Österreichische Chemietage 2013, TU-Graz, Graz, Austria, September 23-26 (2013), p. 40.

J. Yang, **L. Lukashuk,** U. Schubert, Synthesis of CeO_2 from Cerium tert-Butoxide by a Combination of Sol-Gel Solvothermal Processing; **Talk:** 15. Österreichische Chemietage 2013, TU-Graz, Graz, Austria, September 23-26 (2013), p. 39.

Olena Kysil, **Liliana Lukashuk**, Oleksandr Ivaniuta, Oleksii Dubok, Eugenia Buzaneva, Uwe Ritter, Peter Scharff, Design and characterization of photoactive carbon tubes functionalized by the Cu organic complex – histidine as biomedical nanoparticles; Poster: E-MRS Spring Meeting 2013, Strasbourg, France, May 27-31 (2013), U.PII 15.

J. Yang, Ch. Artner, **L. Lukashuk**, U. Schubert, Sol-gel synthesis of CeO_2 by using Cerium tert-butoxide as precursor; Poster: COST Action CM1104-Reducible oxide chemistry, structure and functions, Vienna University of Technology, Vienna, Austria, April 18-19 (2013), p. 62.

M. Goepel, P. C. With, **L. Lukashuk**, C. Küster, D. Enke, R. Gläser, Comparison of Impregnation Methods for the Preparation of Silica-Supported Pt-Catalysts; Poster: 25. Deutsche Zeolith-Tagung, Hamburg, Germany, March 6-8 (2013), p. 96.

H. Gogotsi, I. Sporysh, **L. Lukashuk**, O. Ivanuta, G. Gobsh, U. Ritter, P. Scharff, Sensory elements on the basis of carbon nanotubes: discrete elements; Talk: The VIth International Conference "Electronics and Applied Physics", Kiev, Ukraine, June 16-19 (2010), pp. 47-48.

L. V. Lukashuk, A. B. Lysenko, Coordination polymers of polyoxomolybdates with bifunctional azole ligands; Talk: The 4th International Conference of Chemistry and Modern Technology for Students and Post Graduate Students, Dnepropetrovsk, Ukraine, April 22-24 (2009), p. 48.

L. V. Lukashuk, A. B. Lysenko, Hydrothermal synthesis of Cu(I,II) and Ag(I) polyoxomolybdates with new bifunctional azole ligands; Talk: the IX Ukrainian Conference of Present-Day Problems of Chemistry for Students and Post Graduate Students, Kiev, Ukraine, May 14-16 (2008), p. 35.

TALKS AND POSTER PRESENTATIONS WITHOUT PROCEEDINGS-ENTRY

K. Föttinger, **L. Lukashuk**, Updates and progress on the Co_3O_4-based catalysts; Talk: Catalysis Summit, Filzmoos, Austria, September 24-27 (2015).

L. Lukashuk, E. Kolar, Ch. Rameshan, D. Teschner, A. Knop-Gericke, K. Föttinger, G. Rupprechter, Mechanistic Insights into CO Oxidation and Preferential CO Oxidation over Cobalt Oxide and Promoted Cobalt Oxide Catalysts; Poster: Solids4Fun Summer School 2015, Schloss Hernstein, Austria, June 29 - July 03 (2015).

L. Lukashuk, E. Kolar, K. Föttinger, In situ studies of CO oxidation and preferential CO oxidation on Co_3O_4 and Pd-Co_3O_4 catalysts; Talk: Catalysis Summit, Kaisertal, Austria, September 25-27 (2014).

L. Lukashuk, J. Yang, K. Föttinger, M. Stöger-Pollach, U. Schubert, G. Rupprechter, CO oxidation and preferential CO oxidation on differently prepared CeO_2-modified Co_3O_4 catalysts; Poster: The Summer School of "Solids4Fun" Graduate School, Hernstein, Austria, July 14-18 (2014).

L. Lukashuk, K. Föttinger, G. Rupprechter, Investigation of the catalytic activity of cobalt oxide nanostructures by means of in-situ IR spectroscopy; Talk: The Summer School of "Solids4Fun" Graduate School, Hernstein, Austria, July 08-12 (2013).

SCIENTIFIC REPORTS

Liliana Lukashuk, Nevzat Yigit, Karin Föttinger, In-situ X-ray absorption study of cobalt-based catalysts during preferential CO oxidation, report for MAX IV Laboratory, Lund University, Lund, Sweden; 2016; 3 p.

Liliana Lukashuk, Nevzat Yigit, Karin Föttinger, Investigation of preferential CO oxidation over cobalt-based catalysts by operando X-ray absorption spectroscopy, annual report for MAX IV Laboratory, Lund University, Lund, Sweden; 2016; 2 p.

L. Lukashuk, K. Föttinger, XAS operando studies of Co_3O_4-CeO_2 catalysts during (preferential) CO oxidation: insights into the electronic and geometric structure of Co and Ce, report for MAX IV Laboratory, Lund University, Lund, Sweden; 2015; 3 p.

L. Lukashuk, K. Hradil, N. Yigit, N. Barrabes Rabanal, K. Föttinger, Operando synchrotron X-ray total scattering study of cobalt oxide and promoted cobalt oxide catalysts during (preferential) CO oxidation: insights into the structural, microstructural changes and local/intermediate-range structure, report for PETRA III, Deutsche Elektronen-Synchrotron (DESY), Hamburg, Germany; 2015; 1 p.

K. Föttinger, **L. Lukashuk**, Ch. Rameshan, G. Rupprechter, Structure dependence of CO oxidation over Co_3O_4 nanoshaped catalysts: insights into the nature of active sites and deactivation mechanisms, report

for Helmholtz-Zentrum Berlin für Materialien und Energie, Elektronenspeicherring BESSY II, Berlin, Geremany; 2014; 2 p.

RESUME

LILIANA LUKASHUK

21 Summerhouse Square▪ TS20 1BH Stockton-on-Tees, UK
liliana.lukashuk@gmail.com

Qualifications

Expertise in R&D with background in synthesis, catalysis, chemical engineering, and in situ spectroscopy (5 years)

- Design and conduct of experiments
- Organic and inorganic synthesis, preparation and characterization of catalysts; scale-up of catalyst production, crystallization of coordination polymers; data interpretation
- Catalytic tests: batch reactors and fixed-bed flow reactors, high pressure multipurpose screening rigs (MPSR), detailed kinetic studies and kinetic modeling, design of experiments (DoE)
- Commissioning and improving existing high pressure MPSR for catalytic studies
- Providing recommendation on the design of a pilot plant and developing test programmes for operation
- Proficiency in operation of lab devices: UV-Vis, FTIR, Raman, N_2 sorption, XRD, TGA, GC, MS, in situ FTIR (flow and batch reactors)
- Proficiency in operation of synchrotron-based in situ XRD, in situ XAS, in situ XPS
- Designed and constructed catalytic setup and reaction cell for in situ XAS and in situ XRD synchrotron-based experiments

Communication skills
- Numerous reports, articles (8), proposals for the beamtimes (8 granted & 5 currently under reviewing), presentations for seminars, project meetings & international conferences (>25)

Supervision & training of researchers
- Planned projects, designed experiments, interpreted data, supervised master and bachelor students, corrected manuscripts and reports, trained students to carry out chemical syntheses and to use lab equipment

Collaboration
- Collaborated with scientific institutes and the industrial partners to meet objectives of projects, to prepare scientific papers, conference presentations, and successfully grant beamtime proposals

Soft skills
- Analytical & time management skills • Good team spirit & autonomous • Fast learner & adaptable • Ability to multi-task • Meeting deadlines • Multilingual: Ukrainian, Russian, English, German, Polish

---

Working Experience
Research Experience

December 2015-current	**Johnson Matthey Technology Centre Chilton, Billingham, Cleveland, United Kingdom** **Research Scientist**

- Designing/carrying out/interpreting results of the project and transferring technology/products to the Syn Gas business
- Evaluating project results/making recommendations for the next steps of the project/project resourcing including CAPEX requirements
- Representing Johnson Matthey at technical update meetings with project partners and delivering reports (oral/written) to agreed deadlines
- Commission/operate and maintain/improve existing laboratory and/or pilot equipment
- Setting/maintaining EHS standards and operating procedures for Lab areas
- Supervising and/or managing staff assigned to the project
- PIC and DPIC for Lab areas and equipment
- Writing scientific proposals and case study proposals
- Arranging collaborations between Johnson Matthey and scientific institutes and facilities
- Contributing to the development of close working relationships with business units/external customers/collaborators

October 2012- November 2015

TU Wien, Institute of Materials Chemistry, Vienna, Austria

Project assistant. FWF (The Austrian Science Fund) project: *Cobalt oxide catalysis across the materials and pressure gap*

- Designed and synthesized cobalt oxide and promoted cobalt oxide catalysts, characterized their properties, interpreted data
- Planned & conducted reaction kinetics analysis of catalysts for CO oxidation and preferential CO oxidation (PROX)
- Wrote successful scientific proposals for synchrotron beamtime applications
- Developed in situ cell for XAS and XRD synchrotron-based experiments
- Constructed the catalytic setup for in situ synchrotron-based experiments
- Organized, led and performed the synchrotron-based experiments in BESSY, DESY, SLS, MAX-lab II
- Identified reaction mechanisms for CO oxidation/PROX for industrial-grade cobalt oxide and promoted cobalt oxide catalysts via combination: in-situ XRD, in situ XAS, in situ XPS, in situ FTIR & concentration modulation experiments
- Wrote reports, articles, conference abstracts, and made presentations for academic & industrial public
- Supervised & trained junior graduate and undergraduate students, planned experimental work, corrected scientific reports and conference abstracts
- Coordinated with PANalytical on a project

July 2007- September 2008

Institute of Pharmacology and Toxicology, Academy of Medical Sciences of Ukraine, Kiev, Ukraine
Laboratory assistant (part-time job)
- Synthesized and crystallized physiologically-active substances
- Wrote scientific reports

Teaching experience

April 2013-February 2015	**TU Wien, Institute of Materials Chemistry, Vienna, Austria**
	Teaching assistant • Supervised students during the lab course "Physical Chemistry", corrected protocols and performed examinations

Education

October 2012-current	**TU Wien, Institute of Materials Chemistry, Vienna, Austria**
	Doctoral Candidate in Chemistry
	Thesis: CO oxidation and preferential CO oxidation on cobalt oxide catalysts

October 2010-August 2012	**Leipzig University, Faculty of Chemistry, Leipzig, Germany and Lille 1 University, Faculty of Chemistry, Lille, France**
	Master of Science in Chemistry, international Erasmus Mundus master programme Advanced Spectroscopy in Chemistry. Graduation with distinction
	Thesis: Synthesis, characterization, and catalytic properties of platinum supported on porous glass and silica gel

September 2009-June 2011	**Kiev National Taras Shevchenko University, Faculty of Chemistry, Kiev, Ukraine**
	Master of Science in Chemistry. Graduation with distinction
	Thesis: Hydrothermal synthesis of coordination polymers based upon polyoxomolybdate and bifunctional azole type ligands

September 2005-June 2009	**Kiev National Taras Shevchenko University, Faculty of Chemistry, Kiev, Ukraine**
	Bachelor of Science in Chemistry. Graduation with distinction
	Thesis: Hydrothermal synthesis of Cu(I) and Ag(I) polyoxomolybdates with new bifunctional azole ligands

Professional Trainings and Schools

September 2016 April 2016	**Project Management and Personal Productivity and Time Management trainings**, Johnson Matthey, Royston, UK

September 2016	**Eurokin Summer School on Reaction Kinetics**, Johnson Matthey Technology Centre, Sonning, UK

July 2013-July 2015	**Effective scientific writing and presentation of research; Writing FWF (The Austrian Science Fund) proposals; Project management; Leadership and management**, Internal Continuing Education and Solids4Fun School, Vienna, Austria

March 2015	**Workshop on Analysis of Short Range Order**, TU Wien, Vienna, Austria

March 2015	**9th European NESY Winter School & Symposium on Neutron and Synchrotron Radiation for Industrial Application**, Altaussee, Austria
September 2014	**EXAFS Course**, Max-lab IV, Lund University, Lund, Sweden
July 2014	**Powder Diffraction School & Modern Synchrotron Methods**, Paul Scherrer Institute, Villigen, Switzerland
March 2013	**Electron Microscopy**, USTEM, TU Wien, Vienna, Austria
September 2011	**Advanced Spectroscopy in Chemistry IIIrd International Summer School "New methods in Solid State NMR and related techniques for the analysis of inorganic materials"**, Lille 1 University, Lille, France
August 2010	**The 20th Jyväskylä Summer School, courses: "Polymorphism and crystal forms" and "Future of Main Group Chemistry"**, Jyväskylä, Finland
September 2009	**Summer school "European School on Chemistry and Physics of Materials for Energetics"**, University of Milano-Bicocca, Milan, Italy

Selected Fellowships and Awards

2010-2012	EU Erasmus Mundus scholarship for master course: Advanced Spectroscopy in Chemistry, Leipzig University, Leipzig, Germany and Lille 1 University, Lille, France
2008-2011	Victor Pinchuk Foundation "Zavtra.UA" scholarships (3) for the cycle of research projects, Kiev, Ukraine
2010	DAAD scholarship for a research visit, Ilmenau University of Technology, Faculty of Mathematics and Natural Science, Ilmenau, Germany
March 2010	Award of Kiev National University for the work: "New approaches for design of polyoxomolybdate coordination polymers by means of bifunctional azole ligands", Kiev, Ukraine
2008&2009	Award for the best oral report - Conference for young scientists, Kiev (2008) & Dnepropetrovsk, (2009), Ukraine
2007-2008	Grant Recipient - Maxymovych scholarship, Kiev, Ukraine
2008	DAAD grant for a research visit, Leipzig University, Faculty of Chemistry, Leipzig, Germany

Computer skills

- Proficient user of Microsoft Word and Office, presentation and graphic editor tools for Windows platform, Adobe Photoshop, OriginLab
- Chemistry-oriented software: Cambridge Structure Database analysis, Diamond, ChemDraw, Topas, HighScore, Digital Micrograph, pyPulsar, OPUS, OMNIC, Athena, EXAFSPAK, CasaXPS, Athena Visual Studio, Wonderware InTouch

Languages

Ukrainian (native language), Russian (C1), English (C1), German (B2), Polish (B2), French (A1)

04/11/2016   Liliana Lukashuk